Charles University
Faculty of Science

Immunology

Mgr. Ladislav Sivák

Overcoming cancer resistance to chemotherapy through HPMA copolymer conjugates

Překonání rezistence nádorů k chemoterapii pomocí konjugátů na bázi HPMA kopolymerů

Doctoral thesis

Supervisor: RNDr. Marek Kovář, PhD.

Prague 2019

Prohlášení:

Prohlašuji, že jsem závěrečnou práci zpracoval samostatně a že jsem uvedl všechny použité informační zdroje a literaturu. Tato práce ani její podstatná část nebyla předložena k získání jiného nebo stejného akademického titulu.

Declaration:

I hereby declare that I have written this thesis independently and that I have not used other than the cited sources. I did not use either this thesis or its substantial part as a background to obtain any another academic degree.

Prague, June 2019

Mgr. Ladislav Sivak

Acknowledgments

First and foremost I would like to thank my supervisor RNDr. Marek Kovář, PhD. for the continuous guidance and support he provided during my PhD study, his patience, motivation and immense knowledge.

My sincere thanks also goes to my colleagues from the Laboratory of Tumor Immunology at the Institute of Microbiology for stimulating discussions and for all the advice, practical help and all the fun we have had in the last five years. Without such a team behind me, I doubt that I would be in this place today.

Special thanks must go to my colleagues from the Laboratory of Biomedical Polymers at the Institute of Macromolecular Chemistry, whose development of polymer prodrugs, as well as their expertise and advice, were essential for realization of this study.

Finally I gives thanks with love to my wife Zuzana for her continued support and encouragement throughout this entire process. I was continually amazed by her willingness to make countless sacrifices to help me get to this point and the patience with which she experienced all of the ups and downs of my research.

Abstract

Multidrug resistance (MDR) is a common cause of failure in chemotherapy for malignant diseases. Cancer cells develop MDR most often via the up-regulation of P-glycoprotein (P-gp) expression. P-gp is an efflux pump with broad specificity belonging to ATP-binding cassette (ABC) transporters which decreases the intracellular concentration of various drugs.

We designed polymeric conjugates based on an *N*-(2-hydroxypropyl)methacrylamide (HPMA) bearing a cytostatic drug and/or P-gp inhibitor and tested their cytostatic/cytotoxic activity *in vitro* and their therapeutic efficacy *in vivo* in MDR tumors. We demonstrated that HPMA copolymer conjugates bearing both the cytostatic drug (doxorubicin (Dox) or pirarubicin) and the P-gp inhibitor (derivative of reversin 121 (R121) or ritonavir) possess remarkable cytostatic and cytotoxic activity in MDR tumor cell lines *in vitro* and superior antitumor activity *in vivo*. Notably, the HPMA copolymer conjugate bearing both Dox and R121 showed significant antitumor activity in both P388/MDR and CT26 mouse tumor models and was capable to completely cure 6 out of 8 mice with established CT26 tumors.

We explored the potential of micelle-forming HPMA copolymer-poly(propylene oxide) (PPO) diblock bearing Dox to overcome MDR *in vitro* and *in vivo*. The HPMA copolymer-PPO diblock bearing Dox showed higher cytostatic and cytotoxic activity *in vitro* in comparison to the HPMA copolymer conjugate bearing Dox in MDR murine and human cancer cell lines. Moreover, the HPMA copolymer-PPO diblock bearing Dox showed higher antitumor activity and accumulation in mouse EL4 lymphoma *in vivo* in comparison to the HPMA conjugate bearing Dox.

Finally, we evaluated the potential of polymeric NO donors to improve the therapeutic activity of the HPMA copolymer conjugate bearing Dox through an increase of the enhanced permeability and retention effect. Polymeric NO donors were able to sensitize murine and human cell lines to the cytostatic activity of Dox *in vitro* and significantly improved the treatment of EL4 lymphoma-bearing mice with the HPMA copolymer conjugate bearing Dox *in vivo*.

Abstrakt

Mnohočetná léková rezistence (MDR) představuje jednu z nejběžnějších a z nejzávažnějších komplikací při chemoterapii nádorových onemocnění. Hlavní mechanismem podílejícím se na vzniku MDR nádorových buněk je zvýšená exprese ATP-dependentních ABC transportérů, zejména P-glykoproteinu (P-gp). P-gp jako effluxní pumpa snižuje cytoplazmatickou koncentraci řady protinádorových léčiv.

Otestovali jsme cytotoxický a cytostatický efekt polymerních konjugátů na bázi N-(2-hydroxypropyl)metakrylamidu (HPMA) nesoucí protinádorové léčivo a inhibitor P-gp *in vitro* a *in vivo* na nádorech s MDR. Na MDR myších i lidských nádorových liniích jsme prokázali, že polymerní konjugáty nesoucí protinádorové léčivo a inhibitor P-gp nejenom efektivně inhibují aktivitu P-gp a tím zvyšují intracelulární akumulaci daného cytostatika, ale také zvyšují jeho cytostatickou a cytotoxickou aktivitu *in vitro* a *in vivo*. Léčba pomocí konjugátu nesoucího doxorubicin (Dox) a derivát reversinu 121 (R121) vedla k signifikantní inhibici růstu nádorů a prodloužení doby přežití myší u nádorových modelů P388/MDR a CT26. U modelu CT26 dokonce došlo ke kompletní regresi nádorů u 6 z experimentální skupiny 8 myší nesoucí nádor.

Dále jsme otestovali schopnost diblokového konjugátu nesoucího Dox a skládajícího se z HPMA kopolymerního řetězce a řetězce polypropylen oxidu (PPO) překonávat MDR *in vitro* a *in vivo*. HPMA kopolymer-PPO diblokový konjugát vykazoval vyšší cytostatickou a cytotoxickou aktivitu ve srovnání s HPMA kopolymerním konjugátem nesoucím Dox a to jak na lidských tak myších MDR buněčných liniích *in vitro*. Tento diblokový konjugát měl pak i vyšší terapeutickou účinnost *in vivo* a vykazoval vyšší akumulaci v nádorech ve srovnání s HPMA kopolymerním konjugátem nesoucím Dox.

Nakonec jsme testovali schopnost HPMA kopolymerních konjugátů nesoucí donory NO zvýšit terapeutickou účinnost HPMA konjugátu nesoucího Dox, a to pomocí zvýraznění EPR efektu. Tyto konjugáty nejenom sensitizovali myší a lidské buněčné linie k cytostatické aktivitě Dox *in vitro*, ale také výrazně zvýšili účinnost léčby HPMA kopolymerního konjugátu nesoucího Dox v modelu myšího EL4 lymfomu.

List of Abbreviations

5-FU	5-fluorouracil
ABC	ATP-binding cassette
ALL	acute lymphoblastic leukemia
AML	acute myeloid leukemia
ASK1	apoptosis-regulating kinase 1
Bad	Bcl-2-associated agonist of cell death
Bax	Bcl-2-associated X protein
BCAR	breast cancer anti-estrogen resistance protein
Bcl-2	B-cell lymphoma 2 protein
Bcl-xL	B-cell lymphoma-extra large protein
BCRP	breast cancer resistance protein
BER	base excision repair
BIM	Bcl-2 interacting mediator of cell death
BIR	baculovirus-IAP repeat domain
CAF	cancer-associated fibroblast
CAM-DR	cell adhesion-mediated drug resistance
CFTR	cystic fibrosis transmembrane conductance regulator
cMOAT	canalicular multispecific organic anion transporter
CNS	central nervous system
CsA	cyclosporine A
CTR	copper transporter receptor
CYP3A4	isoform 3A4 of cytochrome P450
DSB	double-strand break
Dctx	docetaxel
DDR	DNA damage repair
DISC	death-inducing signaling complex
DLBCL	diffuse large B-cell lymphoma
Dox	doxorubicin
$E_2$17G	estradiol-17β
ECM	extracellular matrix
EGFR	epidermal growth factor receptor
EMT	epithelial-to-mesenchymal transition
EndMT	endothelial-to-mesenchymal transition
EPR	enhanced permeability and retention
ERCC1	excision repair cross-complementing 1 protein
FR	folate receptor
FTC	fumitremorgin
GCL	γ-glutamylcystein ligase
GFLG	Gly-Phe-Leu-Gly
GGT	γ-glutamyl transpeptidase
GIT	gastrointestinal tract

GSH	glutathione
GSSG	glutathione disulfide
GST	glutathione S-transferase
HGF	hepatocyte growth factor
HMW	high molecular weight
HPMA	*N*-(2-hydroxypropyl)methacrylamide
HRR	homologous recombination repair
HVC	hydrophobic vacuum cleaner
IAP	inhibitor of apoptosis
IL-6	interleukin-6
JNK1	c-Jun N-terminal kinase 1
LMW	low molecular weight
LRP	lung resistance-related protein
LTC_4	leukotriene C_4
LTD_4	leukotriene D_4
LTE_4	leukotriene E_4
MAPK	mitogen-activated protein kinase
Mcl-1	myeloid cell leukemia 1
MDR	multidrug resistance
MDSC	myeloid-derived suppressor cell
MHL1	MutL homolog 1
MMP	matrix metalloproteinase
MMR	mismatch repair
MRP1, 2, 3, 7	multidrug resistance protein 1, 2, 3, 7
MSC	mesenchymal stem cell
MSD	membrane spanning domain
MSH2	DNA mismatch repair protein 2
MTD	maximal tolerated dose
MTX	methotrexate
MutL	mutator L
MVP	major vault protein
NBD	nucleotide-binding domain
NER	nucleotide excision repair
NF-κB	nuclear factor kappa-light-chain-enhancer of activated B cells
NHEJ	non-homologous end-joining
NSCLC	non-small cell lung carcinoma
PARP1	poly(ADP-ribose) polymerase 1
PCFT	proton-coupled folate transporter
PCNSL	primary central nervous system lymphoma
P-gp	P-glycoprotein
PhIP	2-amino-1-methyl-6-phenyllimidazol[4,5-b]pyridine
PI3K	phosphoinositide 3-kinase
PKA	protein kinase A
PKC	protein kinase C

PNA	peanut agglutinin
PPIX	protoporhyrin IX
R121	reversin 121
RAFT	reversible addition-fragmentation chain transfer
Ral	Ras-related protein
Ras	rat sarcoma protein
RFC	reduced folate carrier
RIT	ritonavir
RLIP76	Ral-interacting protein
ROS	reactive oxygen species
S1P	sphingosine-1-phosphate
SCLC	small cell lung carcinoma
siRNA	small interfering RNA
SLC	soluble carrier
SNP	single nucleotide polymorphism
STAT3	signal transducer and activator of transcription 3
SUR	sulfonylurea receptor
TDP1	tyrosyl-DNA phosphodiesterase 1
TGF-β	transforming growth factor-β
THP	pirarubicin
TKI	tyrosine kinase inhibitor
TM	transmembrane
TMD	transmembrane domain
TME	tumor microenvironment
UTR	untranslational region
WGA	wheat germ agglutinin
XRCC1	X-ray repair cross-complementing protein 1

Contents

1 Introduction

Chemotherapy is one of three principal cancer treatment modalities. The effectiveness of chemotherapy is limited by tumor chemoresistance, which represents the most common cause of cancer treatment failure. A diverse range of molecular mechanisms have been implicated in tumor chemoresistance. There are two mechanism-based types of tumor chemoresistance. The first is based on the impairment of the delivery of anticancer drugs to tumor cells and the second is based on cancer cell genetic alterations that affect sensitivity to chemotherapeutics [1, 2].

Tumor chemoresistance mediated by impaired drug delivery results from the reduced accessibility of administered drugs to tumor cells. Factors such as the composition of the extracellular matrix (ECM), increased hydrostatic pressure within solid tumors and altered tumor vascularization were identified as major contributors to this type of chemoresistance mediated by the tumor microenvironment (TME) [3-5]. While some aspects of the TME on tumor growth and progression have long been appreciated, the role of TME in chemoresistance is now increasingly accepted [6-8].

The chemoresistance of cancer cells can be further divided into two categories: intrinsic (natural) and acquired (secondary). Intrinsic resistance means that resistance-mediating factors pre-exist in cancer cells and make chemotherapy ineffective from the onset. Acquired resistance gradually develops during the chemotherapy course and thus initially chemosensitive tumor cells become chemoresistant upon relapse. Alternatively, acquired resistance could arise from the outgrowth of the preexisting subpopulation of tumor cells that already harbored resistance [9].

Loss of sensitivity to a single chemotherapeutic agent, or a class of chemotherapeutic agents with similar mechanisms of action, may not directly cause the loss of sensitivity to other chemotherapeutic agents. However, the development of resistance to chemotherapy is frequently associated with cross resistance to structurally and mechanistically unrelated drugs, suggesting the existence of general mechanisms of chemotherapy resistance. This phenomenon is known as multidrug resistance (MDR) [10].

1.1 Multidrug resistance

MDR is defined as the cross-resistance or insensitivity of cancer cells to the cytostatic and cytotoxic actions of different chemotherapeutic agents commonly used in cancer

chemotherapy which are structurally and functionally unrelated and have different molecular targets [11]. This phenomenon was first discovered in 1968 by Kessel and colleagues. They observed that cells adapted to grow in the presence of daunorubicin did not accumulate as much of the drug as daunorubicin-sensitive cells [12]. Two years later, Biedler and Riehm described the phenomenon called cross-resistance. They found that Chinese hamster lung cells and fibroblasts grown in presence of actinomycin D were resistant not only to actinomycin D but also to vinblastine, vincristine and daunorubicin [13, 14]. Another study showed that daunorubicin was actively transported out of chemoresistant Ehrlich ascites cells, suggesting the existence of a promiscuous membrane transporter that confers MDR [15]. This transporter was later identified by Juliano and Ling in Chinese hamster ovary cells resistant to colchicine and was named P-glycoprotein (P-gp) [16].

MDR can be mediated by numerous mechanisms. Recent studies indicate that there are three major mechanisms: i) the decreased uptake of water-soluble drugs which require transporters to enter the cells; ii) various changes in cancer cells affecting the capacity of anticancer drugs to kill cells, including alterations in the cell cycle or apoptosis induction, increased DNA damage repair and altered drug metabolism; and iii) the increased ATP-dependent efflux of drugs that enter the cancer cells by diffusion through the plasma membrane. These mechanisms could work both independently or together with one another. However, one particular mechanism is usually dominant.

The numerous mechanisms described to explain the MDR phenomenon can be divided into two broad categories: non-cellular and cellular mechanisms. The non-cellular mechanisms involve factors that are extracellular and reduce drug access to the tumor cells, whereas cellular mechanisms include tumor cell-intrinsic factors [17-25].

1.1.1 Non-cellular mechanisms of MDR

Non-cellular mechanisms of chemoresistance are usually associated with solid tumors and occur as a consequence of tumor growth. These mechanisms are typically exhibited in cancers which show inherent resistance to chemotherapy at the initial exposure. The unique features of the TME provide protection for cancer cells from chemotherapeutic agents. A lack of nutrition, hypoxia, higher interstitial fluid pressure and an acidic environment could reduce drug access to the tumor mass and thus confer resistance to chemotherapeutic agents. Recent studies suggest that tumors do not manifest as a proliferation and progression of cancer cells alone, but rather as collaborative interactions between cancer cells and their stroma. These

interactions between cancer cells and non-transformed cells such as endothelium, immune cells and fibroblasts may alter the response to chemotherapeutic agents [26-31]. Another important attribute in non-cellular MDR mechanisms is that cancer cells are genetically heterogeneous. This heterogeneity is now considered an important factor in tumor resistance [27, 32].

1.1.1.1 Role of the TME in MDR

Tumors exist in a close relationship with the surrounding microenvironment. The TME could also affect the sensitivity of tumor cells to drug treatment, in addition to initiating and supporting the tumorigenic process [33]. The first study describing interactions between tumor cells and their microenvironment was performed in 1863 by Rudolph Virchow [34]. The concept that the progression of cancer is regulated by the interactions of cancer cells with their microenvironment was postulated in 1889 by Stephen Paget. Accordingly, Paget is considered the pioneer of the TME concept [35]. The first evidence that the TME participates in tumor resistance to radiotherapy and chemotherapy was described by Sutherland and colleagues. They showed that multicellular spheroids were more resistant to adriamycin than cells cultured in monolayer using Chinese hamster lung fibroblasts and EMT-6 mammary tumor cells [36, 37]. Further work demonstrated that resistant variants of EMT-6 cells cultured in monolayer were no more resistant than the parent cell line. However, upon reinjection of the resistant variant of EMT-6 cells into the mice, they regained their resistant properties [38, 39]. These findings demonstrated that the composition of the TME, including cell-cell and cell-ECM interactions, may contribute to the rapid development of drug resistance in tumors [5].

The TME is composed of a variety of stromal cell types implicated in tumor promotion and progression, such as cancer-associated fibroblasts (CAFs), mesenchymal stem cells (MSCs), lymphocytes, monocytes/macrophages, mast cells and myeloid-derived suppressor cells (MDSCs). Furthermore, the secreted products of these cells, such as cytokines, chemokines and the non-cellular components arranged into the extracellular matrix, are an important part of the TME [40-42]. The stromal cells within the TME substantially support tumor growth and progression in a different manner. For example, endothelial cells provide nutrients through angiogenesis and adipocytes may support cancer growth mainly through the secretion of growth factors and cytokines [43-45]. On the other hand, immune cells could have both pro-tumorigenic and antitumor functions through diverse and complex mechanisms [42, 46-48].

Recent studies have identified mechanisms of resistance to various cancer therapies which were conferred by alteration not in the tumor but rather in the TME (Figure 1.1). TME-mediated drug resistance can be mediated either via soluble factors, such as cytokines and chemokines secreted mainly by CAFs, or cell adhesion-mediated drug resistance (CAM-DR), mediated by the adhesion of cancer cells to components of the ECM [49-58].

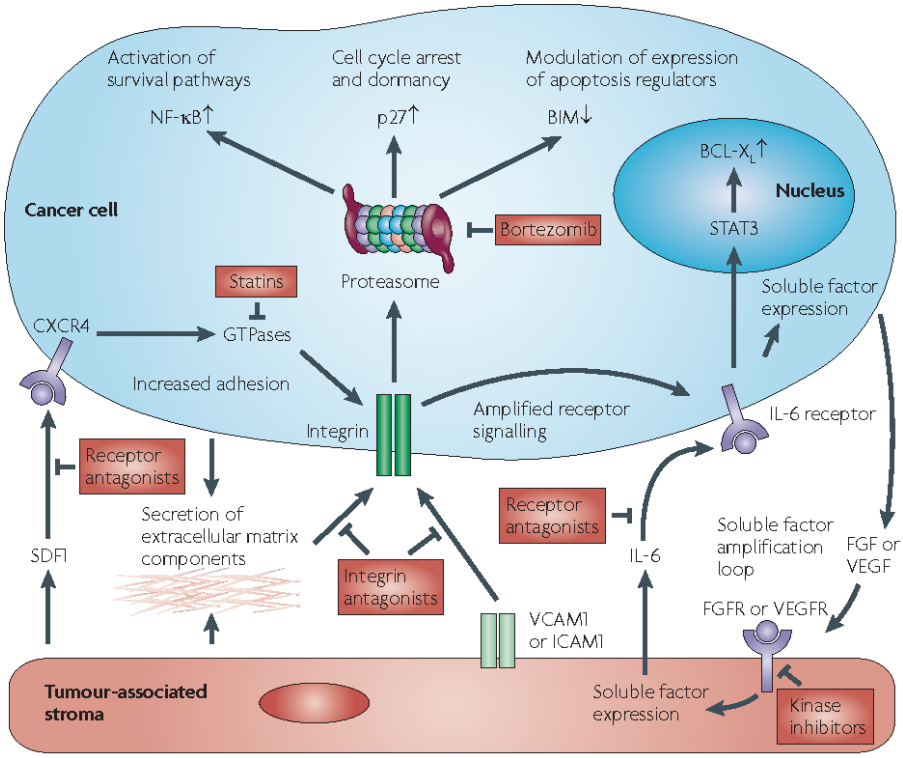

Figure 1.1: Chemoresistance of tumors mediated by the TME. Dynamic interactions between tumor cells and the TME induce a drug resistant phenotype in cancer cells. Integrins on tumor cells could adhere to components of the ECM. These adhesions modulate pro- and anti-apoptotic signals in tumor cells which might induce drug resistance. Moreover, soluble factors secreted by stromal cells upregulate anti-apoptotic proteins in tumor cells and may therefore increase drug resistance. Adopted from Meads et al. [29].

1.1.1.1.1 Soluble factor-mediated drug resistance

CAFs are most abundant stromal components in the TME of solid tumors. Numerous studies demonstrated their prominent roles in cancer pathogenesis [59, 60]. Fibroblasts were first described as spindle-shaped cells capable of collagen synthesis in connective tissue [34]. Fibroblasts synthetize many constituents of the ECM, such as collagen and fibronectin, in addition to contributing to the formation of the basement membrane. In addition, fibroblasts are also an important source of ECM-degrading proteases such as matrix metalloproteinases (MMP) [61-63]. Fibroblasts are usually quiescent. However, they become activated during the

wound healing response and secrete a high amount of ECM components [62]. Fibroblasts associated with tumors exhibit an activation phenotype and different gene expression profile in comparison to normal counterparts [61]. The most unique feature of CAFs is their high capacity for ECM synthesis and remodeling of the local ECM. The deposition of ECM components by CAFs in the tumor stroma can function either as a physical barrier or as a structural scaffold for tumor cells [64].

The most common source of CAFs are normal resident tissue fibroblasts which are activated by neighboring tumor cells [65]. For example, their source could be quiescent stellate cells that share many functions and are considered CAFs in pancreatic and liver cancer [66]. Another source of CAFs are MSCs. Many studies have provided evidence that bone marrow-derived MSCs can differentiate into CAFs in cancers such as glioma, or breast and pancreatic carcinomas [67]. The less common sources of CAFs include epithelial and endothelial cells which could undergo epithelial-to-mesenchymal transition (EMT) or endothelial-to-mesenchymal transition (EndMT), respectively [68-71].

The first evidence of the pro-tumorigenic activity of CAFs was found in a model of human prostate cancer in which immortalized prostate epithelial cells grafted onto mice in combination with CAFs led to the emergence of lesions resembling prostatic intraepithelial neoplasia [72]. Numerous studies have examined the response of CAFs to chemotherapy, as well as their role in cancer chemoresistance (Figure 1.2). These effects are mainly mediated by the secretion of high levels of molecules produced by CAFs, such as interleukin-6 (IL-6), transforming growth factor-β (TGF-β) and hepatocyte growth factor (HGF). IL-6 induces a pro-survival signal in many cancer cells through the overexpression of NF-κB, which confers resistance to cisplatin [53, 73]. HGF is a key regulator of cancer cell resistance to receptor tyrosine kinase inhibitors. The activation of the mitogen-activated protein kinase (MAPK) and the phosphoinositide 3-kinase (PI3K) signaling pathway confers chemoresistance in pancreatic and colorectal cancers [52, 74]. Moreover, recent studies indicate that CAFs can upregulate the glutathione level and thus inhibit the production of reactive oxygen species (ROS) to antagonize chemotherapy-induced cell death in prostate cancer [75]. There is some evidence showing that a unique subset of CAFs are resistant to chemotherapy themselves due to the overexpression of ATP-binding cassette (ABC) transporters [76].

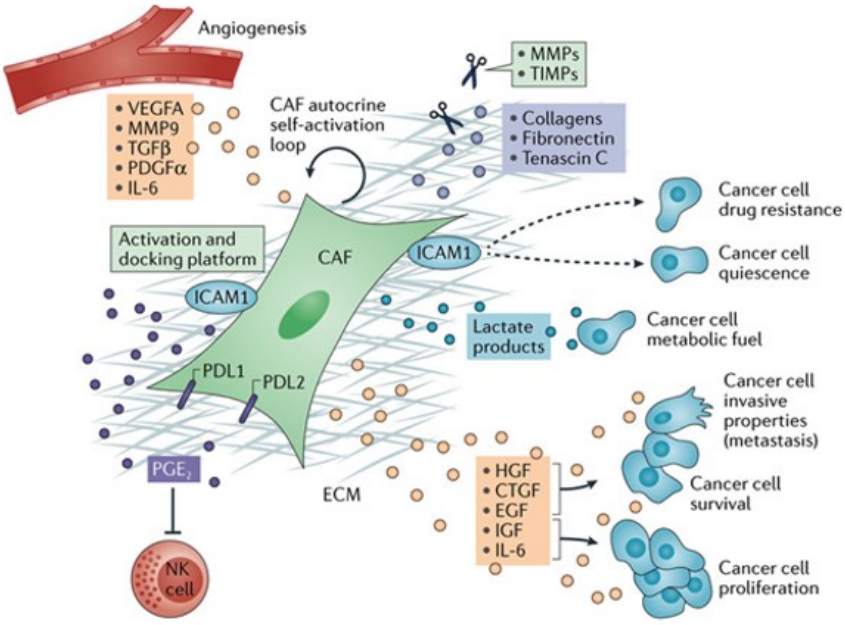

Figure 1.2: The functions of CAFs in tumors. The role of CAFs in tumor growth, progression and resistance. Adopted from Kalluri [77] with minor changes.

1.1.1.1.2 Cell adhesion-mediated drug resistance

The ECM comprises approximately 300 proteins that regulate tissue homeostasis. The major constituents of ECM forming the structural framework are fibrous proteins, such as collagens, fibronectins, laminins and proteoglycans [78-82].

While adhesion is essential for normal cells to grow and survive, independence from adhesion is considered an essential feature of tumor cells [83]. In 1995, Boudreau and colleagues demonstrated that the loss of β1-integrin-mediated adhesion in non-malignant cells led to apoptosis [84]. On the other hand, the adhesion of tumor cells to the ECM through β1-integrin enhances tumor growth and resistance to chemotherapeutic agents in multiple myeloma and small cell lung carcinoma (SCLC) cells [85]. Preventing tumor cell adhesion by blocking β1-integrin interaction with ECM components resulted in the inhibition of tumor growth in mouse multiple myeloma and human breast xenografts [86]. Additionally, the combination of this anti-adhesion approach together with conventional chemotherapeutic drugs showed higher efficacy in tumor growth inhibition than chemotherapy alone [87]. These resistance-promoting effects of cell adhesion were also observed in pancreatic, ovarian, prostate, liver and brain cancer [88-91].

1.1.2 Cellular MDR mechanisms

Cellular mechanisms of tumor chemoresistance are represented by various mechanisms within the cell operating at different levels of the cytotoxic action of the drug. These mechanisms range from a decrease of intracellular drug accumulation to the alteration of apoptosis induction. Such mechanisms can be further classified into non-classical mechanisms and transport-based (classical) mechanisms [26].

1.1.2.1 Non-classical MDR mechanisms

Non-classical mechanisms of chemoresistance are non-transport based mechanisms which are often associated with the altered activity of specific enzymes, such as glutathione S-transferase (GST) and/or topoisomerase I or II, which limit the cytostatic/cytotoxic activity of the drug without altering its concentration inside the cells. Moreover, changes in the expression level of proteins controlling drug metabolism, apoptosis induction and membrane permeability may also reduce the cytotoxic effect of various drugs [26, 92, 93].

1.1.2.1.1 Glutathione-S transferase in tumor chemoresistance

Glutathione (GSH) is a small oligopeptide composed from glutamate, cysteine and glycine which plays an important role in multiple cellular processes such as proliferation, differentiation and apoptosis [94]. Reduced GSH is the major form under physiological conditions, however, it could be converted into GSH disulfide (GSSG) upon reaction with ROS [95]. Elevated GSH levels have been observed in various types of tumors. Moreover, increased concentrations of GSH are typically found together with higher levels of γ-glutamylcysteine ligase (GCL), γ-glutamyl transpeptidase (GGT) and GSH-transporting pumps [96]. The increase in GSH levels and GCL and/or GGT activities are often associated with the chemoresistance of tumor cells [97, 98]. A higher level of GSH per se is a major contributing factor to the chemoresistance of drugs, inducing ROS production and leading to the damage of DNA and proteins [99]. In addition, GGT-overexpressing cells were shown to be more resistant to hydrogen peroxide and chemotherapeutic agents such as doxorubicin (Dox), cisplatin and 5-fluorouracil (5-FU) [100-102]. Recent studies showed coordinated elevated levels of GSH and the overexpression of multidrug resistance protein 2 (MRP2) in chemoresistant colorectal and lung cancer cell lines. The proposed mechanism was that GSH plays a cofactor role in MRP2-mediated efflux [103, 104].

GST represents a classical phase II detoxification enzyme which is primarily responsible for binding GSH to xenobiotics, thus forming conjugates that are subsequently secreted out of the cell (Figure 1.3). There are three types of GST: cytosolic, mitochondrial and nuclear. Cytosolic forms of GST are divided into six classes (α, μ, ω, π, θ and ζ) with 30% sequence homology [105]. GST binds both substrate and GSH and activates the thiol group of GSH to enable nucleophilic attack on the substrate. Accordingly, the elevated expression of GST combined with high GSH levels can increase the rate of conjugation and the detoxification of drugs, thereby increasing chemoresistance [106-108]. Several inhibitors of GSTs were recently developed to improve the response of tumors to chemotherapeutic drugs. Ethacraplatin, ethacrynic acid and its analogs were tested for their toxicity and tolerance in patients with invasive bladder cancer. Collectively, a combination of inhibitors of GSH and GST synthesis might increase the sensitivity of cancer cells to chemotherapeutics and provide viable options for patients with chemotherapy-resistant tumors [106].

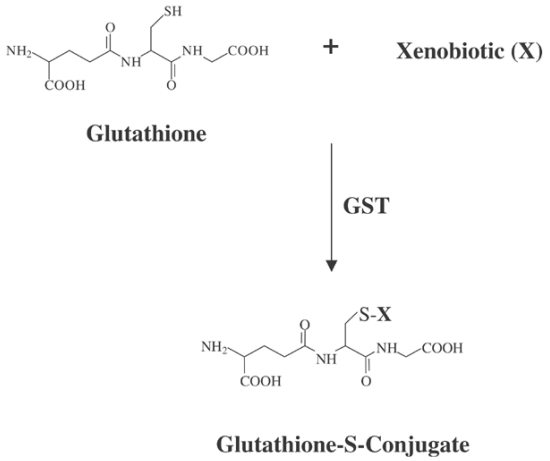

Figure 1.3: The role of GST in xenobiotic detoxification. GSH conjugation to a xenobiotic (X) via GST results in the formation of glutathione-S conjugate. Adopted from Townsend et al. [109].

1.1.2.1.2 Upregulated DNA damage repair in drug resistance

The anticancer activity of most chemotherapeutic drugs relies on the induction of DNA damage. Consequently, the capacity of DNA damage repair (DDR) mechanisms in tumor cells affects the effectiveness of DNA-damaging drugs (Figure 1.4) [110].

There are five major DNA repair pathways. Modified bases are repaired by the base excision repair (BER) pathway [110]. Two other major forms are involved in the repair of DNA double-strand breaks (DBSs). The first is called homologous recombination repair (HRR) and

it is a relatively accurate and efficient repair pathway, however, it depends on the presence of an undamaged sister chromatid. The second mechanism, called the non-homologous end-joining (NHEJ) pathway, is still effective but less accurate. The nucleotide excision repair (NER) mechanism deals with modified nucleotides which distort the structure of the double helix and the mismatch repair (MMR) pathway deals with replication errors, including deletions and insertions [111].

Efficient NER is required for the repair of DNA damage caused by platinum-based drugs [112]. One of the crucial components of the NER pathway is excision repair cross-complementing 1 protein (ERCC1). High expression of ERCC1 has been linked to poor responses to platinum-based drugs in numerous cancer types, including NSCLC, gastric and ovarian cancer [113-115]. Resistance to drugs inducing single-strand breaks arises from the upregulation of proteins of the BER pathway, including poly(ADP-ribose) polymerase 1 (PARP1), X-ray repair cross-complementing protein 1 (XRCC1) and tyrosyl-DNA phosphodiesterase 1 (TDP1). For example, the overexpression of XRCC1 or TDP1 promotes resistance to camptothecin [116-118].

Although there is evidence that the response to chemotherapy could be affected by NER and BER, the sensitivity of cancer cells is preferentially linked to HRR and MMR. Tumors deficient in HRR are highly sensitive to platinum-based drugs. Moreover, two HRR-related genes, breast cancer anti-estrogen resistance protein 1 and 2 (BCAR1 and BCAR2), are frequently inactivated in breast, ovarian and pancreatic tumors [119, 120]. Recent studies showed a link between MMR proteins such as DNA mismatch repair protein 2 (MSH2) and Mutl homolog 1 (MHL1) and resistance to platinum-based compounds. For example, cancer cells deficient in MSH2 protein or with the hyper-methylated *MLH1* gene were more sensitive to cisplatin and carboplatin than control cells [121].

Therefore, inhibition of the main DDR mechanisms in combination with DNA-damaging drugs could represent a promising treatment strategy [110].

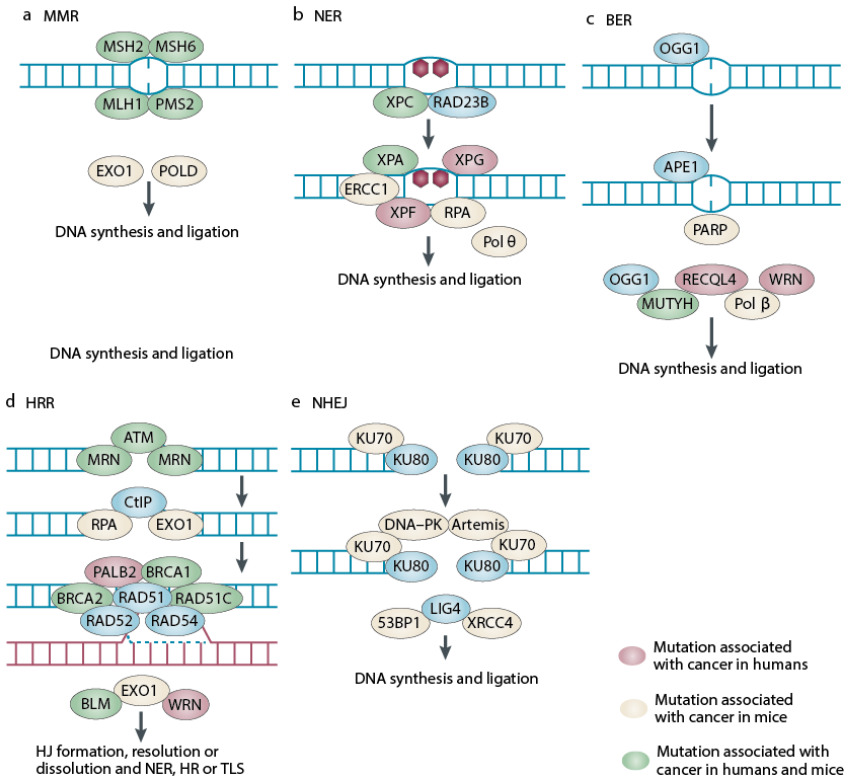

Figure 1.4: DNA repair pathways involved in chemotherapy resistance. Five major DNA repair mechanisms were described including: (a) mismatch repair (MMR); (b) nucleotide excision repair (NER); (c) base excision repair (BER); (d) homologous recombination repair (HRR); and (e) non-homologous end-joining (NHEJ). Together, DNA repair pathways form a highly complex defense against genotoxic damage. The capacity of DDR mechanisms may therefore influence the effectiveness of DNA-damaging chemotherapeutic drugs. Adopted from Bouwman et al. [110] with minor changes.

1.1.2.1.3 Role of apoptosis in cancer resistance

The resistance of cancer cells to apoptosis induction relies on a small number of anti-apoptotic proteins. The most prominent are anti-apoptotic Bcl-2 family members, inhibitors of apoptosis proteins (IAPs) and the caspase 8 inhibitor FLIP [122, 123].

In order to resist apoptosis, cancer cells either upregulate anti-apoptotic Bcl-2 family members, such as B-cell lymphoma 2 protein (Bcl-2) and B-cell lymphoma-extra-large protein (Bcl-xL), or downregulate pro-apoptotic proteins of Bcl-2 family members, including Bcl-2-associated agonist of cell death (Bad) or Bcl-2-associated X protein (Bax) [124-126]. The increased ubiquitination of Bax was found to be positively correlated with the onset of resistance in SCLC cells [127]. Similarly, decreased expression of Bad was associated with resistance to apoptosis in SCLC, breast and pancreatic cancer cells [128, 129]. The overexpression of Bcl-2 or Bcl-xL was demonstrated to be effective in inhibiting apoptosis and

enhancing resistance to a variety of chemotherapeutic agents in various tumor types [130-134]. The expression of both proteins is regulated by transcription factors NF-κB and STAT3, which were found to be overexpressed in many types of chemoresistant tumors. The inhibition of NF-κB activity in murine tumor models resulted in sensitization to a broad spectrum of chemotherapeutic drugs [135]. Further, the constitutively activated STAT3 signaling pathway was demonstrated in many solid tumors [136]. The constitutively activated STAT3 signaling pathway upregulates the expression of anti-apoptotic proteins, including Bcl-xL and myeloid cell leukemia 1 (Mcl-1), which prevent cytochrome c release and the induction of apoptosis. Consequently, the inhibition of either NF-κB or STAT3 signaling in combination with chemotherapy could achieve desirable outcomes [135-138].

Inhibitors of apoptosis (IAPs) block apoptosis by forming a complex with the baculovirus-IAP repeat (BIR) domain of caspases and inhibiting their catalytic activity. The elevated expression of IAPs was demonstrated to be a common feature of various cancer types resistant to apoptosis induction by a large variety of apoptotic stimuli, including chemotherapeutic agents, radiation and immunotherapy [122].

1.1.2.2 Classical transport-based MDR mechanisms

The classical cellular mechanisms of MDR, also known as transport-based mechanisms, involve changes in the efflux or influx of drugs from or to the cancer cells, respectively, by various energy-dependent membrane transport proteins, thereby preventing the drugs from reaching therapeutic concentrations. These mechanisms include a decreased uptake of water-soluble drugs such as folates and nucleotide analogs, and the increased energy-dependent efflux of hydrophobic drugs [139].

1.1.2.2.1 Role of copper transporters in cancer resistance

Platinum-based drugs have a unique role in the treatment of solid tumors and in most cases they are not interchangeable. These agents are most active against testicular, lung, ovarian and bladder cancers. However, resistance to platinum-based drugs (Pt resistance) is very common. Pt resistance is a complex phenomenon which is regulated by a cascade of events that interfere with any of the multiple steps involved in its cytotoxic actions. However, reduced intracellular accumulation is one of the most common features [140]. The decreased expression of platinum-based drug influx transporter copper transporter receptor 1 (CTR1) and the overexpression of platinum-based efflux transporter copper transporter receptor 2 (CTR2), both

belonging to the soluble carrier (SLC) SLC22A2 family, were observed to confer Pt resistance [141]. Conversely, the sensitivity of cisplatin-resistant SCLC cells was restored when CTR1 was introduced into the cells [142]. Similarly, the decreased expression of CTR1 was associated with cisplatin sensitivity in ovarian and colorectal cancer cells, as well as in a mouse model of human cervical cancer in which the levels of cisplatin-induced DNA adducts correlated with CRT1 expression [143-146].

1.1.2.2.2 Antifolate resistance in cancer treatment

One of the first documented mechanisms of antifolate resistance was impaired methotrexate (MTX) transport into cancer cells [147]. The reduced folate carrier (RFC/SLC19A1) was described as a major transporter which facilitates the uptake of antifolates into the cells. The loss of function of the RFC or an inactivating mutation were frequently associated with antifolate resistance [148-152].

Another route of antifolate uptake is mediated via the proton-coupled folate transporter (PCFT/SLC46A1) which functions as a unidirectional symporter that co-transports antifolates along with protons into cells. However, to date no resistance to antifolates has been documented with a loss of function of PCFT [153, 154].

Folate receptors (FRs) are the third route of folate entry into the cell. FRs are high-affinity folate-binding membrane glycoproteins encoded by three different gene loci including FRα, β and γ [21]. Several studies suggested that alterations in FR expression could result in antifolate resistance. It was demonstrated that selection with MTX resulted in decreased levels of FRα, leading to the decreased transport of MTX and drug resistance [155]. Furthermore, the transfection of FRα into human breast carcinoma MCF-7 cells increased their uptake and sensitivity to MTX [156].

These data indicate the importance of understanding the molecular mechanisms underlying antifolate resistance for the design of a new generation of antifolates which aim to overcome this resistance (Figure 1.5) [21].

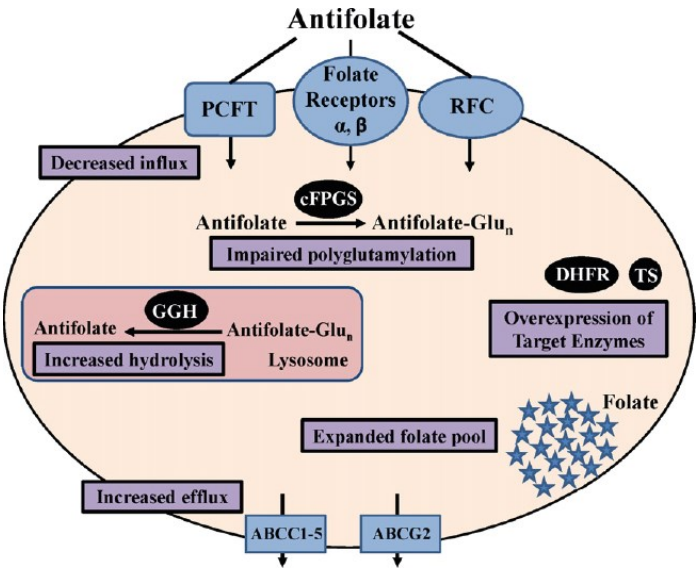

Figure 1.5: Molecular mechanisms of antifolate resistance in cancer. Adopted from Gonen et al. [21].

1.1.2.2.3 Lung resistance-related protein

Lung resistance-related protein (LRP), also known as major vault protein (MVP), was first described in Dox-resistant lung cancer cells [157]. LRP is not a member of the ABC transporters superfamily, however, the expression of LRP is associated with MDR in lung cancer. LRP is primarily located in the cytoplasm and mediates MDR through drug efflux [158, 159]. LRP overexpression was demonstrated in lung cancer cells derived from patients after chemotherapy treatment. It was also documented in B-cell lymphoma and gliomas [160]. Moreover, basal LRP protein expression was associated with resistance to platinum-based drugs, anthracyclines, etoposide and vinblastine in lung cancer cell lines [159].

1.1.2.2.4 RLIP76 in drug resistance

Ral-interacting protein (RLIP76) is an ATP-dependent non-ABC transporter responsible for the efflux of endogenous metabolites, as well as chemotherapeutic agents [161]. RLIP76 actively transports Vinca alkaloids, including vincristine, vinblastine and vinorelbine, leading to decreased drug accumulation within the cell [162]. RLIP76 is expressed in many human tissues and is also overexpressed in multiple cancers. More importantly, the inactivation of RLIP76 results in the sensitization of both NSCLC and SCLC cells to vinorelbine [163].

1.2 ABC transporter superfamily

ABC transporters represent one of the largest and most conserved families of membrane proteins from prokaryotes to humans. The wide-spread presence of these proteins with a relatively conserved structure and function suggests their fundamental role [164]. ABC transporters are usually localized in the plasmatic membranes of cells in the gut, liver and kidney and the epithelia of various tissues. Moreover, the expression of ABC transporters has also been reported in the membrane of intracellular organelles such as the mitochondria, Golgi apparatus and endoplasmic reticulum [165].

The majority of ABC transporters are responsible for the active transport of a wide variety of substrates across the membranes, including steroids, phospholipids, glycolipids or xenobiotics. Various other physiological roles for ABC transporters has been demonstrated, such as defense against oxidative stress and antigen presentation [166]. Some ABC transporters have functions other than substrate translocation, for example, sulfonylurea receptors SUR1 and SUR2 regulate potassium channels, whereas cystic fibrosis transmembrane conductance regulator (CFTR) is an ATP-gated chloride channel [167-169].

The ABC transporter superfamily can be divided into two categories. The first category includes transporters which utilize the energy of ATP hydrolysis to translocate substrates across membranes. Other ABC transporters localized mainly in the cytosol or nucleus play a role in chromatin organization, DNA repair and mRNA transport through the nuclear membrane [31, 170, 171]. Identification and characterization has been performed for 49 members of the ABC transporter superfamily. They are divided into seven subfamilies from ABCA to ABCG based on their gene organization and location, the structure of domains and sequence homology [165, 172, 173].

Mutations or the functional failure of ABC transporters are associated with multiple human diseases, such as cystic fibrosis (associated with the mutation of CFTR, also known as ABCC7), pseudoxanthoma elasticum (associated with the mutation of MRP6, encoded by ABCC6), Stargardt macular degeneration (associated with the mutation of ABCC4), Tangier disease (associated with the mutation of ABCA1), sitosterolemia (associated with the mutation of ABCG5 or BCG8) and harlequin ichthyosis (associated with the mutation of ABCA12) [174].

1.2.1 General structure of ABC transporters

The canonical domain organization of ABC transporters comprises two transmembrane domains (TMDs), which provide a passageway for the cargo and two cytoplasmic nucleotide-binding domains (NBDs), which bind and hydrolyze ATP (Figure 1.6) [175-177].

In eukaryotes, the majority of ABC transporters are composed of a single polypeptide that contains all functional units. Eukaryotic ABC transporters are organized either as full transporters (containing two NBDs and two TMDs), or as half transporters (containing one NBD and one TMD), which form homo- or heterodimers [178].

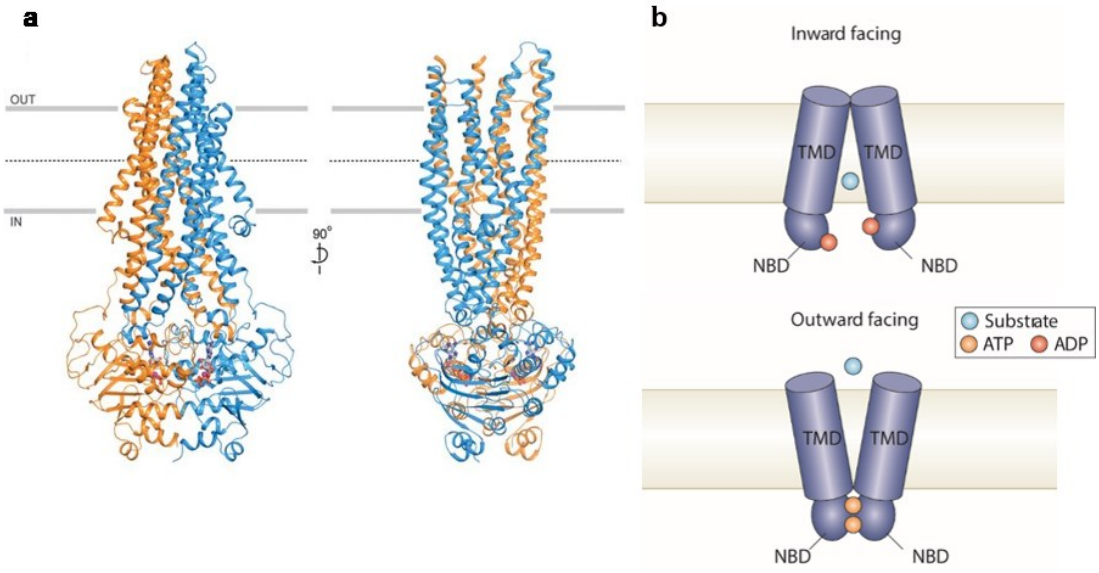

Figure 1.6: Molecular architecture of the ABC transporter. (a) Structure of the human P-gp (E556Q/E1201Q) in complex with ATP. The N-terminal half (TMD1 and NBD1) is colored in orange and the C-terminal half (TMD2 and NBD2) in blue. ATP is shown in ball-and-stick format (gray, carbon; red, oxygen; blue, nitrogen; orange, phosphorus) and Mg^{2+} is shown as a sphere (magenta). (b) Two conformational states model of the ABC transporter, outward facing and inward facing, with the substrate-binding site orientated towards the extracellular and cytoplasmic regions. Adopted from Rees et al. [175] with minor changes.

1.2.1.1 Structure and properties of the NBDs

The nucleotide-binding domains are homologous throughout the members of the ABC transporter family. Each NBD has an L-shaped configuration containing two subdomains and several characteristic conserved motifs. The conserved nature of NBD comprises a RecA-like subdomain with a so-called Rossman fold containing Walker A and Walker B consensus motifs and an α-helical subdomain which contains an LSGGQ sequence also called a “C-loop” or

"ABC signature motif" that contacts the nucleotide in the ATP-bound state and is characteristic of all ABC transporters (Figure 1.7) [179-184].

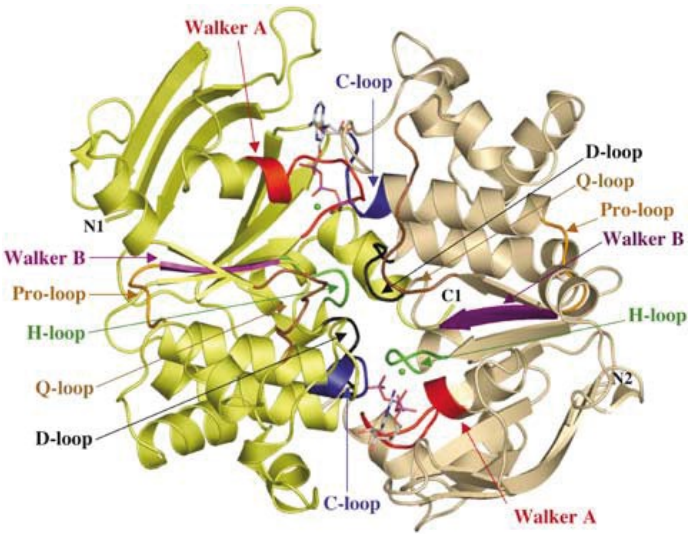

Figure 1.7: Crystal structure of the NBD dimer of the HlyB transporter. NBD dimer representation with bound ATP/$Mg2^{+}$. ATP and $Mg2^{+}$ (green spheres) are sandwiched at the interface of the two NBD monomers (shown in light tan and yellow). N- and C-termini of the individual monomers are labeled. Conserved motifs are colored accordingly. Adopted from Zaitseva et al. [185].

The crystal structures of isolated NBDs bound to ATP show the two NBDs engaged in a symmetric dimer with the two ATP molecules sandwiched in the dimer interface. This arrangement is called a sandwich dimer or head-to-tail arrangement. As a consequence of this organization, the ATP-binding sites are formed between the P-loop of one NBD and the LSGGQ motif of the other and vice versa [186-188].

1.2.1.2 Structure and properties of the TMDs

Unlike NBDs, the TMDs vary in their primary sequence, length, architecture and the number of transmembrane (TM) α-helices, depending on the transporter class. ABC exporters contain conserved 12 TM α-helices, whereas ABC importers feature 10 to 20 TM α-helices. The lack of primary structure conservation in the TMDs is likely due to the diverse nature of the transporting substrates. Transporting substrates interact with residues of the TM α-helices which line the TM pore. The TM α-helices of the TMDs form a TM pore which is either accessible from the cytoplasm (inward facing) or from the outside of the cell (outward facing) (Figure 1.6). Several overlapping drug-binding sites were identified in multidrug transporter P-

glycoprotein. Accordingly, the drug binding pocket of P-glycoprotein has been described as polyspecific [189-191]. Conformational changes at the NBDs are transmitted to TMDs via coupling helices, also called intracytosolic loops (ICLs). The coupling helices are embedded in a grove on the surface of the NBDs at the boundary between the Rec-like and α-helical subdomain [192-194].

1.2.2 ATPase catalytic cycle of ABC transporters

The crystal structures of transporters provided a framework for formulating the reaction mechanisms of ATP-driven substrate transport. Numerous distinct mechanisms were proposed to describe how ATP binding and hydrolysis by NBDs might be coupled to inward-facing or outward-facing conformations of the TMDs. Three major mechanistic models were proposed: the ATP-switch model, constant contact model and the reciprocating twin-channel model (Figure 1.8) [195].

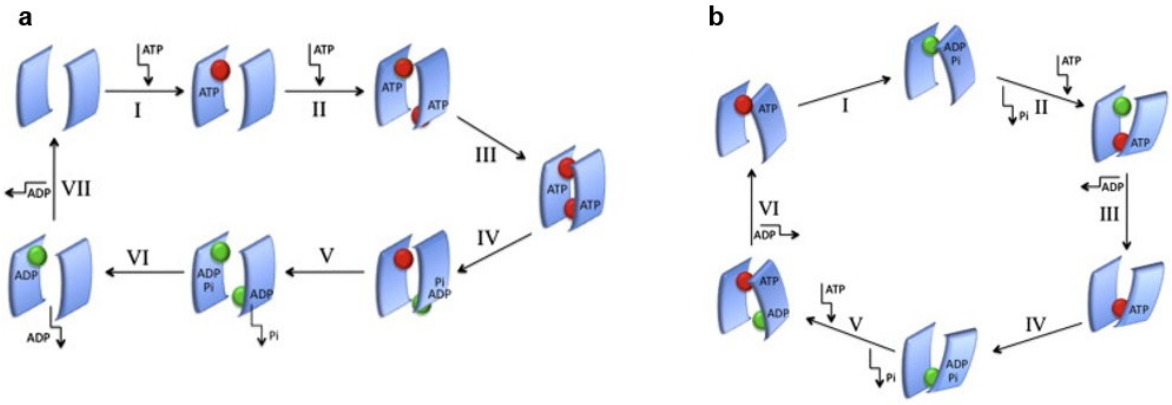

Figure 1.8: Models of the ATP catalytic cycle in the ABC transporters. (a) ATP-switch model; and (b) constant contact model. Adopted from George et al. [196].

1.2.2.1 The ATP-switch model

The ATP-switch model was proposed to explain the mechanism of substrate transport via ABC transporters, specifically how cycling between high and low-affinity states for ligands on different sides of the membrane are coupled to the ATP catalytic cycle. The characteristic feature of the ATP-switch model is that transport mechanisms are divided into several steps and the transmission from one step to next is mediated by conformational changes. The transporter is in the nucleotide-free basal state at start of cycle with a high affinity for a ligand and NBDs

are in an open dimer configuration with a low affinity to ATP. The transport cycle is initiated by the binding of the substrate to its high affinity sites in TMDs, causing conformational changes in the NBDs transduced via coupling helices. As a result, the affinity of NBDs for ATP is increased by lowering the activation energy for the closed dimer formation. Next, the cooperative binding of two molecules of ATP to NBD monomers generates the formation of the sandwich dimer around ATP molecules. The closed NBD dimer induces a conformational changes in TMDs to initiate substrate translocation. These conformational changes involve the breaking of interactions between TM α-helices and the formation of new contacts. These new interactions allow the relocation of the substrate binding site from the cytoplasmic to the extracellular face. The extracellular exposure of the binding site reduces its affinity to the substrate and allows the substrate release. Next, ATP is sequentially hydrolyzed to form a transition state and the sequential release of phosphate and ADP restore the transporter to its basal configuration.

This model highlights the close crosstalk between the two halves of the ABC transporter which is essential for forming the ATP hydrolysis sites and the drug translocation pathway. It also helps to explain how substrate binding can stimulate ATP binding instead of ATP hydrolysis [194, 195, 197].

1.2.2.2 The constant contact model

The major difference between the constant contact model and the ATP-switch model is that in the former, NBDs remain in contact throughout the cycle. There are two distinct versions of the constant contact model. The symmetric working model assumes ATP hydrolysis in each NBD, with one site opening at the point of ATP hydrolysis and second site remaining closed with ATP bound and occluded. The enzymatically supported asymmetric model proposes that one nucleotide-bound active site is occupied with ATP while other is empty and accessible to ATP [187, 198, 199].

1.3 Role of ABC transporters in MDR

The MDR phenotype represents the dominant mechanism in the development of resistance to chemotherapeutic drugs in cancer cells. It is associated with the overexpression of ABC transporters, reducing the intracellular concentration of drugs. To date, 15 members of the ABC transporter superfamily which confer a MDR phenotype have been identified. The most common members of ABC transporters mediating cancer MDR are P-glycoprotein (P-gp),

multidrug resistance protein 1, 2, 5, 7 (MRP1, 2, 5, 7) and breast cancer resistance protein (BCRP). Moreover, these transporters can be simultaneously expressed in tumor cells [200-202].

1.3.1 P-glycoprotein

The first correlations between cell membrane transporters and drug resistance were made in Chinese hamster ovary cell lines, in which it was shown that a 170 kDa glycoprotein, called P-gp (ABCB1 or MDR1), correlated with the degree of drug resistance. P-gp was purified in 1979 as a surface glycoprotein. Strong evidence supporting its role in pleiotropic drug resistance came in 1982 when it was shown that DNA from a resistant cell line which was transferred to non-resistant cells was able to confer resistance [203]. P-gp represents the most studied member of the ABC transporters mediating MDR in tumor cells [8, 165]. P-gp can transport a large variety of hydrophobic compounds, either neutral or with a positive charge, including numerous anticancer agents. The overexpression of P-gp is the most common mechanism of MDR in human tumors [139].

1.3.1.1 Structural features of P-gp

P-gp is encoded by the human *ABCB1 (MDR1)* gene located on chromosomal region 7q21. In mice, there are two closely related homologous genes, *Abcb1a* (*Mdr1a*) and *Abcb1b* (*Mdr1b*) [204, 205]. The *MDR1* gene consists of 28 exons encoding a protein which is 1,280 amino acids in length. It has been shown that the MDR1 gene is highly polymorphic, with 50 single nucleotide polymorphisms (SNPs) and three insertion/deletion polymorphisms reported so far. Several SNPs are currently considered to be the most clinically relevant: G2677T/A in exon 21, C3435C/T in exon 26 and C1236C/T in exon 12. The SNP in exon 26 was associated with a two-fold reduction of intestinal P-gp expression, which caused a higher digoxin plasma concentration after oral administration. All three abovementioned SNPs were positively correlated with the progression-free survival of patients after paclitaxel treatment [206-208].

P-gp is a single polypeptide chain organized in two similar halves. Each half contains one homologous NBD and one homologous TMD consisting of six membrane-spanning α-helices [209]. P-gp contains three putative glycosylation sites, which represent asparagines 91, 94 and 99 and two phosphorylation sites for protein kinases A (PKA) and C (PKC), which correspond to serines 669 and 681 in the linking region [210, 211].

It is still unclear whether P-gp contains a single or multiple drug binding sites in its drug-binding cavity. So far, three drug binding sites in P-gp have been identified, the H-site, which preferentially interacts with Hoechst 33342, the R-site interacting with Rhodamine 123 and the P-site, with a positive allosteric effect on the H- an R-sites. Interestingly, nearly 18% of amino acids involved in drug-binding possess aromatic residues [209, 212].

1.3.1.2 Mechanism of drug efflux

One of the most interesting features of P-gp is that it recognizes an extremely wide spectrum of chemical structures as substrates. Its substrates are typically of a hydrophobic nature. Nevertheless, P-gp substrates are also amphipathic molecules which align in the interfacial region rather than being uniformly distributed in the hydrophobic part of the lipid bilayer. Three models of the P-gp drug efflux mechanism have been proposed, namely the classical pore pump model, the hydrophobic vacuum cleaner (HVC) model and the flippase model (Figure 1.9) [213].

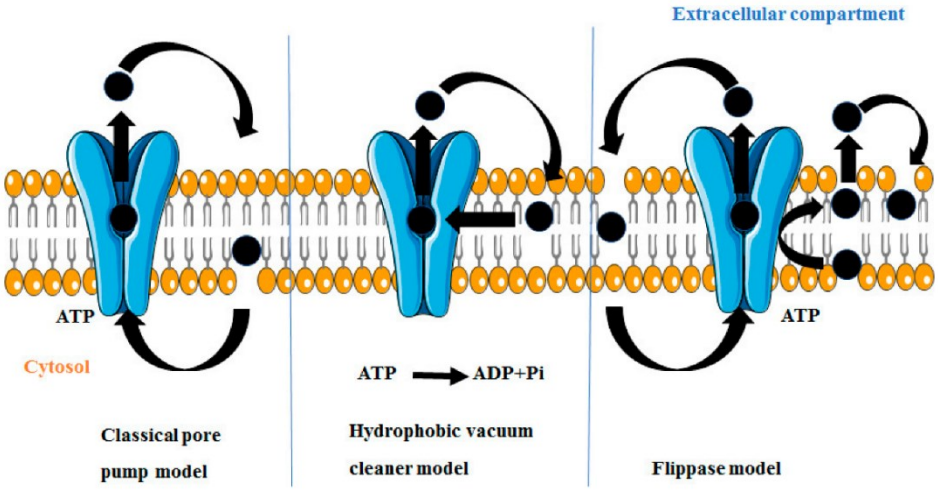

Figure 1.9: Different functional models of P-gp-induced MDR. Adopted from Dewanjee et al. [213].

Drug molecules associated with P-gp in the cytosolic compartment are transported out of the cell through the protein channel in the classical pore pump model, thus keeping the substrate away from the hydrophobic lipid phase of the membrane [214].

According to the HVC model, P-gp drives the efflux of drugs directly from the membrane rather than the aqueous phase. This model suggests that P-gp interacts with its substrates within the membrane through two portals formed by TM domains 4/6 and 10/12, due

to the hydrophobic nature of most P-gp substrates, allowing the substrate to enter the cavity and be subsequently effluxed to the extracellular space [215].

In the flippase model, substrates located in the inner leaflet of the plasma membrane are translocated to the outer leaflet of the lipid bilayer, from which they passively diffuse into the extracellular environment. This model assumes that substrates have specific localizations within each bilayer leaflet. Substrates exert a slower rate of passive transbilayer flip-flop than the rate of P-gp-mediated flipping, therefore the concentration of substrates remain higher in the outer leaflet [216].

1.3.1.3 Physiological role of P-gp

P-gp is constitutively expressed in various normal tissues including in the kidneys, liver, pancreas, small and large intestine, brain, testes, adrenal glands and the placenta. This tissue distribution implies an important physiological role in the protection against a wide range of potentially toxic substances [7].

P-gp is located on the apical membrane of intestinal epithelial cells, ensuring the transport of substrates from cells into the intestinal lumen [217]. An intriguing feature of P-gp in the gastrointestinal tract (GIT) is the interaction with drug metabolizing enzymes, particularly with the 3A4 isozyme of cytochrome P450 (CYP3A4). P-gp and CYP3A4 share many substrates and have a common tissue distribution. This considerable overlap in substrate selectivity and tissue localization had led to hypothesis that this enzyme pair acts as coordinated barrier against xenobiotics in GIT [218].

P-gp is expressed on the luminal side of the proximal tubule cells in the kidneys as well as in other parts of the nephrons, such as the loop of Henle or collecting ducts. Many studies have shown that P-gp plays a key role in the renal elimination of certain molecules by means of active secretion into the urine and it most likely limits the re-absorption of these molecules filtered in the glomerulus [219].

P-gp is also expressed on the apical membrane of endothelial cells lining the brain capillaries. These cells form a continuous monolayer called the blood-brain barrier, which represents an important physical and biochemical transport barrier leading to the limited access of xenobiotics to the central nervous system (CNS). P-gp transports substrates to the blood and accordingly, it is probably a major limiting factor of xenobiotic entry into the brain. This hypothesis is supported by studies in knockout mice lacking P-gp. These animals have a normal lifespan and appear healthy and fertile. However, when certain drugs (P-gp substrates) are

administrated, these drugs accumulate at very high levels in the brain compared with wild-type mice [220].

1.3.1.4 Role of P-gp in cancer MDR

Studies performed over the last two decades showed that the intrinsic and acquired expression of P-gp plays a significant role in the clinical chemoresistance of human malignancies. According to the analysis of *MDR1* RNA levels in more than 400 different tumor samples, tumors can be classified into three categories: i) usually positive (intrinsically chemoresistant tumors such as in colon, kidney and pancreatic cancer); ii) occasionally positive (e.g., neuroblastoma); and iii) generally negative (e.g., lung, ovarian and prostate cancer and melanoma). The low level or absence of *MDR1* gene expression in some chemoresistant tumors suggests that other mechanisms of MDR exist. However, there is a strong correlation between MDR1 expression and drug resistance in many types of cancer [221].

The overexpression of P-gp confers resistance to a wide variety of neutral and cationic hydrophobic chemotherapeutics including taxanes (e.g., paclitaxel and docetaxel), epipodophyllotoxins (e.g., etoposide and teniposide), Vinca alkaloids (e.g., vinblastine and vincristine), anthracyclines (e.g., Dox and daunorubicin), actinomycin D or tyrosine kinase inhibitors (TKIs, e.g., imatinib, nilotinib and erlotinib) [139, 172]. It was therefore important to identify the mechanisms regulating P-gp expression and activity. Several potential mechanisms were suggested: i) amplification of the *MDR1* gene; ii) increased transcription of the *MDR1* gene; iii) changes in ABCB1 translation efficiency; iv) mutations in the *MDR1* gene; and v) chromosomal rearrangements that produce hybrid *MDR1* genes [222, 223].

P-gp can also confer resistance to apoptosis induced by diverse non-drug stimuli including Fas, TNF, γ-irradiation and serum starvation [200]. The exact mechanism by which P-gp inhibits apoptosis is not clear. However, different theories have been proposed, including interference with the death-inducing signaling complex (DISC) and the inhibition of caspase-8 activation [213]. Moreover, P-gp could prevent apoptosis by regulating the intracellular levels of the lipid molecules involved in apoptotic signaling pathways, such as the sphingolipids and their metabolites, particularly ceramide and sphingosine-1-phosphate (S1P) [221]. Furthermore, the overexpression of sphingosine kinase, which is the enzyme involved in the production of S1P, leads to the upregulation of P-gp [224, 225].

1.3.2 Multidrug resistance proteins

The multidrug resistance proteins (MRPs) belong to the C subfamily of the ABC transporters (ABCC). The ABCC subfamily contains thirteen members. Nine are MRPs, designated MRP1-MRP9 (ABCC1-ABCC6 and ABCC10-ABCC12). The other three members of the ABCC subfamily, namely CFTR (ABCC7), SUR1 (ABCC8) and SUR2 (ABCC9), are not involved in MDR but rather play a role as chloride- or potassium-selective channels. Finally, ABCC13 lacks Walker A, Walker B and the ABC signature motif and it is most likely a non-functional ABC transporter [226].

MRPs share several common structural features, including TM α-helices arranged in membrane spanning domains (MSDs), as well as NBDs at the intracellular site, similarly to other members belonging to the ABC transporter superfamily. Two MSDs and two NBDs are commonly observed in the ABC transporter superfamily and also in MRP4, MRP5, MRP8 and MRP9 (ABCC4, ABCC5, ABCC11 and ABCC12, respectively). This group of transporters is designated short MRPs. However, MRP1, MRP2, MRP3, MRP6 and MRP7 (ABCC1, ABCC2, ABCC3, ABCC6 and ABCC10, respectively) have an additional N-terminus-proximal MSD0 and are therefore defined as long MRPs (Figure 1.10) [227].

MRPs share a similar transport mechanism, although they are structurally different. Most MRPs were initially cloned from tumors, but they are also broadly found in normal tissues. A wide range of endo- and xenobiotics can be transported by MRPs and different MRPs may have similar substrate specificity. Accordingly, the function of MRPs is a primary tissue defense in different locations [228].

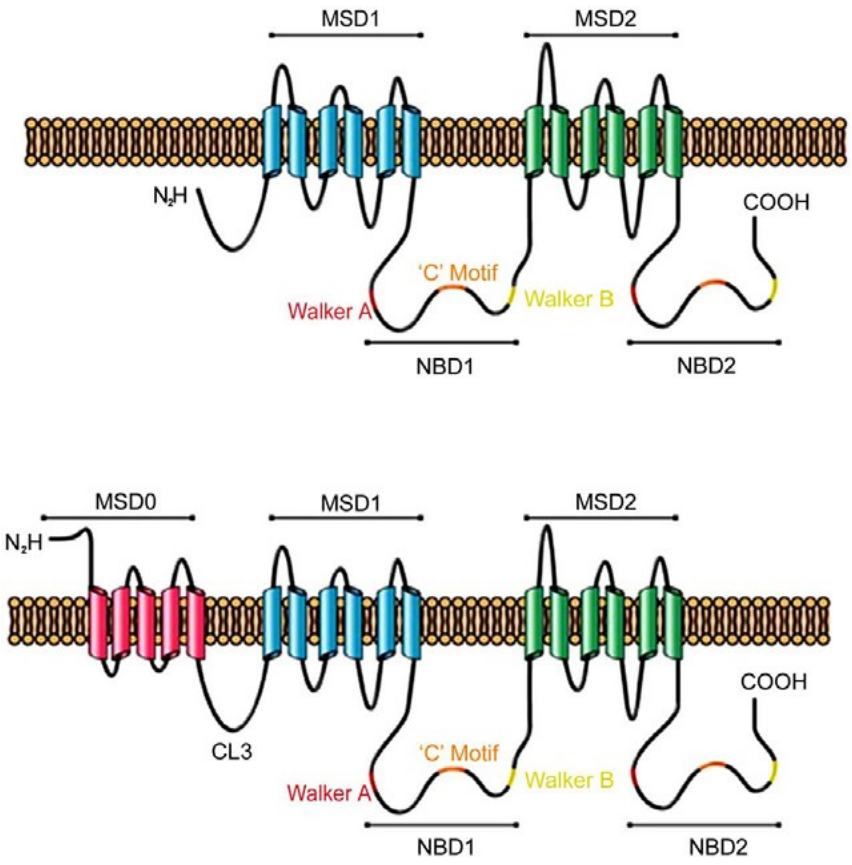

Figure 1.10: Schematic illustration of MRP topology. The MRPs can be divided into two classes, short (MRP4, -5, -8 and -9) and long (MRP1, -2, -3, -6 and -7). Short MRPs have a canonical ABC transporter structure with two membrane spanning domains (MSD) and two nucleotide-binding domains (NBD), whereas long MRPs have three MSDs and two NBDs. Adopted from Deeley et al. [228] with minor changes.

1.3.2.1 Structure of MRP1

MRP1 (ABCC1) was first cloned in 1992 from the Dox-selected human lung cancer cell line H69/AR. The human *ABCC1* gene has been mapped to chromosome 16p13.1 and spans approximately 200 kb. It contains 31 exons encoding a 1,531 amino acid protein [229]. The murine ortholog of human MRP1 (*Mrp1/Abcc1*) was identified in 1996. Although these proteins share 88% of amino acid sequence homology, functional differences are present. For example, murine MRP1 is not capable of conferring resistance to anthracyclines, although it mediates resistance to vincristine and etoposide. Newly synthetized MRP1 is a 170 kDa polypeptide, rapidly processed into a 190 kDa protein via N-terminal glycosylation [230-232].

The MRP1 has a five-domain structure with two NBDs and three MSDs. The exact function of the N-terminal MSD0 in MRP1 remains uncertain and may depend on the cell type [233]. The cavity in the membrane through which substrates are effluxed is formed by MSD1 and MSD2. The orientation of MSD0 to MSD1 and MSD2, as well as its role in substrate

translocation, is poorly understood [234]. The MSDs have the highest sequence divergence within the ABC transporter superfamily and an abundance of evidence indicates that they largely, but not exclusively, dictate transporter substrate selectivity [235, 236]. TM α-helices of MSD1 and MSD2 contain a high frequency of polar amino acids. In particular, the last two TM α-helices of MSD1 and MSD2 (TM10-11 and TM16-17, respectively) are amphipathic and contain polar amino acids clustered on one side of the α-helix [237]. Multiple studies indicate that the polarity of these amino acids is important for substrate binding and transport in MRP1 [238-241].

1.3.2.2 MRP1 mechanism of function

The transport of substrate by MRP1 is similar to other ABC transporters, as it is powered by the hydrolysis of ATP which facilitates protein conformational change. Each NBD contains three key motifs common among all ABC transporters and forms a characteristic sandwich dimer with bound ATP. The ATP-binding sites of MRP1 are not functionally equivalent. Whereas NBD1 has an ATP-binding site called the degenerate site, with a high affinity for ATP but very low ATPase activity, NBD2 has a so-called consensus site with much a higher capacity for ATP hydrolysis [242]. This functional asymmetry represents a feature of ABCC transporters, as well as several heterodimeric transporters, which is distinct from canonical ABC transporters. Such asymmetry is explained by differences in the canonical sequences and spacing of the three key motifs [196].

The substrate binds to the high-affinity binding site in MSD during the first step of MRP1-mediated efflux. This causes the recruitment of ATP to NBD1. ATP binding causes further conformational changes resulting in the interaction of NBD1 with NBD2 and the recruitment of a second ATP molecule. These two NBDs are arranged in a head-to-tail orientation with the two ATP molecules positioned in-between. The dimerization of the two NBDs causes conformational changes in MSDs, resulting in the transport of the substrate to the low-affinity binding site and its release into the extracellular environment [243]. MRP1 is an atypical ABC transporter due the presence of MSD0, however, the deletion of this additional MSD does not affect the transporter's function [244].

1.3.2.3 Role of MRP1 in cancer chemoresistance

MRP1 is overexpressed in many cancers, such as breast, brain, pancreatic and prostate carcinoma, NSCLC and SCLC, melanoma, neuroblastoma, myeloid leukemia and acute

lymphoblastic leukemia (AML and ALL), in which it may play a key role in chemoresistance development and tumor progression. MRP1 contributes to cancer chemoresistance by exporting different classes of drugs, ranging from amphipathic anions to hydrophobic molecules. It also mediates the efflux of amphipathic drugs conjugated with sulfate, glutathione and glucuronic acid. These drugs include anthracyclines, Vinca alkaloids, epipodophyllotoxins, camptothecins, methotrexate, mitoxantrone and tyrosine kinase inhibitors [245]. However, unlike P-gp, MRP1 does not confer resistance to taxanes, which is an important feature of P-gp-mediated resistance [246]. Nonetheless, the clinical correlations of MRP1 overexpression and MDR are extremely variable amongst tumor types. For example, the clinical prognostic value of MRP1 remains questionable in breast cancer despite its well-described capacity to provide a MDR phenotype *in vitro* [247]. It is noteworthy that the elevated expression of MRP1 has been observed in cells isolated from metastatic lesions and metastatic lymph nodes, suggesting a possible contribution of MRP1 to metastatic spread [248]. MRP1 was also found to be localized within intracellular compartments including mitochondria, endoplasmic reticulum and endocytic vesicles. The presence of MRP1 in mitochondria may protect mitochondrial DNA from damage and mitochondrial-induced cell death, thus serving as a sequestering mechanism to prevent drugs reaching their intracellular target. Moreover, recent studies demonstrated that intracellular MRP1 may serve as a reservoir for the rapid restoration of surface levels when required [249].

MRP1 is also expressed in many normal tissues, such as the testes, lungs, skin, skeletal muscles, heart, kidneys and small intestine. Accordingly, MRP1 may affect the efficacy of drugs used to treat non-malignant diseases by transporting various antibiotics, opiates, antiviral agents and statins [250].

1.3.2.4 MRP2 structure and function

Multidrug resistance protein 2 (MRP2, ABCC2) was first identified and cloned from rat hepatocytes as a homolog of MRP1 and named the canalicular multispecific organic anion transporter (cMOAT). MRP2 has three MSDs and two NBDs. Amino acid residues in TM α-helices, particularly TM6, TM9, TM16 and TM17, are essential for the recognition and binding of substrates [251]. MRP2 shares 49% of amino acid sequence homology with MRP1, but it has a different expression pattern [252].

MRP2 is expressed at the apical membrane of the polarized cells of various tissues including hepatocytes, proximal tubule cells, enterocytes, bladder epithelial cells and cells of the placenta [253]. One of the main physiological functions of MRP2 is to transport conjugated

metabolites into the bile canaliculus in the liver. Mice with impaired MRP2 transporters showed decreased hepatobiliary excretion of glucuronide conjugates and developed Dubin-Johnson syndrome [254]. MRP2 actively transports a spectrum of physiological compounds, such as glutathione, glucuronides and sulfate conjugates, leukotriene D_4 (LTD_4), leukotriene E_4 (LTE_4), LTC_4 and estradiol-17β ($E_2$17G). However, the affinity of MRP2 for these substrates is significantly lower than that of MRP1 [255, 256].

Chemoresistance conferred by MRP2 has been demonstrated in a variety of cancer types such as lung, GIT and liver cancer. The overexpression of MRP2 corresponds to etoposide, vincristine, cisplatin, Dox, epirubicin and MTX resistance. Therefore, MRP2 appears to be involved in the resistance to various chemotherapy agents in many types of tumors [257].

1.3.3 Breast cancer resistant protein

The breast cancer resistance protein (BCRP) is the second member of the G subfamily of the ABC transporter superfamily (ABCG2). BCRP was first identified in 1998 in a multidrug resistant human breast cancer cell line, MCF-7/Adr, which does not express other known multidrug efflux transporters [258]. Human BCRP is encoded by the *ABCG2* gene located on chromosome 4q22. It is a 72 kDa glycoprotein containing 665 amino acids. The murine ortholog shares 81% of amino acid sequence homology with human ABCG2 and was found to confer drug resistance in a pattern indistinguishable from human ABCG2 [259]. It contains three potential N-glycosylation sites at Asn^{418}, Asn^{557} and Asn^{596}. However, the elimination of these N-glycosylation sites did not affect the expression, subcellular trafficking or the overall function of ABCG2 [260-262].

Several unique features of BCRP distinguish it from most other ABC transporters. First, BCRP is the first described half transporter mediating MDR, with one MSD and one NBD (Figure 1.11). Second, the NBD precedes the MSD, a domain organization that is opposite to that in P-gp and MRP1. Third, BCRP is active upon the homodimerization or oligodimerization of either itself or with other transporters from the ABCG subfamily, such as ABCG5 and ABCG8. Such unique structural features imply that BCRP employs quite a different transport mechanism in comparison to P-gp and MRP1 [263].

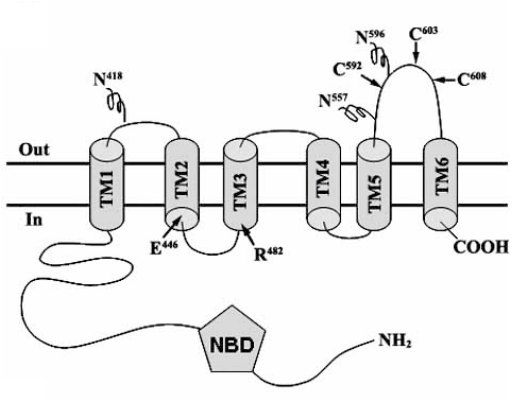

Figure 1.11: Model of the putative structure of BCRP. BCRP as a half transporter contains a single NBD followed by six TM α-helices organized into the single MSD with three N-glycosylation sites. Adopted from Xu et al. [263] with minor changes.

BCRP is widely expressed in normal human tissues with higher expression on the apical membrane of syncytiotrophoblast cells. In addition, BCRP is prominently expressed on the apical membrane of cells in the small intestine, colon, liver canaliculi membrane and the endothelial cells of capillaries in the blood-testis and blood-brain barriers. This localization implies that BCRP can play a crucial role in limiting the absorption, distribution and elimination of various xenobiotics [264, 265]. Interestingly, BCRP is also expressed on the plasma membrane of mature erythrocytes with reduced cellular protoporphyrin IX (PPIX) levels in rodents. It is possible that BCRP plays an important role in protecting these erythrocytes from oxidative damage, because the elevated cellular accumulation of PPIX is associated with the formation of ROS [266].

High BCRP expression has been detected in many chemoresistant hematological malignancies and solid tumors, indicating that it is responsible for MDR in these cancers. BCRP is also overexpressed in a subpopulation of cancer cells also known as the side population in AML, neuroblastoma, sarcoma, breast cancer, SCLC and glioblastoma. These stem-like cells may have an important role in conferring resistance to chemotherapeutic drugs, thereby contributing to relapses [267].

Substrates of BCRP include organic anionic molecules, nucleoside analogs, organic dyes, TKIs, anthracyclines, camptothecin-derived topoisomerase I inhibitors, MTX and flavopiridols [10]. Other BCRP substrates are toxins, such as carcinogen 2-amino-1-methyl-6-phenyllimidazo[4,5-b]pyridine (PhIP), or flavonoids such as genistein, uric acid and vitamins. Accordingly, BCRP has a very broad substrate specificity that is substantially distinct from that of P-gp and MRPs [263].

1.3.4 Modulation of ABC transporter-mediated MDR

There is an ongoing effort to develop drugs capable of either inhibiting or inactivating ABC transporters to increase the concentration of anticancer drugs within cancer cells. The inhibition of ABC transporters has been evaluated with synthetic or natural inhibitors, including competitive and non-competitive inhibitors. Competitive inhibitors exert their function by tight binding and blocking the substrate binding pocket. Non-competitive inhibitors exert their function by binding to a non-substrate binding site and inhibiting the ATPase activity or modulating transporter function allosterically. Another potential strategy to circumvent MDR is the downregulation of the expression of ABC transporters by microRNA or small interfering RNA (siRNA). A third approach is based on the rational design of new chemotherapeutics which are not substrates of ABC transporters [8].

1.3.4.1 Inhibitors of ABC transporters

Compounds with the ability to reverse the chemoresistance mediated by ABC transporters belong to a number of different chemical classes, including calcium channel blockers, vasodilators, indole alkaloids, hormones and surfactants. The process of chemosensitization involves the co-administration of an inhibitor with the anticancer drug in order to increase intracellular anticancer drug accumulation by impairing ABC transporter function [8].

Three generations of P-gp inhibitors have been described to date. The first generation of P-gp inhibitors includes verapamil, cyclosporine A (CsA) and quinine. These inhibitors are pharmaceutically active molecules themselves and they were not specifically developed for ABC transporter inhibition. Moreover, these P-gp inhibitors are substrates of P-gp and as a result, they show effective inhibition of P-gp only at high dosages that result in serious side effects. The second generation of inhibitors was developed through the modification of the first generation in order to acquire higher potency and specificity, but lower toxicity. These inhibitors, such as CsA analog valspodar, verapamil analog dex-verapamil and biricodar (VX-710), showed higher efficacy than the first generation of P-gp inhibitors when used in combination with conventional chemotherapeutic drugs. However, these drugs were also inhibitors of hepatic and intestinal cytochrome P450 enzymes. As such, they decreased the metabolism and clearance of cytostatics, causing systemic toxicity [139]. The continuous problem with MDR inhibitors led to the development of the third generation of P-gp inhibitors, including tariquidar (XR9576), zosuquidar (LY335979), laniquidar (R101933) and elacridar

(F12091) [245]. Although these compounds were less toxic and significantly inhibited P-gp function at nanomolar concentrations, clinical trials revealed that the results of combined treatment with chemotherapeutics were not improved [268, 269].

Most of the abovementioned molecules inhibit only P-gp. However, some drugs capable of inhibiting other ABC transporters have also been developed. For example, agosterol-A, LTC_4 and LTD_4 receptor agonist (MK571), raloxifine analogs and isoxazole-derived molecule PAK-104P significantly inhibited MRP1- and MRP2-mediated MDR [270]. In contrast, inhibitors for other ABC transporters of the ABCC subfamily have not been developed [270, 271].

A large number of BCRP inhibitors with diverse chemical structures have been identified. The typical example of a highly selective BCRP inhibitor is fumitremorgin C (FTC), produced by *Aspergillus fumigatum*. However, the neurotoxicity of FTC precludes its use *in vivo* [272]. Several FTC analogs, including Ko132, Ko134 and Ko143 with a much higher inhibitory activity, remarkable selectivity and low neurotoxicity have been developed [273]. Other notable BCRP inhibitors are novobiocin, tamoxifen and its derivatives, TAG-11 and TAG139, and reserpine and dietary flavonoids such as chrysin and biochanin A. Moreover, several non-specific inhibitors, such as elacridar and biricodar, known to inhibit P-gp and MRP1, were also identified as BCRP inhibitors [263]. Several studies have reported in the last decade that BCRP can be inhibited by TKIs, such as imatinib, nilotinib and apatinib, and by HIV-protease inhibitors, such as ritonavir, nelfinavir and saquinavir [274].

1.3.4.2 Novel strategies to overcome MDR

MicroRNAs are small, non-coding RNAs that bind to the 3'UTR of mRNA and inhibit the expression of proteins at the translational level. MicroRNAs are generally dysregulated in cancer cells and alterations in microRNAs levels may play a role in MDR. Several studies reported that microRNAs can regulate MDR by modulating P-gp expression [275]. For example, the upregulation of microRNA-331-5p and microRNA27a can decrease P-gp expression and thus cause the reversal of MDR in the Dox-resistant leukemia cell lines K562 and HL60 [276].

Synthetic siRNAs are also extensively used to reverse chemoresistance by inhibiting the expression of MDR genes such as *ABCB1*, *ABCB4* and *ABCG2*. An example is the reduced expression level of the *ABCC4* gene using RNA interference in chemoresistant gastric cancer cells. This inhibition resulted in the increased sensitivity of cancer cells to chemotherapeutic drugs [277, 278].

Another approach to overcome MDR is to develop drugs that are not substrates of ABC transporters. Accordingly, new anticancer drugs that are not transported by P-gp and/or other ABC transporters were developed. These drugs are, for example, taxane analogs DJ-927 [279], BMS-184476 [280] and ortataxel [281]. However, they have been evaluated in preclinical trials for their capacity to overcome MDR in both sensitive and resistant tumor cell lines, with negative outcomes due to significant adverse effects [245].

1.4 HPMA copolymer-based drug delivery systems

Conventional chemotherapy plays an important role in cancer treatment. However, unfavorable pharmacokinetics and the severe side effects of low molecular weight (LMW) anticancer drugs are a limiting disadvantage. As a consequence, numerous polymer drug-carrier systems have been developed. Polymeric drug carriers are characterized by their high molecular weight (HMW) and can be divided into naturally occurring or synthetic carriers. Synthetic polymers can be tailor-made to have properties suitable for the particular need and consequently, they are used more frequently in comparison to polymers of natural origin. The majority of synthetic polymer drug carrier systems, e.g., nanoparticles or liposomes, usually have the drug entrapped inside the carrier-formed particles. On the other hand, water-soluble polymer-drug conjugates have pharmacologically active molecules covalently bound to the polymer chain via a defined spacer, enabling controlled drug release. Among them, synthetic polymer carriers based on *N*-(2-hydroxypropyl)methacrylamide (HPMA) copolymers are one of most intensively studied systems [282-284].

HPMA copolymers were developed at the Institute of Macromolecular Chemistry in Prague by Kopecek and co-workers several decades ago. Due to their suitable biological properties and biocompatibility, HPMA copolymers have been tested for their potential use in various medical applications. Nevertheless, their most important and promising application is in the field of anticancer drug delivery [285-287].

HPMA copolymers bearing anticancer drugs substantially reduce the side toxicity of the attached drug by preventing its release in the bloodstream during transport to the tumor. Unlike free LMW drugs, HPMA copolymer conjugates preferentially accumulate in the solid tumors due to the enhanced permeability and retention (EPR) effect (see page 43). Once they reach the tumor, the drug is released either in the tumor interstitium or within the cancer cells, providing a sufficient drug concentration to trigger cancer cell death. In addition, the long half-life in the

bloodstream and the solubilization of even highly hydrophobic anticancer drugs makes this drug delivery system particularly attractive [288].

1.4.1 Structure and synthesis of HPMA copolymer carriers

HPMA copolymer-drug conjugates are composed of several distinct parts: a water-soluble HPMA copolymer backbone, spacer/linker and anticancer drug(s), in addition to an optional targeting moiety (Figure 1.12) [284].

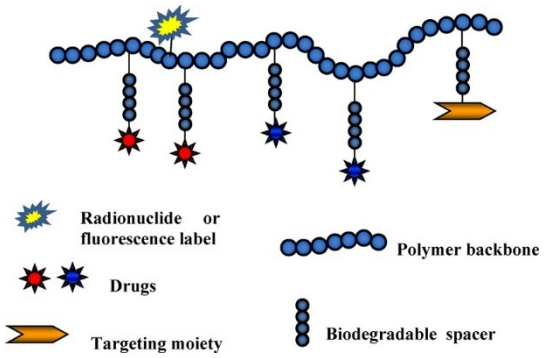

Figure 1.12: Schematic of a polymer-drug conjugate. The polymer conjugate consists of a polymer backbone and one or more kinds of anticancer drugs attached by a biodegradable bond, in addition to an optional targeting moiety. Adopted from Ulbrich et al. [289].

HPMA copolymer-drug conjugates were originally prepared using the free radical copolymerization of HPMA with respective co-monomers bearing reactive 4-nitrophenyl ester groups or other functional groups, followed by conjugation with an anticancer drug. All reactive polymer precursors were multivalent HPMA copolymers with various amounts of reactive groups randomly distributed along the polymer chain. The molecular weight of the copolymers usually ranges from 20,000-35,000, due to chain-transfer reactions and steric hindrance in the precipitation of growing polymer radicals [290-292].

The low polydispersity of polymer-drug conjugates is an important requirement for *in vivo* application and regulatory authorities such as the FDA. Unfortunately, HPMA copolymer-drug conjugates synthetized by free radical copolymerization exhibited polydispersity higher than 1.5 and often close to 2. A new technique using controlled radical polymerization, namely reversible addition-fragmentation chain transfer (RAFT), was used. RAFT-controlled radical copolymerization of HPMA enabled the synthesis of a copolymer with a molecular weight of

3-135 kDa and polydispersity of 1.1-1.3. The resulting polymer-drug conjugates therefore exhibited a well-defined structure [293, 294].

Anticancer drugs are bound to the polymeric carrier via a covalent bond which is stable in the bloodstream but cleavable within the tumor cells, particularly in the lysosomal compartment [295]. One strategy is to use the pH differences between the blood and lysosomes and bind the drug via a pH-sensitive hydrazone bond [296] or *cis*-aconityl [297] and maleic [298] spacers. The other option is to design spacers which are cleavable by specific lysosomal enzymes. The best stability in the bloodstream and a fair degradability in the presence of the lysosomal enzyme cathepsin B has been shown for the oligopeptidic Gly-Phe-Leu-Gly (GFLG) spacer [299, 300].

Optionally, a targeting moiety could be used for the increased accumulation of polymer-drug conjugates in the target cells. The active targeting of polymer-drug conjugates can be achieved through the incorporation of target-cell-specific ligands such as peptides, carbohydrates, lectins, transferrin, antibodies or antibody fragments [301-303].

1.4.2 HPMA copolymer-drug conjugates without a targeting moiety

Malignant cells within the tumor mass are characterized by phenotypic diversity. Accordingly, several generally applicable approaches for targeting solid tumors in general have been developed. The most important approach is based on the enhanced permeability and retention (EPR) effect (Figure 1.13). The EPR effect can be exploited for the so-called passive targeting of antitumor drugs into solid tumors [304]. The EPR effect was first reported by Matsumura and Maeda in 1986 [305]. They showed that most solid tumors have leaky blood vessels with defective architecture, absent or impaired lymphatic drainage and produce an extensive amount of various vascular permeability factors. Newly formed blood vessels in solid tumors usually have defective endothelial cells with wide fenestration of approximately 200 to 700 nm and lack a smooth muscle layer. The EPR effect exploits this unique pathophysiological nature of tumor blood vessels for the transport of macromolecules into the tumor tissue. Macromolecules larger than 40 kDa, as well as small particles approximately 20-500 nm in diameter, can easily leak from tumor vessels and accumulate in tumor tissue. Impaired lymphatic drainage then further increases the accumulation of such molecules within the tumor. The main advantage of the EPR effect in solid tumors is its universality, which enables the use of this drug delivery approach in many types of tumors [306, 307].

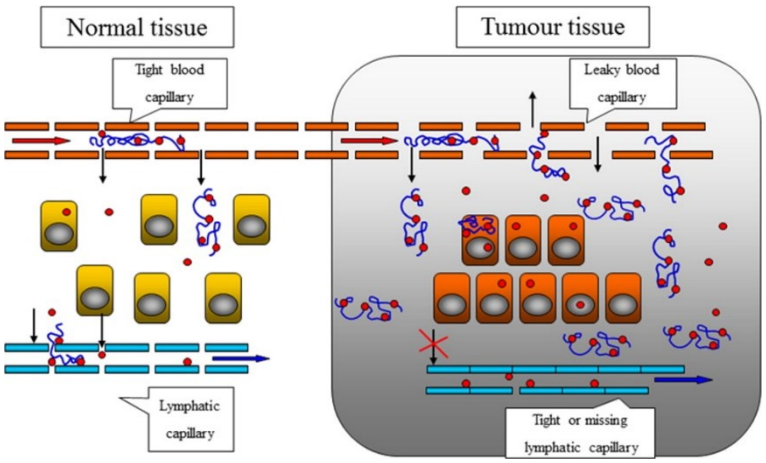

Figure 1.13: Schematic of the EPR effect. The accumulation of macromolecules in solid tumors due to the EPR effect. Red dots represent the LMW drug and the blue lines represent macromolecules. Adopted from Ulbrich et al. [289].

Various anticancer drugs have been attached to non-degradable linear HPMA copolymer carriers such as Dox, puromycin, MTX, taxanes and 5-FU [308-310]. However, the first HPMA copolymer conjugate bearing Dox bound through an amide bond and via a GFLG spacer subjected to Phase I/II clinical trial was Dox^{AM}-PHPMA (PK1) (Figure 1.14). The results of the clinical trial confirmed most of the findings obtained *in vivo* in animal models, such as low toxicity and improved pharmacokinetics, including significantly prolonged drug circulation and the increased the accumulation of the drug within the solid tumors. Nevertheless, the introduction of HPMA copolymer-drug conjugates which are activated by lysosomal enzymes (via an oligopeptide spacer) into clinical practice has been declined [311-313].

The next generation of linear HPMA copolymer-drug conjugates bearing Dox bound via a pH-sensitive hydrazone bond, Dox^{HYD}-PHPMA (Figure 1.14), was introduced about two decades after PK1 [314]. This conjugate exhibited remarkable antitumor activity in mice and induced a specific antitumor immune response that could be transferred to naive mouse recipients [315]. Moreover, this structurally simpler HPMA copolymer-drug conjugate has a maximal tolerated dose (MTD) which is three times higher than PK1 [316].

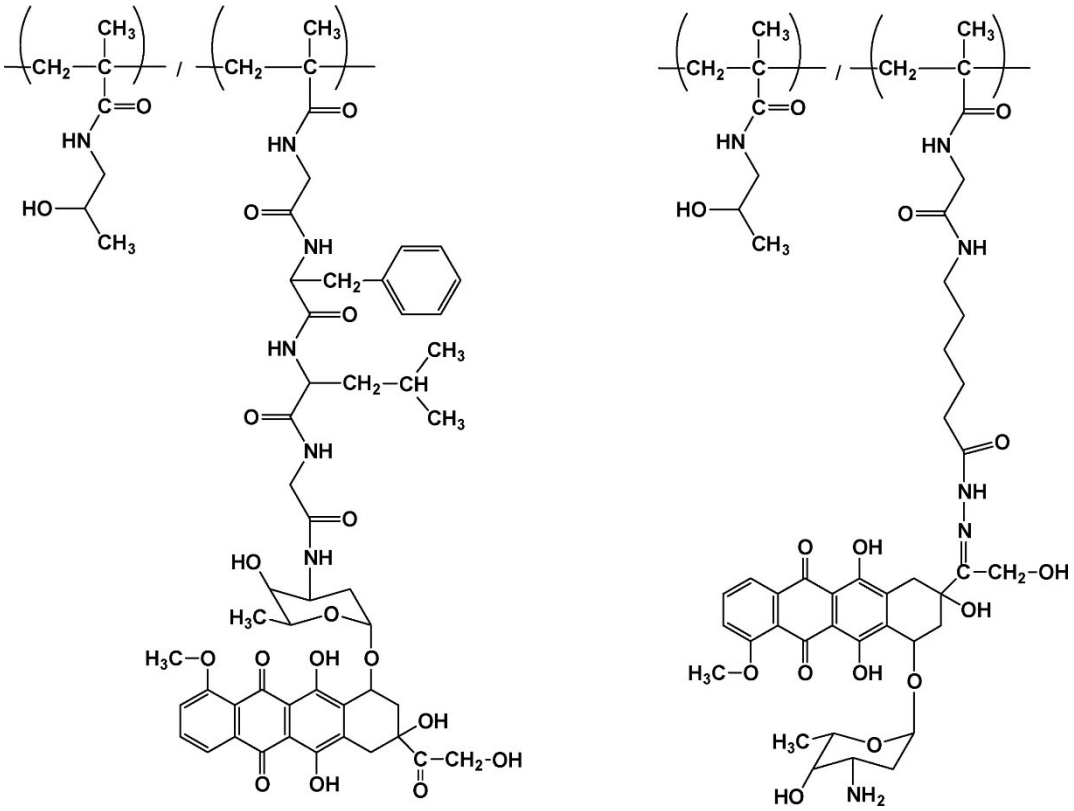

Figure 1.14: HPMA copolymer conjugates bearing Dox. Polymer conjugates bearing Dox bound via an enzymatically degradable GFLG spacer and amide bond (left) or pH-sensitive hydrazone bond (right). Adopted from Ulbrich et al. [289].

The accumulation of HPMA copolymer-drug conjugates in solid tumors due to the EPR effect improves with the increasing molecular weight of the polymer carrier (up to~250 kDa) [317, 318]. As such, the use of linear HPMA copolymers with molecular weights of about 40 kDa as carriers for efficient passive tumor targeting is somehow limited [319]. Accordingly, HMW HPMA copolymers such as branched [320], grafted [317], diblock, multiblock [321] and star [318] conjugates have been designed and synthetized (Figure 1.15). However, these HMW copolymers with molecular weights above the renal threshold need to be biodegradable to enable the excretion of the short polymer chains through the urine [318].

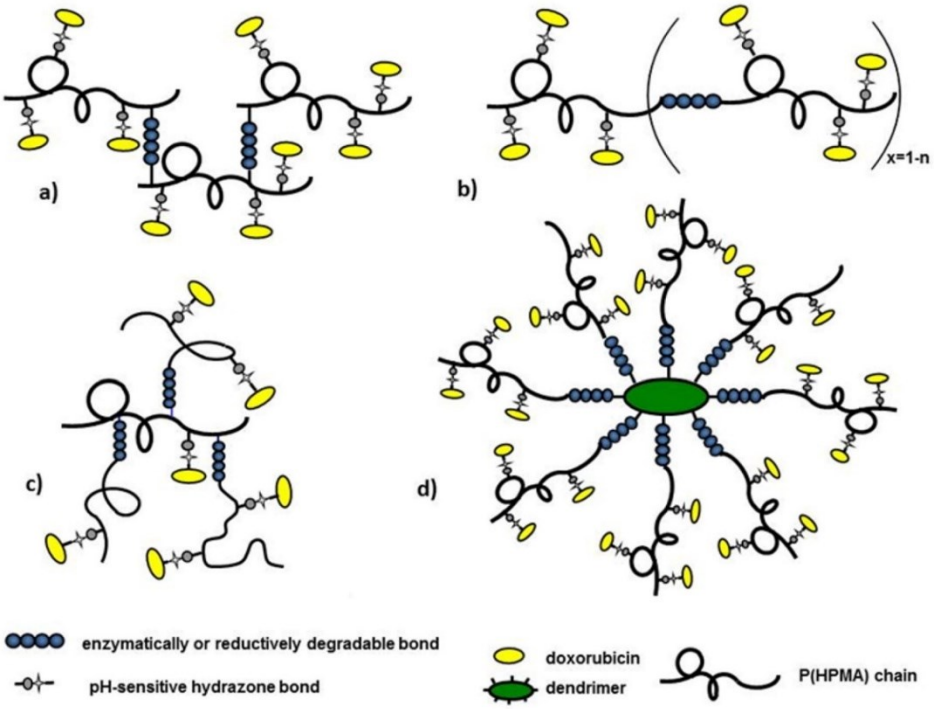

Figure 1.15: Schematic structures of biodegradable HMW drug conjugates based on HPMA copolymers. (a) Branched polymer carrier; (b) linear diblock and multiblock carrier; (c) grafted polymer carrier; and (d) star polymer carrier. Adopted from Ulbrich et al. [289].

1.4.3 Active targeting of HPMA copolymer-drug conjugates

Active targeting is an approach based on the specific interactions between a surface antigen and a complementary ligand bound to the polymeric carrier. Actively targeted polymer-drug conjugates can be highly selective and effective against tumors which are less sensitive to passively targeted polymer-drug conjugates. Nevertheless, the process of the active targeting of polymer-drug conjugates begins through passive accumulation in tumor tissue via the EPR effect [289].

Various targeting moieties have been employed in HPMA copolymer-drug conjugates to achieve specific delivery. HPMA copolymer-dug conjugates bearing Dox via the oligopeptide spacer GFLG and a targeting moiety, such as antibodies, transferrin, lectins, saccharides or melanocyte-stimulating hormone (MSH), were evaluated [284]. The results of these studies showed that such targeting moieties can significantly influence the systemic distribution of polymer-drug conjugates and promote receptor-mediated targeting *in vivo* [284, 322].

One of the HPMA copolymer conjugates bearing Dox and targeted B1 monoclonal Ab was used in the treatment of mouse B-cell leukemia BCL1. This conjugate was found to completely cure up to 70% of mice bearing B-cell leukemia BCL1 after a single intravenous dose. Similar results were obtained with mice bearing B-cell lymphoma 38C13 and treated with αCD71 mAb-targeted conjugate, or T-cell lymphoma EL4 and treated with αThy1.2 mAb-targeted conjugate. However, significant drawbacks of using Ab as a targeting moiety are the high cost and poor reproducibility of the synthesis [323].

HPMA copolymer conjugates bearing Dox have also been conjugated with targeting lectins such as wheat germ agglutinin (WGA) or peanut agglutinin (PNA) and evaluated in human colorectal carcinoma SW620 *in vitro* [289].

The HPMA copolymer conjugate bearing Dox via a GFLG spacer and targeted by a galactosamine called PK2 was the first actively targeted HPMA-based conjugate which entered Phase I/II clinical trials. However, due to the comparable drug accumulation in tumor and normal liver tissues, further testing was declined [324].

2 Aims of the thesis

The aim of this study was to design and evaluate the biological activity of HPMA copolymer conjugates capable of overcoming P-gp mediated MDR or enhancing the EPR effect. This general aim can be dived into three partial tasks:

1. The characterization of the biological activity of new HPMA copolymer conjugates bearing a P-gp inhibitor and cytostatic drug (Dox, pirarubicin) in MDR cell lines *in vitro* and *in vivo*.
   a. The evaluation of the P-gp inhibitory activity of HPMA copolymer conjugates bearing P-gp inhibitor (derivative of reversin 121 (R121) or ritonavir (RIT)).
   b. The determination of the cytotoxic and cytostatic activity of HPMA copolymer conjugates bearing a P-gp inhibitor and cytostatic drug *in vitro*.
   c. The efficacy of HPMA copolymer conjugates bearing a P-gp inhibitor and cytostatic drug in the treatment of murine model tumors expressing P-gp.

2. The evaluation of the therapeutic potential of micelle-forming HPMA copolymer-poly(propylene oxide) (PPO) diblock bearing anticancer drug and its capability to inhibit P-gp per se.
   a. The determination of the P-gp inhibitory activity of HPMA copolymer-PPO diblock in MDR cell lines *in vitro*.
   b. The evaluation of the cytotoxic activity and cellular uptake of HPMA copolymer-PPO diblock in various cancer cell lines *in vitro*.
   c. The evaluation of the therapeutic efficacy of HPMA copolymer-PPO diblock in the treatment of murine model tumors.

3. The investigation of the biological activity of HPMA copolymer conjugates bearing organic nitrates as polymeric NO donors.
   a. The evaluation of NO release from the polymeric carrier and the effect of polymeric NO donors on proliferation in cancer cell lines *in vitro*.
   b. The characterization of the cytostatic activity of Dox in the presence of the polymeric NO donors in tumor cell lines *in vitro*.
   c. The estimation of the MTD of selected polymeric NO donors.
   d. The evaluation of the effect of polymeric NO donors on the treatment of solid tumors by the HPMA copolymer conjugates bearing Dox by increasing the EPR effect.

3 List of publications

This thesis was prepared on the basis of the following publications:

Koziolová E, Janoušková O, Cuchalová L, Hvězdová Z, Hraběta J, Eckschlager T, Sivák L, Ulbrich K, Etrych T, Šubr V. Overcoming multidrug resistance in Dox-resistant neuroblastoma cell lines via treatment with HPMA copolymer conjugates containing anthracyclines and P-gp inhibitors. *Journal of Controlled Release*. **2016** Jul 10; 233:136-46.

IF = 7.786

PMID: 27189135

Contribution of the author: 10%; I performed the *in vitro* testing of the cytostatic activity of the HPMA copolymer conjugates with various molar ratios between the cytostatic drug and the P-gp inhibitor. I also contributed to manuscript preparation.

Sivak L, Subr V, Tomala J, Rihova B, Strohalm J, Etrych T, Kovar M. Overcoming multidrug resistance via simultaneous delivery of cytostatic drug and P-glycoprotein inhibitor to cancer cells by HPMA copolymer conjugate. *Biomaterials*. **2017** Jan 1; 115:65-80.

IF = 8.806

PMID: 27886555

Contribution of the author: 60%; I was responsible for most of the experiments in the biological part of the work. I also contributed to data analysis and manuscript preparation.

Braunová A, Kostka L, Sivák L, Cuchalová L, Hvězdová Z, Laga R, Filippov S, Černoch P, Pechar M, Janoušková O, Šírová M. Tumor-targeted micelle-forming block copolymers for overcoming of multidrug resistance. *Journal of Controlled Release*. **2017** Jan 10; 245:41-51.

IF = 7.877

PMID: 27871991

Contribution of the author: 20%; I established and performed the calcein AM assay which I utilized for the determination of the P-gp inhibitory activity of HPMA copolymer-PPO diblock. I also carried out the experiments focused on the sensitization of mouse tumor cell lines to the cytostatic activity of Dox. I contributed to manuscript preparation.

Studenovsky M, Sivak L, Sedlacek O, Konefal R, Horkova V, Etrych T, Kovar M, Rihova B, Sirova M. Polymer nitric oxide donors potentiate the treatment of experimental solid tumours

by increasing drug accumulation in the tumour tissue. *Journal of Controlled Release.* **2018** Jan 10; 269:214-24.

IF = 7.877

PMID: 29154977

Contribution of the author: 20%; I established and performed the cell-based NO assay which I utilized for intracellular NO detection. I also carried out confocal microscopy experiments and assays based on the Griess reaction for the detection of generated NO. I contributed to manuscript preparation.

I hereby confirm that the author of the thesis, Ladislav Sivák, has substantially contributed to the publications listed above. He performed the majority of the experimental work and significantly contributed to the manuscript preparation in the case of his first-author publication.

RNDr. Marek Kovář, PhD.

Journal of Controlled Release 233 (2016) 136–146

Contents lists available at ScienceDirect

Journal of Controlled Release

journal homepage: www.elsevier.com/locate/jconrel

Overcoming multidrug resistance in Dox-resistant neuroblastoma cell lines *via* treatment with HPMA copolymer conjugates containing anthracyclines and P-gp inhibitors

Eva Koziolová [a], Olga Janoušková [a], Lucie Cuchalová [a], Zuzana Hvězdová [a], Jan Hraběta [b,c], Tomáš Eckschlager [b,c], Ladislav Sivák [d], Karel Ulbrich [a], Tomáš Etrych [a], Vladimír Šubr [a,*]

[a] Institute of Macromolecular Chemistry, The Czech Academy of Sciences, v.v.i., Heyrovsky Sq. 2, 162 06 Prague 6, Czech Republic
[b] Charles University Prague, 2nd Medical Faculty, Department of Pediatric Hematology and Oncology, 150 06 Prague 5, Czech Republic
[c] University Hospital Motol, 150 06 Prague 5, Czech Republic
[d] Institute of Microbiology, The Czech Academy of Sciences, v.v.i., Videňská 1083, 142 20 Prague 4, Czech Republic

ARTICLE INFO

Article history:
Received 17 February 2016
Received in revised form 9 May 2016
Accepted 13 May 2016
Available online 14 May 2016

Keywords:
N-(2-hydroxypropyl)methacrylamide copolymers
Multidrug resistance
P-glycoprotein inhibitors
Reversin 121
Ritonavir
Doxorubicin
Pirarubicin
Neuroblastoma

ABSTRACT

Water-soluble *N*-(2-hydroxypropyl)methacrylamide copolymer conjugates bearing the anticancer drugs doxorubicin (Dox) or pirarubicin (THP), P-gp inhibitors derived from reversin 121 (REV) or ritonavir (RIT)), or both anticancer drug and P-gp inhibitor were designed and synthesized. All biologically active molecules were attached to the polymer carrier *via* pH-sensitive spacer enabling controlled release in mild acidic environment modeling endosomes and lysosomes of tumor cells. The cytotoxicity of the conjugates against three sensitive and Dox-resistant neuroblastoma (NB) cell lines, applied alone or in combination, was studied *in vitro*. All conjugates containing THP displayed higher cytotoxicity against all three Dox-resistant NB cell lines compared with the corresponding Dox-containing conjugates. Furthermore, the cytotoxicity of conjugates containing both drug and P-gp inhibitor was up to 10 times higher than that of the conjugate containing only drug.
In general, the polymer-drug conjugates showed higher cytotoxicity when conjugates containing inhibitors were added 8 or 16 h prior to treatment compared with conjugates bearing both the inhibitor and the drug. The difference in cytotoxicity was more pronounced at the 16-h time point. Moreover, higher inhibitor:drug ratios resulted in higher cytotoxicity. The cytotoxicity of the polymer-drug used in combination with polymer P-gp inhibitor was up to 84 times higher than that of the polymer-drug alone.

© 2016 Elsevier B.V. All rights reserved.

1. Introduction

Neuroblastoma, the most frequent solid extracranial neoplasm in children, often exhibits intrinsic or acquired multidrug resistance (MDR) and therefore resists intensive multimodal chemotherapy [1]. Three decades of research focused on MDR cancer cells have identified a wide range of mechanisms through which MDR cells can elude chemotherapy. In fact, resistance has developed against every antitumor drug, even the newest agents. Thus, the ability to identify and overcome MDR may significantly improve the efficacy of cancer treatment. MDR is in many cases caused by the overexpression of adenosine 5 -triphosphate (ATP)-binding cassette (ABC) transporters in tumor cells, especially P-glycoprotein (P-gp) [2]. In healthy tissues, P-gp plays an important role in the elimination of undesirable or harmful compounds from cells. This protective function of P-gp is also utilized as a survival mechanism by cancer cells, leading to the elimination of anticancer drugs, *e.g.*, anthracyclines, from the cells, resulting in the low efficacy or even the failure of cancer treatment [3,4].

Various low-molecular-weight P-gp inhibitors have been used to overcome MDR [5,6]. However, the administration of free inhibitor also causes P-gp inhibition in healthy cells, leading to serious side effects [7,8]. Additionally, the simultaneous presence of adequate levels of both a cytostatic agent and an inhibitor in the tumor is essential to achieve a desirable effect.

Drug delivery systems based on nanomedicines, including polymer conjugates, due to their prolonged circulation and ability to accumulate in solid tumors due to EPR [9] effect are able to deliver high concentrations of chemotherapeutic drugs and/or MDR inhibitors to tumors and enable controlled release of the active agents at the site of interest [10–12].

Numerous nanocarriers with physically loaded chemotherapeutics and MDR inhibitors, *e.g.*, hydrogels [13], liposomes [14] or nanoparticles [15] seem to overcome the drawbacks of using free inhibitors both *in vitro* and *in vivo*. Nevertheless, drug/inhibitor release by these carriers is usually not controlled. We found that water-soluble *N*-(2-

* Corresponding author.
E-mail address: subr@imc.cas.cz (V. Šubr).

http://dx.doi.org/10.1016/j.jconrel.2016.05.036
0168-3659/© 2016 Elsevier B.V. All rights reserved.

hydroxypropyl)methacrylamide (HPMA) copolymer-based conjugates with P-gp inhibitors derived from ritonavir (RIT) or reversin 121 (REV), bound *via* a pH-sensitive hydrazone bond to polymer carrier significantly increased the cytotoxic effect of doxorubicin (Dox) conjugate toward the Dox-resistant murine monocytic leukemia P388/MDR cell line *in vitro* [16].

Here, we compared the cytotoxicity of two conjugates with the anticancer agents doxorubicin (Dox) or 4-O-tetrahydropyranyl doxorubicin (pirarubicin, THP; for the structure, see Fig. 1 in the supplement file), administered together with P-gp inhibitor conjugates, both of which were attached to the polymer carriers *via* a pH-sensitive hydrazone bond-containing spacer, using three Dox-resistant NB cell lines (NB4-Dox, NB3-Dox and IMR32-Dox) with different resistance factors.

In the present study, Dox served as a control for Dox-resistant cells; THP is an efficient anthracycline anticancer agent with a cellular uptake rate that is 30–100 times faster than that for Dox [17–19]. The first clinical application of a THP-containing polymer conjugate based on a HPMA copolymer with THP bound *via* a hydrazone bond has recently been reported, yielding remarkable results for the treatment of a patient with metastatic prostate cancer, including a drop in tumor markers to normal levels and significant metastasis regression. At the same time, no noticeable signs of toxicity were observed [20].

Moreover, the literature data concerning the efflux of THP *via* P-gp diverge significantly. Some studies have observed the P-gp-driven efflux of THP, and an increase in the intracellular drug concentration after application of P-gp inhibitors [21,22] or increased THP cytotoxicity due to P-gp down-regulation [23,24]. On the other hand, THP is considered to be able to overcome P-gp related MDR in Dox-resistant cells [25], and the rate of THP transmembrane transport in Dox-resistant cells is thought to be relatively high, with efflux mediated by protein transporters unable to keep pace [26]. Therefore, we believe that using polymer conjugates to enable the simultaneous, tumor-specific delivery of a P-gp inhibitor together with the cytostatic drug THP can help to overcome MDR in cancer cells and thus significantly improve the treatment of resistant tumors. This paper should contribute to the verification of this idea.

2. Materials and methods

2.1. Materials

Ritonavir was purchased from ChemPacific Corp. (Baltimore, MD, USA). Doxorubicin hydrochloride (Dox) and pirarubicin (THP) were purchased from Meiji Seika, Tokyo, Japan. *N*-(2-Hydroxypropyl)methacrylamide (HPMA) was synthesized as described previously [27].

N′-[6-(2-Methyl-acryloylamino)-hexanoyl]-hydrazine carboxylic acid *tert*-butyl ester (Ma-Ahx-NH-NH-Boc) was prepared as described previously [16].

MeOHe-Asp(OBzl)-Lys(Z)-OtBu (REV; for the structure, see Fig. 2a) in the supplement file) was prepared by two-step synthesis as described previously [16].

5-Methyl-4-oxohexanoyl-ritonavir ester (RIT; for the structure, see Fig. 2b) in the supplement file) was prepared as described previously [16].

All other chemicals and solvents were of analytical grade. The solvents were dried and purified using conventional procedures and distilled before use.

2.2. Synthesis of the P-Ahx-NH-NH_2 precursor

The polymer precursor P-Ahx-NH-NH-Boc (in general, P indicates HPMA copolymer) was prepared by reversible addition-fragmentation chain transfer (RAFT) copolymerization as described previously [16]. The polymer precursor *P1*, used for the synthesis of polymer conjugates *P-REV–P-RIT*(*THP*) (see Table 1.), was prepared by removing the Boc protecting group in the presence of TFA [28].

Table 1
Characteristics of polymer precursor and polymer conjugates.

HPMA copolymer precursor and conjugates	M_w	Đ	Hydrazide content mol%	REV/RIT content mol%/wt%	Dox/THP content mol%/wt%
P1	31,600	1.17	6.4	–	–
P-REV	34,200	1.23	–	2.9/11.8	–
P-REV(*Dox*)	37,100	1.20	–	2.23/8.5	2.4/8.0
P-REV(*THP*)	36,800	1.19	–	1.76/7.0	1.9/7.1
P-RIT	32,900	1.22	–	1.34/7.3	–
P-RIT(*Dox*)	37,400	1.2	–	1.78/7.3	2.87/9.4
P-RIT(*THP*)	36,500	1.19	–	1.76/8.5	3.18/8.4
P-Dox	32,000	1.8	–	–	2.27/9.4
P-THP	39,000	2.1	–	–	2.14/9.6

2.3. Synthesis of polymer conjugates with inhibitor derivatives and anticancer drug

The conjugates *P-REV*(*Dox*) and *P-RIT*(*Dox*) for simultaneous co-delivery of both the drug and inhibitor attached to the same polymer carrier were synthesized as described previously [14]. The same procedure was used for the synthesis of conjugates *P-REV*(*THP*) and *P-RIT*(*THP*). For example, *P-REV*(*THP*) was synthesized as follows: Polymer precursor *P1* (50 mg), REV (9 mg, 0.013 mmol) and THP (5.75 mg, 0.009 mmol) were dissolved in dry methanol (350 μL), after which acetic acid (14 μL) was added. The reaction was carried out for 16 h in the dark. The reaction mixture was diluted with dry methanol (2 mL), and the conjugate *P-REV*(*THP*) was purified by column chromatography on a Sephadex LH-20 column with methanol as the mobile phase. The conjugate was then precipitated into ethyl acetate, isolated by filtration and dried under a vacuum. The yield was 52 mg of *P-REV*(*THP*), which contained 7.0 wt% REV and 7.1 wt% THP. For examples of the structures of the polymer conjugates *P-REV*(*THP*) and *P-RIT*(*THP*) are shown in Fig. 1. The conjugates *P-REV* and *P-RIT* were synthesized by reacting *P1* with REV or RIT using the above procedure. The conjugates *P-Dox* and *P-THP* were prepared according to the literature [29,30].

2.4. Characterization of monomers, polymer precursor and conjugates

The structures of monomers and inhibitor derivatives were confirmed by ^{1}H NMR (300 MHz) using a Bruker DPX 300 spectrometer, elemental analysis and by determination their molecular weights with a mass spectrometer (MS LCQ Fleet, Thermo Fisher Scientific).

The purity of monomers and inhibitor derivatives was checked using a HPLC Shimadzu system with a reverse-phase column (Chromolith®HighResolution RP-18e, 100 × 4.6 mm) (Merck, Germany) equipped with a UV/VIS photodiode array detector. Gradient elution with 5–95% of acetonitrile for 15 min at a flow rate of 1.0 mL/min was used.

The number average molecular weights (M_n), weight-average molecular weights (M_w), and polydispersities (*Đ*) of the polymer precursors and conjugates were measured using size-exclusion chromatography (SEC) on a HPLC Shimadzu system equipped with a UV detector, an Optilab®rEX differential refractometer and multi-angle light scattering DAWN® 8™ (Wyatt Technology, USA) detector. The Mw, Mn and Đ were calculated using the Astra V software. The refractive index increment dn/dc = 0.167 mL/g was used for calculation. For these experiments, a 20% 0.3 M acetate:80% methanol (v/v) buffer and either a TSKgel G3000SW or a TSKgel G4000SW column were used.

The content of the inhibitor in the polymer conjugates was determined by amino acid analysis of the hydrolyzed polymer conjugates (6 M HCl, 115 °C, 18 h in a sealed ampoule) using a reverse-phase column (Chromolith®HighResolution RP-18e, 100 × 4.6 mm) (Merck, Germany) after pre-column derivatization with *o*-phthaldialdehyde (OPA) and 3-sulfanylpropanoic acid using fluorescence detector (excitation at

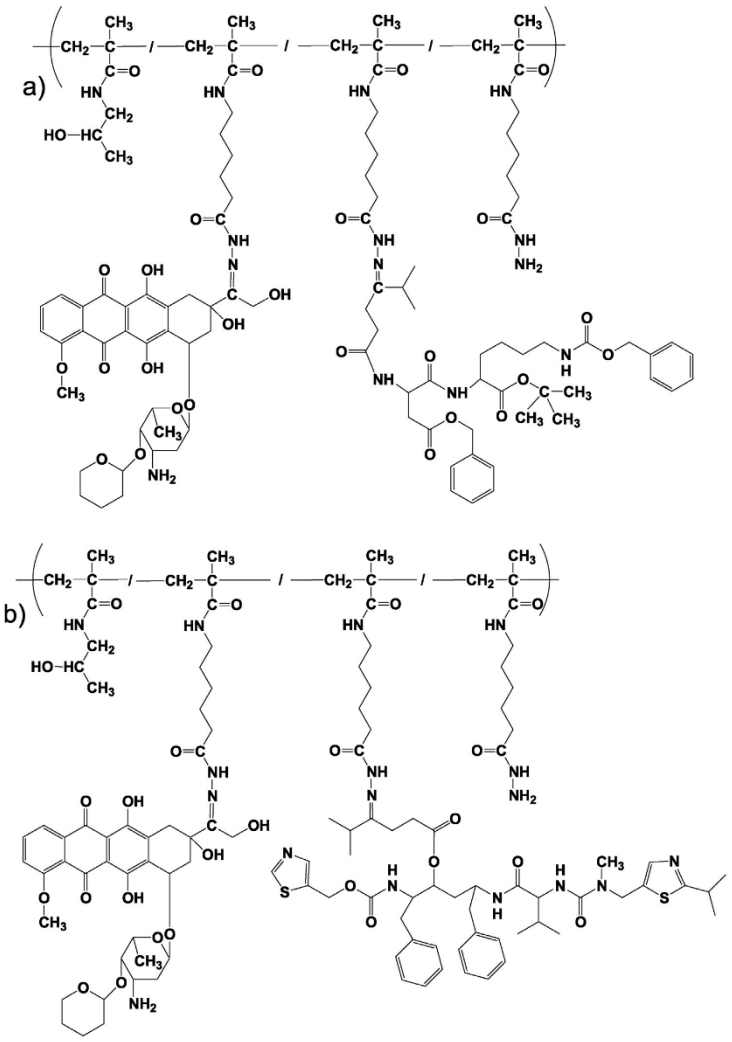

Fig. 1. Structure of conjugates a) *P-REV(THP)* and b) *P-RIT(THP)*.

229 nm, emission at 450 nm). Gradient elution with 10–100% solvent B for 35 min at a flow rate of 1.0 mL/min was used, where solvent A was 0.05 M sodium acetate buffer, pH 6.5, and solvent B was 300 mL of 0.17 M sodium acetate and 700 mL of methanol.

The Dox and THP content in conjugates was determined spectrophotometrically on a Specord 205 (Jena Analytics) spectrophotometer ($\varepsilon_{488,Dox} = 10.700\ L \cdot mol^{-1} \cdot cm^{-1}$; $\varepsilon_{488,THP} = 11.300\ L \cdot mol^{-1} \cdot cm^{-1}$ methanol), and the content of the hydrazide groups was determined by the TNBSA method ($\varepsilon_{500} = 17.550\ L \cdot mol^{-1} \cdot cm^{-1}$; borate buffer pH 9.3).

2.5. In vitro release of inhibitors and drugs from the polymer conjugates

The release rates of RIT, REV, Dox and THP from the polymer conjugates *P-REV(Dox)*, *P-REV(THP)*, *P-RIT(Dox)* and *P-RIT(THP)* were investigated in phosphate buffers at pH 5.0 or 7.4 (0.1 M, with 0.05 M NaCl) at 37 °C. The amount of released RIT and REV was determined after chloroform extraction of RIT and REV using HPLC with a reverse-phase column and UV-detection at 220 nm as previously described [16]. The amount of released Dox and THP was determined by HPLC with a SEC column (described above). The relative area of the peaks (PDA detection at 488 nm) corresponds to the released Dox and THP and the polymer-bound Dox and THP. The values shown are the mean values obtained from three independent experiments.

2.6. Cell lines

The parental human neuroblastoma cell lines UKF-NB4 (NB4), UKF-NB3 (NB3), and UKF-IMR32 (IMR32), as well as chemoresistant

derivatives UKF-NB4-Dox (NB4-Dox), UKF-NB3-Dox (NB3-Dox), and UKF-IMR32-Dox (IMR32-Dox), were obtained from the laboratory of Prof. Eckschlager (Department of Pediatric Hematology and Oncology, 2nd Medical Faculty of Charles University in Prague and University Hospital in Motol) [31]. The chemoresistant cells were established by exposing parental cells to increasing concentrations of the Dox. The initial Dox concentration was 2 ng/mL. The resistant sublines were grown for >6 months in Iscove's modified Dulbecco's medium (IMDM) supplemented with 10% fetal calf serum and the concentration of Dox was gradually increased up to 100 ng/mL. Cells were subcultured at 5-day intervals [32]. Cells were cultivated in IMDM (Life Technology, Prague, Czech Republic) supplemented with heat-inactivated 10% fetal bovine serum (FCS), 100 U/mL penicillin and 100 μg/mL streptomycin.

2.7. In vitro cell viability assay

The cells ($5 \cdot 10^3$ or $7 \cdot 10^3$ for IMR and IMR-Dox cell lines, respectively) were seeded in 100 μL of media into 96-well flat-bottom plates (TPP, St. Louis, MO, USA) 24 h before the addition of polymer conjugates containing both drug and inhibitor on the same carrier (*P-REV*(*Dox*), *P-REV*(*THP*), *P-RIT*(*Dox*) and *P-RIT*(*THP*)) or a combination of polymer conjugates bearing inhibitor (***P-REV*** and *P-RIT*) together with polymer conjugates bearing either Dox or THP (*P-Dox* and *P-THP*). For cytotoxicity testing the concentrations of the conjugates (*P-REV*(*Dox*), *P-REV*(*THP*), *P-RIT*(*Dox*) and *P-RIT*(*THP*)) ranged from 0.1 to 45 μM of the drug equivalent. To testing the combinatorial effect of the drug and inhibitor conjugates (*P-REV*, *P-RIT*, *P-Dox* and *P-THP*), the conjugates with inhibitors (*P-REV* and *P-RIT*) (concentrations ranged from 0.001 to 5 μM for an inhibitor:drug (I:D) ratio of 1:1 and 0.004–20 μM for an I:D ratio of 4:1) were added 8 or 16 h before the addition of the conjugates with drugs (*P-Dox* and *P-THP*). The cells were subsequently cultivated for 72 h in 5% CO_2 at 37 °C. Then, 10 μL of Alamar Blue® cell viability reagent (Life Technologies, Prague, Czech Republic) was added to each well and incubated for 4 h at 37 °C. The active component of the Alamar Blue reagent, resazurin, was reduced to the highly fluorescent compound resorufin only in viable cells. The fluorescence of resorufin was detected on a Synergy Neo plate reader (Bio-Tek, Prague, Czech Republic) at 570 nm excitation and at 600 nm emission. Cells cultivated in medium without the conjugates were used as controls. Three wells were used for each concentration. The assay was repeated three times. Statistical analysis was performed using Student's *t*-test and GraphPad Prism Software.

2.8. RNA isolation and real-time PCR

Total RNA was isolated from the cultured cells using RNA Blue (Top Bio, Prague, Czech Republic) according to the manufacturer's protocol. The concentration and purity of the RNA samples were determined by measuring the absorbance at 260 nm. Residual DNA was removed using TURBO DNase (Life Technologies, Prague, Czech Republic). Total RNA (2 μg) was reverse-transcribed to cDNA using the High-Capacity cDNA Reverse Transcription Kit (Life Technologies). All real-time PCR reactions were performed using the StepOnePlus™ Real-Time PCR System (Applied Biosystems, Carlsbad, CA, USA), and the amplifications were performed using gene-specific probes (Life Technologies) and qPCR ProbesMaster with lowROX (Jena Bioscience GmbH, Jena, Germany). The thermal cycling conditions comprised an initial denaturation step at 95 °C for 2 min, 40 cycles at 95 °C for 30 s and 60 °C for 1 min. The experiments were carried out in duplicate for each data point. Gene expression differences were determined using the $2^{-\Delta\Delta C_T}$ method [33]. Gene expression was related to the NB3 cell line, which expressed the lowest levels of P-gp among the tested parental cell lines. Glyceraldehyde 3-phosphate dehydrogenase was used as an internal control/housekeeping gene.

2.9. Detection of P-gp expression by flow cytometry

To determine P-gp expression on the cell membrane, the cells were first washed with PBS containing 0.5% bovine albumin serum (0.5% BSA-PBS). Afterward approximately $5 \cdot 10^5$ of cells in 50 μL were labeled for 30 min at r.t. with 5 μL of Anti-human CD243-PE monoclonal antibody (Exbio, Vestec, Czech Republic), which recognizes the multi-drug resistance (mdr)-1 gene product. As a control, cells were labeled with the isotype antibody. Afterwards, cells were washed with 0.5% BSA-PBS and diluted in 0.5 mL of 0.5% BSA-PBS containing 1 μg/mL 7-Aminoactinomycin D (Thermo Scientific, Prague, Czech Republic) to mark dead cells. We determined the median fluorescence intensity and compared the expression of resistant and parental cell lines. Samples were analyzed using an FACS Verse (BD Bioscience, San Jose, CA, USA) and FlowJo software (Tree Star, Ashland, OR, USA).

2.10. Calcein efflux assay

The ability of REV and RIT, as well as the polymer conjugates bearing the inhibitors (*P-REV* and *P-RIT*), to block the MDR pumps was assessed using the Calcein^{AM} efflux assay. Cells were seeded at $5 \cdot 10^3$ cells per well (in 100 μL of culture IMDM medium) in 96-well plates (TPP Techno Plastic Products AG). The assay was performed 48 h later (with respect to the time intervals). At the time of the study, the tested inhibitors and control (10 μM Cyclosporine A) were added in triplicate in 10 μL of IMDM medium and incubated for defined time intervals: 30 min, 2 h, and 4 h in the case of the free inhibitors; 4 h, 8 h, and 18 h in the case of the conjugates *P-REV* and *P-RIT*; and always 30 min for the control. The concentrations of each inhibitor and control were selected based on our previous work [16]. Subsequently, Calcein^{AM} was added (final concentration 0.3 μM per well), and the cells were incubated for another 20 min. The uptake of Calcein^{AM} was stopped by centrifugation (1500 rpm, 3 min, and 4 °C). Cells were washed twice with 400 μL PBS and resuspended in 200 μL PBS. The fluorescence of the accumulated Calcein^{AM} was measured on a plate reader (Synergy H1 Hybrid Reader, Biotek, Winooski, VT, USA) at 485 nm excitation and 530 nm emission. Each experiment was performed two or three times.

2.11. Comparison of uptake of polymer conjugates in NB4-Dox cell line studied by laser scanning confocal microscopy (LSCM)

NB4-Dox cell line (8×10^4 cells) were seeded in 1 mL of media on a 35 mm glass bottom dish with four chambers, a 20 mm micro well, and a# 1 cover glass (0.13–0.16 mm) (Bio-Port Europe, Czech Republic) one day before incubation with polymer conjugates. The polymers were added in accordance to the cytotoxicity assays. The conjugates (*P-REV*(*Dox*), *P-REV*(*THP*), *P-RIT*(*Dox*) and *P-RIT*(*THP*)) were added in concentration 14 μM of the inhibitors equivalent and signal of Dox or THP was detected after 2, 4, 8 and 24 h of incubation. In the case of polymer conjugates combination *P-REV* or *P-RIT* (concentrations 14 μM) were added 8 or 16 h before the addition *P-Dox* or *P-THP* (concentration 3.5 μM). The molar ratio of inhibitor and drug was 4:1. The signal of Dox or THP was detected after 2, 4, 8 and 24 h of incubation.

Prior to the end of the incubation time (10 min) Hoechst 33,342 (5 μg/mL, Thermo Scientific, Czech Republic) was added for the labeling of the nucleus. The Dox and THP were excited at 488 nm and the emitted light was detected through 500–600 nm filter. Hoechst 33,342, dye labeling the nuclei, was excited at 405 nm and emitted light was detected through 425–500 nm filter. The laser scanning confocal microscope Olympus IX83 with FV10-ASW software (Olympus, Czech Republic) was used to observe the fluorescence light. The samples were scanned with a 60× oil immersion objective Plan ApoN (1.42 numerical aperture).

3. Results and discussion

In this work, we describe the synthesis, physicochemical characterization and *in vitro* biological behavior of eight types of HPMA copolymer conjugates containing the anticancer agents Dox or THP, P-gp inhibitors derived from reversin 121 or ritonavir, or a combination of drug and inhibitor. We focused our study on overcoming multidrug resistance of cancer cells by inhibiting Pgp-mediated efflux of drugs – one of the most important factors in MDR. The description and results of the characterization of polymer precursor *P1* and polymer conjugates are provided in Table 1. The conjugates *P-Dox* and *P-THP* were designed as an efficient polymer drug-carrier system to facilitate tumor-targeted drug delivery due to the EPR effect [28,30]. In addition, the conjugates *P-REV* and *P-RIT*, containing *P*-gp inhibitors, administered simultaneously with the polymer conjugates *P-Dox* and *P-THP*, as well as the conjugates *P-REV*(*Dox*), *P-REV*(*THP*), *P-RIT*(*Dox*) and *P-RIT*(*THP*), which contain both drug and inhibitor attached to the same polymer carrier *via* a pH-sensitive hydrazone bond, should lead to enhanced antitumor activity in MDR cell lines. Such enhanced activity has already been demonstrated for combination therapy using Dox conjugates along with conjugates of reversin 121 or ritonavir derivatives in the P388/MDR lymphoma cell line [16].

3.1. Synthesis of conjugates

Because the polymer backbone of HPMA copolymers is not biodegradable, only polymers with molecular weights below the renal filtration limit (M_w below 50,000 g/mol for HPMA copolymers) can be used as drug carriers without fearing potential side effects caused by the long-term accumulation of the polymer conjugate in the body. The polymer precursor *P1* was prepared by RAFT copolymerization, resulting in copolymer with a distribution of molecular weights (Đ) close to 1 (Table 1). The amount of hydrazide groups in *P1* (6.4 mol%) was sufficient to bind both drug and inhibitor. The M_w of *P1* and its narrow Đ enable the renal excretion of the carrier together with enhanced tumor accumulation versus the equivalent polymer precursors prepared by free radical polymerization [34]. The polymer conjugates *P-Dox* and *P-THP* with higher dispersity Đ, were used because they have previously been used in many *in vitro* and *in vivo* studies [28,30].

All of the drugs and inhibitors were attached to polymer precursor *via* pH-sensitive hydrazone bond were synthesized by reacting the hydrazide groups of the copolymer precursor *P1* with the keto groups of Dox, THP, REV or RIT in methanol in the presence of acetic acid. The inhibitors REV and RIT were selected based on previous results, as these inhibitors showed the highest difference in release rate at pH 5.0 and pH 7.4 and adequate P-gp-inhibition activity [16]. The characteristics of all of the conjugates are summarized in Table 1.

3.2. In vitro release of the P-gp inhibitors and drugs from conjugates P-REV(Dox), P-RIT(Dox), P-REV(THP) and P-RIT(THP)

The polymer conjugates accumulate in solid tumor tissues in which the extracellular pH decreases below physiological levels due to insufficient oxygen and nutrient supply [35]. In addition, macromolecules such as the polymer conjugates, unlike low-molecular-weight compounds, cannot enter cells by diffusion, and thus their cellular uptake is restricted to passive or active endocytosis/pinocytosis, which localizes the conjugates in endosomes. Endosomes subsequently fuse with lysosomes, which possess a low pH of approximately 5 and contain various enzymes [36]. The *in vitro* release of REV, RIT, THP and Dox from polymer conjugates *P-REV*(*THP*), *P-RIT*(*THP*), *P-REV*(*Dox*), *P-RIT*(*Dox*) in PBS buffer at pH 5.0 and 7.4, which mimics the conditions inside the cell and in the circulation, are shown in Figs. 2 and 3.

The pH-sensitive hydrazone bond between the active agent and the polymer backbone is relatively stable at pH 7.4. The amount of REV and THP released from polymer conjugate *P-REV*(*THP*) at pH 7.4 was below

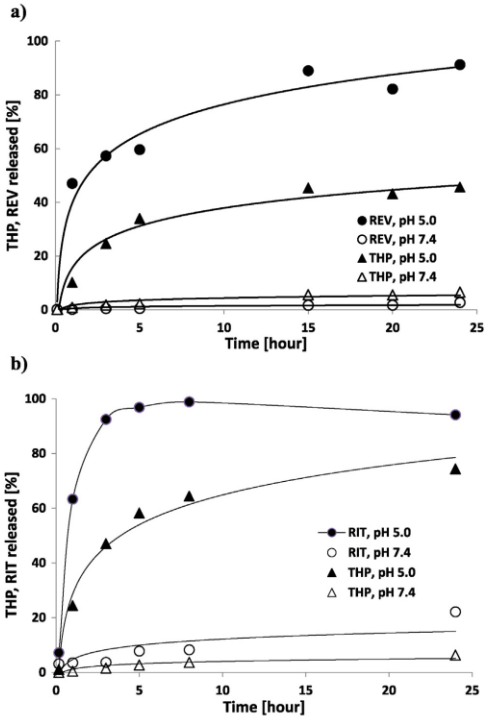

Fig. 2. *In vitro* release of THP and P-gp inhibitor (REV, RIT) from polymer conjugates *P-REV*(*THP*) (a) and *P-RIT*(*THP*) (b) in PBS buffer at pH 5.0 and 7.4; 37 °C. Standard deviation of the measurements was <10%.

10% within 24 h. The amount of RIT released from polymer conjugate *P-RIT*(*THP*) at pH 7.4 was 20% within 24 h, and the amount of THP released at pH 7.4 was comparable to that released from conjugate *P-REV*(*THP*). However, the drug/inhibitor release rate from conjugates *P-REV*(*THP*) and *P-RIT*(*THP*) in a mildly acidic environment of a tumor tissue (below pH 7) increases with decreasing pH reaching maximum at pH 5.0 (modeling the environment in secondary endosomes and lysosomes) (60 to 80% of inhibitor and 35 to 60% of THP was released within 5 h). The release of REV and RIT from polymer conjugates *P-REV*(*Dox*) and *P-RIT*(*Dox*) at pH 5.0 and 7.4 was comparable with the release from conjugates *P-REV*(*THP*) and *P-RIT*(*THP*). The release rate of Dox from *P-REV*(*Dox*) and *P-RIT*(*Dox*) at pH 7.4 was below 10% within 24 h and was much faster at pH 5.0 (55% of Dox released within 5 h). The release rate of the active agents is in agreement with published data [16,28,30]. Thus, we can conclude that attachment of both, drug and inhibitor, to single polymer chain does not change the release rate of the active compounds. In summary, the active agents can be released from the conjugates in the slightly acidic environment of the target tumor tissue or within the endosomes/lysosomes of tumor cells, whereas the conjugates keep their satisfactory stability at pH of blood circulation [30].

3.3. Characterization of neuroblastoma cell lines

Neuroblastomas are known for their clinical heterogeneity, which is caused by their diverse genotype and therefore phenotype [37]. Three pairs of NB cell lines (each pair consists of a parental and a Dox-resistant cell line) were characterized, and the treatment efficiency was subsequently evaluated in all of them. The NB cell lines NB3, NB3-Dox, NB4,

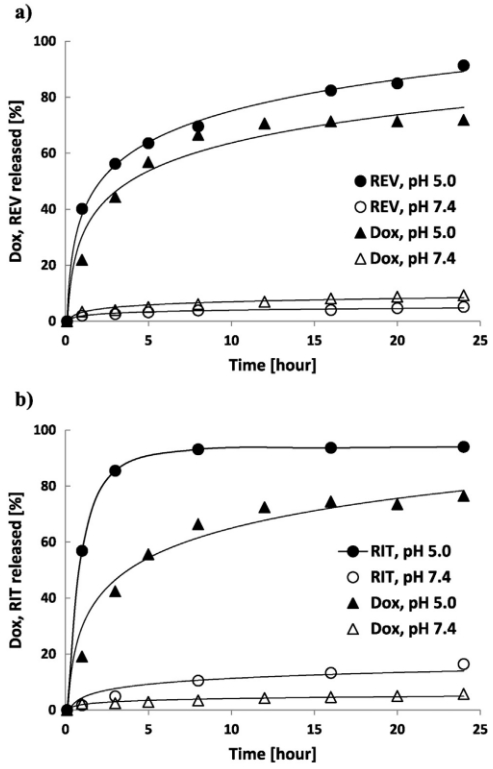

Fig. 3. *In vitro* release of Dox and P-gp inhibitor (REV, RIT) from polymer conjugates *P-REV*(*Dox*) (a) and *P-RIT*(*Dox*) (b) in PBS buffer at pH 5.0 and 7.4; 37 °C. Standard deviation of the measurements was < 10%.

NB4-Dox, IMR32, and IMR32-Dox were cultivated as described in the Materials and Methods. The cell lines were analyzed between passages 2–5 from refreezing to minimize changes caused by long-term passaging. The cells were characterized for their P-gp content at the mRNA and protein level.

3.3.1. ABCB1 mRNA expression in neuroblastoma cell lines

The overexpression of P-gp plays a crucial role in the resistance to several cytostatic drugs including Dox in cancer cells. The mRNA level of the ABCB1 gene, which encodes P-gp, was determined using real-time PCR. The relative quantification of gene expression was determined using the $2^{-\Delta\Delta C_T}$ method [33]. According to the real-time PCR results, P-gp expression was significantly higher in the Dox-resistant cell lines compared with the parental cell lines (see Fig. 4). The NB3-Dox cell line exhibited the highest ABCB1 gene expression, and the IMR32-Dox resistant cell line exhibited the lowest expression. As for the parental cell lines, NB4 that was established from chemoresistant recurrent neuroblastoma showed a significantly higher level of ABCB1 gene expression compared with NB3 and IMR32 that were established from tumors before chemotherapy.

The gene expression of other common markers that cause MDR (ABCG2, ABCC1 and ABCC2) was also evaluated in the resistant and parental cells by real-time PCR. The expression levels of these tested markers were negligible in the parental cell lines and did not change significantly in resistant cell lines (unpublished results).

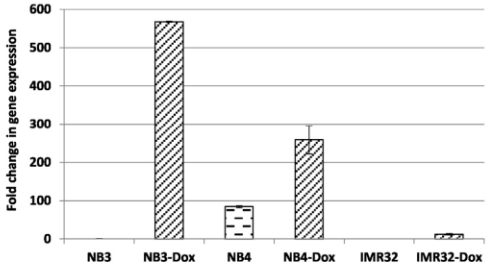

Fig. 4. Changes in ABCB1 gene expression in parental and Dox-resistant NB cell lines. The ABCB1 gene expression level of NB3 was used as the basal level.

3.3.2. NB cell characterization at the protein level

To verify the elevated expression of P-gp not only at the mRNA level but also at the protein level, the presence and level of P-gp were evaluated in all six NB cell lines using flow cytometry (see Fig. 5). The NB4 parental cell line expressed the highest level of P-gp compared with the IMR32 and NB3 cell lines, consistent with the mRNA expression results. The highest median fluorescent intensity of labeled P-gp was detected in the NB4-Dox cell line, which corresponds to previously published data [31]. However, NB3-Dox showed no significant difference in P-gp expression compared with the NB4-Dox cell line. The median fluorescent intensity of labeled NB3-Dox was only 1.3 times lower than that of NB4-Dox. Due to the elevated P-gp expression level in the NB4 parental cell line, NB4-Dox expresses only 4 times more P-gp than the parental cell line, compared with NB3-Dox, which expresses 118 times more P-gp than its parental cell line. The IMR32-Dox cell line expresses very low level of P-gp, which is only 2 times higher than that of the parental IMR32 cell line.

3.3.3. In vitro inhibitory activity of conjugates P-REV and P-RIT

The increased P-gp expression in NB4-Dox and NB3-Dox cells was confirmed at both the mRNA and protein level. Therefore, the ability to block MDR pumps with the free inhibitors REV and RIT (see Fig. 4 in the supplement file) and the polymer conjugates *P-REV* and *P-RIT* (see Fig. 6) was studied in NB4-Dox and NB3-Dox cell lines using the Calcein^{AM} efflux assay.

The most effective inhibition induced by the inhibitor derivatives, REV and RIT, was reached after 0.5 to 2 h of incubation (see Fig. 3 in the supporting information). The decrease in P-gp inhibition shown in the figure documents rather cytotoxic effect of inhibitors. At highest inhibitor concentrations the cells stopped proliferation and thus the signal of incorporated calcein was lower. The measured IC50 for P-gp inhibitor RIT was 20–30 μM for parental and resistant NB4 and NB3 cell lines, for REV the IC50 was in the same range for NB4/NB4-Dox and for NB3/NB3-Dox cell lines was lower, between 10 and 20 μM. In contrast to that, for the polymer conjugates *P-REV* and *P-RIT* the most effective inhibition was reached after 8 to 18 h of incubation time. Parental cell lines and IMR32-Dox cells incubated with inhibitors showed no difference in the accumulation of Calcein^{AM} compared with control cells without inhibitors (data not shown).

3.4. In vitro cytotoxicity of polymer-bound anthracyclines and P-gp inhibitors

We tested the cytotoxic effect of polymer conjugates with Dox and THP, as well as the enhancement of their cytotoxicity by the addition of polymer bound P-gp inhibitors, REV and RIT, on 3 different Dox-resistant NB cells lines – NB4-Dox, NB3-Dox, and IMR32-Dox. The parental non-resistant cell lines NB4, NB3 and IMR32 were used as controls.

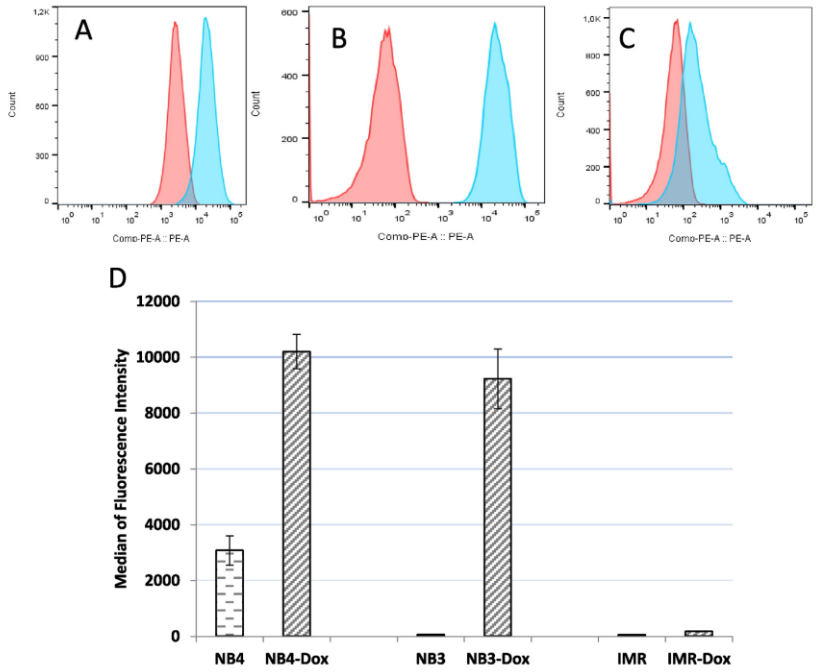

Fig. 5. Expression of P-gp in parental and Dox-resistant cell lines evaluated by FACS. Red histogram - parental cell line, blue histogram - resistant cell line; A-NB4/NB4-Dox cell lines; B-NB3/NB3-Dox cell lines; C-IMR32/IMR32_Dox cell lines; D-bar graph of flow cytometry data (n = 3).

3.4.1. In vitro cytotoxic activity of the conjugates P-Dox and P-THP in parental and Dox-resistant cell lines

The ability of the polymer conjugate *P-THP* to overcome MDR in Dox-resistant NB cell lines was tested in comparison with the conjugate *P-Dox*. The IC50 values of *P-THP* and *P-Dox* are displayed in Table 2.

The Dox-resistant cell lines NB4-Dox and NB3-Dox were both significantly less sensitive to treatment with conjugate *P-Dox* ($P < 0.0001$) compared with the parental cell lines, whereas the difference between the IC50s of *P-Dox* for the IMR32-Dox and IMR32 cell lines were not significant due to the low P-gp expression in IMR32-Dox. The highest resistance factor RF for *P-Dox* was observed for the NB3-Dox/NB3 cell lines ($RF = 363$), where the increase in P-gp mRNA expression in NB3-Dox compared with NB3 was the highest of all the tested cell lines. The RF for *P-Dox* was lower for the NB4-Dox/NB4 cell lines ($RF = 19$), because the parental NB4 cell line exhibits the highest *P*-gp expression compared with the other two parental cell lines. *P*-gp expression in the IMR32-Dox cell line is lower compared with the NB4-Dox and NB3-Dox cell lines, therefore the RF for *P-Dox* was relatively low ($RF = 2.0$).

The increase in the IC50 values of *P-THP* in Dox-resistant cells compared with the parental cells was also significant only for NB4-Dox and NB3-Dox ($P < 0.01$). The RFs for *P-THP* were 51, 23 and 2.0 for NB4-Dox, NB3-Dox and IMR32-Dox, respectively. The increase in IC50 values indicates that neither *P-Dox* nor *P-THP* conjugates could completely overcome MDR in the Dox-resistant NB4-Dox, NB3-Dox and IMR32-Dox cell lines, which differ in their expression of P-gp.

P-THP showed generally higher cytotoxicity compared with that of conjugate *P-Dox*. The higher cytotoxicity of *P-THP* may be explained by quicker uptake of THP released from the conjugate in incubation media and its conjugate by the cells compared with the uptake of free Dox and its conjugate *P-Dox* [38] which is in good agreement with the much more rapid incorporation of free THP into tumor cells compared with Dox [17–19,30]. On the other hand, both treatment with *P-THP* and with *P-Dox* showed differing trends for the NB4/NB4-Dox, NB3/NB3-Dox and IMR32/IMR32-Dox cell lines. In the case of IMR32/IMR32-Dox, the difference in the IC50 of *P-THP* and *P-Dox* was minimal – < 1.5 times for IMR32 and 1.3 times for IMR32-Dox, which corresponds to the negligible increase in P-gp expression in the resistant cell line. In the case of NB4/NB4-Dox, the IC50 of *P-THP* was considerably lower than that of *P-Dox* for both cell lines – 15.3 times for NB4 and 5.7 times for NB4-Dox. The IC50 of *P-THP* for the NB3 cell line was similar to that of *P-Dox* (only 1.3 times lower) but was 20.7 times lower for the NB3-Dox cell line. The difference in cytotoxicity between the parental cell lines NB3 and NB4 corresponds to their distinct P-gp levels. The NB4 cell line behaves similarly to the resistant cell line, because its expression of MDR factors is believed to be higher than that of the NB3 cell line, which expresses minimal basal levels of P-gp. These results reflect the heterogeneity of NB cell lines and their diverse adaptation to drug treatment.

3.4.2. Sensitization of Dox-resistant cells to the cytotoxicity of polymer drug conjugates with P-gp inhibitors in vitro

Using different NB cell lines isolated from patients, we compared the cytotoxicity of *P-Dox* and *P-THP* with the cytotoxicity of the conjugates *P-REV*(*Dox*), *P-RIT*(*Dox*), *P-REV*(*THP*) and *P-RIT*(*THP*), which contain both drug and inhibitor attached simultaneously to the same polymer carrier *via* hydrazone bonds.

Moreover, we determined the cytotoxicity of the conjugates *P-Dox* and *P-THP* in NB cell lines that were pretreated with the conjugates *P-REV* and *P-RIT*. Two intervals of 8 h and 16 h were selected for the cell pretreatment based on the Calcein assays results for P-gp inhibition. In addition, the influence of the ratio of the polymer-inhibitor conjugates *P-REV* and *P-RIT* to the polymer-drug conjugates *P-Dox* and *P-THP* on

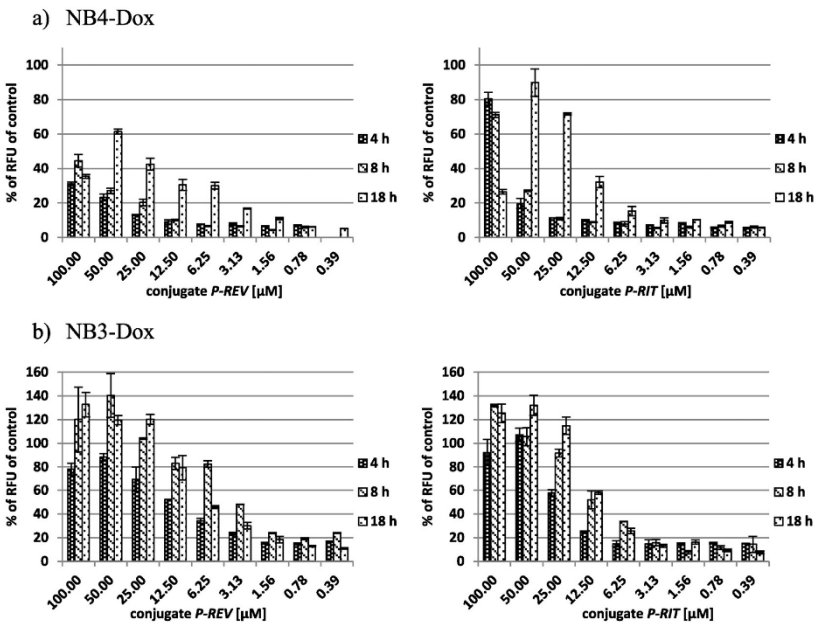

Fig. 6. Ability of polymer conjugates *P-REV* and *P-RIT* to inhibit P-gp function in NB3-Dox and NB4-Dox cells, as measured by the Calcein^{AM} efflux assay. Cyclosporine A was used as a control. The rate of Calcein^{AM} accumulation and thus the inhibitor efficacy of the tested conjugates were expressed as the percentage of relative fluorescence units (RFU) with respect to the control.

the IC50 for polymer cytostatics was studied. The ratio between polymer-bound inhibitor and polymer-bound drug was related to the molar ratio of inhibitor and drug bound to the polymer and is hereafter referred to as the inhibitor:drug (I:D) ratio.

The efficacy of treating NB3-Dox and NB4-Dox cell lines with conjugates that combine both a drug and an inhibitor or with polymer-drug and polymer-P-gp inhibitor mixtures is shown in Figs. 7 and 8. The absolute IC50 values are shown in Tables 1 and 2 in the supporting information.

Due to the low P-gp expression in IMR32-Dox, the difference in the IC50 values obtained for parental IMR32 and resistant IMR32-Dox was not substantial. In IMR32-Dox, treatment with the polymer-bound inhibitors did not considerably affect the cytotoxicity of the polymer-bound drugs (data not shown); therefore, further discussion of the efficacy of the combinatorial therapy concerns only the resistant NB3-Dox and NB4-Dox cell lines.

The conjugate *P-REV*(*Dox*) showed significantly ($P < 0.01$) higher cytotoxicity in the NB4-Dox and NB3-Dox cell lines compared with the *P-Dox* conjugate. These results are in agreement with results obtained previously for conjugate *P-REV*(*Dox*) in the Dox-resistant P388/MDR cell line [16]. When the cells were treated with combination of the conjugates, higher cytotoxicity than that of *P-REV*(*Dox*) was achieved in both cell lines with *P-Dox* pretreated with *P-REV* for 8 h or 16 h at both ratios of the conjugates (1:1 or 4:1). In general, longer pretreatment and higher I:D ratio led to higher cytotoxicity – the IC50 values decreased by up to 97% and 99% for the NB4-Dox and NB3-Dox cell lines, respectively. However, we observed slight differences between the efficiency of each treatment in the NB4-Dox and NB3-Dox cell lines. In the NB4-Dox cell line, the differences between each treatment were less pronounced than in the NB3-Dox cell line, where the cytotoxicity showed a steeper dependence on the pretreatment duration and the I:D ratio. These results can be explained by different adaptation of each cell line to the inhibitor treatment.

All of the *P-THP* treatments accompanied by *P-REV* pretreatment resulted in decreased IC50 values compared with the IC50 values obtained for single *P-THP* in both cell lines. Conjugate *P-REV*(*THP*) showed significantly ($P < 0.01$) higher cytotoxicity compared with conjugate *P-THP* in the NB4-Dox cell line; however, in the NB3-Dox cell line, the difference between the IC50 for *P-REV*(*THP*) and that for *P-THP* was not statistically significant. Interestingly, *P-REV*(*THP*) induced the highest cytotoxic effect in the NB4-Dox cell line (IC50 decreased by 90%), and a dependence of the cytotoxicity on the pretreatment duration or I:D ratio was not

Table 2
IC50 values (μM of Dox/THP eq.) for free Dox and THP and polymer conjugates *P-Dox* and *P-THP*.

Polymer conjugate	NB4	NB4-Dox		NB3	NB3-Dox		IMR32	IMR32-Dox	
	IC50	IC50	RF*	IC50	IC50	RF	IC50	IC50	RF
Dox	0.10 ± 0.02	6.77 ± 4.75		0.01 ± 0.002	0.78 ± 0.36		0.02 ± 0.02	0.05 ± 0.01	
THP	0.03 ± 0.01	7.67 ± 1.29		0.01 ± 0.001	0.10 ± 0.01		0.02 ± 0.001	0.03 ± 0.001	
P-Dox	2.3 ± 0.39	43.87 ± 3.93	19	0.04 ± 0.02	14.54 ± 0.41	363	0.06 ± 0.003	0.12 ± 0.001	2
P-THP	0.15 ± 0.02	7.67 ± 1.29	51	0.03 ± 0.01	0.7 ± 0.08	23	0.04 ± 0.003	0.09 ± 0.01	2

*RF** Resistance factor - $RF = \frac{IC50\ of\ resistant\ cells}{IC50\ of\ parental\ cells}$.

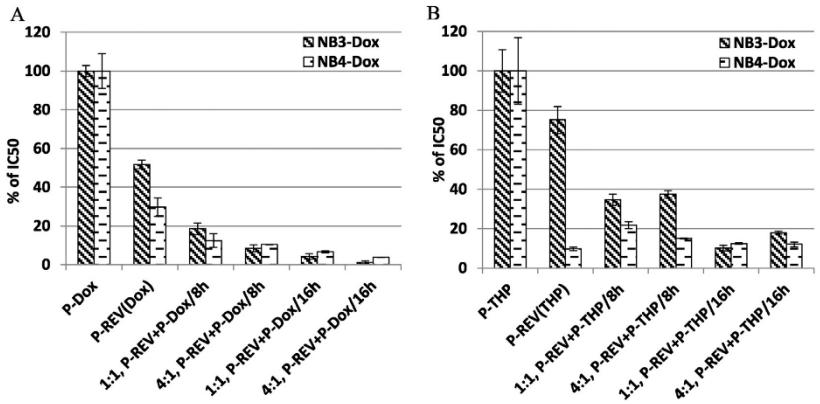

Fig. 7. Cytotoxicity of *P-REV*(*Dox*) (A), *P-REV*(*THP*) (B) and the combination of *P-REV* with *P-Dox* (A) or *P-THP* (B) against NB3-Dox and NB4-Dox. The efficacy of each treatment is displayed as the % decrease in the IC50, where 100% is the IC50 of the conjugates *P-Dox* or *P-THP*.

observed. In the NB3-Dox cell line, the 16 h pretreatment resulted in the most significant IC50 decrease (by 88%), whereas the I:D ratio did not affect the efficacy considerably. In general, the cytotoxicity of the THP conjugates was improved to a smaller extent than the cytotoxicity of the Dox conjugates by combined treatment with the inhibitor conjugates. These differences could be caused by faster penetration of THP conjugates through the plasma membrane and their faster accumulation inside cancer cells compared with the Dox conjugates.

As shown by confocal microscopy, fluorescence signal of THP in comparison with Dox after 24 h incubation of NB4-Dox cells with polymer conjugates *P-Dox* and *P-THP* (see Fig. 4A in supporting information) is significantly higher which proves faster (the signal of THP was detected earlier than signal of Dox (data not shown)) and more effective uptake of THP by these cells and which corresponds to higher toxicity of *P-THP* (Table 2). This is in line with the data obtained in more detailed study by Nakamura H. et al. [38].

Dox and THP after 24 h incubation of NB4-Dox cells with *P-REV*(*Dox*), *P-REV*(*THP*), *P-RIT*(*Dox*) and *P-RIT*(*THP*) exhibited higher fluorescence than in cells incubated with *P-Dox* resp. *P-THP* (Fig. 4, A-C in supporting informations) which could be connected with the ability of RIT and REV to facilitate transport of the conjugates through the cells membrane.

The highest fluorescence intensity of Dox and THP was observed when the NB4-Dox cells were by 8 or 16 h preincubated with *P-REV* or *P-RIT* before treatment with *P-Dox* or *P-THP* (data for 16 h preincubation are given in Fig. 4, D-E in supporting information).

The signals of both anthracyclines were localized in cytoplasm and slightly in nucleus after 24 h incubation. There are also marked signals localized in vesicles, which can be partly due to the type of cell line and partly due to characteristics of this type of polymer endocytosis pathway.

In addition, the response to each treatment was different in the NB3-Dox and NB4-Dox cell lines. The NB4-Dox cell line is less sensitive to cytotoxic treatment probably because its parental cell line already exhibits some attributes of MDR. The absolute IC50 values for the NB4-Dox cell line are higher for each treatment than the corresponding IC50 values for the NB3-Dox cell line (see the Tables 1 and 2 in the supplement file). The feedback regulation of *P*-gp activity in the NB4-Dox cell line after treatment with polymer-bound inhibitors may prevent the IC50 values of the polymer-bound drugs from decreasing when compared to NB3 cell line.

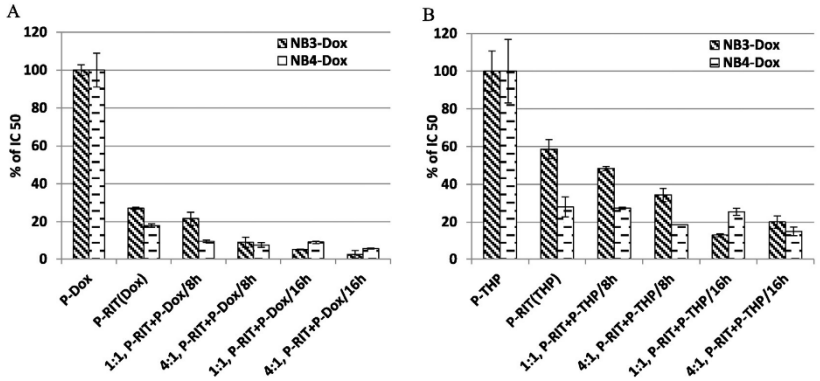

Fig. 8. The cytostatic activity of *P-RIT*(*Dox*) (A), *P-RIT*(*THP*) (B) and of the combination of *P-RIT* with *P-Dox* (A) or *P-THP* (B) against NB3-Dox and NB4-Dox. The efficacy of each treatment is displayed as the % decrease in IC50, where 100% is the IC50 of the conjugates *P-Dox* or *P-THP*.

Not only *P-REV*(*Dox*) but also *P-RIT*(*Dox*) showed significantly ($P < 0.01$) higher cytotoxicity in the NB4-Dox and NB3-Dox cell lines compared with *P-Dox*. In both cell lines, combined treatment with *P-RIT* and *P-Dox* was more efficient than that with *P-RIT*(*Dox*) and followed the same trend as the pretreatment with *P-REV* – the 16 h pretreatment with an I:D ratio of 4:1 was the most efficient treatment and improved the cytotoxicity by 95% and 92% for the NB3-Dox and NB4-Dox cell lines, respectively. In addition, the two resistant cell lines reacted differently to each treatment. In the NB3-Dox cell line, the time and ratio dependence of the cytotoxicity were steeper than in NB4-Dox cells, and the IC50 decrease was more pronounced.

Compared with *P-REV*(*THP*), the conjugate *P-RIT*(*THP*) showed significantly ($P < 0.05$) higher cytotoxicity than *P-THP* in both the NB4-Dox and NB-3-Dox cell lines. The impact of *P-RIT* addition on the cytotoxicity of *P-THP* followed approximately the same trend as for the polymer-bound REV, and compared with Dox conjugates, the cytotoxicity enhancement was less apparent. Furthermore, the *P-THP* cytotoxicity was dependent on the pretreatment duration in the NB3-Dox cell line, but compared with *P-REV*, mixtures with higher I:D ratios were more efficient with the 8 h pretreatment. As in the case of *P-REV*, the most effective treatment in the NB3-Dox cell line (IC50 decreased by 87%) consisted of 16 h pretreatment with *P-RIT* at I:D ratio of 1:1. The descending trend of IC50 with longer pretreatment and higher I:D ratio was also less pronounced in the NB4-Dox cell line, and the differences between each treatment with the *P-RIT* and *P-THP* or with *P-RIT*(*THP*) were less distinct than in the NB3-Dox cell line. However, unlike *P-REV*, the IC50 decrease with higher I:D ratio was significant ($P < 0.05$) for both treatments, and the most effective treatment in the NB4-Dox cell line was induced by *P-RIT* and *P-THP* at an I:D ratio 4:1 with a 16 h pretreatment (IC50 decreased by 85%).

4. Conclusions

HPMA copolymer conjugates with P-gp inhibitors derived from ritonavir or reversin 121 and/or with the anthracycline cytostatics Dox or THP were synthesized, and their cytotoxic activity was tested, as was their ability to overcome MDR. Neither Dox conjugate nor THP conjugate completely overcame MDR in the NB4-Dox and NB3-Dox resistant cells, as the IC50 values obtained upon treating the resistant cell lines with polymer cytostatics were higher than those obtained upon treatment of the corresponding parental cell lines. Compared with the Dox-containing conjugate, the conjugate containing THP exhibited higher cytotoxicity toward all of the Dox-resistant cell lines. In the NB4-Dox and NB3-Dox cell lines, the co-administration of the P-gp inhibitor conjugates decreased the IC50 values for both Dox- and THP-bearing conjugates. The sensitization of MDR cells was less pronounced for the THP conjugate and varied with different Dox-resistant cell lines. In general, a longer pretreatment period and a higher I:D ratio led to a higher cytotoxic effect. These results are unexpected in light of previous results showing that the conjugates *P-REV*(*Dox*) and *P-RIT*(*Dox*) were more efficient compared with a simultaneously added mixture of conjugates *P-REV* and *P-Dox* or *P-RIT* and *P-Dox* in the P388/MDR cell line [16]. We hypothesize that pretreatment facilitates inhibitor release from the conjugates and sufficient P-gp inhibition before exposure of the cells to the drug conjugate, whereas the simultaneous addition of the P-gp inhibitor conjugate and the drug conjugate did not have the same effect.

Suitable pretreatment with P-gp inhibitor conjugates played an important role in the eventual cytotoxicity of the drug conjugates, and the optimal dosage scheme varied for different Dox-resistant cell lines and for the polymer drug used (Dox or THP). Considerable differences between the sensitization efficacy of the two conjugates with the different P-gp inhibitors, RIT and REV, were not observed. The simultaneous tumor-specific delivery of these inhibitors together with cytostatic drugs conjugated to the same polymer carriers can significantly improve the treatment of resistant tumors thus documenting importance of P-gp inhibition in overcoming MDR.

Acknowledgement

The work was supported by the Czech Science Foundation (Grant No. P301/12/1254) and Ministry of Education, Youth and Sports of the Czech Republic within the National Sustainability Program I (Project POLYMAT LO1507).

Appendix A. Supplementary data

Supplementary data to this article can be found online at http://dx.doi.org/10.1016/j.jconrel.2016.05.036.

References

[1] J.M. Maris, K.K. Matthay, Molecular biology of neuroblastoma, J. Clin. Oncol. 17 (1999) 2264–2279.
[2] M.M. Gottesman, T. Fojo, S.E. Bates, Multidrug resistance in cancer: role of ATP-dependent transporters, Nat. Rev. Cancer 2 (2002) 48–58.
[3] S.V. Ambudkar, S. Dey, C.A. Hrycyna, M. Ramachandra, I. Pastan, M.M. Gottesman, Biochemical, cellular, and pharmacological aspects of the multidrug transporter, Annu. Rev. Pharmacol. Toxicol. 39 (1999) 361–398.
[4] J.W. McCormick, P.D. Vogel, J.G. Wise, Multiple drug transport pathways through human P-glycoprotein, Biochemistry 54 (2015) 4374–4390.
[5] B.L. Lum, M.P. Gosland, Mdr expression in normal-tissues — pharmacological implications for the clinical use of P-glycoprotein Inhibitors, Hematol. Oncol. Clin. North Am. 9 (1995) 319–336.
[6] M. Falasca, K.J. Linton, Investigational ABC transporter inhibitors, Expert Opin. Investig. Drugs 21 (2012) 657–666.
[7] D.R. Ferry, H. Traunecker, D.J. Kerr, Clinical trials of P-glycoprotein reversal in solid tumours, Eur. J. Cancer 32A (1996) 1070–1081.
[8] A.K. Tiwari, K. Sodani, C.L. Dai, C.R. Ashby, Z.S. Chen, Revisiting the ABCs of multidrug resistance in cancer chemotherapy, Curr. Pharm. Biotechnol. 12 (2011) 570–594.
[9] H. Maeda, Y. Matsumura, Tumoritropic and lymphotropic principles of macromolecular drugs, crit. Rev. Ther. Drug Carrier Syst. 6 (1989) 193–210.
[10] A. Ganoth, K.C. Merimi, D. Peer, Overcoming multidrug resistance with nanomedicines, Expert Opin. Drug Deliv. 12 (2015) 223–238.
[11] S. Kunjachan, B. Rychlik, G. Storm, F. Kiessling, T. Lammers, Multidrug resistance: physiological principles and nanomedical solutions, Adv. Drug Deliv. Rev. 65 (2013) 1852–1865.
[12] G.L. Beretta, F. Cavalieri, Engineering nanomedicines to overcome multidrug resistance in cancer therapy, Curr. Med. Chem. 23 (2016) 3–22.
[13] M. Šťastný, D. Plocová, T. Etrych, K. Ulbrich, B. Říhová, HPMA-hydrogels result in prolonged delivery of anticancer drugs and are a promising tool for the treatment of sensitive and multidrug resistant leukaemia, Eur. J. Cancer 38 (2002) 602–608.
[14] N.R. Patel, A. Rathi, D. Mongayt, V.P. Torchilin, Reversal of multidrug resistance by co-delivery of tariquidar (XR9576) and paclitaxel using long-circulating liposomes, Int. J. Pharm. 416 (2011) 296–299.
[15] Y. Patil, T. Sadhukha, L. Ma, J. Panyam, Nanoparticle-mediated simultaneous and targeted delivery of paclitaxel and tariquidar overcomes tumor drug resistance, J. Control. Release 136 (2009) 21–29.
[16] V. Šubr, L. Sivák, E. Koziolová, A. Braunová, M. Pechar, J. Strohalm, M. Kabešová, B. Říhová, K. Ulbrich, M. Kovář, Synthesis of poly[*N*-(2-hydroxypropyl)methacrylamide] conjugates of inhibitors of the ABC transporter that overcome multidrug resistance in doxorubicin-resistant P388 cells in vitro, Biomacromolecules 15 (2014) 3030–3043.
[17] S. Kunimoto, K. Miura, K. Umezawa, C.Z. Xu, T. Masuda, T. Takeuchi, H. Umezawa, Cellular uptake and efflux and cytostatic activity of 4′-O-tetrahydropyranyladriamycin in adriamycin-sensitive and resistant tumor-cell lines, J. Anthropol. 37 (1984) 1697–1702.
[18] S. Kunimoto, K. Miura, Y. Takahashi, T. Takeuchi, H. Umezawa, Rapid uptake by cultured tumor-cells and intracellular behavior of 4′-O-tetrahydropyranyladriamycin, J. Anthropol. 36 (1983) 312–317.
[19] T. Sugiyama, Y. Sadzuka, K. Nagasawa, N. Ohnishi, T. Yokoyama, T. Sonobe, Membrane transport and antitumor activity of pirarubicin, and comparison with those of doxorubicin, Jpn. J. Cancer Res. 90 (1999) 775–780.
[20] H. Dozono, S. Yanazune, H. Nakamura, T. Etrych, P. Chytil, K. Ulbrich, J. Fang, T. Arimura, T. Douchi, H. Kobayashi, M. Ikoma, H. Maeda, HPMA copolymer-conjugated pirarubicin in multimodal treatment of a patient with stage IV prostate cancer and extensive lung and bone metastases, Target. Oncol. 11 (2016) 101–106.
[21] J. Meesungnoen, J.P. Jay-Gerin, S. Mankhetkorn, Relation between MDR1 mRNA levels, resistance factor, and the efficiency of P-glycoprotein-mediated efflux of pirarubicin in multidrug-resistant K562 sublines, Can. J. Physiol. Pharmacol. 80 (2002) 1054–1063.
[22] D. Glowacka-Rogacka, M. Arciemiuk, A. Kupiec, M.M. Bontemps-Gracz, E. Borowski, J. Tarasiuk, The activity of latent benzoperimidine esters to inhibit P-glycoprotein and multidrug resistance-associated protein 1 dependent efflux of pirarubicin from several lines of multidrug resistant tumor cells, Cancer Detect. Prev. 28 (2004) 283–293.
[23] K. Wu, B. Wang, Y. Chen, J. Zhou, J. Huang, K. Hui, J. Zeng, J. Zhu, K. Zhang, L. Li, P. Guo, X. Wang, J.T. Hsieh, D. He, J. Fan, DAB2IP regulates the chemoresistance to pirarubicin and tumor recurrence of non-muscle invasive bladder cancer through STAT3/Twist1/P-glycoprotein signaling, Cell. Signal. 27 (2015) 2515–2523.

[24] T. Kubota, T. Furukawa, H. Tanino, S. Oura, H. Murata, S. Yuasa, K. Morita, J. Ueno, R. Kozakai, T. Yano, Pirarubicin might partly circumvent the P-glycoprotein-mediated drug resistance of human breast cancer tissues, Anticancer Res. 18 (1998) 967–972.
[25] T. Kubota, T. Furukawa, H. Tanino, A. Suto, Y. Otani, M. Watanabe, T. Ikeda, M. Kitajima, Resistant mechanisms of anthracyclines–pirarubicin might partly break through the P-glycoprotein-mediated drug-resistance of human breast cancer tissues, Breast Cancer 8 (2001) 333–338.
[26] C. Marbeuf-Gueye, D. Ettori, W. Priebe, H. Kozlowski, A. Garnier-Suillerot, Correlation between the kinetics of anthracycline uptake and the resistance factor in cancer cells expressing the multidrug resistance protein or the P-glycoprotein, Biochim. Biophys. Acta, Mol. Cell Res. 1450 (1999) 374–384.
[27] P. Chytil, T. Etrych, L. Kostka, K. Ulbrich, Hydrolytically degradable polymer micelles for anticancer drug delivery to solid tumors, Macromol. Chem. Phys. 213 (2012) 858–867.
[28] T. Etrych, T. Mrkvan, P. Chytil, Č. Koňák, B. Říhová, K. Ulbrich, *N*-(2-hydroxypropyl)methacrylamide-based polymer conjugates with pH-controlled activation of doxorubicin. I. New synthesis, physicochemical characterization and preliminary biological evaluation, J. Appl. Polym. Sci. 109 (2008) 3050–3061.
[29] T. Etrych, M. Jelínková, B. Říhová, K. Ulbrich, New HPMA copolymers containing doxorubicin bound via pH-sensitive linkage: synthesis and preliminary in vitro and in vivo biological properties, J. Control. Release 73 (2001) 89–102.
[30] H. Nakamura, T. Etrych, P. Chytil, M. Ohkubo, J. Fang, K. Ulbrich, H. Maeda, Two step mechanisms of tumor selective delivery of *N*-(2-hydroxypropyl)methacrylamide copolymer conjugated with pirarubicin via an acid-cleavable linkage, J. Control. Release 174 (2014) 81–87.
[31] J. Bedrníček, A. Vícha, M. Jarošová, M. Holzerová, J. Činátl, M. Michaelis, J. Činátl, T. Eckschlager, Characterization of drug-resistant neuroblastoma cell lines by comparative genomic hybridization, Neoplasma 52 (2005) 415–419.
[32] R.A. Blaheta, F.H. Daher, M. Michaelis, C. Hasenberg, E.M. Weich, D. Jonas, R. Kotchetkov, H.W. Doerr, J. Činátl Jr., Chemoresistance induces enhanced adhesion and transendothelial penetration of neuroblastoma cells by down-regulating NCAM surface expression, BMC Cancer 6 (2006) 294.
[33] K.J. Livak, T.D. Schmittgen, Analysis of relative gene expression data using real-time quantitative PCR and the $2^{-\Delta\Delta C_T}$ method, Methods 25 (2001) 402–408.
[34] P. Chytil, M. Šírová, E. Koziolová, K. Ulbrich, B. Říhová, T. Etrych, The comparison of in vivo properties of water-soluble HPMA-based polymer conjugates with doxorubicin prepared by controlled RAFT or free radical polymerization, Physiol. Res. 64 (Suppl. 1) (2015) S41–S49.
[35] L.E. Gerweck, K. Seetharaman, Cellular pH gradient in tumor versus normal tissue: potential exploitation for the treatment of cancer, Cancer Res. 56 (1996) 1194–1198.
[36] Selective endocytosis of macromolecular drug carriers, in: R. Duncan, J.R. Robinson, W.H.L. Lee (Eds.), Controlled Drug Delivry, CRC Press, Boca Raton 1987, pp. 581–621.
[37] G.M. Brodeur, A. Nakagawara, Molecular-basis of clinical heterogeneity in neuroblastoma, Am. J. Pediatric Hematol. Oncol. 14 (1992) 111–116.
[38] H. Nakamura, E. Koziolová, P. Chytil, K. Tsukigawa, J. Fang, M. Haratake, K. Ulbrich, T. Etrych, H. Maeda, Pronounced cellular uptake of pirarubicin in comparison with other anthracycline conjugates in the HPMA copolymer of pirarubicin and doxorubicin, Biomaterials (2016) submitted for publication.

Biomaterials 115 (2017) 65–80

Contents lists available at ScienceDirect

Biomaterials

journal homepage: www.elsevier.com/locate/biomaterials

Overcoming multidrug resistance via simultaneous delivery of cytostatic drug and P-glycoprotein inhibitor to cancer cells by HPMA copolymer conjugate

Ladislav Sivak [a], Vladimir Subr [b], Jakub Tomala [a], Blanka Rihova [a], Jiri Strohalm [b], Tomas Etrych [b], Marek Kovar [a, *]

[a] Institute of Microbiology of the Czech Academy of Sciences, v.v.i., Videnska 1083, 14220 Prague, Czechia
[b] Institute of Macromolecular Chemistry of the Czech Academy of Sciences, v.v.i., Heyrovskeho nam. 2, 16206 Prague, Czechia

ARTICLE INFO

Article history:
Received 27 July 2016
Received in revised form
9 November 2016
Accepted 11 November 2016
Available online 12 November 2016

Keywords:
Multidrug resistance
P-glycoprotein
Doxorubicin
Reversin 121
HPMA copolymer carrier
Polymer-drug conjugate

ABSTRACT

Multidrug resistance (MDR) is a common cause of failure in chemotherapy for malignant diseases. MDR is either acquired as a result of previous repeated exposure to cytostatic drugs (P388/MDR cells) or naturally, as some tumors are congenitally resistant to chemotherapy (CT26 cells). One of the most common mechanisms of MDR is upregulation of P-glycoprotein (P-gp) expression. Here, we used HPMA copolymer conjugates, whereby the cytostatic drug doxorubicin (Dox) or the derivative of the P-gp inhibitor reversin 121 (R121) or both were covalently bound through a degradable pH-sensitive hydrazone bond. We proved that R121, when bound to a polymeric carrier, is capable of inhibiting P-gp in P388/MDR cells and sensitizing them in relation to the cytostatic activity of Dox. Conjugate bearing both Dox and R121 was found to be far more potent in P388/MDR cells than conjugate bearing Dox alone or a mixture of conjugates bearing either Dox or R121 when cytostatic activity *in vitro*, cell cycle arrest, accumulation of Dox in cells and induction of apoptosis were determined. Importantly, conjugate bearing R121 is also effective *in vivo* as it inhibits P-gp in P388/MDR tumors after intraperitoneal administration, while both the conjugate bearing Dox and R121 induces apoptosis in P388/MDR tumors more effectively than conjugate bearing Dox alone. Only conjugate bearing Dox and R121 significantly inhibited P388/MDR tumor growth and led to the prolonged survival of treated mice. However, the most dramatic antitumor activity of this conjugate was found in the CT26 tumor model where it completely cured six out of eight experimental mice, while conjugate bearing Dox alone cured no mice.

© 2016 Elsevier Ltd. All rights reserved.

1. Introduction

Multidrug resistance (MDR) is defined as the cross-resistance or insensitivity of cancer cells to the cytostatic/cytotoxic actions of various anticancer drugs, which are structurally unrelated and have different molecular targets [1]. Two main types of MDR are found in tumors, namely, natural, in which tumor cells are congenitally resistant to chemotherapy, and acquired, which results from previous drug exposure [2]. One of the principal mechanisms by which many cancers develop MDR is upregulation of the P-glycoprotein (P-gp) expression. It is a broad-specificity transmembrane efflux pump belonging to ATP-binding cassette (ABC) transporters, which reduces intracellular concentration of a wide variety of drugs below the effective cytotoxic threshold [3–6].

Considerable effort has been devoted to the development of small molecules that can inhibit the function of P-gp in order to sensitize tumors to conventional chemotherapeutics [7–10]. Among them, a series of short hydrophobic peptides called reversins, which have the ability to increase the constitutive ATPase activity of P-gp, have been described [11]. The potential of different reversins to inhibit P-gp activity has been studied in various MDR cancer cell lines *in vitro*, with reversin 121 identified as the most promising P-gp inhibitor [12–14].

No P-gp inhibitor has been approved for clinical use so far, despite the considerable effort to develop such drugs [7]. This is mainly due to the low selectivity of P-gp inhibitors leading to intolerable toxicity of either the P-gp inhibitor itself or anticancer drugs upon coadministration with a P-gp inhibitor, since P-gp is

* Corresponding author.
E-mail address: makovar@biomed.cas.cz (M. Kovar).

http://dx.doi.org/10.1016/j.biomaterials.2016.11.013
0142-9612/© 2016 Elsevier Ltd. All rights reserved.

naturally expressed in a variety of tissues, such as the gut, liver or kidneys [15]. A relevant strategy would be to utilize drug delivery systems (DDSs), such as polymer-drug conjugates, liposomes, nanoparticles or self-assembled micelles, to ensure more selective delivery of the P-gp inhibitor and the cytostatic drug into the tumor [16–20]. These kinds of DDS possess a more favorable pharmacokinetic profile than parent cytostatic drugs and P-gp inhibitors. Moreover, they are passively accumulated in solid tumors due to the enhanced permeability and retention effect (EPR) [21]. Further, there are studies showing that some DDS are able, at least partially, to overcome P-gp-mediated MDR through intracellular delivery of cytostatic drugs [22–26].

In our previous work, we have synthesized a series of derivatives of reversin 121 containing carbonyl group enabling covalent linkage to the HPMA copolymer carrier through the hydrazone bond. Next, we tested these derivatives for their potential to inhibit P-gp. Reversin 121, modified with 5-methyl-4-oxohexanoic acid (henceforth R121), was found to be an even more potent P-gp inhibitor than unmodified reversin 121 and was chosen for further development. Additionally, we compared the cytotoxicity of two conjugates bearing either doxorubicin (Dox) or 4-*O*-tetrahydropyranyl doxorubicin (THP) administered together with P-gp inhibitor R121 or ritonavir modified with 5-methyl-4-oxohexanoic acid bound to the polymer carrier in Dox-resistant human neuroblastoma cell lines solely *in vitro*. Polymeric conjugates bearing R121 or ritonavir significantly increased cytotoxicity of the Dox/THP and mixture of conjugates bearing either ABC transporter inhibitor or Dox/THP was found to be more potent than conjugate bearing both [27].

In the present study, we designed, synthesized and tested *in vitro* and *in vivo* biologic activity of conjugates, bearing either Dox or the P-gp inhibitor R121, or both, which are bound via a pH-sensitive hydrazone bond to the HPMA copolymer carrier. Such conjugates have significantly prolonged half-life in circulation [28], improved solubility [29] and achieved targeted delivery of their payload into a solid tumor via the EPR effect [30–32]. Here, we have demonstrated that the codelivery of Dox and R121, which are bound to the same polymeric carrier, results in superior cytostatic/cytotoxic activity *in vitro* and antitumor activity *in vivo* in mouse tumor models with both acquired and natural MDR.

2. Materials and methods

2.1. Materials

Methacryloyl chloride, 1-amino-propan-2-ol, 2,2′-azobis(2-methylbutyronitrile) (AIBN), 4,5 dihydro-thiazole-2-thiol (TT), Boc-hydrazide, 2-cyanopropan-2-yl benzodithioate (CTA), succinic anhydride, iron(III) acetylacetonate, isopropylmagnesium chloride (2 M solution in THF), 4-(dimethylamino)pyridine (DMAP), *N*-ethyl-*N*′-(3-dimethylaminopropyl)carbodiimide hydrochloride (EDC), 2,4,6-trinitrobenzene sulfonic acid (TNBSA), *N*,*N*-diisopropylethylamine (DIPEA), *N*,*N*-dimethyl formamide (DMF), dimethyl sulfoxide (DMSO), *tert*-butyl alcohol (t-BuOH), dichloromethane (DCM) and silica gel 60 were purchased from Sigma-Aldrich in the Czech Republic. *N*-α-t-Boc-L-aspartic acid β-benzyl ester (Boc-Asp(OBzl)-OH), L-Aspartic acid β-benzyl ester (H-Asp(OBzl)-OH) and *N*-ε-CBZ-L-lysine *t*-butyl ester hydrochloride (H-Lys(Z)-OtBu.HCl) were purchased from Novabiochem. Doxorubicin hydrochloride (Dox.HCl) was purchased from Meiji Seika in Tokyo, Japan. Cy7.5 NHS ester was purchased from Lumiprobe GmbH in Hannover, Germany. Initiator 2,2′-azobis[2-(2-imidazolin-2-yl)propane]dihydrochloride (VA-044) was purchased from Wako Chemicals GmbH in Germany. All other chemicals and solvents were of analytical grade. The solvents were dried and purified using conventional procedures and distilled before use.

2.2. Synthesis of monomers, reversin derivative and chain transfer agent CPETC

N-(2-Hydroxypropyl)methacrylamide (HPMA) was synthesized as described previously [33].

N′-[6-(2-Methyl-acryloylamino)-hexanoyl]-hydrazine carboxylic acid *tert*-butyl ester (Ma-Ahx-NHNH-Boc) was prepared as described previously [34]. (6-Methacrylamido hexanoyl)hydrazine (Ma-Ahx-NHNH$_2$) was prepared as described previously [35]. 5-Methyl-4-oxohexanoic acid (MeOHe-OH) was synthesized according to Barberis et al. [36]. Reversin 121 derivative MeOHe-Asp(OBzl)-Lys(Z)-OtBu (R121) was prepared by two-step synthesis as described previously [34].

The trithiocarbonate chain transfer agent S-2-cyano-2-propyl S′-ethyl trithiocarbonate (CPETC) was synthesized as described by Ishitake et al. [37]. CPETC was obtained as a red-orange oil. The HPLC showed a single peak with a retention time at 10.7 min. ^{1}H NMR, δ: 1.36 (t, 3H, SCH2CH3), δ: 1.88 (s, 6H, C(CH3)2CN), δ: 3.35 (q, 2H, SCH2CH3).

2.3. Synthesis of the P-Ahx-NHNH$_2$ precursor and conjugates

The copolymer P-Ahx-NHNH-Boc was prepared by reversible addition–fragmentation chain transfer (RAFT) copolymerization of HPMA with Ma-Ahx-NHNH-Boc by using the chain transfer agent 2-cyanopropan-2-yl benzodithioate and the initiator AIBN at 70 °C for 16 h, as described previously [34]. The terminal dithiobenzoate group was removed using the method described in Perrier et al. [38]. The polymer precursor P-Ahx-NHNH$_2^*$ was prepared by removing the Boc protecting group in the presence of TFA [35]. The synthetic scheme is shown in Suppl. Scheme 1.

The copolymer P-Ahx-NHNH$_2^{\#}$ was prepared by RAFT copolymerization of HPMA (2.0 g, 14 mmol) with Ma-Ahx-NHNH$_2$ (0.330 g, 1.55 mmol) dissolved in 20 mL mixture of methanol/sodium acetate buffer, pH 5.2 (1:3), by using the chain transfer agent CPETC (14.3 mg, 0.0698 mmol) and the initiator VA-044 (7.45 mg, 0.023 mmol) at 45 °C for 5 h. The molar ratio of HPMA:Ma-Ahx-NHNH$_2$ was 90:10 and the ratio of monomers:CPETC:VA-044 was 200:1:0.33. The copolymer was isolated by column chromatography using Sephadex G-25 in distilled water, followed by lyophilization. The yield was 1.5 g (64%). The trithiocarbonate end group was removed using the method described previously [39]. The polymer was isolated by precipitation into ethyl acetate, then filtered off and dried in a vacuum. The synthetic scheme of polymer precursors P-NH-NH$_2^{\#}$ and P-NH-NH$_2^{\S}$ is shown in Suppl. Scheme 2.

The conjugate P-R121 was prepared from the polymer precursor P-Ahx-NH-NH$_2^*$ (1000 mg, 0.52 mmol NHNH$_2$ groups). The polymer was dissolved in dry methanol (7.0 mL) and R121 (150 mg, 0.225 mmol) was added, followed by the addition of acetic acid (140 μL). The reaction mixture was stirred for 16 h at room temperature (RT). The reaction mixture was then diluted with dry methanol (30 mL), while the conjugate P-R121 was purified by column chromatography using a Sephadex LH-20 column in methanol with UV detection at 220 nm. The compound was precipitated in ethyl acetate, isolated by filtration and dried under vacuum conditions. The yield was 1000 mg and the R121 content was 9.86 wt%.

The conjugate P-Dox was prepared by the same methods as P-R121. P-Ahx-NH-NH$_2^*$ (2000 mg, 1.09 mmol NHNH$_2$ groups) was dissolved in dry methanol (14.0 mL) and Dox.HCl (220 mg, 0.379 mmol) was added, followed by the addition of acetic acid

(280 μL). The reaction mixture was stirred for 16 h at RT. The reaction mixture was then diluted with dry methanol (60 mL), while the conjugate P-Dox was purified by column chromatography using a Sephadex LH-20 column in methanol with UV detection at 488 nm. The compound was precipitated into ethyl acetate, isolated by filtration and dried under vacuum conditions. The yield was 2000 mg and the Dox content was 9.65 wt%.

The conjugates P-R121(Dox) for simultaneous codelivery of both the drug and the inhibitor attached to the same polymer carrier were synthesized by the reaction of the polymer precursor P-Ahx-$NHNH_2^{\#}$ (1200 mg, 0.34 mmol $NHNH_2$ groups), R121 (200 mg, 0.3 mmol) and Dox (32.4 mg, 0.056 mmol) in dry methanol (8400 μL) on the addition of acetic acid (168 μL). The reaction was carried out for 16 h in the dark. The reaction mixture was diluted with dry methanol (40 mL), while the conjugate P-R121(Dox) was purified by column chromatography using a Sephadex LH-20 column using methanol as the mobile phase with UV detection at 488 nm. The conjugate was then precipitated into ethyl acetate, isolated by filtration and dried under vacuum conditions. The yield was 1100 mg of P-R121(Dox), which contained 9.9 wt% R121 and 2.63 wt% Dox. The structure and synthetic scheme of polymer conjugate P-R121(Dox) is shown in Suppl. Scheme 3.

The polymer conjugate P-R121stab(Dox) was prepared by two-step synthesis. In the first step, the hydrazone bond in P-R121 conjugate was stabilized by the reaction with sodium cyanoborohydride in methanol. The conjugate P-R121 (1550 mg) was dissolved in methanol (8.7 mL) and sodium cyanoborohydride (50 mg, 0.79 mmol) was added, followed by the addition of acetic acid (300 μL). The reaction mixture was stirred for 1 h at laboratory temperature. The conjugate P-R121stab was purified using a Sephadex LH-20 column with methanol, precipitated into ethyl acetate, filtered and dried in a vacuum. The yield was 1100 mg. In the second step, the Dox was bound to residual hydrazide groups by P-R121stab via a hydrazone bond with the same method as described above. The yield was 1.05 g, while the content of R121 was 12.8 wt% and Dox was 5.79 wt%. The synthetic scheme of polymer conjugate P-R121stab(Dox) is shown in Suppl. Scheme 4.

Polymer conjugate P-CY7.5(R121, Dox) was synthesized by two-step synthesis. The polymer precursor P-Ahx-NH-$NH_2^{\$}$ (350 mg, 0.16 mmol $NHNH_2$ groups) and CY7.5 NHS ester (4 mg, 0.0051 mmol) were dissolved in DMSO (1.9 mL), after which DIPEA (4 μL, 0.023 mmol) added. Reaction mixture was stirred for 16 h in the dark. The polymer, bound with CY7.5, was isolated by precipitation into ethyl acetate and dried in a vacuum. P-Cy7.5 (330 mg), R121 (42 mg, 0.063 mmol) and Dox (15 mg, 0.026 mmol) were dissolved in dry methanol (1.9 mL), after which acetic acid (70 μL) was added. The reaction was carried out for 16 h in the dark. The reaction mixture was diluted with dry methanol (2 mL), while the conjugate P-CY7.5(R121, Dox) was purified by column chromatography using a Sephadex LH-20 column with methanol as the mobile phase. The conjugate was then precipitated into ethyl acetate, isolated by filtration and dried under a vacuum. The yield was 320 mg of P-CY7.5(R121, Dox), which contained 9.07 wt% R121, 4.87 wt% Dox.HCl and 0.95 wt% Cy7.5. Structure and synthetic scheme of the polymer conjugate P-Cy7.5(R121, Dox) is shown in Suppl. Scheme 5.

2.4. Characterization of monomers, polymer precursors and conjugates

The structures of monomers and R121 were confirmed by ^1H NMR (300 MHz) using a Bruker DPX 300 spectrometer and elemental analysis, while their molecular weights were determined by a mass spectrometer (MS LCQ Fleet, Thermo Fisher Scientific).

The purity of monomers, the inhibitor derivative and CPETC was checked using a HPLC Shimadzu system with a reversed-phase column (Chromolith®HighResolution RP-18e, 100 × 4.6 mm) (Merck, Germany), which was equipped with a UV/VIS photodiode array detector. Gradient elution with 5–95% of acetonitrile for 15 min at a flow rate of 1.0 mL/min was used.

The number average molecular weights (M_n), the weight average molecular weights (M_w) and polydispersities ($Đ$) of the polymer precursors and conjugates were measured using size-exclusion chromatography (SEC) on an HPLC Shimadzu system equipped with a UV detector, an Optilab®rEX differential refractometer and a multi-angle light scattering DAWN® 8™ detector (Wyatt Technology, USA). The M_w, M_n and Đ were calculated using the Astra V software. The refractive index increment dn/dc = 0.167 mL/g was used for calculation. For these experiments, a 20% 0.3 M acetate:80% methanol (v/v) buffer, along with either a TSKgel G3000SW or a TSKgel G4000SW column, were used.

The hydrodynamic radius of conjugates (R_H) in phosphate buffers (pH 7.4, 0.1 M with 0.05 M NaCl) was determined by a Nano-ZS Zetasizer (model ZEN 3600, Malvern, UK). The polymer concentration was c = 5 g l^{-1}. The intensity of the scattered light was detected at an angle θ = 173° using a laser with a wavelength of 632.8 nm. The DTS (Nano) software was used for the dynamic light scattering data evaluation. The values were equivalent to the mean of at least five independent measurements. The values were not extrapolated to the zero concentration.

The Dox and CY7.5 content in conjugates was determined spectrophotometrically by a Specord 205 (Jena Analytics) spectrophotometer ($\varepsilon_{488,Dox}$ = 10,300 L mol^{-1} cm^{-1}; $\varepsilon_{786,Cy7.5}$ = 223,000 L mol^{-1} cm^{-1}), while the content of the hydrazide groups was determined by the TNBSA method (ε_{500} = 17,550 L mol^{-1} cm^{-1}; borate buffer pH 9.3).

The content of the R121 in the polymer conjugates was determined by amino acid analysis of the hydrolyzed polymer conjugates (6 M HCl, 115 °C, 18 h in a sealed ampoule) using a reversed-phase column (Chromolith®HighResolution RP-18e, 100 × 4.6 mm) (Merck, Germany) after pre-column derivatization with *o*-phthaldialdehyde (OPA) and 3-sulfanylpropanoic acid using a fluorescence detector (excitation at 229 nm, emission at 450 nm). Gradient elution, with 10–100% solvent B for 35 min at a flow rate of 1.0 mL/min, was used, where solvent A was 0.05 M of sodium acetate buffer, pH 6.5, and solvent B where solvent A was 0.05 M of sodium acetate buffer, pH 6.5, and solvent B was composed of 0.17 M sodium acetate (300 mL) and methanol (700 mL).

2.5. In vitro release of R121 and Dox from the polymer conjugate P-R121(Dox)

The release rates of R121 and Dox from the polymer conjugate P-R121(Dox) was investigated in phosphate buffers at pH 5.0 or 7.4 (0.1 M, with 0.05 M NaCl) at 37 °C. The amount of released R121 was determined after chloroform extraction R121 using HPLC with a reverse-phase column and UV-detection at 220 nm as previously described [34]. The amount of released Dox was determined by HPLC Shimadzu with a SEC column TSK 3000SW and UV detector. The 20% 0.3 M acetate: 80% methanol (v/v) buffer and flow rate 0.5 ml/min were used. The relative area of the peaks at 488 nm corresponds to the released Dox and the polymer-bound Dox. The values shown are the mean values obtained from three independent experiments.

2.6. Cell lines and cell cultures

The murine monocytic leukemia cell line P388 (parental cell line) and its Dox-resistant subline P388/MDR (cell line overexpresses P-gp) were obtained from Professor I. Lefkovits (Basel

Institute for Immunology, Basel, Switzerland). Both cell lines were propagated in RPMI-1640 medium (Sigma-Aldrich, Czech Republic), which was supplemented with heat-inactivated fetal bovine serum (FBS), 2 mM glutamine, 100 U/mL penicillin (Gibco™, BRL), 1 mM sodium pyruvate (Gibco™, BRL), 100 μg/mL streptomycin (Gibco™, UK) and 5 mL nonessential amino acids (Sigma-Aldrich, Czech Republic). The P388/MDR cells were grown in the continuous presence of 750 ng/mL of Dox to maintain the MDR-phenotype. One day before each experiment, the cells were transferred to Dox-free medium. The murine colon carcinoma cell line CT26 was purchased from ATCC (Manassas, VA, USA) as a model of natural Dox resistance. The CT26 (CRL-2638, *H-2^d*) cells were cultured in the same medium as the P388 cell line, but additionally supplemented with 4.5 g/L of glucose and 10 mM of HEPES. Cells showing exponential growth with viability greater than 95% were used for all experiments. Cultures were maintained under standard conditions (37 °C, 5% CO_2 atmosphere). All cell lines were tested for mycoplasma infection (MycoAlert Mycoplasma Detection Kit, Lonza, Switzerland).

2.7. Mice

Mice of the inbred strain DBA/2NCrl (*H-2^d*) were obtained from Charles River's breeding colonies (Charles Rivers, Sulzfeld, Germany). Inbred Balb/c (*H-2^d*) mice were obtained from the animal facility at the Institute of Physiology in the Academy of Sciences of the Czech Republic, v.v.i. Female athymic CD1 Nu/Nu (nude) mice (seven to nine weeks old, 20 g on average) were obtained from Charles River's breeding colonies (Charles Rivers, Sulzfeld, Germany). Food and water were given *ad libitum* to the mice, which were aged between nine and 15 weeks of age and in the 19–22 g weight range. In all animal work, institutional guidelines for the care and use of laboratory animals were strictly followed in line with a protocol approved by the Institutional Animal Care and Use Committee of the Academy of Sciences of the Czech Republic, as well as conducted in compliance with local and European guidelines.

2.8. Cellular drug sensitivity assay

To test the cytostatic activity of the drugs in the presence or absence of chemosensitizers, cell growth inhibition was determined using the [^{3}H]-thymidine incorporation assay. The cells (1×10^4 per well for P388 and P388/MDR, or 5×10^3 per well for CT26) were seeded in a 96-well flat bottom tissue culture plate (Nunc, Denmark). Various concentrations of the samples were added to the wells to reach a final volume of 250 μL. Triplicate wells were used for each test condition. The plates were incubated in a 5% CO_2 atmosphere at 37 °C for 72 h. After the incubation period, each well was pulsed with 1 μCi (37 kBq) of [^{3}H]-thymidine for 6 h. The cells were then collected on glass fiber filters (Filterman, Wallac, Finland) using a cell harvester (Tomtec, Orange, CT, USA), while the radioactivity of the samples was measured in a scintillation counter (1450 Microbeta TriLux, Wallac, Finland). Cells cultivated in a fresh medium were used as controls. The activity of control cells was always higher than 30,000 cpm/well. The inhibition of tumor cell growth is expressed as the IC_{50}, that is, the concentration of Dox (or equivalent) that inhibited cell growth by 50%. All reported IC_{50} values are the mean of at least three independent experiments.

2.9. Calcein efflux assay

The P388/MDR and CT26 cells were seeded at a concentration of 1×10^5 per well (150 μL per well) in culture medium. Then, 50 μL of the tested compounds or controls (in duplicate) were added and the cells were incubated for 8 or 16 h. After the incubation period, calcein acetoxymethyl ester (calcein) was added (final concentration: 0.2 μM), and the cells were incubated for another 30 min in the dark. After the incubation period, the CT26 cells were detached by phosphate-buffered saline (PBS) supplemented with 1% bovine serum albumin (Sigma-Aldrich, Czech Republic), 1 mM of EDTA (GibcoTM, BRL) and 1 mM of EFTA (Sigma-Aldrich, Czech Republic). Both cell lines were then washed and centrifuged twice (200G, 5 min, 4 °C) with 200 μL and resuspended in 100 μL of cold FACS buffer (PBS with 2% FCS and 2 mmol of EDTA). The flow cytometric analysis was performed using the LSRII instrument (BD Bioscience), while the data were analyzed using FlowJo software (Tree Star, Inc., Ashland, OR, USA). Nonliving cells were detected and gated out using Hoechst 33258 staining (Sigma-Aldrich, Czech Republic). The total number of cells counted per well was 50,000. All incubation steps were conducted in a 5% CO_2-humidified atmosphere at 37 °C. The results are reported as an average of three independent experiments, each conducted in duplicate.

2.10. Measurement of apoptosis

The pattern of cell death was determined using flow cytometry by simultaneous staining with Annexin V-Dyomics 647 (Appronex, Czech Republic) and Hoechst 33258 (Invitrogen, USA). Annexin V has a high affinity with phosphatidylserine, which is translocated from the inner to the outer leaflet of the plasma membrane at an early stage of apoptosis. The use of Hoechst 33258 helps distinguish between apoptosis and necrosis due to the difference in the permeability of cell membranes of live and damaged cells. P388/MDR and CT26 cells were seeded at a concentration of 1×10^5 cells per well in 100 μL of culture medium using 96-well flat bottom tissue culture plates (Nunc, Denmark). Subsequently, 50 μL of the desired concentrations of the inhibitors and cytostatic drugs were added to the final volume of 200 μL. Following treatments for 24 h (the incubation steps were conducted in a 5% CO_2-humidified atmosphere at 37 °C), the cells were collected by centrifugation (200G, 5 min, 4 °C), transferred into 96-well culture tissue plates with a conical bottom (Nunc, Denmark) and washed twice with 200 μL of annexin binding buffer (10 mM HEPES buffer, 140 mM NaCl, 2 mM $CaCl_2$, pH 7.4). Cells were then stained in 10 μL of Annexin V-Dyomics 647 (1:100) and incubated for 15 min at RT in the dark. After the incubation period, the annexin binding buffer and Hoechst 33258 (0.1 μg/mL) were added to the final volume of 100 μL, then immediately analyzed using the LSRII instrument flow cytometer (BD Biosciences, USA). At least 50,000 cells were analyzed for each sample. Data were analyzed using FlowJo software (Tree Star, Inc., Ashland, OR, USA). The positioning of quadrants on Annexin V-Dyomics 647/Hoechst 33258 dot plots were performed to distinguish between living cells (annexin V / Hoechst), early apoptotic cells (annexin V$^+$/Hoechst), late apoptotic cells (annexin V$^+$/Hoechst$^+$) and necrotic cells (annexin V /Hoechst$^+$).

2.11. Cell cycle analysis

The cell cycle distribution was carried out by staining the DNA with propidium iodide (PI), followed by cytometric measurement of the fluorescence. The P388/MDR and CT26 cells were seeded at a density of 5×10^5 cells per well in 48-well culture tissue plates and incubated with the cytostatic drug in the presence or absence of P-gp inhibitors for 24 h in a 5% CO_2-humidified atmosphere at 37 °C. Following the treatments, the cells were harvested and washed twice with PBS. Then, the pellets were fixed with ice-cold 70% ethanol and stored at −4 °C overnight. After the incubation period, the cells were collected by centrifugation (850G, 10 min, 4 °C),

washed twice with ice-cold PBS and resuspended in 300 μL of PI staining solution, which contained 0.1% v/v of Triton X-100 (Sigma-Aldrich, Czech Republic), 50 μg/mL of RNase A (Sigma-Aldrich, Czech republic) and 50 μg/mL of PI (Sigma-Aldrich, Czech Republic). The cells were then incubated for 60 min at 4 °C in the dark. The labeled cells were analyzed by flow cytometry using the LSRII instrument (BD Biosciences, USA). Data were analyzed using FlowJo software (Tree Star, Inc., Ashland, OR, USA). For each experiment, 30,000 events per sample were recorded. The scale of cells in the G0/G1, S and G2/M phases was described as a DNA histogram.

2.12. Intracellular accumulation of Dox

To investigate the relationship between cytotoxicity and intracellular accumulation of chemotherapeutic agents, P388/MDR and CT26 cells were seeded into 96-well flat bottom tissue culture plates (Nunc, Denmark), at a density of 5×10^5 per well, and treated with different concentrations of free Dox or HPMA copolymer conjugate, bearing Dox via a hydrazone bond, in the presence or absence of a P-gp inhibitor for 24 h. After treatment, the cells were collected by centrifugation (200G, 5 min, 4 °C), transferred into 96-well culture tissue plates with a round bottom (TPP, Switzerland) and washed twice with 200 μL of ice-cold FACS buffer (PBS with 2% FCS and 2 mmol of EDTA). Cell pellets were resuspended in 100 μL of ice-cold FACS buffer and then analyzed by flow cytometry. Flow cytometric analysis was performed on an LSRII (BD Bioscience, USA) instrument, while the data were analyzed using FlowJo software (Tree Star, Inc., Ashland, OR, USA). The untreated cells served as a negative control. Nonliving cells were detected and gated out by Hoechst 33258 staining (Sigma-Aldrich, Czech Republic). For each experiment, 50,000 events per sample were recorded. The mean fluorescence signal was recorded in all experiments, which were repeated three times.

2.13. In situ P-glycoprotein assay

To determine whether P-R121 conjugate, bearing the P-gp inhibitor R121, selectively inhibits P-gp within the tumor, the female athymic CD1 NuNu (nude) mice (seven to nine weeks old, 20 g on average) were subcutaneously inoculated with 1×10^6 P388/MDR cells. Eight days after tumor inoculation, the mice that developed palpable tumors reaching 4–9 mm were randomly distributed into groups (three mice per group) and injected with a single 208 mg dose of R121/kg of P-R121 conjugate, bearing the P-gp inhibitor R121 bound via a hydrazone bond. The mice that were inoculated with the tumor cells and injected with PBS alone were used as controls. After 24 h or 48 h, the animals were sacrificed and a single cell suspension was prepared from harvested tumors by GentleMACS Dissociator (Miltenyi Biotec GmbH, Bergisch Gladbach, Germany). Afterwards, red blood cells (RBC) and lysis cells were resuspended in FACS buffer, calcein acetoxymethyl ester (calcein-AM) was added (final concentration 0.5 μM) and the cells were incubated for 30 min in the dark. After the incubation period, cells were resuspended in FACS buffer (PBS with 2% FCS and 2 mmol of EDTA), blocked by 20% mouse serum for 10 min on ice and stained with fluorochrome-labeled monoclonal antibody antimouse APC-MHC I (H2Kd, clone SF1-1.1.1, eBioscience, San Diego, CA, USA) or isotype control mouse APC-IgG1κ (clone P3.6.2.8.1, eBioscience, San Diego, CA, USA), which was diluted 1:200 in FACS buffer. Cells were then washed twice and analyzed using the LSRII instrument (BD Bioscience). Data were analyzed using FlowJo software (Tree Star, Inc., Ashland, OR, USA). Nonliving cells were detected and gated out using Hoechst 33258 staining (Sigma-Aldrich, Czech Republic). The results shown are representative plots of three experiments.

2.14. Immunohistochemical analysis of cleaved caspase-3

The immunohistochemical analysis of cleaved caspase-3 within the tumor was conducted to evaluate the therapeutic effect of HPMA copolymer conjugates on the process of cell apoptosis in which caspase-3 plays an irreplaceable role. Female DBA/2 mice (six to seven weeks old, 18–20 g) were subcutaneously transplanted with 1×10^6 P388/MDR on the right anterior shaven flank in 100 μl of sterile PBS. Eight days after tumor inoculation, the mice that developed palpable tumors reaching 4–9 mm were randomly distributed into groups (three mice per group), with a single 50 mg dose of Dox/kg of P-R121(Dox) or P-Dox conjugate administered intraperitoneally in 1 ml of sterile PBS. The doses of polymeric conjugates were determined as equivalents of Dox/kg, based on the mean body weight in every experimental group at the time of drug administration. The mice that were inoculated with the tumor cells and injected with PBS alone were used as controls. After 24 h or 48 h, the mice were sacrificed by cervical dislocation, while serial sections of a 5 μm thickness were from formalin-fixed, paraffin-embedded blocks and mounted on poly-*l*-lysine-coated glass slides (Menzel Gläser, Braunshwein, Germany) for hematoxylin and eosin staining, as well as cleaved caspase-3 immunohistochemical staining. Afterwards, tumor sections were dewaxed in xylene, rehydrated in graded alcohols and placed in dH_20. Antigen retrieval was performed by boiling in citrate buffer (pH 6.0) for 15 min. To reduce the nonspecific binding of the antibody, sections were incubated with 2% bovine serum albumin in Tris-buffered saline (TBS) for 30 min at RT. After quenching the endogenous peroxidases with 3% hydrogen peroxide in methanol for 30 min at RT, followed by two rinses with Tris-HCl buffer, the sections were incubated with rabbit anticleaved caspase-3 Asp-175 in a 1:100 dilution (Cell Signaling Technology, Beverly, MA, USA) for 1 h. After two washes in TBS the standard streptavidin-biotin-peroxidase complex technique, using 20 min of incubation with biotinylated linking antibody and peroxidase-labeled streptavidin was performed. 3,3-diaminobenzidine tetrachloride was used as a substrate chromogen solution for the development of the peroxidase activity. The immunohistochemical expression of cleaved caspase-3 was evaluated microscopically, then scanned and digitized using the virtual microscopy scanner Axio Scan.Z1 (Carl Zeiss, Jena, Germany) in brightfield mode. All sections were observed by an investigator who was blinded in line with the study protocol.

2.15. TUNEL assay

The presence of apoptotic cells within the tumor was determined using the In Situ Cell Death Detection Kit (Fluorescein, Roche Applied Science, Mannheim, Germany). Female DBA/2 mice (six to seven weeks old, 18–20 g) were subcutaneously transplanted with 1×10^6 P388/MDR on the right anterior shaven flank in 100 μl of sterile PBS. Eight days after tumor inoculation, the mice that developed palpable tumors reaching 4–9 mm were randomly distributed into groups (three mice per group) and injected with a single 50 mg dose of Dox/kg of P-R121(Dox) or P-Dox conjugate, which was administered intraperitoneally in 1 ml of sterile PBS. The doses of polymeric conjugates were determined as equivalents of Dox/kg, based on the mean body weight in every experimental group at the time of drug administration. The mice that were inoculated with the tumor cells and injected with PBS alone were used as controls. After 24 h or 48 h, mice were sacrificed and tumor tissues were harvested. Tissue block were embedded in OCT cryo-embedding media (Tissue Tek, Germantown, NY, USA) and immediately frozen in liquid nitrogen. Subsequently, the frozen sections (10 μm) were mounted on glass slides (SuperFrost, Menzel Gläser,

Braunshwein, Germany), dried overnight and stored at −20 °C until use. The TUNEL assay was performed by incubating frozen tumor sections with a TUNEL reaction mixture for 1 h. All sections were counterstained with DAPI (1 μg/ml) for 15 min at 37 °C. Finally, the sections were mounted with antifade mounting medium and analyzed with an Olympus FV-1000 confocal microscope (Olympus, Tokyo, Japan). The specificity of the TUNEL assay was tested by staining the sections with the labeling solution without terminal transfers (negative control). Random images were obtained, while the frequency of TUNEL-positive cells was determined using ImageJ software (National Institutes of Health, Bethesda, MD, USA) [40].

2.16. Whole body imaging of biodistribution of P-CY7.5(R121, DOX)

Nu/Nu (four per group) mice were subcutaneously injected with 5×10^6 P-388-MDR tumor cells in the left lower back region seven days prior to the intravenous application of 15 mg/kg of the Dox HPMA-based polymer conjugate P-CY7.5(R121, DOX), labeled with the NIR dye Cyanine 7.5 (CY7.5), for whole body imaging. All measurements were performed on a Bruker Xtreme instrument (Bruker Biospin). Each mouse was anesthetized (Zoletil, by IM) and measured at selected time points to acquire an X-ray image (general anatomy of the animal) and a fluorescence signature (fluorescence signal of the tracking dye). Fluorescence was acquired with an excitation wavelength set to 760 nm, while emission was taken via an 830/15 nm wavelength filter with an exposure time of 1 s. Molecular imaging software (Bruker Biospin) was used for quantification of fluorescence signal in tumors. X-ray image was generated by standard mild x-ray imaging (0.4 mm aluminum filter, energy 35 kV, exposure time 1 s).

2.17. In vivo toxicity

Tumor-free Balb/c mice (n = 5) were intraperitoneally injected with a single 50 mg/kg (Dox equivalent) dose of conjugates P-R121(Dox), P-Dox or 208 mg/kg (R121 equivalent) of P-R121, or with a mixture of conjugates P-Dox/P-R121. With the three-dose schedule, mice were injected with 25 mg/kg of P-R121(Dox) (Dox equivalent) on days −3, −6 and day 0 (the last dose). The mice that were injected with physiological solution (PBS) were used as controls. All mice were observed throughout the duration of the experiment for signs of dehydration, inability to eat or drink, weakness or change in activity level. The weight loss was monitored three times a week throughout the experiment. No *in vivo* toxicity was observed in any animal group following the treatment (weight loss should not exceed 15% of the body mass) [41].

2.18. Histopathological analysis

For the observation of potential side effects in the treated mice, a histological analysis was conducted of the five mice from the groups that were intraperitoneally injected in 1 ml of sterile PBS with a single 50 mg dose of Dox/kg or 208 mg of R121/kg or three 25 mg doses of Dox/kg of P-R121(Dox) conjugate on days −3, −6, and 0. The doses of polymeric conjugates were determined as equivalents of Dox/kg or the P-gp inhibitor R121/kg, based on the mean body weight in every experimental group at the time of drug administration. The mice that were inoculated with the tumor cells and injected with PBS alone were used as controls. Seven days after injection, the mice were sacrificed by cervical dislocation, with their organs (brain, heart, kidney, large intestine, liver, lung, lymph nodes, pancreas, skeletal muscle, small intestine, spleen and bone marrow) harvested. The tissue samples were fixed in 10% neutral buffered formalin for at least 48 h. The fixed samples were processed by standard histological methods using an automated tissue processor (Leica ASP6025, Leica Microsystems, Germany), after which they were embedded in paraffin blocks using a Leica EG 1150H paraffin embedding station (Leica Microsystems, Germany). Slices with a thickness of between 3 and 5 μm were cut from each sample using a microtome, were stained (Leica RM2255, Leica Microsystems, Germany) and mounted on standard glass slides (Bammed, Czech Republic). The slices were stained with hematoxylin and eosin (DiaPath Srl., Italy). The prepared samples were evaluated as light-microscopic images, which were obtained using a Carl Zeiss Axio Scope A1 (Carl Zeiss, Jena, Germany) and an Axio Scan.Z1 slide scanner (Carl Zeiss, Jena, Germany).

2.19. Serum biochemical analysis

Tumor-free mice Balb/c (n = 5) were intraperitoneally injected with a single dose of conjugate P-R121(Dox) (50 mg of Dox/kg), P-Dox (50 mg of Dox/kg), P-R121 (208 mg R121/kg) or with a mixture of conjugate P-Dox/P-R121. In the three-dose schedule, mice were administered with 25 mg of Dox/kg P-R121(Dox) conjugate on days −3, −6 and 0.200 μL of blood was collected from the tail vein two and nine days after the last dose of drug treatment using a Microvette 200 capillary (Sarstedt, Germany). Blood samples were incubated on ice for 30 min in order to coagulate them, after which they were centrifuged for 10 min at 300 G at RT. Using a fully automated clinical chemistry analyzer, serum biochemical analysis was performed. The levels of aspartate aminotransferase (AST) and alanine transaminase (ALT) were measured in order to evaluate liver functions. The serum creatinine kinase (CK) level was used as a marker for the diagnosis of cardiac toxicity. The serum level of

Table 1
Characteristics of polymer precursors and polymer conjugates.

HPMA copolymer precursors and conjugates	M_w	Đ	$NHNH_2$ content mol%	R121 content mol%/wt %	Dox content mol%/wt%	Cy7.5 content mol%/wt%	R_H [nm]
P-NH-NH_2^A	30,300	1.09	8.4	–	–	–	3.49 ± 0.29
P-NH-NH_2^B	35,300	1.10	6.8	–	–	–	3.71 ± 0.26
P-NH-NH_2^B	32,200	1.12	4.2	–	–	–	3.64 ± 0.32
P-R121	45,400	1.22	–	1.20/9.86	–	–	5.80 ± 0.27
P-R121stab	35,800	1.15	–	2.34/9.76	–	–	n.d.
P-R121(Dox)^A	40,600	1.16	–	1.01/3.83	3.99/13.17	–	n.d.
P-R121(Dox)^B	41,400	1.14	–	3.12/11.1	3.47/10.73	–	n.d.
P-R121(Dox)^C	39,600	1.15	–	3.19/12.9	1.57/5.16	–	n.d.
P-R121(Dox)	39,100	1.09	–	2.72/10.86	0.76/2.61	–	5.57 ± 0.26
P-R121(Dox)^D	42,300	1.16	–	2.83/11.31	0.56/1.95	–	n.d.
P-R121stab(Dox)	43,100	1.20	–	3.43/12.8	1.79/5.79	–	5.70 ± 0.72
P-Dox	41,400	1.07	–	–	2.66/9.65	–	3.82 ± 0.26
P-Cy7.5(R121, Dox)	n.d.[a]	n.d.	–	2.31/9.07	1.43/4.87	–/0.95	n.d.

[a] GPC profile of the fluorescently labeled conjugate was similar to that of the corresponding polymer precursor; however, the precise calculation of M_w cannot be executed due to the interaction of the LS detector laser light with the fluorescent dye.

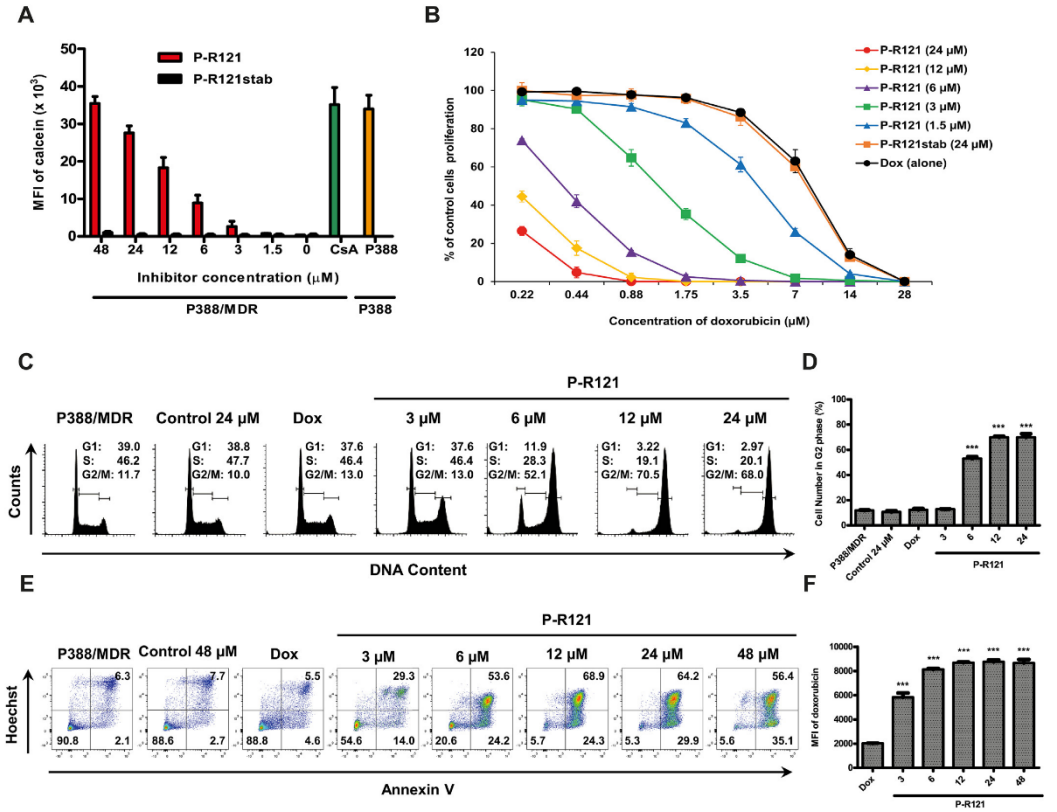

Fig. 1. Effect of conjugate P-R121 on P-gp function and cytotoxic activity of Dox in P388/MDR cells. (A) Capacity of conjugates P-R121 and P-R121stab, bearing P-gp inhibitor R121 via a pH-sensitive or non-biodegradable bond, respectively, to inhibit P-gp function in P388/MDR cells determined by calcein efflux assay after 16 h of incubation (5% CO_2, 37 °C). P388/MDR cells incubated with 10 μM of cyclosporine A and sensitive P388 cells incubated with calcein only were used as positive controls. Each experimental value is the average of three independent experiments ± SD. (B) Sensitization of P388/MDR cells to cytostatic activity of Dox with the titrated concentrations of conjugate P-R121 using [^{3}H]-thymidine incorporation assay. The results are shown as the proliferation of the exposed cells relative to controls (cells incubated in medium only). Each experimental point is the average of three experiments. (C) Flow cytometry analysis of cell cycle in P388/MDR cells exposed to 1.75 μM of Dox alone or in combination with various concentrations of conjugate P-R121 for 24 h. Representative histograms of three independent experiments are shown. (D) Percentage of cells in G2/M phase from three independent experiments as shown. (E) Apoptosis determined by annexin V/Hoechst 33258 after double staining in P388/MDR cells incubated in 14 μM Dox alone or together with titrated concentrations of conjugate P-R121 for 24 h. Numbers in each quadrant indicate the percentage of cells. The results shown are representative plots of three experiments. (F) Accumulation of Dox in P388/MDR cells incubated with Dox alone (14 μM) or in combination with titrated concentrations of conjugate P-R121 for 24 h. The results are expressed as a mean fluorescence intensity (MFI) of Dox ± SD. Significant differences from the respective control (Dox) are shown ($^{***}P \leq 0.001$).

creatinine was measured to assess the kidney functions.

2.20. Inhibition of tumor growth in vivo

The Dox-resistant subline of murine monocytic leukemia P388/MDR and murine colon carcinoma CT26 were used as drug-induced or natural resistance models, respectively, for the *in vivo* evaluation of antitumor activity of the linear *P*(HPMA) formulation of Dox. Female DBA/2 mice (six to seven weeks old, 18–20 g) and Balb/c mice (seven to eight weeks old, 20–22 g) were subcutaneously transplanted with 1×10^6 P388/MDR or 2×10^5 CT26 cells, respectively, on the right anterior shaven flank in 100 μl of sterile PBS. Eight days (for the P388/MDR xenograft tumor) or 10 days (for the CT26 xenograft tumor) after tumor inoculation, the mice that developed palpable tumors reaching 4–9 mm were randomly distributed into eight groups (eight mice per group) for different treatment. For the chemotherapy treatment groups, the mice received a single dose (on day eight for P388/MDR or on day 10 for CT26) of 50 mg of Dox/kg or 208 mg of R121/kg, or three doses (on days eight, 11 and 13 for P388/MDR or on days 10, 13 and 16 for CT26) of 25 mg of Dox/kg or 104 mg of R121/kg, which were administered intraperitoneally in 1 ml of sterile PBS. The mice that were inoculated with the tumor cells and injected with PBS alone were used as controls. The doses of polymeric conjugates were determined as equivalents of Dox/kg or the P-gp inhibitor R121/kg, based on the mean body weight in every experimental group at the time of drug administration. The animals were observed three times per week for signs of tumor progression. Measurements of tumor size were carried out using caliper. The tumor size, body weight and survival time were determined. The mice that survived

Table 2
IC_{50} values determined in multidrug resistant (P388/MDR) cell line for different HPMA copolymer conjugates.

Type of conjugate	IC_{50}[a] (μM of Dox eq.)
P-Dox	162 ± 12.5
P-R121(Dox)	4.78 ± 1.12
P-R121 + P-Dox	8.06 ± 0.85
P-R121stab(Dox)	154 ± 11.6

[a] IC_{50} (μM) values were calculated as a concentration of Dox, which inhibits the incorporation of [^{3}H]-thymidine into the exposed cells to 50% of the controls after 72 h of cultivation. Cells cultivated in the medium only were used as controls. The activity of control cells was always higher than 50,000 cpm/well. Experiments were repeated three to five times and average values ± SD shown. P-Dox: HPMA copolymer conjugate bearing Dox; P-R121: HPMA copolymer conjugate bearing R121; P-R121(Dox): HPMA copolymer conjugate bearing both Dox and R121 at a molar ratio of 1:1; P-R121stab(Dox): HPMA copolymer conjugate bearing both Dox and R121 with nondegradable bond between polymeric carrier and R121.

Table 3
IC_{50} values determined in multidrug resistant (P388/MDR) cell line for HPMA copolymer conjugate P-R121(Dox) at various R121:Dox ratios.

Type of conjugate	Molar ratio R121/Dox	IC_{50}[a] (μM of Dox eq.)
P-R121(Dox)^A	0.25:1	21.7 ± 0.92
P-R121(Dox)^B	1:1	4.78 ± 1.12
P-R121(Dox)^C	2:1	3.68 ± 0.48
P-R121(Dox)	4:1	2.81 ± 0.22
P-R121(Dox)^D	6:1	3.16 ± 0.36

[a] IC_{50} (μM) values were calculated as a concentration of Dox, which inhibits the incorporation of [^{3}H]-thymidine into the exposed cell to 50% of the controls after 72 h of cultivation. Cells cultivated in the medium only were used as controls. The activity of the control was always higher than 50,000 cpm/well. Experiments were repeated three to five times and average values ± SD are shown. P-R121(Dox): HPMA copolymer conjugate bearing both Dox and R121. [A,B,C,D] See Table 1 in Materials and Methods.

until day 120 without any signs of a tumor were considered as LTSs.

2.21. Statistical analysis

All experiments were carried out at least in triplicate and results were expressed as the mean ± standard deviation (SD). Statistical analysis was performed using GraphPad Prism (GraphPad Software, San Diego, CA, USA). The difference between the two groups was analyzed by the two-tailed Student's t-test. Multigroup comparisons of the means were carried out by the one-way analysis of variance (ANOVA) test followed by Dunnett's post hoc test in order to compare the difference between the experimental groups and the control group. Survival analysis was computed by the Kaplan-Meier method and compared using the log-rank test. The confidence level of the current study is 95%. Differences with $^*P \leq 0.05$, $^{**}P \leq 0.01$, $^{***}P \leq 0.001$ were considered as statistically significant.

3. Results and discussion

3.1. Synthesis of HPMA copolymer conjugates

The polymer precursors were prepared by RAFT copolymerization, resulting in the distribution of molecular weights (Đ) below 1.2 (see Materials and Methods, Table 1). As the polymer backbone of HPMA precursors is not biodegradable, precursors with an average molecular weight M_w under the renal filtration limit (M_w below 50,000 g/mol) were used as drug carriers. The use of the trithiocarbonate chain transfer agent S-2-cyano-2-propyl S′-ethyl trithiocarbonate (CPETC) enables the synthesis of P-Ahx-$NHNH_2^{\#}$ by copolymerization of HPMA with unprotected Ma-Ahx-$NHNH_2$. The polymer conjugates were synthesized by the reaction of hydrazide groups of P-Ahx-$NHNH_2$ with carbonyl groups of Dox and R121 in methanol in the presence of acetic acid. The inhibitor R121, which was selected on the basis of the previous results, exerts the highest difference in the release rate at pH 5.0 and pH 7.4 from the polymeric carrier out of all derivatives of reversin 121 tested [34].

The pH-sensitive hydrazone bond between the active agent and the polymer backbone is relatively stable at pH 7.4. The amount of R121 and Dox released from polymer conjugate P-R121(Dox) at pH 7.4 was below 10% within 24 h. However, the drug/inhibitor release rate from conjugate P-R121(Dox) in a mildly acidic environment of a tumor tissue (below pH 7.0) increases, reaching maximum at pH 5.0, modeling the environment in secondary endosomes and lysosomes (Suppl. Fig. 1).

3.2. HPMA copolymer conjugate bearing R121 bound through a hydrazone bond effectively inhibits P-gp activity and sensitizes P388/MDR cells to Dox

The HPMA copolymer conjugate bearing R121, bound through a pH-sensitive hydrazone bond, was tested in a P388/MDR cell line for the inhibition of P-gp activity. P388/MDR is a commonly used model of cancer cell line with acquired MDR [42,43]. It exerts a resistance to Dox that is about 1000 times higher in comparison to the drug-sensitive counterpart cell line P388 [44,45]. Conjugate with a nondegradable bond between the polymeric carrier and R121 (henceforth P-R121stab) was synthesized to confirm that P-gp inhibition is due to the release of R121 from the polymeric carrier. Conjugate P-R121 inhibits P-gp activity in a dose-dependent manner and completely blocks P-gp activity at a concentration of 48 μM (R121 equivalent), since calcein accumulation in P388/MDR cells was comparable to those incubated with 10 μM of cyclosporine A or to P388 sensitive cells (Fig. 1A). Control conjugate P-R121stab showed no effect on calcein accumulation in P388/MDR cells. Conjugate P-R121 also markedly sensitized P388/MDR cells to the cytostatic activity of Dox (~50 times), while the control conjugate had no effect (Fig. 1B). We recorded significant cell cycle arrest in the G2/M phase when P388/MDR cells were exposed to 1.75 μM of Dox plus titrated concentrations of conjugate P-R121 (Fig. 1C and D) but not to 1.75 μM of Dox alone, thereby further supporting the sensitization of P388/MDR cells to the cytostatic activity of Dox, since Dox is known to inhibit proliferating cells in the G2/M phase [46]. Conjugate P-R121 also sensitized P388/MDR cells to the cytotoxic activity of Dox as the percentage of live P388/MDR cells (annexin V /Hoechst) dramatically decreased when cells were incubated with 14 μM of Dox plus titrated concentrations of conjugate P-R121, but not with 14 μM of Dox alone (Fig. 1E). The decrease in life cell counts was accompanied by a robust increase in early (annexin V^+/Hoechst) and late (annexin V^+/$Hoechst^+$) apoptotic cells. We have also seen increased accumulation of Dox (~four times) in P388/MDR cells incubated with Dox and conjugate P-R121, in comparison to cells incubated with Dox only (Fig. 1F), thus providing further evidence that conjugate P-R121 effectively blocks P-gp in P388/MDR cells. Contrary, conjugate P-R121 had no effect on cytostatic and cytotoxic activity of Dox in drug-sensitive P388 cell line (Suppl. Fig. 2).

3.3. Superior cytostatic activity of HPMA copolymer conjugates bearing both Dox and R121 in P388/MDR cell line in vitro

Polymeric conjugate bearing only Dox (henceforth P-Dox) shows very low cytostatic activity in P388/MDR cells (Table 2). However, similar conjugate bearing both Dox and R121 at a molar ratio of 1:1 exerts cytostatic activity more than 30 times higher

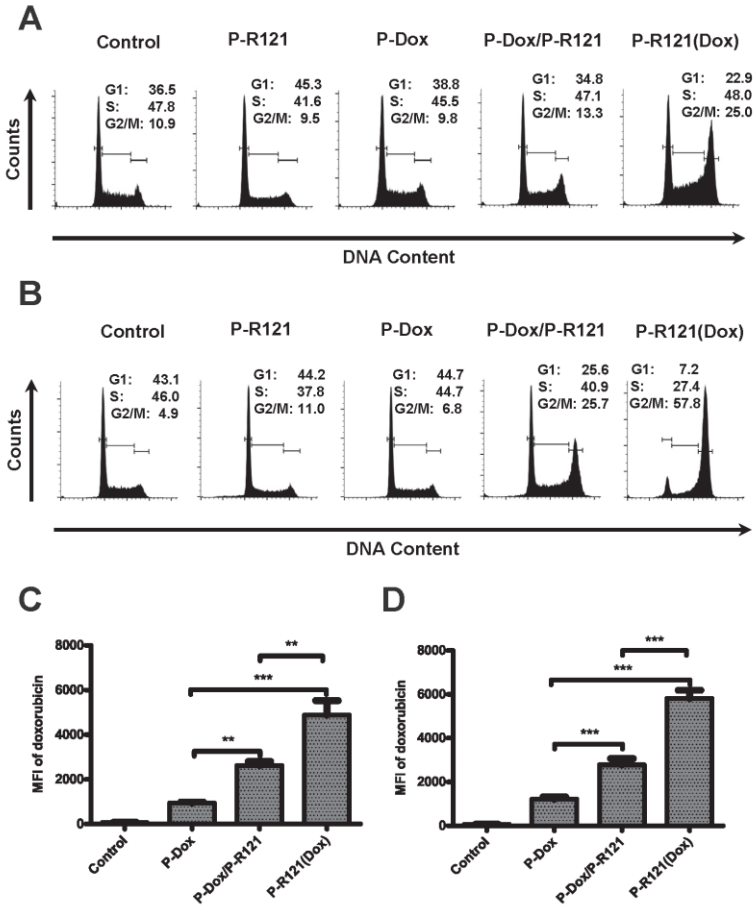

Fig. 2. The effect of conjugate P-R121(Dox) on cell cycle and accumulation of Dox in P388/MDR cells. P388/MDR cells were exposed to a 14 μM Dox concentration of conjugate P-R121(Dox), a mixture of conjugates P-Dox/P-R121 or conjugate P-Dox for 24 h (A) or 48 h (B), with the cell cycle analyzed by measuring DNA content after staining with propidium iodide using flow cytometry. Cells incubated in medium only and with P-R121 conjugate at the concentration of R121, corresponding to the same concentration as in case of conjugate P-R121(Dox), and a mixture of conjugates P-Dox/P-R121 were used as controls. The representative histograms of three independent experiments with similar results are shown. Accumulation of Dox in P388/MDR cells, incubated with conjugates bearing Dox or controls (cells incubated with medium only) after 24 h (C) and 48 h (D), were determined by flow cytometry. Results are expressed as MFI of Dox ± SD of at least three experiments. Significant differences are shown ($^{**}P \leq 0.01$, $^{***}P \leq 0.001$).

than P-Dox (IC_{50} being 162 μM vs. 4.78 μM Dox). Interestingly, a mixture of conjugates P-Dox and P-R121, at the same molar ratio (1:1), shows cytostatic activity that is about twice as low as conjugate bearing both Dox and R121. Thus, we proved that, when a cytostatic drug and a P-gp inhibitor are bound to the same polymeric chain, the *in vitro* cytostatic activity in P-gp-expressing cells is higher than in the corresponding mixture of two conjugates bearing either a cytostatic drug or a P-gp inhibitor. This is an opposite finding to that one we did previously in human neuroblastoma cell lines where mixture of conjugates bearing either P-gp inhibitor or cytostatic drug was more effective than conjugate bearing both [27]. However, tumor cells were pre-incubated with polymeric conjugate bearing P-gp inhibitor prior of adding polymeric conjugate bearing cytostatic drug in this study. Conjugate bearing both Dox and R121, where hydrazone bonds between polymeric carrier and R121 were reduced and thus made nondegradable (i.e., R121 is not released from conjugate, henceforth P-R121stab(Dox)), possesses comparable cytostatic activity to conjugate P-Dox in P388/MDR cells (Table 2).

Next, we have synthesized a series of conjugates bearing both R121 and Dox at different molar ratios (from 0.25:1 to 6:1). Table 3 shows that conjugate with a molar ratio R121:Dox corresponding to 4:1 is most effective in inhibiting the proliferation of P388/MDR cells *in vitro*. Thus, we decided that this conjugate (henceforth P-R121(Dox)) was used in further studies.

3.4. Cell cycle analysis, induction of apoptosis and Dox accumulation in P388/MDR cells exposed to conjugate P-R121(Dox)

P388/MDR cells incubated for 24 h with conjugate P-R121(Dox)

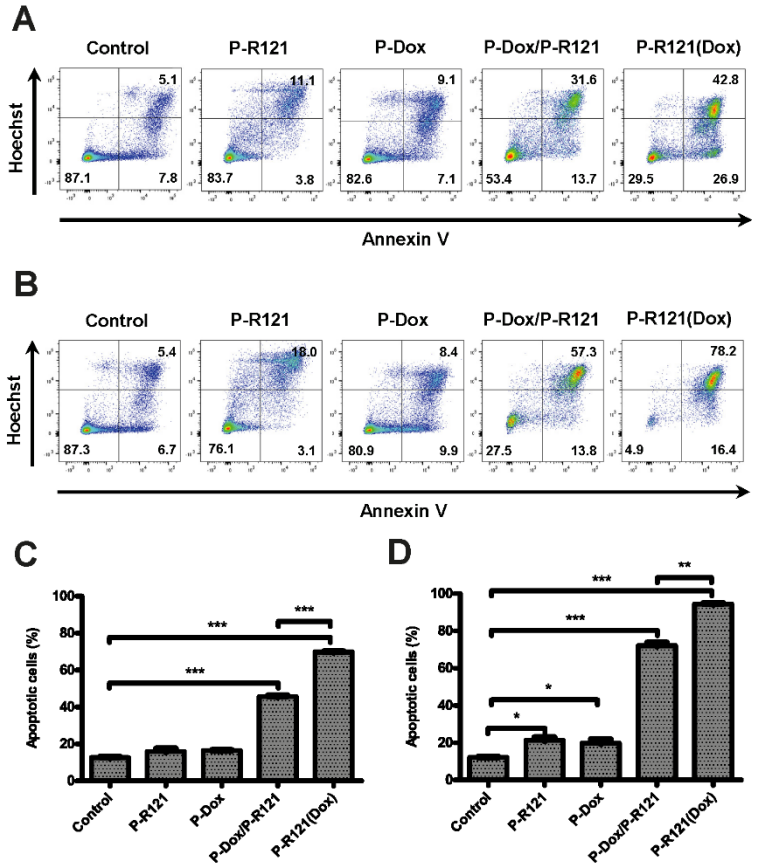

Fig. 3. The cytotoxicity of conjugate P-R121(Dox) in P388/MDR cells. Apoptosis was determined in P388/MDR cells incubated with a 14 μM Dox concentration of conjugate P-R121(Dox), a mixture of conjugates P-Dox/P-R121 or conjugate P-Dox for 24 h (A) or 48 h (B) by annexin V-FITC/Hoechst 33258 double staining using flow cytometry. The numbers in quadrants indicate the percentage of cells in the given population. The results are shown as representative plots from three independent experiments with similar results. The percentage of all apoptotic cells (early and late apoptosis) after 24 h (C) or 48 h (D) incubation from all three experiments are analyzed as a bar graph. Cells incubated in medium only and with P-R121 conjugate at the concentration of R121, corresponding to the same concentration as in P-R121(Dox) and P-Dox/P-R121, were used as controls. Significant differences are shown ($^{*}P \leq 0.05$, $^{**}P \leq 0.01$, $^{***}P \leq 0.001$).

at a concentration corresponding to 14 μM of Dox showed noticeable cell cycle arrest in the G2/M phase in comparison to control cells (~25% vs. 11% of cells in the G2/M phase; Fig. 2A). Neither cells incubated with conjugate P-Dox, nor cells incubated with a mixture of conjugates P-Dox and P-R121 at the same Dox concentration, showed cell cycle arrest in the G2/M phase. P388/MDR cells incubated with conjugate P-R121(Dox) for 48 h showed profound cell cycle arrest in the G2/M phase (58% of cells in the G2/M phase; Fig. 2B), while cells incubated with a mixture of conjugates P-Dox and P-R121 showed cell cycle arrest comparable to that seen with conjugate P-R121(Dox) after 24 h. Conjugate P-Dox did not show any effect after 48 h. P388/MDR cells incubated with conjugate P-R121(Dox) also showed a higher accumulation of Dox in comparison to a mixture of conjugates P-Dox and P-R121 (~two times) and in comparison to conjugate P-Dox (~five times), both at 24 h and 48 h time intervals (Fig. 2C and D). No cell cycle arrest (Suppl. Fig. 3A) or difference in Dox accumulation (Suppl. Fig. 3C) were observed after 24 h of incubation with respective conjugates in sensitive P388 cells.

Trends similar to those found in cell cycle arrest could be seen during the induction of apoptosis (Fig. 3). Conjugate P-R121(Dox) was more potent in inducing the apoptosis in P388/MDR cells than a mixture of conjugates P-Dox and P-R121 at both 24 h and 48 h time intervals. Conjugate P-Dox did not induce apoptosis at either time point when used at the same concentration of Dox (14 μM). Conjugate P-Dox, mixture of conjugates P-Dox and P-R121 and conjugate P-R121(Dox) had the same effect at the concentration of Dox 14 nM on induction of apoptosis (Suppl. Fig. 3B).

3.5. *Inhibition of P-gp and overcoming the MDR within P388/MDR tumors in situ*

To determine whether conjugate P-R121 is capable of inhibiting P-gp in MDR tumor cells *in vivo* after IP injection, we established

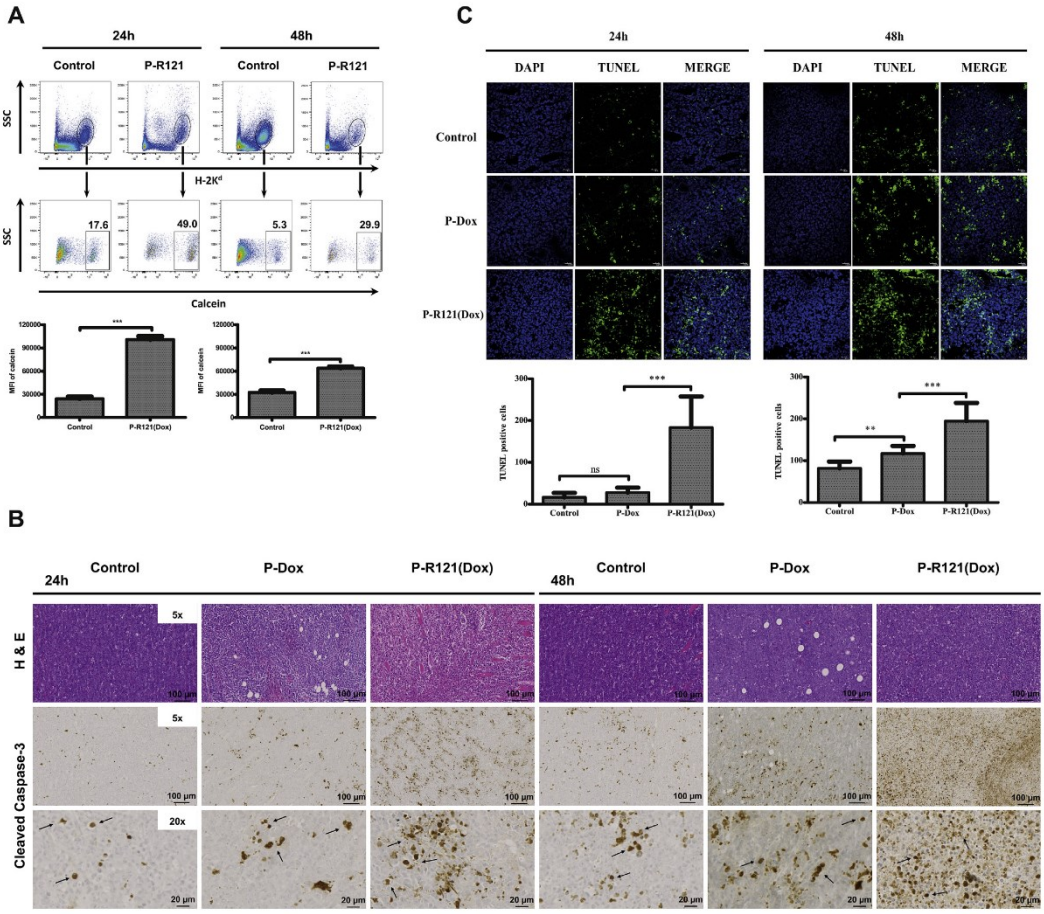

Fig. 4. Inhibition of P-gp with conjugate P-R121 and induction of apoptosis with P-R121(Dox) conjugate *in vivo*. (A) Nude mice were subcutaneously injected with 1×10^6 P388/MDR cells (H-2K^d). Mice with developed tumors of about 50–100 mm^2 were intraperitoneally injected with conjugate P-R121 (208 mg R121/kg). Mice were sacrificed 24 h or 48 h after injection and single cell suspension from tumors were incubated with calcein for 30 min *in vitro*, labeled with anti-H-2K^d mAb and analyzed by flow cytometry. Upper dot plots show the gating of tumor cells. The bottom dot plots show the accumulation of calcein in the cells. The quantification of MFI of calcein positive cells is shown in bar graphs for 24 h (left) and 48 h (right). (B) DBA/2 mice were subcutaneously inoculated with P388/MDR cells. Mice were intraperitoneally injected with conjugate P-R121(Dox) or P-Dox (50 mg of Dox/kg), when tumors reached the size of about 50–100 mm^2. Representative images of tumor sections examined by immunohistochemical staining for cleaved caspase-3 (middle and bottom rows) as well as histological hematoxylin and eosin staining (upper row). Cleaved caspase-3 positive cells are in brown. (C) Representative images of tumor sections, which were prepared as in (B), were examined by TUNEL assay. The quantification of TUNEL-positive cells from three independent experiments is shown in bar graphs. All data are the mean ± SD of at least three independent experiments performed. Significant differences are shown ($^{**}P \leq 0.01$, $^{***}P \leq 0.001$). (For interpretation of the references to colour in this figure legend, the reader is referred to the web version of this article.)

P388/MDR tumors (H-2K^d) in CD1 nude mice. Mice with tumors of an average size of 50–100 mm^2 were intraperitoneally injected with conjugate P-R121 and cells isolated from resected tumors either 24 h or 48 h after P-R121 administration were tested in calcein assay and analyzed by flow cytometry. Labeling with anti-H-2K^d mAb enabled us to identify the tumor cells. The higher fraction of tumor cells isolated from mice injected with P-R121 showed increased accumulation of calcein in comparison to tumor cells isolated from control mice at 24 h after injection (49% vs. 17.6%), as well as at 48 h after injection (29.9% vs. 5.3%), as seen in Fig. 4A. Moreover, calcein-positive tumor cells showed higher MFI when isolated from mice injected with P-R121, compared with those from control mice (Fig. 4A, bottom). Thus, systemic administration of conjugate P-R121 is able to inhibit P-gp in P388/MDR tumors.

Next, we focused our attention on whether conjugate P-R121(Dox) has the potential to induce apoptosis in MDR tumors *in vivo*. We established P388/MDR tumors in syngeneic DBA/2 mice and injected mice with conjugate P-R121(Dox). Mice were euthanized either 24 h or 48 h after injection, with tumors used for staining of cleaved (i.e., activated) caspase-3 via immunohistochemistry and for TUNEL assay. We found that injection of

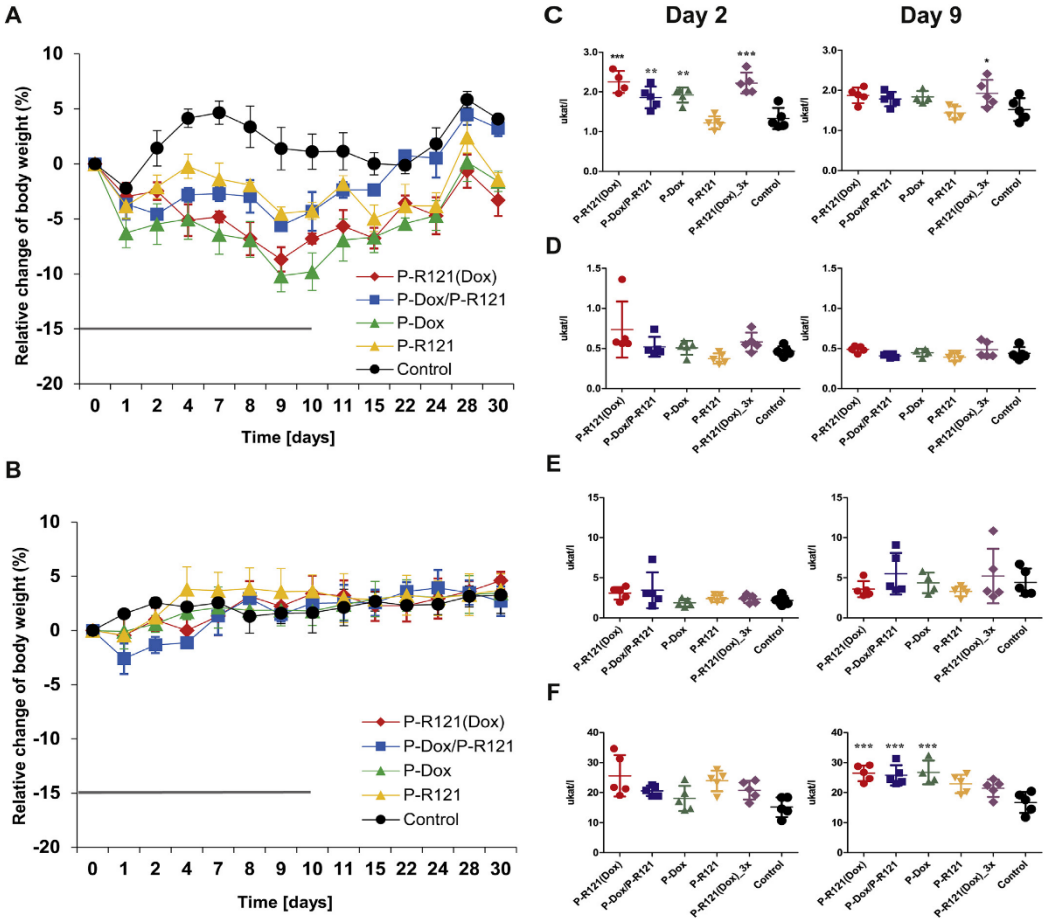

Fig. 5. Toxicity of conjugates P-R121(Dox), P-Dox, P-R121 and a mixture of P-Dox/P-R121 in mice. BALB/c mice (five per group) were intraperitoneally injected with tested conjugates in a single dose (A) or in a three-dose schedule (B). Control mice were intraperitoneally injected with the same volume of physiological solution. One dose contained 50 mg of Dox/kg of body weight and/or 208 mg of R121/kg of body weight in the single dose schedule, and 25 mg of Dox/kg of body weight and/or 104 mg of R121/kg of body weight in the three-dose schedule (_x3). The single dose was administered on day 0 and the three doses were administered on days −6, −3 and 0. The body weight of mice was recorded on a daily basis. Blood was collected from mice on day 2 (left) and day 9 (right), while serum (C) aspartate aminotransferase (AST), (D) alanine aminotransferase (ALT), (E) creatine kinase (CK) and (F) lactate dehydrogenase (LDH) levels were determined. The experiment was repeated twice with similar results. Statistical significances are shown ($^{*}P \leq 0.05$, $^{**}P \leq 0.01$, $^{***}P \leq 0.001$).

conjugate P-R121(Dox) induces the cleavage of caspase-3 in P388/MDR tumors at a markedly higher frequency compared to tumors from mice injected with conjugate P-Dox using the same dose of 50 mg of Dox/kg (Fig. 4B). Caspase-3 is an "executory" caspase and its activation is an irreversible process leading to apoptotic cell death [47]. Thus, we decided to check whether the increased activation of caspase-3 in P388/MDR tumors from mice injected with conjugate P-R121(Dox) is also reflected in TUNEL assay, which detects DNA fragments caused by DNA degradation in the final stage of apoptosis [48,49]. Indeed, we recorded significantly more TUNEL-positive cells in P388/MDR tumors from mice injected with P-R121(Dox) than those from mice injected with conjugate P-Dox using the same dose of 50 mg of Dox/kg (Fig. 4C). We clearly confirmed here that conjugate P-R121(Dox) possesses significantly higher potency for inducing apoptosis in P388/MDR tumors than conjugate bearing only Dox.

3.6. Toxicity of conjugate P-R121(Dox) in mice

We realized it was necessary to assess the toxicity of conjugate P-R121(Dox) and estimate the safe dosage before *in vivo* experiments took place to evaluate the antitumor activity in mouse tumor models. We found in our previous work that the maximal tolerated dose of conjugate P-Dox given as a bolus IV injection is 85 mg of Dox/kg [41]. Thus, mice were intraperitoneally injected with a single dose of conjugate P-R121(Dox), corresponding to 50 mg of Dox/kg (on day 0) or with three doses of conjugate P-R121(Dox), where one dose corresponded to 25 mg of Dox/kg (on days −6, −3

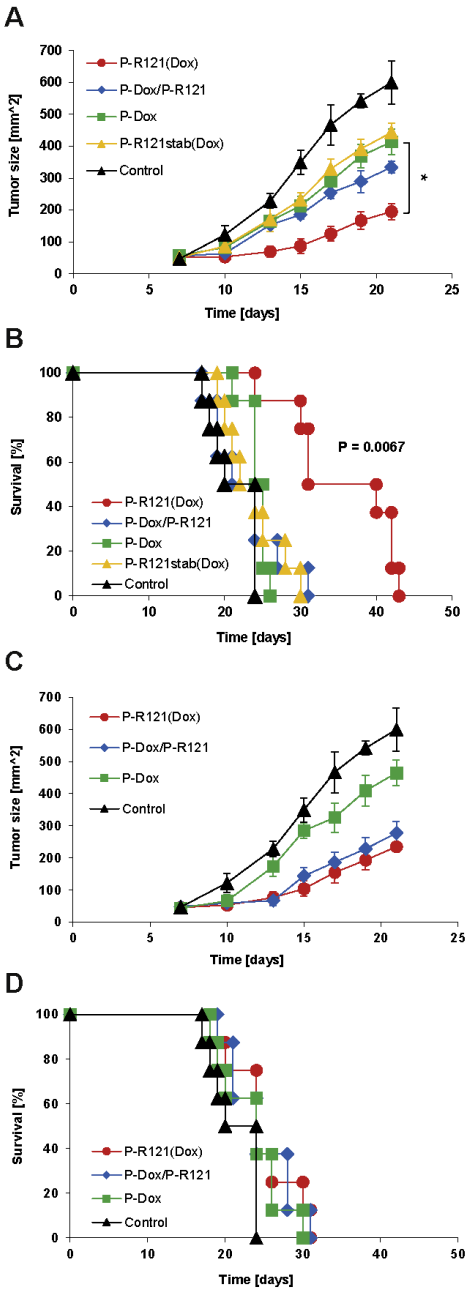

Fig. 6. Antitumor activity of conjugate P-R121(Dox) in mice bearing P388/MDR tumors. DBA/2 mice (eight per group) were subcutaneously inoculated with 1×10^6 P388/MDR cells on day 0. Mice were intraperitoneally injected, either with a single dose of polymeric conjugates on day 7 (A–B) or with three doses on days 7, 10 and 13 (C–D). One dose contained 50 mg of Dox/kg and/or 208 mg of R121/kg where the single dose was applied, and 25 mg of Dox/kg and/or 104 mg of R121/kg where three doses were applied. Untreated mice or mice treated with conjugate P-R121stab(Dox), where R121 is bound through a nondegradable bond, were used as controls. Tumor size (A, C) and survival (B, D) of the experimental mice were monitored. Statistical significance is shown (*$P < 0.05$).

and 0). The body weight as a sign of acute toxicity was recorded. Fig. 5A shows that a single dose of conjugate P-R121(Dox) did not result in body weight loss higher than 10%, nor was it more toxic than conjugate P-Dox. This was an important finding, since it is known that the coadministration of P-gp inhibitors and cytostatic drugs can lead to a profound increase in toxicity [8]. The toxicity was even lower when conjugate P-R121(Dox) was given in three doses, as mice did not lost more than 5% of their initial body weight (Fig. 5B).

We injected mice as described above and collected blood samples on days 2 and 9. Blood samples were investigated for serum levels of aspartate aminotransferase (AST; Fig. 5C), alanine aminotransferase (ALT; Fig. 5D), creatine kinase (CK; Fig. 5E) and lactate dehydrogenase (LDH; Fig. 5F). Elevated levels of AST and ALT are markers of hepatotoxicity [50], while elevation in CK and LDH point to cardiotoxicity [51]. The mild increase in AST levels is obviously associated with administration of conjugates bearing Dox, which could indicate a decent hepatotoxicity. However, ALT levels are normal, indicating that liver toxicity of conjugate P-R121(Dox) is low indeed. Serum levels of CK in mice injected with conjugate P-R121(Dox) and other tested conjugates are also completely comparable to controls. There is a slight increase of LDH levels on day 9 in sera from mice injected with a single dose of all conjugates bearing Dox, which could possibly be attributed to cardiotoxicity of Dox. This cardiotoxicity was comparable in mice injected with conjugates P-R121(Dox) and P-Dox, such that polymer-bound R121 does not increase cardiotoxicity of polymer-bound Dox. Similarly, a normal level of creatinine did not point to nephrotoxicity of conjugate P-R121(Dox) (Suppl. Fig. 4). This is a quite important finding since P-gp is expressed in kidneys [52,53]. Thus, it was concluded that the chosen dosage of conjugate P-R121(Dox) is safe, given that any signs of toxicity are limited, which is comparable to conjugate P-Dox.

3.7. Overcoming of MDR in cytostatic drug-induced P388/MDR tumor model

P388/MDR cells growing in syngeneic DBA/2 mice represent a tumor model with an extremely high level of MDR, which is practically insensitive to treatment with free Dox, even when given at a maximal tolerated dose (Suppl. Fig. 5). We employed the P388/MDR tumor model to evaluate the antitumor activity and potential of conjugate P-R121(Dox) to overcome the high level of drug-induced MDR. To prove that conjugate P-R121(Dox) is accumulated in P388/MDR tumors via the EPR effect, we synthesized a similar conjugate, but with the addition of near-infrared (NIR) fluorescent dye Cy7.5 (see Materials and Methods), and used it for whole body imaging of the biodistribution of this conjugate. It can be clearly seen that the conjugate is accumulated at the site of tumor upon i.v. injection because a strong fluorescent signal is located at the lower left flank of the mice (the site of tumor cell inoculation), although a very week signal is obtained from the ventral view (Suppl. Fig. 6). Similar data has been found for i.p. injection although with different kinetics of conjugate accumulation in tumor and in CT26 model (Suppl. Figs. 7 and 8).

Next, DBA/2 mice with established P388/MDR tumors of about 25–50 mm^2 were intraperitoneally injected with conjugate P-

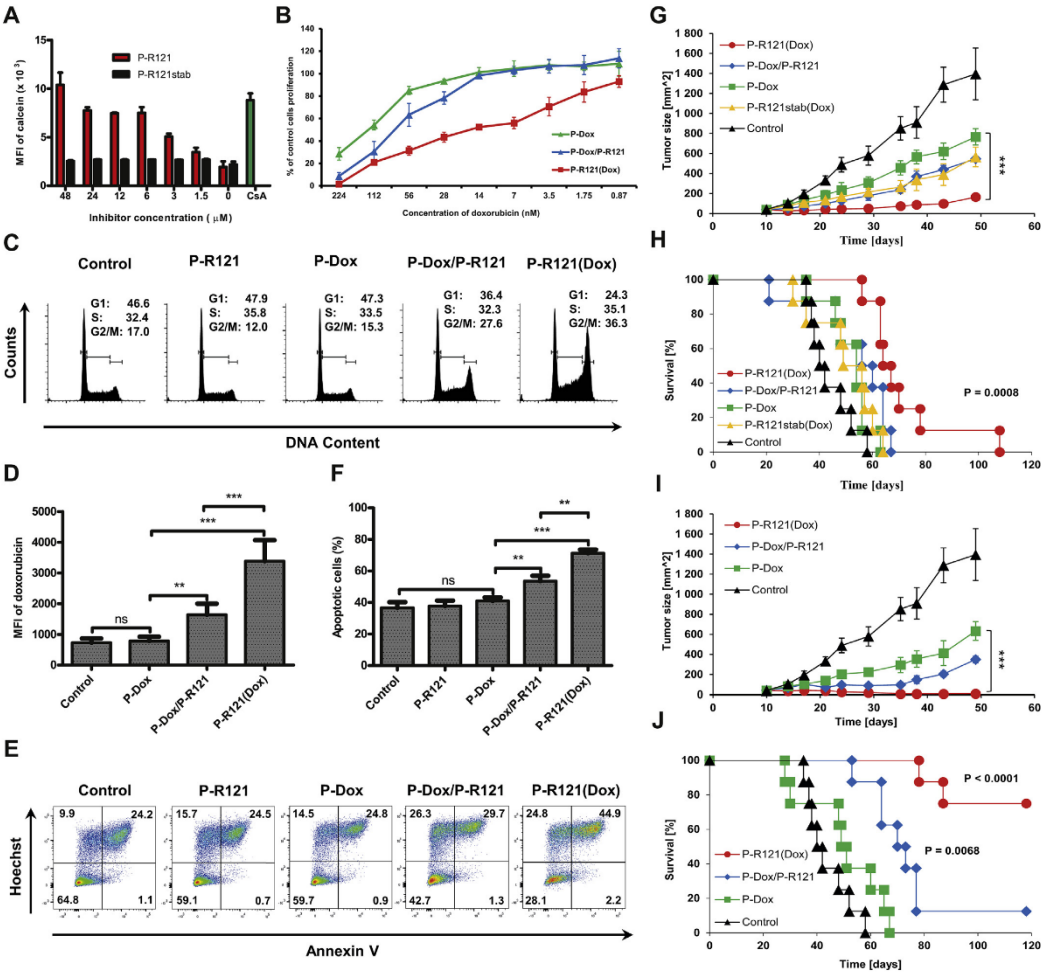

Fig. 7. Overcoming naturally occurring MDR in CT26 tumor cells by conjugate P-R121(Dox). (A) Inhibition of P-gp function in CT26 cells by conjugate P-R121 and by similar conjugate bearing R121 bound through a non-degradable bond (P-R121stab) determined by calcein assay after 16 h of incubation. CT26 cells incubated with 10 μM of cyclosporine A were used as a positive control. (B) *In vitro* cytostatic activity of polymeric conjugates in CT26 cells determined by [^{3}H]-thymidine incorporation assay. Results are shown as the inhibition of exposed cell proliferation relative to controls (cells incubated in medium only). Each experimental point is the average of three independent experiments + SD. (C) Cell cycle analysis of CT26 cells exposed to a 28 nM Dox concentration of polymeric conjugates, which are determined by measuring the DNA content after propidium iodide staining. Cells incubated in medium only were used as controls. The representative histograms of three independent experiments with similar results are shown. (D) Accumulation of Dox in CT26 cells, incubated for 24 h with polymeric conjugates bearing Dox or controls (cells incubated in medium only), determined by flow cytometry and expressed as the MFI of Dox. Results are shown as the mean + SD of at least three experiments. (E) Induction of apoptosis in CT26 cells incubated with a 28 nM Dox concentration of polymeric conjugates for 24 h. Cells were stained with annexin V-FITC/Hoechst 33258 and analyzed by flow cytometry. The number in each quadrant indicates the percentage of cells in the given population. The results are shown as representative plots of three independent experiments. Cells incubated in medium only were used as controls. (F) Quantification of the percentage of all apoptotic cells (early and late apoptosis) from all three experiments. (G–J) BALB/c mice (eight per group) were subcutaneously inoculated with 2×10^5 CT26 cells on day 0. Mice were intraperitoneally injected either with a single dose of polymeric conjugates on day 10 (G–H) or with three doses on days 10, 13 and 16 (I–J). One dose contained 50 mg of Dox/kg and/or 208 mg of R121/kg where the single dose was applied, or 25 mg of Dox/kg and/or 104 mg of R121/kg where the three doses were applied. Untreated mice or mice treated with conjugate P-R121stab(Dox), where R121 is bound through a non-degradable bond, were used as controls. Tumor size (G, I) and survival (H, J) of the experimental mice were monitored. Statistical significances are shown (*$P \leq 0.05$, **$P \leq 0.01$, ***$P \leq 0.001$).

R121(Dox), using either a single dose corresponding to 50 mg of Dox/kg or three doses given every third day, where one dose corresponded to 25 mg of Dox/kg. Conjugate P-R121(Dox), which was given in one dose, showed a significantly stronger inhibition of P388/MDR tumor growth than conjugate P-Dox, as well as a higher therapeutic efficacy than a mixture of conjugates P-Dox and P-R121 (Fig. 6A). However, conjugate P-R121stab(Dox) and non-releasing R121 inhibited tumor growth to the same extent as conjugate P-Dox. This clearly demonstrates that conjugate bearing both Dox and R121 is capable of overcoming MDR, when both cytostatic drug and

P-gp inhibitor are bound through a pH-sensitive bond and are thus intracellularly releasable. The survival of DBA/2 mice bearing P388/MDR tumors (Fig. 6B) was significantly prolonged by conjugate P-R121(Dox) alone in a single-dose schedule. Conversely, conjugate P-R121(Dox), when given in three lower doses, indicated comparable inhibition of tumor growth to a mixture of conjugates P-Dox and P-R121 (Fig. 6C), but did not significantly prolong the survival of experimental mice (Fig. 6D). The treatment of P388/MDR tumors with conjugate P-R121(Dox) is, therefore, more effective when a single higher dose is used instead of three lower doses, although the cumulative dose of these three doses is higher than the single dose (75 vs. 50 mg of Dox/kg). We have seen a similar pattern within the treatment of some non-MDR mouse tumors with HPMA copolymer-bound Dox conjugates [41].

3.8. Overcoming MDR in a naturally resistant CT26 tumor model

The final set of experiments was performed using the CT26 tumor model. CT26 cells were described to express low levels of P-gp without being exposed to cytostatic drugs [54,55], thereby representing a model of low-level natural MDR. CT26 cell line differs from P388/MDR not only by level of P-gp expression. CT26 tumors show slower progression upon s.c. inoculation in comparison to P388/MDR. Moreover, the frequency of metastazing is significantly lower in CT26 model which is reflected in remarkably longer lifespan of mice bearing CT26 tumors. To prove that CT26 cells indeed express P-gp, we incubated them with conjugate bearing R121, which was bound through either pH-sensitive degradable hydrazone bond (P-R121) or nondegradable reduced hydrazone bond (P-R121stab), and tested them in calcein assay. Conjugate P-R121 increased calcein accumulation in CT26 cells in a dose-dependent manner, resulting in a calcein accumulation that was ~five times higher at the highest concentration tested (48 μM R121) than non-treated cells (Fig. 7A). Conjugate P-R121stab had no effect. Next, we compared the cytostatic activity of conjugates P-Dox and P-R121(Dox) in the CT26 cell line *in vitro*. Conjugate P-R121(Dox) exerted almost one order higher in cytostatic activity than conjugate P-Dox, while also being more potent than a mixture of conjugates P-Dox and P-R121 (Fig. 7 B). Analogically, conjugate P-R121(Dox) induced cell cycle arrest in the G2/M phase more effectively than a mixture of conjugates P-Dox and P-R121 at a Dox concentration of 28 nM (Fig. 7C). Conjugate P-Dox at the same concentration had no effect on the cell cycle. Accumulation of Dox was significantly higher in CT26 cells incubated with conjugate P-R121(Dox) than conjugate P-Dox or a mixture of conjugates P-Dox and P-R121 (Fig. 7D). Conjugate P-R121(Dox) was also superior during the induction of apoptosis in CT26 cells at a Dox concentration of 28 nM (Fig. 7E and F). These data demonstrate that the inhibition of P-gp by R121 increases cytostatic and cytotoxic activity of Dox in CT26 cells, while the most effective overcoming of MDR is achieved by conjugate bearing both Dox and R121.

Finally, we evaluated the antitumor activity and potential of conjugate P-R121(Dox) to overcome low-level natural MDR in CT26 tumors. BALB/c mice, with established CT26 tumors of about 25–50 mm^2, were intraperitoneally injected with conjugate P-R121(Dox) using either a single dose corresponding to 50 mg of Dox/kg or three doses given every third day, where one dose corresponded to 25 mg of Dox/kg. Conjugate P-R121(Dox), when given in a single dose, showed powerful inhibition of CT26 tumor growth, as tumors were 10 times smaller on average than those in the control mice at day 48 (Fig. 7G). Similar to the P388/MDR tumor model, conjugate P-R121(Dox) was more effective than conjugate P-Dox regarding inhibition of tumor growth. Conjugate P-R121(Dox) was also the only treatment modality that significantly prolonged the survival of mice in a one-dose schedule (Fig. 7H). The therapeutic effect of conjugate P-R121(Dox), when given in three lower doses, was generally much stronger in the CT26 tumor model than the P388/MDR model. Mice treated with conjugate P-R121(Dox) completely rejected tumors in most cases (Fig. 7I), while six out of eight experimental mice were long-term survivors (LTSs) without any sign of a tumor up to day 120 (termination of the experiment; Fig. 7J). Treatment with a mixture of conjugates P-Dox and P-R121 also led to a remarkably strong inhibition regarding tumor growth, although only one out of eight mice was a LTS. P-Dox conjugate inhibited the growth of tumors less efficiently than a mixture of conjugates P-Dox and P-R121 (~two times larger tumors on average on day 48) and did not produce any LTSs.

4. Conclusions

We have demonstrated that HPMA copolymer conjugate bearing both cytostatic drug Dox and P-gp inhibitor R121, bound through pH-sensitive hydrazone bonds, is capable of overcoming MDR in highly resistant P388/MDR cells *in vitro* and *in vivo*. Such conjugate is superior to a mixture of conjugates bearing either Dox or R121, thereby showing that cytostatic drugs and P-gp inhibitors need to be bound to the same polymeric carrier for maximal potency. Polymeric conjugate bearing both Dox and R121 also potently overcome natural MDR in CT26 cells, as documented by powerful antitumor activity *in vivo*. Polymeric conjugates bearing not only a cytostatic drug, but also a P-gp inhibitor, could thus improve the performance of polymer-bound drug conjugates and intensify treatment of some common cancers where natural MDR is common, i.e., colon, pancreatic or kidney cancer.

Author contributions

L.S. and J.T. performed biological studies *in vitro* and *in vivo*; V.S., J.S. and T.E. performed the chemical synthesis and characterization of polymeric conjugates; L.S. J.T. and V.S. prepared the Figures and Tables; L.S., V.S. and M.K. wrote the manuscript; M.K., B.R. and V.S. supervised the research.

Acknowledgment

The work was supported by the Czech Science Foundation (grant number P301/12/1254), the Ministry of Education, Youth and Sports of the Czech Republic, within the LQ1604 National Sustainability Program II (Project BIOCEV-FAR), and by the project "BIOCEV" (CZ.1.05/1.1.00/02.0109) and the Institutional Research Concept RVO 61388971. The authors would like to thank Pavlina Jungrova, Helena Misurcova and Tereza Pelikanova for their excellent technical assistance. Conflicts of interest: none.

Appendix A. Supplementary data

Supplementary data related to this article can be found at http://dx.doi.org/10.1016/j.biomaterials.2016.11.013.

References

[1] M.M. Gottesman, How cancer cells evade chemotherapy: sixteenth richard and hinda rosenthal foundation award lecture, Cancer Res. 53 (1993) 747–754.
[2] D.B. Longley, P.G. Johnston, Molecular mechanisms of drug resistance, J. Pathol. 205 (2005) 275–292.
[3] F.X. Mahon, F. Belloc, V. Lagarde, C. Chollet, F. Moreau-Gaudry, J. Reiffers, et al., MDR1 gene overexpression confers resistance to imatinib mesylate in leukemia cell line models, Blood 101 (2003) 2368–2373.
[4] C. Holohan, S. Van Schaeybroeck, D.B. Longley, P.G. Johnston, Cancer drug resistance: an evolving paradigm, Nat. Rev. Cancer 13 (2013) 714–726.
[5] T. Mizutani, M. Masuda, E. Nakai, K. Furumiya, H. Togawa, Y. Nakamura, et al.,

Genuine functions of P-glycoprotein (ABCB1), Curr. Drug Metab. 9 (2008) 167–174.
[6] R. Krishna, L.D. Mayer, Multidrug resistance (MDR) in cancer. Mechanisms, reversal using modulators of MDR and the role of MDR modulators in influencing the pharmacokinetics of anticancer drugs, Eur. J. Pharm. Sci. Off. J. Eur. Fed. Pharm. Sci. 11 (2000) 265–283.
[7] S. Shukla, C.P. Wu, S.V. Ambudkar, Development of inhibitors of ATP-binding cassette drug transporters: present status and challenges, Expert Opin. Drug Metab. Toxicol. 4 (2008) 205–223.
[8] G. Szakacs, J.K. Paterson, J.A. Ludwig, C. Booth-Genthe, M.M. Gottesman, Targeting multidrug resistance in cancer, Nat. Rev. Drug Discov. 5 (2006) 219–234.
[9] H.M. Coley, Overcoming multidrug resistance in cancer: clinical studies of p-glycoprotein inhibitors, Methods Mol. Biol. 596 (2010) 341–358.
[10] S. Nobili, I. Landini, T. Mazzei, E. Mini, Overcoming tumor multidrug resistance using drugs able to evade P-glycoprotein or to exploit its expression, Med. Res. Rev. 32 (2012) 1220–1262.
[11] A. Koubeissi, I. Raad, L. Ettouati, D. Guilet, C. Dumontet, J. Paris, Inhibition of P-glycoprotein-mediated multidrug efflux by aminomethylene and keto-methylene analogs of reversins, Bioorg. Med. Chem. Lett. 16 (2006) 5700–5703.
[12] K. Hoffmann, R. Bekeredjian, J. Schmidt, M.W. Buchler, A. Marten, Effects of the high-affinity Peptide reversin 121 on multidrug resistance proteins in experimental pancreatic cancer, Tumour Biol. J. Int. Soc. Oncodev. Biol. Med. 29 (2008) 351–358.
[13] F.J. Sharom, X. Yu, P. Lu, R. Liu, J.W. Chu, K. Szabo, et al., Interaction of the P-glycoprotein multidrug transporter (MDR1) with high affinity peptide chemosensitizers in isolated membranes, reconstituted systems, and intact cells, Biochem. Pharmacol. 58 (1999) 571–586.
[14] O. Arnaud, A. Koubeissi, L. Ettouati, R. Terreux, G. Alame, C. Grenot, et al., Potent and fully noncompetitive peptidomimetic inhibitor of multidrug resistance P-glycoprotein, J. Med. Chem. 53 (2010) 6720–6729.
[15] D.R. Ferry, H. Traunecker, D.J. Kerr, Clinical trials of P-glycoprotein reversal in solid tumours, Eur. J. Cancer 32A (1996) 1070–1081.
[16] L. Yang, L. Meng, X. Zhang, Y. Chen, G. Zhu, H. Liu, et al., Engineering polymeric aptamers for selective cytotoxicity, J. Am. Chem. Soc. 133 (2011) 13380–13386.
[17] J.K. Oh, D.I. Lee, J.M. Park, Biopolymer-based microgels/nanogels for drug delivery applications, Prog. Polym. Sci. 34 (2009) 1261–1282.
[18] B. Li, H. Xu, Z. Li, M. Yao, M. Xie, H. Shen, et al., Bypassing multidrug resistance in human breast cancer cells with lipid/polymer particle assemblies, Int. J. Nanomed. 7 (2012) 187–197.
[19] X.-X. Wang, Y.-B. Li, H.-J. Yao, R.-J. Ju, Y. Zhang, R.-J. Li, et al., The use of mitochondrial targeting resveratrol liposomes modified with a dequalinium polyethylene glycol-distearoylphosphatidyl ethanolamine conjugate to induce apoptosis in resistant lung cancer cells, Biomaterials 32 (2011) 5673–5687.
[20] Y. Gao, Y. Chen, X. Ji, X. He, Q. Yin, Z. Zhang, et al., Controlled intracellular release of doxorubicin in multidrug-resistant cancer cells by tuning the shell-pore sizes of mesoporous silica nanoparticles, ACS Nano 5 (2011) 9788–9798.
[21] H. Maeda, H. Nakamura, J. Fang, The EPR effect for macromolecular drug delivery to solid tumors: improvement of tumor uptake, lowering of systemic toxicity, and distinct tumor imaging in vivo, Adv. Drug Deliv. Rev. 65 (2013) 71–79.
[22] A.V. Kabanov, E.V. Batrakova, V.Y. Alakhov, Pluronic block copolymers as novel polymer therapeutics for drug and gene delivery, J. Control. Release Off. J. Control. Release Soc. 82 (2002) 189–212.
[23] E.V. Batrakova, A.V. Kabanov, Pluronic block copolymers: evolution of drug delivery concept from inert nanocarriers to biological response modifiers, J. Control. Release Off. J. Control. Release Soc. 130 (2008) 98–106.
[24] T. Minko, HPMA copolymers for modulating cellular signaling and overcoming multidrug resistance, Adv. Drug Deliv. Rev. 62 (2010) 192–202.
[25] T. Minko, P. Kopeckova, J. Kopecek, Comparison of the anticancer effect of free and HPMA copolymer-bound adriamycin in human ovarian carcinoma cells, Pharm. Res. 16 (1999) 986–996.
[26] T. Minko, P. Kopeckova, J. Kopecek, Chronic exposure to HPMA copolymer-bound adriamycin does not induce multidrug resistance in a human ovarian carcinoma cell line, J. Control. Release Off. J. Control. Release Soc. 59 (1999) 133–148.
[27] E. Koziolova, O. Janouskova, L. Cuchalova, Z. Hvezdova, J. Hrabeta, T. Eckschlager, et al., Overcoming multidrug resistance in Dox-resistant neuroblastoma cell lines via treatment with HPMA copolymer conjugates containing anthracyclines and P-gp inhibitors, J. Control. Release Off. J. Control. Release Soc. 233 (2016) 136–146.
[28] B. Rihova, L. Kovar, M. Kovar, O. Hovorka, Cytotoxicity and immunostimulation: double attack on cancer cells with polymeric therapeutics, Trends Biotechnol. 27 (2009) 11–17.
[29] B. Rihova, M. Kovar, Immunogenicity and immunomodulatory properties of HPMA-based polymers, Adv. Drug Deliv. Rev. 62 (2010) 184–191.
[30] T. Etrych, V. Subr, J. Strohalm, M. Sirova, B. Rihova, K. Ulbrich, HPMA copolymer-doxorubicin conjugates: the effects of molecular weight and architecture on biodistribution and in vivo activity, J. Control. Release Off. J. Control. Release Soc. 164 (2012) 346–354.
[31] H. Maeda, Tumor-selective delivery of macromolecular drugs via the EPR effect: background and future prospects, Bioconj. Chem. 21 (2010) 797–802.
[32] Y. Matsumura, H. Maeda, A new concept for macromolecular therapeutics in cancer chemotherapy: mechanism of tumoritropic accumulation of proteins and the antitumor agent smancs, Cancer Res. 46 (1986) 6387–6392.
[33] P. Chytil, T. Etrych, J. Kriz, V. Subr, K. Ulbrich, N-(2-Hydroxypropyl)methacrylamide-based polymer conjugates with pH-controlled activation of doxorubicin for cell-specific or passive tumour targeting. Synthesis by RAFT polymerisation and physicochemical characterisation, Eur. J. Pharm. Sci. Off. J. Eur. Fed. Pharm. Sci. 41 (2010) 473–482.
[34] V. Subr, L. Sivak, E. Koziolova, A. Braunova, M. Pechar, J. Strohalm, et al., Synthesis of poly[N-(2-hydroxypropyl)methacrylamide] conjugates of inhibitors of the ABC transporter that overcome multidrug resistance in doxorubicin-resistant P388 cells in vitro, Biomacromolecules 15 (2014) 3030–3043.
[35] T. Etrych, T. Mrkvan, P. Chytil, C. Konak, B. Rihova, K. Ulbrich, N-(2-hydroxypropyl)methacrylamide-based polymer conjugates with pH-controlled activation of doxorubicin. I. New synthesis, physicochemical characterization and preliminary biological evaluation, J. Appl. Polym. Sci. 109 (2008) 3050–3061.
[36] M. Barberis, J. Perez-Prieto, Enantioselective synthesis of sabina ketone, Tetrahedron Lett. 44 (2003) 6683–6685.
[37] K. Ishitake, K. Satoh, M. Kamigaito, Y. Okamoto, Stereogradient polymers formed by controlled/living radical polymerization of bulky methacrylate monomers, Angew. Chem. 48 (2009) 1991–1994.
[38] S. Perrier, P. Takolpuckdee, C.A. Mars, Reversible addition-fragmentation chain transfer polymerization: end group modification for functionalized polymers and chain transfer agent recovery, Macromolecules 38 (2005) 2033–2036.
[39] A. Postma, T.P. Davis, G. Moad, M.S. O'Shea, Thermolysis of RAFT-synthesized polymers. A convenient method for trithiocarbonate group elimination, Macromolecules 38 (2005) 5371–5374.
[40] D.E. Maidana, P. Tsoka, B. Tian, B. Dib, H. Matsumoto, K. Kataoka, et al., A novel ImageJ macro for automated cell death quantitation in the retina, Investig. Ophthalmol. Vis. Sci. 56 (2015) 6701–6708.
[41] B. Tomalova, M. Sirova, P. Rossmann, R. Pola, J. Strohalm, P. Chytil, et al., The structure-dependent toxicity, pharmacokinetics and anti-tumour activity of HPMA copolymer conjugates in the treatment of solid tumours and leukaemia, J. Control. Release Off. J. Control. Release Soc. 223 (2016) 1–10.
[42] T. Tsuruo, H. Iida, S. Tsukagoshi, Y. Sakurai, Increased accumulation of vincristine and adriamycin in drug-resistant P388 tumor cells following incubation with calcium antagonists and calmodulin inhibitors, Cancer Res. 42 (1982) 4730–4733.
[43] M. Raymond, E. Rose, D.E. Housman, P. Gros, Physical mapping, amplification, and overexpression of the mouse mdr gene family in multidrug-resistant cells, Mol. Cell. Biol. 10 (1990) 1642–1651.
[44] M. St'astny, J. Strohalm, D. Plocova, K. Ulbrich, B. Rihova, A possibility to overcome P-glycoprotein (PGP)-mediated multidrug resistance by antibody-targeted drugs conjugated to N-(2-hydroxypropyl)methacrylamide (HPMA) copolymer carrier, Eur. J. Cancer 35 (1999) 459–466.
[45] M. Inaba, H. Kobayashi, Y. Sakurai, R.K. Johnson, Active efflux of daunorubicin and adriamycin in sensitive and resistant sublines of P388 leukemia, Cancer Res. 39 (1979) 2200–2203.
[46] A. Malugin, P. Kopeckova, J. Kopecek, Liberation of doxorubicin from HPMA copolymer conjugate is essential for the induction of cell cycle arrest and nuclear fragmentation in ovarian carcinoma cells, J. Control. Release Off. J. Control. Release Soc. 124 (2007) 6–10.
[47] S. Shalini, L. Dorstyn, S. Dawar, S. Kumar, Old, new and emerging functions of caspases, Cell Death Differ. 22 (2015) 526–539.
[48] Y. Gavrieli, Y. Sherman, S.A. Ben-Sasson, Identification of programmed cell death in situ via specific labeling of nuclear DNA fragmentation, J. Cell Biol. 119 (1992) 493–501.
[49] F. Labat-Moleur, C. Guillermet, P. Lorimier, C. Robert, S. Lantuejoul, E. Brambilla, et al., TUNEL apoptotic cell detection in tissue sections: critical evaluation and improvement, J. Histochem. Cytochem. Off. J. Histochem. Soc. 46 (1998) 327–334.
[50] S. Shrestha, C.M.Y. Yeung, C. Nunnerley, S.C. Tsang, Comparison of morphology and electrical conductivity of various thin films containing nanocrystalline praseodymium oxide particles, Sens. Actuators A Phys. 136 (2007) 191–198.
[51] I. Andreadou, F. Sigala, E.K. Iliodromitis, M. Papaefthimiou, C. Sigalas, N. Aligiannis, et al., Acute doxorubicin cardiotoxicity is successfully treated with the phytochemical oleuropein through suppression of oxidative and nitrosative stress, J. Mol. Cell. Cardiol. 42 (2007) 549–558.
[52] A.H. Schinkel, J.J. Smit, O. van Tellingen, J.H. Beijnen, E. Wagenaar, L. van Deemter, et al., Disruption of the mouse mdr1a P-glycoprotein gene leads to a deficiency in the blood-brain barrier and to increased sensitivity to drugs, Cell 77 (1994) 491–502.
[53] A.H. Schinkel, E. Wagenaar, L. van Deemter, C.A. Mol, P. Borst, Absence of the mdr1a P-Glycoprotein in mice affects tissue distribution and pharmacokinetics of dexamethasone, digoxin, and cyclosporin A, J. Clin. Investig. 96 (1995) 1698–1705.
[54] D. Fan, P. Beltran, Y. Wang, C. Bucana, S. Yoon, A. Deguzman, et al., Cell density-dependent regulation of mdr-1 gene expression in murine colon cancer cells, Int. J. Oncol. 9 (1996) 865–878.
[55] F. Lin, L. Hoogendijk, L. Buil, J.H. Beijnen, O. van Tellingen, Sildenafil is not a useful modulator of ABCB1 and ABCG2 mediated drug resistance in vivo, Eur. J. Cancer 49 (2013) 2059–2064.

Journal of Controlled Release 245 (2017) 41–51

Contents lists available at ScienceDirect

Journal of Controlled Release

journal homepage: www.elsevier.com/locate/jconrel

Tumor-targeted micelle-forming block copolymers for overcoming of multidrug resistance

Alena Braunová [a], Libor Kostka [a], Ladislav Sivák [b], Lucie Cuchalová [a], Zuzana Hvězdová [a], Richard Laga [a], Sergey Filippov [a], Peter Černoch [a], Michal Pechar [a], Olga Janoušková [a], Milada Šírová [b], Tomáš Etrych [a,*]

[a] Institute of Macromolecular Chemistry, Czech Academy of Sciences, Heyrovského nám. 2, 162 06 Prague, Czech Republic
[b] Institute of Microbiology, Czech Academy of Sciences, Vídeňská 1083, 142 20 Prague, Czech Republic

ARTICLE INFO

Article history:
Received 11 August 2016
Received in revised form 31 October 2016
Accepted 17 November 2016
Available online 18 November 2016

Keywords:
Multidrug resistance
P-glycoprotein inhibitor
EPR effect
HPMA copolymer
Poly(propylene oxide)
Micellar drug conjugate

ABSTRACT

New amphiphilic diblock polymer nanotherapeutics serving simultaneously as a drug delivery system and an inhibitor of multidrug resistance were designed, synthesized, and evaluated for their physico-chemical and biological characteristics. The amphiphilic character of the diblock polymer, containing a hydrophilic block based on the *N*-(2-hydroxypropyl)methacrylamide copolymer and a hydrophobic poly(propylene oxide) block (PPO), caused self-assembly into polymer micelles with an increased hydrodynamic radius (R_h of approximately 15 nm) in aqueous solutions. Doxorubicin (Dox), as a cytostatic drug, was bound to the diblock polymer through a pH-sensitive hydrazone bond, enabling prolonged circulation in blood, the delivery of Dox into a solid tumor and the subsequent stimuli-sensitive controlled release within the tumor mass and tumor cells at a decreased pH. The applicability of micellar nanotherapeutics as drug carriers was confirmed by an *in vivo* evaluation using EL4 lymphoma-bearing C57BL/6 mice. We observed significantly higher accumulation of micellar conjugates in a solid tumor because of the EPR effect compared with similar polymer-drug conjugates that do not form micellar structures or with the parent free drug. In addition, highly increased anti-tumor efficacy of the micellar polymer nanotherapeutics, even at a sub-optimal dose, was observed. The presence of PPO in the structure of the diblock polymer ensured, during *in vitro* tests on human and mouse drug-sensitive and resistant cancer cell lines, the inhibition of P-glycoprotein, one of the most frequently expressed ATP-dependent efflux pump that causes multidrug resistance. In addition, we observed highly increased rate of the uptake of the diblock polymer nanotherapeutics within the cells. We suppose that combination of unique properties based on MDR inhibition, stimuli sensitiveness (pH sensitive activation of drug), improved pharmacokinetics and increased uptake into the cells made the described polymer micelle a good candidate for investigation as potential drug delivery system.
© 2016 Elsevier B.V. All rights reserved.

1. Introduction

Multidrug resistance (MDR) is one of the main causes of the imperfect or even ineffective treatment of many types of haematological malignancies and solid tumors. The resistance of cancer cells to current chemotherapy is associated with the overexpression of at least two ATP-dependent efflux pumps, P-glycoprotein (P-gp; MDR1) and multidrug resistance-associated protein 1 (MRP1), both belonging to a superfamily of ATP-binding cassette (ABC) transporters [1,2]. These overexpressed proteins participate in the preferential active transport of cytotoxic drugs out of cancer cells before the therapeutic effect of drugs. Thus, the intracellular concentration of drugs in tumors is decreased, and conversely, the probability of the survival of tumor cells increases. An inhibition of the membrane transporters [3–5] should improve the retention of chemotherapeutics inside tumor cells, allowing a more effective cancer therapy to be achieved. The application of low-molecular weight (LMW) P-gp inhibitors (cyclosporine A, verapamil, ritonavir, vincristine, tamoxifen, *etc.*) with non-selective biodistribution represents a serious risk associated with the inhibition of P-gp in healthy tissues. Although P-gp protects the organism against xenobiotics in normal cells, this protein contributes to the resistance of tumors towards cytostatic drugs in cancer cells.

It has been previously found [6–11] that the high-molecular weight (HMW) polymer carriers and their polymer-drug conjugates are subject to so-called passive accumulation in solid tumors. This phenomenon is called the EPR (enhanced permeability and retention) effect [6,12–15]. HMW compounds are preferably accumulated in solid tumors because of the leaky tumor neovasculature, but they are not eliminated because of the damaged or completely missing lymphatic drainage in solid tumor tissues. Currently, the EPR effect is highly utilized in the design and application of polymer-drug conjugates tailor-made for passive accumulation in solid tumors. The use of HMW polymer-drug conjugates also offers an option for the inhibition of P-gp, provided that part of the

* Corresponding author.
E-mail address: etrych@imc.cas.cz (T. Etrych).

http://dx.doi.org/10.1016/j.jconrel.2016.11.020
0168-3659/© 2016 Elsevier B.V. All rights reserved.

polymer carrier acts as a P-gp inhibitor. Kabanov and coworkers [2,16–21] studied micellar carriers based on various types of pluronic triblock copolymers of poly(ethylene oxide) (PEO) and poly(propylene oxide) (PPO), where PPO block was responsible for sensitizing resistant cells to cytostatics. Consequently, the cytotoxic activity of the drug was increased [2]. The major and limiting disadvantage of these systems with non-covalently incorporated drugs in the hydrophobic core of the micelle could be continuous non-controlled drug release within the whole organism caused by diffusion and micelle disintegration during its circulation in blood. Recently, micellar polymer systems become extensively studied as drug delivery systems. Various amphiphilic block copolymer, including amphiphilic block copolymer with poly(*N*-(2-hydroxypropyl)methacrylamide) synthesized using RAFT polymerization as the hydrophilic block, were studied as precursors for self-assembling micellar systems [22–24].

Here, we present the design, synthesis and evaluation of the physico-chemical and biological properties of amphiphilic diblock copolymers containing a hydrophilic copolymer of *N*-(2-hydroxypropyl)methacrylamide (HPMA) with 1-(*tert*-butoxycarbonyl)-2-(6-methacrylamidohexanoyl)hydrazine (Ma-Ah-NHNH-Boc) and hydrophobic PPO. We hypothesized that the replacement of the hydrophilic PEO block in the pluronic polymer with another hydrophilic polymer, such as a HPMA copolymer, might lead to block copolymers with similar P-gp-inhibiting properties as the pluronic polymer. At the same time, the block copolymer may serve as a carrier of an anticancer drugs, like doxorubicin (Dox), covalently linked to the copolymer *via* a pH-sensitive hydrazone bond, which is biodegradable inside cancer cells and stable during the transport in the organism [2,15,25–28]. The amphiphilic dual character of the synthesized diblock polymer precursor **DB** (Synthesis on Fig. 1A) and the polymer-drug conjugate **DB-Dox** (Fig. 1B) enables the formation of micelles in aqueous environments (Fig. 1C) as well as increases in apparent molecular weight and size in solution. This provides a great advantage for the preferential passive targeting of the system into solid tumors driven by the EPR effect. After the disintegration of the micelles to unimers because of their gradual dilution below the critical micellar concentration (CMC) in targeted cells/tumor tissue, the unimers should be excreted from the organism by glomerular filtration, as their molecular weight is well below the renal filtration limit (M_n = 12,950 g/mol; Đ = 1.18). We found that this micellar system can serve as both a passively targeted drug delivery system and a polymer inhibitor of P-gp because of the presence of the PPO block in its structure. In consequence, the proposed polymer system could be a good candidate for the effective treatment of various tumors, even those that are resistant.

2. Material and methods

2.1. Synthesis of the monomers and initiator

N-(2-Hydroxypropyl)methacrylamide (HPMA) was synthesized according to the literature [29]. M.p. 69–70 °C; Elemental analysis: calculated/found: C 58.72/58.98%, H 9.15/9.18%, N 9.78/9.82%. 1-(*tert*-Butoxycarbonyl)-2-(6-methacrylamidohexanoyl)hydrazine (Ma-Ah-NHNH-Boc) was prepared as described previously [30]. M.p. 114–116 °C; Elemental analysis: calculated/found: C 57.49/58.26%; H 8.68/8.95%; N 13.41/13.25%.

2-[1-Cyano-1-methyl-4-oxo-4-(2-thioxo-thiazolidin-3-yl)-butylazo]-2-methyl-5-oxo-5-(2-thioxothiazolidin-3-yl)-pentanenitrile (ABIC-TT) was prepared as described previously [31]. Elemental analysis:

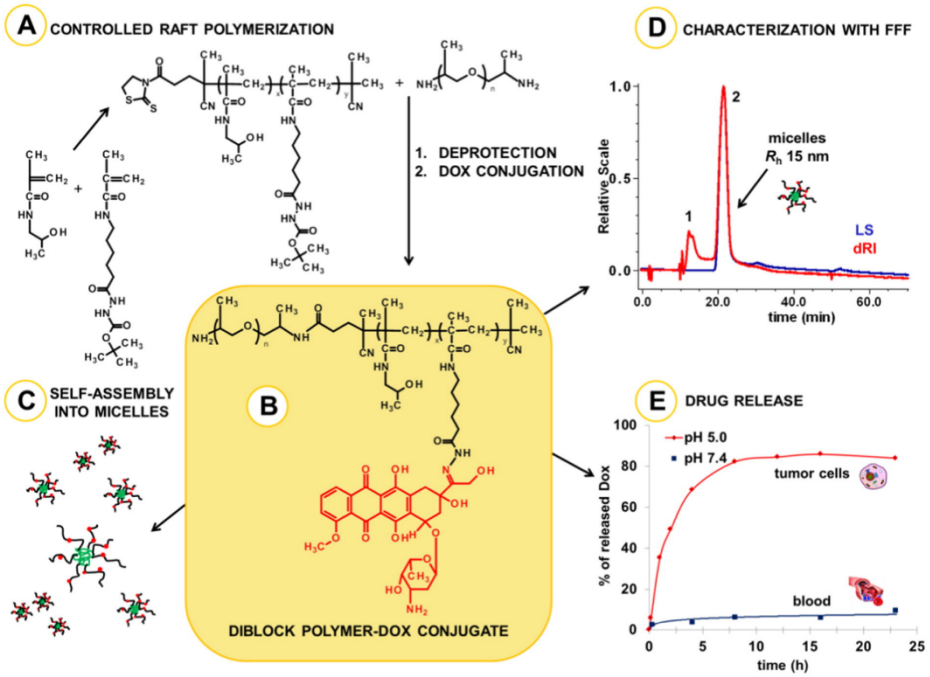

Fig. 1. Overall description of the micellar diblock polymer system with Dox: synthesis (A), schematic structure (B), self-assembly into micellar structures (C), characterization with the FFF method (D), and drug release in aqueous media mimicking the conditions of the bloodstream and intracellular environment (E).

calculated/found: C 44.79/45.10%; H 4.59/4.69%; N 17.41/16.89%; S 26.57/26.05%. ESI–MS: $m/z = 504.83$ $(M+Na)^+$.

2.2. Synthesis of the functionalized chain transfer agent

Dithiobenzoic acid 1-cyano-1-methyl-4-oxo-4-(2-thioxothiazolidin-3-yl)butyl ester (CTA-TT) was synthesized according to the literature [32]. ESI − MS: $m/z = 380.92$ $(M+Na)^+$.

2.3. Synthesis of hydrophilic block

Poly(HPMA-co-Ma-Ah-NHNH-Boc)-TT with terminal TT groups and NHNHBoc groups along the polymer chain was synthesized by RAFT polymerization with molar ratio ABIC-TT/CTA-TT/comonomers 1/2/150. The ratio of comonomers HPMA/Ma-Ah-NHNHBoc was 92/8 mol%. HPMA (1000 mg; 6.983 mmol) was dissolved in *tert*-butanol (6.747 mL), Ma-Ah-NHNHBoc (190 mg; 0.607 mmol), ABIC-TT (24.425 mg; 5.060×10^{-2} mmol) and CTA-TT (38.517 mg; 0.101 mmol) were dissolved in DMSO (1.687 mL). The polymerization mixture was bubbled with argon for 15 min. The copolymerization was performed in the sealed ampoule at 70 °C for 16 h. The product was isolated by precipitation to the mixture acetone/diethylether (1:1), the precipitate was centrifuged, filtered and dried. Reactive ω-end dithiobenzoate groups (DTB) were removed with 2.2′-azobisisobutyronitrile (AIBN) as described in literature [33]. The semitelechelic copolymer was characterized by SEC ($M_n = 8,450$ g/mol; $Đ = 1.20$). The content of TT groups ($F_{TT} = 0.98$, where F_{TT} is $M_{n,T}/M_n$, molecular weight determined for polymer containing 1 mol of main chain-end TT groups divided by molecular weight determined by SEC). Content of $NHNH_2$ groups (5.94 mol%) was determined spectrophotometrically after removal of Boc groups with a mixture of 95% trifluoracetic acid (TFA)/2.5% triisopropylsilane (TIS)/2.5% water. The conversion was 46% (833 mg) and R_h 4.5 nm.

2.4. Purification of commercial hydrophobic block

Commercial poly(propylene oxide) bis(2-aminopropyl ether) (Aldrich; NH_2-PPO-NH_2; M = 4000 g/mol) was purified by column chromatography (Sephadex LH-20, MeOH – HPLC grade) before using. For detection of polymer was used UV detector (230 nm) and TLC in chloroform/methanol 5:1 with special developing solution of NH_4SCN (3.40 g) and $Co(NO_3)_2$ (0.56 g) in H_2O (20 mL). The content of NH_2 end groups on purified PPO 1.52 was determined spectrophotometrically (as described below).

2.5. Synthesis of the diblock polymer precursor (DB)

The hydrophobic block (NH_2-PPO-NH_2; M = 4000 g/mol; 33.2 mg; 8.30×10^{-3} mmol) as well as the hydrophilic block (poly(HPMA-co-Ma-Ah-NHNH-Boc)-TT) (86 mg; 9.96×10^{-3} mmol, $M_n = 8450$ g/mol, $F_{TT} = 0.98$) were dissolved separately in 1 mL dimethylacetamide (DMA). The solution of hydrophilic block was slowly added to the hydrophobic block solution under stirring and the reaction mixture was reacted overnight. After 16 h, the reaction was purified by column chromatography (Sephadex LH-20 in MeOH) with RI, UV (230 nm) and TLC detection. The solvents were removed under vacuum and the final product was dried to the constant weight yielded 80 mg (77%). Boc-protecting groups were removed by a mixture of 95% trifluoracetic acid (TFA)/2.5% triisopropylsilane (TIS)/2.5% water. The solvents were removed under vacuum after polymer dissolution immediately. The residue was dissolved in borate buffer (pH 8.0) and pH of polymer solution was adjusted to a value 6.5–8.0 by concentrated NaOH solution. The crude unprotected product was desalinated and purified by column chromatography (Sephadex G-25 – column PD10, water). The final product was isolated by freeze-drying. Yield was 40 mg (78%). **DB** (poly(HPMA-co-Ma-Ah-$NHNH_2$)-PPO-NH_2) was characterized by SEC ($M_w = 15,230$ g/mol, $M_n = 12,950$ g/mol, $Đ = 1.18$) and DLS ($R_h = 14$ nm).

2.6. Synthesis of diblock polymer-Dox conjugate (DB-Dox)

Attachment of the drug Dox to **DB** through pH-sensitive hydrazone bond was carried out by procedure described in the literature earlier [25,26]. Briefly, the corresponding **DB** with free hydrazide groups was dissolved in anhydrous methanol (MeOH) and the polymer solution with concentrated acetic acid as a catalyst was added to the solid drug Dox.HCl. The reaction mixture was reacted under vigorous stirring overnight in the dark. The crude product was purified by column chromatography in MeOH (Sephadex LH-20). The solvent from polymer conjugate fraction was removed under vacuum and sample was dried to the constant weight. The content of bound Dox was determined spectrophotometrically (water, $\varepsilon_{488} = 9800$ L × mol^{-1} × cm^{-1}). Yield was 80% (96 mg), the content of Dox was 8.7 wt%. The structure of **DB-Dox** is shown in Fig. 1B.

2.7. Synthesis of linear polymer-drug conjugate pHPMA-Dox

The linear polymer-drug conjugate **pHPMA-Dox** based on copolymer of HPMA and Ma-Ah-$NHNH_2$ with Dox attached *via* hydrazone bond ($M_w = 30,000$ g/mol) was synthesized according to the literature [26].

2.8. Preparation of the lyophilized form of DB-Dox for easy-to-use administration of sample

DB-Dox (100 mg; 8.7 wt% Dox), $NaH_2PO_4 \times 2\ H_2O$ (2.40 mg), $Na_2HPO_4 \times 2\ H_2O$ (9.54 mg) and lactose (332 mg) were dissolved in distilled water, the solution was quickly frozen by dry ice and lyophilized. For physico-chemical characterization (CMC, R_h) or biological tests, the final lyophilizate (100 mg of the origin diblock polymer-Dox conjugate) was reconstituted in aqueous NaCl solution (17.2 mL; concentration 9 g/L).

2.9. Release of the drug Dox

Diblock polymer drug conjugate **DB-Dox** was incubated at 37 °C in 0.1 M phosphate buffers (with 0.05 M NaCl) adjusted to pH 5.0 mimicking the environment in endosomes and lysosomes of cancer cells (intracellular environment), to 6.5 and 6.9 mimicking the extracellular tumor environment and 7.4, that served as a model of bloodstream. The amount of released Dox was determined by SEC (80% methanol and 20% of 0.3 M sodium acetate buffer with pH 6.7; isocratic flow; 0.3 mL/min; Shimadzu system, Japan) on column TSK 3000 Super SW and detection by UV detector (484 nm).

2.10. Synthesis of fluorescently labelled polymer conjugates DB(Cy5.5)-Dox and pHPMA(Cy5.5)-Dox

DB-Dox (10 mg) and 2.5 wt% of Cyanine 5.5 NHS ester (0.25 mg; Cy5.5; product of Lumiprobe) was dissolved in dry MeOH (300 μL). The reaction mixture was reacted under vigorous stirring in the dark overnight. The fluorescently labelled product was purified in the dark by column chromatography (Sephadex LH-20) in MeOH from the mixture of MeOH (75%) and PBS buffer (25%; pH 7.4) for injection. The solvent from the product fraction was removed under vacuum, **DB(Cy5.5)-Dox** was isolated by freeze-drying from water. The content of bound Cy5.5 was determined spectrophotometrically (MeOH, $\varepsilon_{680} = 209,000$ L × mol^{-1} × cm^{-1}). The content of free Cyanine 5.5 was determined by HPLC system equipped with UV-VIS detector (Shimadzu SPD-10AVvp) using methanol-sodium acetate buffer (80:20 vol%) TSK gel Super SW 3000 (Tosoh Bioscience) column. Content of free Cyanine

5.5 was below 0.5% of total dye content. Yield was 80% (8.13 mg), the content of bound Cy5.5 was 0.5 wt%. **pHPMA(Cy5.5)-Dox** was synthesized and characterized by the analogous way as **DB(Cy5.5)-Dox** (the content of bound Cy5.5 was 0.75 wt%).

2.11. General methods

The initiator ABIC-TT and CTA agent CTA-TT were characterized by mass spectrometry on an LCQ Fleet mass analyzer with electrospray ionization (ESI-MS) (Thermo Fisher Scientific, Inc., MA, USA). The content of terminal NH_2 groups on purified PPO were determined in non-aqueous environment by a UV/VIS spectrophotometer Specord 205 (Analytik Jena, Germany) using a modified TNBSA assay [25]. Molar absorption coefficient for amino groups $\varepsilon_{421} = 16,000\ L \times mol^{-1} \times cm^{-1}$, acquired for the model reaction of *N*-(3-aminopropyl)methacrylamide hydrochloride with TNBSA after 60 min incubation in a mixture of methanol/0.1 M sodium tetraborate buffer (pH 9.3) ~60/40, was determined and used. Thin layer chromatography (TLC) of PPO and PPO derivatives was performed on silica-gel 60 F254 (Merck, Germany) with a mixture of chloroform/methanol 5:1 for developing of plates and detection with a solution of NH_4SCN (3.40 g) and $Co(NO_3)_2$ (0.56 g) in H_2O (20 mL). TLC plates of derivatives of doxorubicin (Dox) were performed in a mixture MeOH:$CHCl_3$:CH_3COOH (2:8:1). The molecular weights (M_w, M_n) and polydispersity (Đ) of prepared copolymers and the amount of the released drug Dox were determined by size-exclusion chromatography (SEC) on HPLC system (Shimadzu, Japan) equipped with UV, differential refractive index (Optilab rEX; Wyatt Technology Corp., USA) and multi-angle light scattering (LS) DAWN Helleos II (Wyatt Technology Corp., USA) detectors using column TSK gel Super SW 3000 (Tosoh Bioscience) and 20% acetate buffer (0.3 M; pH 6.5)/80% MeOH as a mobile phase for the analysis. The content of terminal DTB and TT groups, the content of $NHNH_2$ groups that are located along the polymer chain as well as the content of drug doxorubicin (Dox) linked to the polymer conjugates through hydrolytically degradable hydrazone bond were determined spectrophotometrically on a UV/VIS spectrophotometer Specord 205 (Analytik Jena, Germany) using the molar absorption coefficients for TT groups in methanol ($\varepsilon_{305} = 10,800\ L \times mol^{-1} \times cm^{-1}$) [34], for DTB groups in methanol ($\varepsilon_{302} = 12,400\ L \times mol^{-1} \times cm^{-1}$), for $NHNH_2$ groups after their Boc deprotection with TFA/TIS/H_2O (95%/2,5%/2,5%) by TNBSA assay [25] in 0.1 M $Na_2B_4O_7 \cdot H_2O$ with pH 9.3 ($\varepsilon_{500} = 17,200\ L \times mol^{-1} \times cm^{-1}$) and for Dox in water ($\varepsilon_{488} = 9,800\ L \times mol^{-1} \times cm^{-1}$). The molecular weight of formed micelles were determined by field flow fractionation technique (FFF; Eclipse 3+ modul) equipped with DLS (DAWN 8+; Wyatt Technology Corp., USA), UV and RI (Optilab rEX; Wyatt Technology Corp., USA) detection using regenerated cellulose membrane (10 kDa) for the analysis and a mixture water/NaN_3 as a mobile phase. The concentration of the sample was 3 mg/mL. Sizes (R_h) of micelles formed from the diblock polymer precursor (**DB**) and the diblock polymer drug conjugate (**DB-Dox**) in an aqueous environment (PBS buffer, pH 7.4) were performed on a ZEN 3600 (Zetasizer Nano instruments, Malvern, UK) at scattering angle Θ 173° by dynamic light scattering (DLS) as well as the long term stability of these micelles in aqueous media. The micelles were incubated 70 h in PBS buffer (pH 7.4) at 37 °C to determine their stability in aqueous environment (Fig. S1, given in Electronic Supplementary Information (ESI)). All solutions were filtrated with 0.22 μm PVDF filter into dust-free cell prior to DLS experiments.

2.12. Cell lines and cultures

The parental human neuroblastoma cell lines UKF-NB4 (NB4) and UKF-NB3 (NB3) and their chemoresistant sublines UKF-NB4-Dox (NB4/Dox) and UKF-NB3-Dox (NB3/Dox) were provided as a kind gift by Prof. T. Eckschlager, (Department of Pediatric Hematology and Oncology, 2nd Medical Faculty of Charles University in Prague and University Hospital in Motol) [35,36]. The neuroblastoma cells were cultivated in IMDM medium (Life Technology), supplemented with 10% heat inactivated fetal calf serum, and antibiotics (penicillin/streptomycin, Sigma-Aldrich; medium further referred as complete medium), as described elsewhere [36].

Murine monocytic leukemia cell line P388 (parental cell line) and its doxorubicin-resistant subline P388/MDR (overexpressing P-gp) were kindly donated by Prof. I. Lefkovits (Basel Institute for Immunology, Basel, Switzerland). The cells were subcultured and propagated as described before, using complete RPMI 1640 (Sigma-Aldrich); supplemented with 1 mM sodium pyruvate, 0.1 mM non-essential aminoacids, antibiotics (all Sigma-Aldrich), and 10% heat inactivated fetal calf serum (Invitrogen), and antibiotics [37].

2.13. Calcein efflux assay

Calcein^{AM} is a substrate for P-gp (MDR1) or MRP1 multidrug resistance proteins. The ability of their inhibition by **DB** was determined as a fluorescent activity of calcein measured in the drug-sensitive and drug-resistant sublines of human neuroblastoma (NB3, NB4, NB3/Dox, NB4/Dox), and murine lymphoma (P388, P388/MDR) cells. The cells were incubated with various concentration of the diblock polymer precursor **DB** or **DB-Dox** at 5% CO_2, 37 °C. The neuroblastoma cells were seeded at 5×10^3 cells/well in 100 μL culture IMDM medium and cultivated for 48 h allowing the cells to adhere to the plastic (96-well flat bottom TPP Techno Plastic, Switzerland). Subsequently, the cells were incubated with titrated concentrations of **DB** or **DB-DOX** for another 2 or 6 h. The lymphoma cells were seeded at 1×10^5 cells per well (150 μL per well; flat-bottom plates; Thermo Fisher Scientific) in culture medium, and incubated with **DB** at titrated concentrations for 4, 8, or 24 h. As a positive control, the cells were incubated with 10 μM cyclosporine A (CsA). Calcein^{AM} was added for the last 20 min of incubation at final concentration of 0.3 μM for neuroblastoma cells, 0.1 μM for lymphoma cells, protected from light.

The uptake of Calcein^{AM} was stopped by centrifugation (200 g, 5 min, 4 °C) and the cells were washed twice with PBS. The neuroblastoma cells were then resuspended in 200 μL PBS and their calcein fluorescence was measured using a plate reader (Synergy H1 Hybrid Reader, BioTek, Winooski, VT, USA) at 485 nm excitation and 530 nm emission, with the **DB**-untreated cells with calcein set as a background. The lymphoma cells were washed twice and the pellets resuspended in 100 μL of cold FACS buffer (PBS with 2% FCS and 2 mmol EDTA). The flow cytometry analysis was performed using an LSRII instrument (BD Biosciences), and the data were analyzed using FlowJo software (Tree Star, Inc.). For analysis, non-living cells were detected and gated out using Hoechst 33258 staining (Sigma-Aldrich). The results were calculated as percent of the positive control (CsA) or as a mean fluorescence intensity (MFI).

2.14. In vitro cytotoxicity assays

Neuroblastoma cell lines: To determine the cytostatic activity of Dox, **pHPMA-Dox**, and **DB-Dox** with/without presence of **DB**, sensitive and resistant neuroblastoma cells were cultivated in complete IMDM medium in the presence of titrated concentrations of the drugs in 96-well flat bottom plates (Thermo Fisher Scientific) for 72 h, 5% CO_2 at 37 °C. The cells were seeded to let the cells adhere, and **DB** was added to the cells 1 h before the samples containing Dox. At the end of the cultivation period, overall metabolic activity was detected by adding 10 μL Alamar blue® (Life Technologies) for the last 4 h. The active component of the reagent, resazurin, is reduced to the highly fluorescent compound resorufin only in viable/metabolically active cells. The fluorescence of resorufin was detected using Synergy Neo plate reader (BioTek) at 570 nm excitation, 600 nm emission wavelengths.

Triplicate wells were used for each test condition. The inhibition of tumor cell growth was expressed as IC_{50} value, meaning the

concentration of Dox (or equivalent) that inhibited the cell metabolic activity by 50%. The reported data are representative of at least three independent experiments.

Lymphoma cell line: Cytostatic activity of Dox and **pHPMA-Dox** in the presence/absence of diblock polymer precursor **DB** in sensitive P388 and resistant P388/MDR lymphoma cell line, the standard [^{3}H]-thymidine incorporation assay was explored. The cells (1×10^4 per well) were seeded in 96-well flat bottom tissue culture plate (Thermo Fisher Scientific) and cultivated in complete RPMI-1640 medium. Various concentrations of diblock polymer precursor **DB** were added to the wells to reach a final volume of 250 μL. Triplicate wells were used for each test condition. The plates were incubated in 5% CO_2, 37 °C for 72 h. At the end of the incubation period, each well was pulsed with 1 μCi (37 kBq) of [^{3}H]-thymidine (Perkin Elmer) for 6 h. The cells were then collected on glass fiber filters (Filtermat, Perkin Elmer) using cell harvester (Tomtec Mach III,) and the radioactivity of the samples was measured in a scintillation counter (1450 Microbeta TriLux, Wallac) with solid scintillator (Meltilex; PerkinElmer). Cells cultivated in fresh medium were used as controls. The activity of control cells was always higher than 30, 000 cpm/well.

2.15. Polymer conjugate uptake evaluated by laser scanning confocal microscopy

Parental human neuroblastoma NB3 cells and resistant NB3/Dox cells were used for the evaluation of polymer conjugate uptake using confocal laser scanning microscopy. Fluorescently labelled diblock polymer-drug conjugates **DB(Cy5.5)-Dox** and **pHPMA(Cy5.5)-Dox** as a control polymer based on the linear conjugate **pHPMA-Dox** with covalently bound Cy5.5 were incubated with neuroblastoma cells NB3 or NB3/Dox for 2 or 4 h in a 5% CO_2 atmosphere at 37 °C. The amount of the polymer conjugates added to the cell suspensions was normalized to the Cyanine 5.5 content (0.5 μg/mL). The normalization to the dye was used to evaluate the difference in internalization rate between linear and micellar polymer conjugate. After incubation, the cells were washed two times with PBS and the cells were labelled with Hoechst 33342 in PBS (5 μg/mL). The polymer-bound dye Cyanine 5.5 was excited at 647 nm and the emitted light was detected through 650–750 nm filter. Hoechst 33342 dye labelling the nuclei was excited at 405 nm and emitted light was detected through 425–500 nm filter. The laser scanning confocal microscope Olympus IX83 with FV10-ASW software (Olympus, Czech Republic) was used to observe the fluorescence and transmitted light. The samples were scanned with a 60× oil immersion objective Plan ApoN (1.42 numerical aperture).

2.16. In vivo accumulation of drug in solid tumors and drug circulation in bloodstream

Drug accumulation in solid tumor, heart, liver, kidney and blood circulation was performed on mice with inoculated T-cell lymphoma EL4. At day 8 post tumor transplantation, the mice were intravenously (i.v.) injected with DB-Dox, pHPMA-Dox, or free Dox (Adriblastina; Teva), at a dose eq. of 10 mg Dox/kg. Immediately after the treatment administration, the mice were placed in metabolic cages (Tecniplast), with food and water *ad libitum*, in order to collect urine. Mouse blood and tumor, heart, kidney and liver samples were drawn in predetermined time intervals. Tumor, kidney, liver and heart samples were homogenized and analyzed to obtain the content of drug Dox, which was determined after acid hydrolysis in 1 M HCl at 50 °C. Under these conditions Dox is cleaved to aglycon, which is extracted into chloroform and analyzed on HPLC (Shimadzu HPLC system equipped with reverse phase column Chromolith Performance RP-18e, 100 × 4.6 mm, and with UV–vis detector Shimadzu SPD-10AVvp, 230 nm; eluent water/acetonitrile with gradient 50–100 vol% of acetonitrile, flow 0.5 mL × min^{-1}).

2.17. Experimental tumor model and treatment

C57BL/6 female mice were purchased from Institute of Physiology, ASCR (Prague, Czech Republic) and bred under conventional conditions. In all animal work, institutional guidelines for care and use of laboratory animals were strictly followed under a protocol approved by the Institutional Animal Care and Use Committee of the Academy of Sciences of the Czech Republic, and conducted in compliance with local and European guidelines. EL4 lymphoma cells (ATCC TIB-39) were cultivated in RPMI 1640 medium (Sigma-Aldrich) supplemented with 4 mM L-glutamine, 4.5 g/L glucose, 1 mM Na pyruvate (Invitrogen) antibiotics (pen/strept; Sigma-Aldrich), and 10% heat inactivated fetal calf serum (Invitrogen). The mice were subcutaneously (s.c.) injected with 1×10^5 EL4 cells, and treated in a therapeutic regime (*i.e.*, after the tumors developed to a measurable size 6–8 mm in diameter). The treatments were injected intravenously (i.v.) as a single dose eq. 7.5 mg Dox/kg at day 8. Free Dox was injected in two i.v. injections, each 5 mg/kg at days 8 and 12. Tumor growth, potential signs of overall toxicity, such as hunched posture, cachexia, disturbed food and water intake, and survival were monitored. The tumor size was calculated as $V = a*b^2/2$, where a = longer diameter, b = shorter diameter. Statistical differences in survival times were evaluated by Log-rank (Mantel-Cox) test using GraphPad software.

3. Results and discussion

3.1. Synthesis of diblock polymer-Dox conjugate

The hydrophilic block (pHPMA) was synthesized by reversible addition-fragmentation chain transfer (RAFT) polymerization of the comonomers HPMA and Ma-Ah-NHNHBoc. The chain transfer agent dithiobenzoic acid 1-cyano-1-methyl-4-oxo-4-(2-thioxothiazolidin-3-yl)butyl ester (CTA-TT) and the initiator 2-[1-cyano-1-methyl-4-oxo-4-(2-thioxo-thiazolidin-3-yl)-butylazo]-2-methyl-5-oxo-5-(2-thioxothiazolidin-3-yl)-pentanenitrile (ABIC-TT) containing aminoreactive thiazolidine-2-thione groups were used during the semitelechelic polymer synthesis. **DB**, poly(HPMA-co-Ma-Ah-$NHNH_2$)-PPO-NH_2, was prepared by the reaction of the terminal TT groups of the hydrophilic pHPMA block and the aminoderivative of PPO (hydrophobic block) followed by a Boc deprotection with a mixture 95% trifluoracetic acid/2.5% triisopropylsilane/2.5% water. Dox was attached to **DB** *via* a biodegradable hydrazone bond to yield **DB-Dox**. The synthesized polymers were characterized by size exclusion chromatography (SEC), field flow fractionation (FFF), UV/VIS spectrophotometry and dynamic light scattering (DLS).

Although SEC in organic solvents showed a monodisperse diblock polymer with a M_w of approximately 15,000 g/mol, after the dissolution of **DB** in aqueous media, the FFF and DLS proved the formation of supramolecular structures. FFF documented that >85% of all injected mass was during the analysis in the form of nanoparticles, probably micelles (Fig. 1D: peak 2 (micelles): M_n = 1,110,000 g/mol, Đ = 1.31), during the incubation in non-physiologic aqueous media (water with sodium azide).

Similarly, the DLS data showed in both cases (**DB** and **DB-Dox**) that the particle size was approximately 16–20 nm in the hydrodynamic radius (R_h) showing only one peak of micelles and no peak of unimer (Fig. S1, see in ESI) in physiologic-like aqueous media. The good stability of the formed micellar structures of **DB** during the 70 h incubation in PBS buffer (pH 7.4) at 37 °C is demonstrated in Fig. S2 (see in ESI). We suppose that formation of stable micelles in aqueous solution will favorable change the pharmacokinetics of polymer prodrug, *e.g.* prolong the circulation in blood, and enhance the tumor accumulation *via* EPR effect. Moreover, we observed very small negative ζ-potential for both **DB** and **DB/Dox**, ζ-potential (**DB**) = -1.02; ζ-potential (**DB-Dox**) = −1.98, which further increase the stability of the micelles in the aqueous solution.

3.2. In vitro drug release

The stability of the hydrazone bond between **DB** and the anticancer drug Dox at various pH values was verified by the incubation of **DB-Dox** in buffers modeling the bloodstream, extra- and intracellular tumor conditions, PBS buffers with pH 7.4, 6.9, 6.5 and 5.0, respectively. **DB-Dox** was fairly stable in pH 7.4 that mimicked the bloodstream, releasing up to only 10% of the Dox within 24 h. In comparison with the results obtained for pH 7.4 mimicking the environment in bloodstream, we observed faster hydrolysis of hydrazone bond at pH 6.9 and 6.5 mimicking extracellular conditions in tumor mass. There was 23% of released Dox at pH 6.5 and about 17% in pH 6.9 after 24 h of incubation in model buffer media. Even a small decrease in pH from bloodstream values accelerates the drug release, thus confirming the pH-sensitive activation of drug already in extracellular tumor environment. Moreover, the highly accelerated release was found at a pH 5, modeling the situation in the endosomes and the lysosomes of target cancer cells (Fig. 1E).

Our results are consistent with results of the hydrolytic release of the hydrazone bond obtained previously [6,15,25–27] and fully support the applicability of **DB-Dox** as a suitable system for controlled drug delivery.

3.3. In vitro disintegration of micellar polymer carrier

For any clinical use, all nanosized delivery systems have to be able to be excreted, either after controlled degradation or disassembling into fragments, ensuring the removal of the carrier from the body. Micellar systems disassemble after the concentration drop below the CMC. The CMC measurement of the micelles has been conducted using DLS over a broad concentration range, 0.5–0.0025 mg/mL. The obtained intensity-weighted distribution functions of the hydrodynamic radius W (R_h) at different concentrations were inspected for the presence of unimers. It is well known that large objects give a much higher scattering intensity than smaller ones. For this reason, the intensity-weighted distribution functions were further converted to volume-weighted distribution functions, which give more a realistic picture of the size distribution of particles in solution. At high concentrations, a volume-weighted distribution function has a single peak with a R_{h1} value of 15 nm (Fig. 2). This peak was attributed to polymeric micelles. At a high dilution, the ratio of scattering from polymer solution over the solvent was very low. Thus, longer measuring times were required in this case to obtain a correlation function with good signal-to-noise statistics. At concentrations below 0.01 mg/mL, a peak with a R_{h1} value of several nanometers appeared in the distribution function (Fig. 2). This could be ascribed to the unimers of **DB**. We conclude that the micelles were disintegrated at concentrations below 0.01 mg/mL, which could be regarded as the CMC value for the system. Moreover, the presence of a very small portion of large aggregates (<0.4%) was visible in the correlation function at low dilutions as the second peak (R_{h2}). We speculate that this small peak could be ascribed to a very small portion of the PPO block, which was either not reacted into the diblock or was released from **DB** by very slow, spontaneous hydrolysis during the incubation in PBS buffer. The described hydrophobic PPO finally formed large aggregates in aqueous solution after the disintegration of micelles.

3.4. In vitro inhibitory activity of diblock polymer and DB-Dox conjugate

A biological evaluation of the diblock copolymers and its drug conjugate was performed with the aim to simultaneously verify the ability of P-gp inhibition and the drug delivery using polymer nanotherapeutics. Dox-sensitive human neuroblastoma cell lines NB3 and NB4, the murine lymphoma P388 cell line, and their MDR analogues resistant to Dox, NB3/Dox, NB4/Dox, and P388/MDR cell lines, were first tested for their *in vitro* cytotoxic sensitivity to **DB**. After 72 h of incubation with various concentrations of **DB**, no cytotoxicity was determined throughout the measured concentration range. Even at a concentration 500 μg/mL **DB** for neuroblastoma cells or 250 μg/mL **DB** for lymphoma cells, **DB** did not show any cytotoxic effect on the cells (data not shown).

The ability of the diblock polymer precursor **DB** to inhibit transmembrane efflux pumps, especially P-gp, was evaluated using a calcein efflux assay. Previously, it has been demonstrated [36] that drug resistance is caused mainly by the overexpression of P-gp, both in neuroblastoma and lymphoma cells. The significant P-gp inhibition by **DB** was detected in all studied Dox-resistant cell lines, NB3/Dox, NB4/Dox and P388/MDR (Fig. 3).

In the NB3/Dox and NB4/Dox resistant cell lines, the highest P-gp inhibition was apparent between 250 and 125 μg/mL and declined with decreasing **DB** concentration. In P388/MDR, the highest P-gp inhibition was found in the concentration range of 31–125 μg/mL. The difference between the P-gp inhibitory concentration observed in the neuroblastoma cell lines and the lymphoma P388/MDR cell line could be because of the different type and origin of the cancer cell lines, neuroblastoma *versus* lymphoma and mouse *versus* human cells. In addition, the higher

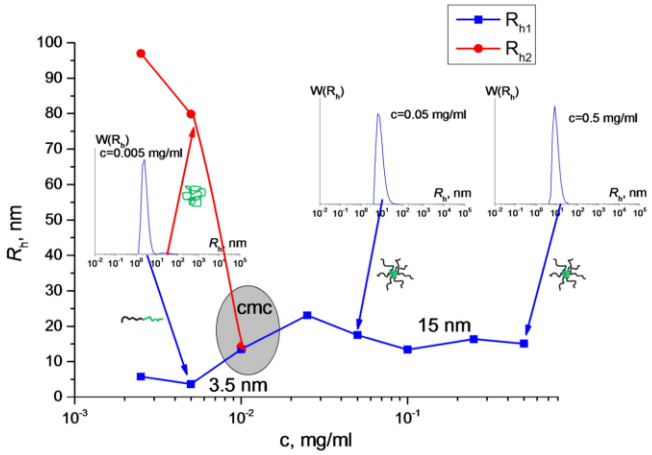

Fig. 2. CMC determination of the diblock polymer precursor **DB**. The dependence of R_h, determined by DLS, on the concentration of **DB** is plotted. Insets: Volume-weighted distribution functions at different concentrations. A schematic description of the PPO block, the unimer of the diblock copolymer **DB**, and the micelle of the diblock copolymer **DB**.

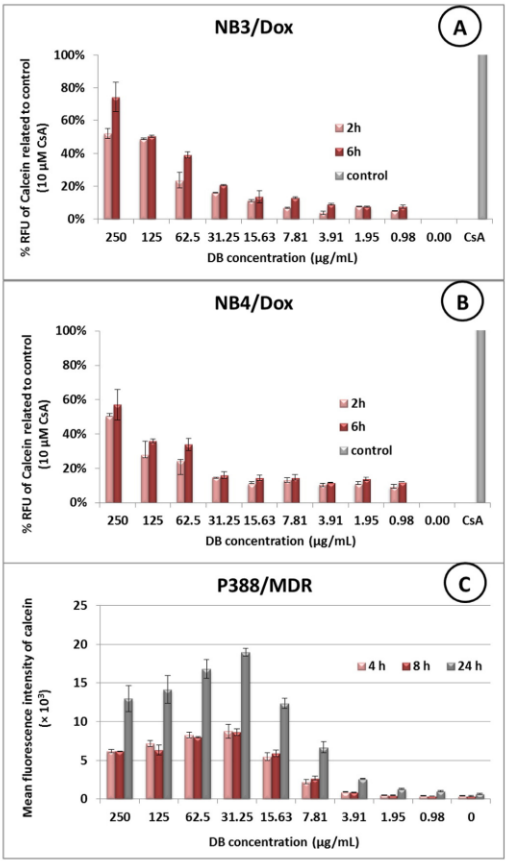

Fig. 3. Calcein efflux assay tested in neuroblastoma NB3/Dox (A) and NB4/Dox (B), and lymphoma P388/MDR (C) cell lines. The ability of **DB** to inhibit the activity of ABC transporters is expressed as percent of the positive control (10 μM cyclosporin A) in neuroblastoma cell lines or as the mean fluorescence intensity (MFI) in lymphoma P388/MDR cells. The MFI values in P388/MDR positive control (10 μM cyclosporin A) were ~50.000.

effect of **DB**, which was observed in neuroblastoma drug-resistant cancer cells, especially NB3/Dox, is driven by the higher expression of P-gp and other ABC transporters in neuroblastoma cells compared to lymphoma cancer cell lines. No significant effect in the calcein efflux assay was observed in the parental drug-sensitive cell lines NB3, NB4 and P388. This agrees with their very low or undetectable expression of P-gp [36]. We have not observed significant difference between **DB** and **DB-Dox** potency to inhibit P-gp, compare Fig. 3 and S3 in ESI. **DB-Dox** was also able to inhibit the P-gp and similarly the highest P-gp inhibition was apparent between 250 and 125 μg/mL in neuroblastoma cell lines. Importantly, the concentrations of **DB** or **DB-Dox** in the range of 30–250 μg/mL corresponded to concentrations that we presume are achievable in polymer systems utilized for the *in vivo* treatment of drug-resistant solid tumors [6]. Thus, we can conclude that the proposed diblock polymer system is able to significantly help to overcome MDR during cancer treatment.

3.5. In vitro cytotoxicity and cellular uptake of polymer conjugate

To further verify our hypothesis that **DB** alone can serve as a P-gp inhibitor and can enable drug penetration and retention in the cancer cells, we tested the effect of P-gp inhibition mediated by **DB** on the cytotoxicity of various types of Dox formulations. For this purpose, we used i) free doxorubicin, ii) **pHPMA-Dox** (a linear conjugate based on the copolymer of HPMA and Ma-Ah-$NHNH_2$ with Dox attached *via* a hydrazone bond, M_w = 30,000 g/mol[26]), and iii) **DB-Dox**. Adding **DB** to the samples increased their cytotoxicity, thus decreasing the IC_{50} value, in all three drug-resistant cell lines (Fig. 4).

The addition of the diblock precursor **DB** at both concentrations (250 μg/mL and 125 μg/mL) induced a significant increase in the cytotoxicity of all Dox formulations tested; a decrease in the IC_{50} value by one order of magnitude, 4 to 7 times, respectively, was observed for free Dox for NB3/Dox, NB4/Dox or P388/Dox. In concordance with the results obtained in the calcein efflux assay (Fig. 3), a greater effect on the cytotoxicity of Dox was observed in NB3/Dox cells expressing a 2-fold higher amount of P-gp than NB4/Dox and P388/Dox [29]. This further supports the hypothesis that the effect of diblock precursor **DB** on ABC transporters predominantly depends on P-gp. The chemosensitivity of cells induced by the addition of the diblock precursor **DB** was more pronounced with the free drug compared with the polymer conjugate **pHPMA-Dox**. These results are not surprising, considering the fact that the polymer conjugates can enter target cells by endocytosis, thereby partially overcoming of membrane drug transporters [38,39]. The diblock polymer-drug conjugate **DB-Dox** itself exhibits 3–5 times higher cytotoxicity on neuroblastoma resistant cancer cell lines in comparison with the linear polymer analogue **pHPMA-Dox**. Similarly, we have found 2–5 times higher cytotoxicity for **DB-Dox** in non-resistant neuroblastoma and lymphoma cell lines, see Table S1 in ESI. Generally, the IC_{50} values were much lowered in sensitive cell lines and no additional effect of **DB** addition was found on NB3 and P388 cell lines, as the cells do not express P-gp. Small effect of **DB** addition, 2–3 times higher cytotoxicity, was found in the sensitive NB4 cell line, as the line contains small amount of P-gp. To further clarify the finding of much higher cytotoxicity for **DB-Dox** compared with **pHPMA-Dox**, we evaluated the polymer conjugate uptake on the sensitive cancer cell line NB3 and resistant cell line NB3/Dox using confocal laser scanning microscopy. We observed a much faster uptake in the case of **DB-Dox** compared to the linear conjugate after the incubation of NB3 or NB3/Dox cells with polymer-Dox conjugates fluorescently labelled with Cyanine 5.5 dye, **DB(Cy5.5)-Dox** and **pHPMA(Cy5.5)-Dox** (Fig. 5). Thus, **DB-Dox** is greatly capable to increase the uptake of itself and consequently of the carried drug into cancer cell lines in both, non-resistant and resistant cell lines.

DB addition to **DB-Dox** caused a smaller increase in the cytotoxicity of **DB-Dox** in neuroblastoma resistant cell lines than in the case of **pHPMA-Dox** or free Dox. We assume that this is because the inhibition of membrane transporters by **DB** is already significantly present in the biological activity of **DB-Dox** and further **DB-Dox** increases the uptake of Dox into cells, allowing the additional diblock polymer **DB** to have only a partial effect. Thus, the addition of **DB** showed only a complementary effect on the cytotoxicity of **DB-Dox**. In summary, the diblock polymer **DB**, itself or in the form of the polymer conjugate with Dox, is able to significantly increase the cytotoxic effect of a drug in selected MDR cancer cell lines. This effect was verified both for the polymer prodrugs (linear or diblock polymer conjugates based on the pHPMA copolymer with hydrazone-bound Dox) and for free Dox. Furthermore, the polymer conjugate with Dox based on the amphiphilic diblock copolymer pHPMA-PPO (**DB-Dox**) exhibited a significantly higher cytotoxic effect on resistant, and also sensitive, cancer cell lines than the analogous polymer systems based only on hydrophilic **pHPMA-Dox**.

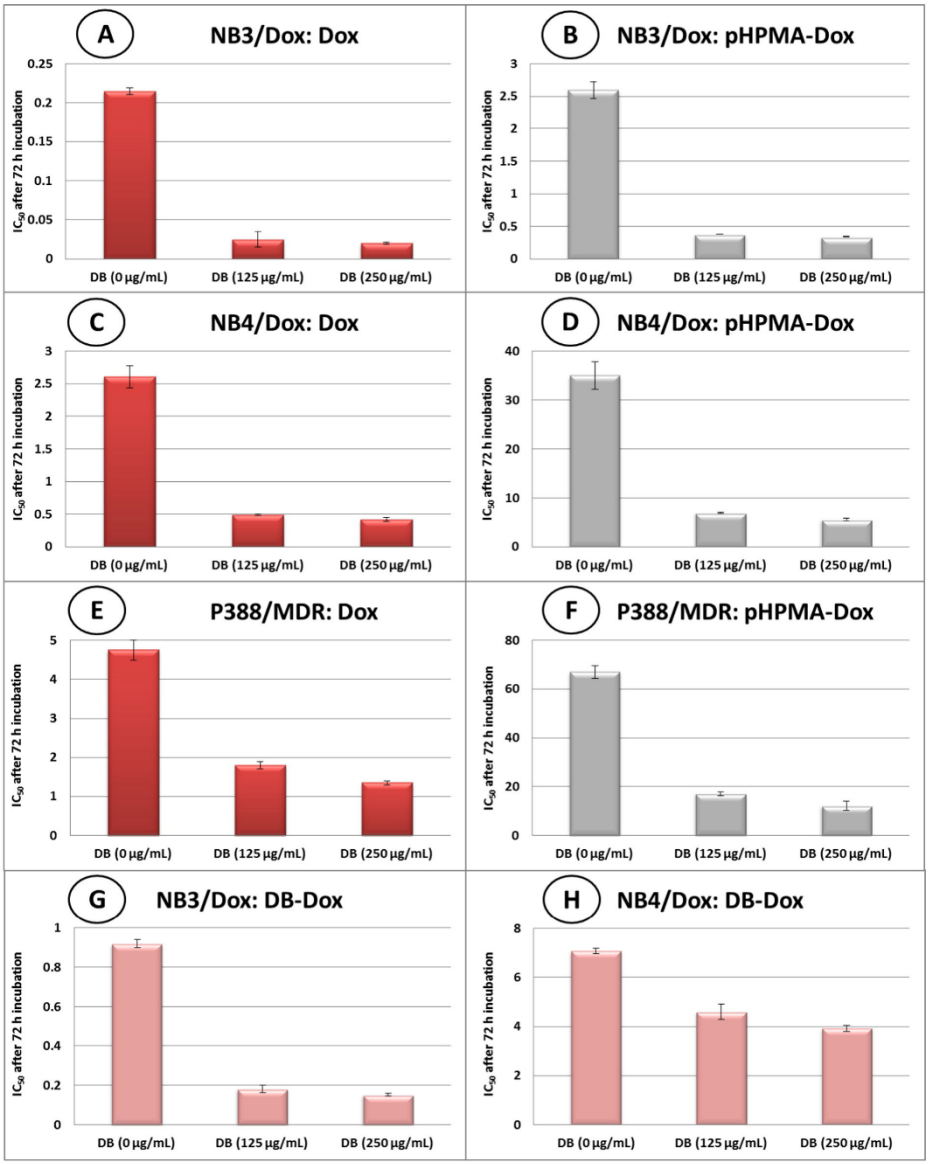

Fig. 4. Increase in the cytotoxicity of three Dox formulations (free parent Dox – A, C, E; linear **pHPMA-Dox** – B, D, F; and diblock polymer-drug conjugate **DB-Dox** – G, H) caused by the inhibition of drug efflux pumps. In the neuroblastoma cell lines NB3/Dox (A, B, G) and NB4/Dox (C, D, H), the overall metabolic activity was determined after 72 h of cultivation using AlamarBlue. The effect of increasing the concentration of the diblock polymer precursor **DB** on the cytostatic effect of free Dox or **pHPMA-Dox** in the lymphoma cell line P388/MDR (E, F) was detected by a standard proliferation assay after 72 h. The results are expressed in all cases as IC_{50} values in μg Dox/mL.

3.6. In vivo therapeutic activity and biodistribution

Proper pharmacokinetics, in particular, the ability to circulate in the organism for sufficient time to achieve increased accumulation within the target tissue, is a key issue for the efficient therapeutic activity of any drugs, including nanotherapeutics. Therefore, we performed a pharmacokinetic study of the *in vivo* drug accumulation in solid tumors and the blood circulation time using mice bearing EL4 T-cell lymphoma. A therapeutically relevant dose of all the Dox formulations (10 mg Dox eq./kg) was administered in mice, and samples of blood, tumor, heart, kidney and liver were collected at predetermined time intervals. We observed a 4-fold higher content of Dox in the tumor tissue

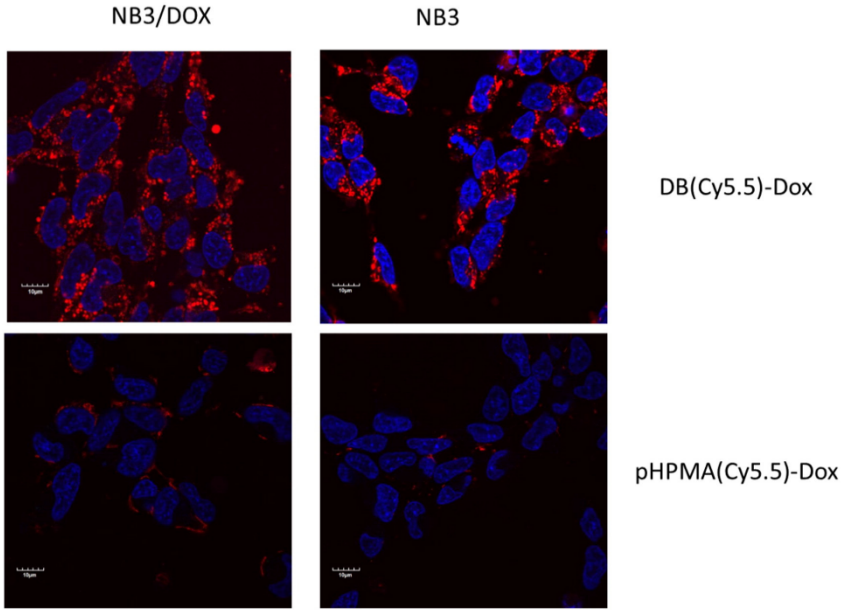

Fig. 5. Uptake of polymer conjugates labelled by fluorescent dye Cyanine 5.5 (coloured in red), nucleus stained with Hoechst 33342 (coloured in blue), after incubation of parental human neuroblastoma NB3 or resistant NB3/Dox cell line 4 h with fluorescently labelled polymer conjugates (micellar **DB(Cy5.5)-Dox** (upper row) and linear **pHPMA(Cy5.5)-Dox** (bottom row)) at 37 °C and 5% CO_2. (For interpretation of the references to colour in this figure legend, the reader is referred to the web version of this article.)

after the administration of micellar polymer conjugate **DB-Dox** than in the case of the linear **pHPMA-Dox** conjugate (Fig. 6B). Furthermore, we observed more than a 20-fold higher accumulation of **DB-Dox** (12 h or 24 h after administration) than that of the parent free drug after the administration of the maximum tolerated dose (MTD) [40]. The drug bound to the diblock polymer conjugate **DB-Dox** circulated in the bloodstream significantly longer than the Dox bound to the linear polymer **pHPMA-Dox** or the parent free Dox (Fig. 6A). This could be described to the increased hydrodynamic size of micellar diblock conjugate, which is higher than the limit of the renal threshold. In contrast to that, free drug and **pHPMA-Dox** are eliminated by renal filtration quickly; their size is lower than the renal limit. In addition, the tumor-to-blood ratio was calculated, showing the increasing value for **DB-Dox**. It was 11.3 after 48 h and 12.2 after 96 h with increasing tendency, while maintaining a value of approximately 1 for free Dox in the whole time interval tested. We have not observed any significant accumulation of free Dox, **pHPMA-Dox** or **DB-Dox** in samples of heart, kidney and liver, see Fig. 6C–E. The concentration of Dox in all the organ samples decreased with increasing time after injection corresponding with blood clearance. Thus, we can conclude that the diblock polymer conjugate **DB-Dox** is suitable to deliver a significantly higher amount of drug into a solid tumor, while keeping the side effects substantially reduced. We also analyzed the amount of Dox in urine at interval 0–96 h after drug administration. After 96 h, we have determined cumulative amounts of Dox: 7% of drug for micellar diblock polymer conjugate **DB-Dox**, 72% for linear polymer conjugate **pHPMA-Dox** and about 19% for free Dox. The decreased amount of Dox in urine observed in case of administration of **DB-Dox** was caused by increased hydrodynamic radius of micellar system, which ensures its prolonged circulation in blood and does not allow the fast urine elimination. A pharmacokinetic study demonstrated a significantly better pharmacokinetic profile for **DB-Dox** than for the linear conjugate **pHPMA-Dox** and the parent free drug. The ability of **DB-Dox** to mediate such a high accumulation of Dox in the tumor tissue is a consequence of the formation of micelles with a hydrodynamic size in the range of 30–35 nm, exhibiting a pronounced EPR effect-driven accumulation.

The treatment of murine EL4 lymphoma tumors, already shown to have sensitivity towards polymer-Dox conjugates based on HPMA [6, 41], was performed to document the ability of **DB-Dox** to act as an efficient drug delivery system, exploiting the EPR effect. **DB-Dox** at a dose as low as 7.5 mg Dox eq./kg induced significant tumor growth reduction (Fig. S4, given in ESI) and complete tumor regression in 3 out of 8 mice in the group (Fig. 6C), whereas **pHPMA-Dox** at an equivalent dose reduced the tumor growth to a lesser extent, curing only one animal. Free Dox, injected at an even higher dose close to the MTD (total 10 mg/kg, injected at day 8 and 12), was not sufficient to induce a complete cure. The applied dose of **DB-Dox** is far below the MTD determined for **DB-Dox** (~25 mg/kg); thus, we can anticipate that the escalation of the dose can further improve the therapeutic outcome of **DB-Dox** treatment.

4. Conclusions

In conclusion, we summarize that the new diblock micellar carrier and the corresponding polymer conjugate with Dox covalently bound *via* a pH-sensitive hydrazone bond are highly potent polymer-based nanotherapeutics for neoplastic treatment. The design of the polymer carrier system significantly reduced the drug side effects, prolonged blood circulation, highly increased accumulation within the target tumor tissue and provided concentration-controlled disassembly of the micellar carrier. The block copolymers enabled the stimuli-sensitive activation of the polymer-bound drugs within the target tumor tissue and cells. In addition, they overcame the P-gp mediated MDR of the cancer cells and highly increased the uptake of the carried drug. We demonstrated the potent activity of the presented micellar carrier (**DB**) and its corresponding conjugate with the drug (**DB-Dox**) in inhibiting

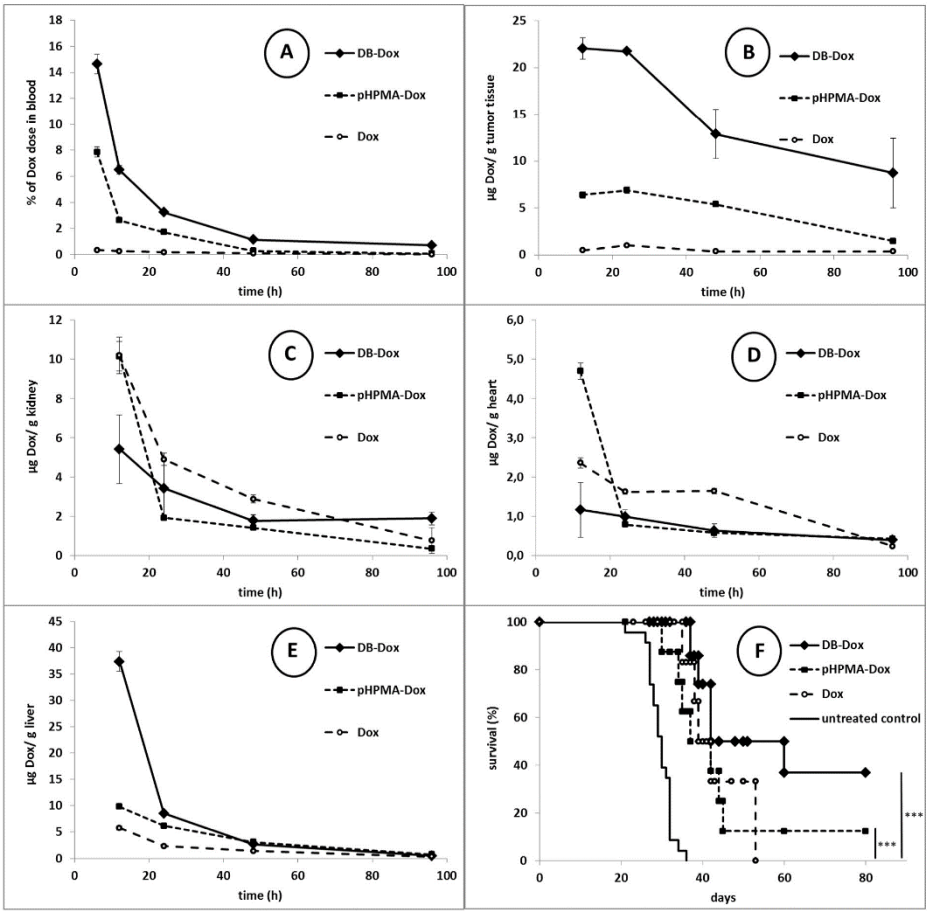

Fig. 6. *In vivo* blood clearance (A), accumulation of Dox in tumor tissue (B), accumulation of Dox in kidney (C), accumulation of Dox in heart (D), accumulation of Dox in liver (E) and survival of EL4 lymphoma-bearing mice after treatment with **DB-Dox**, **pHPMA-Dox**, or free Dox (F). Number of mice analyzed per group/interval in (A, B, C, D, E) n = 3. Number of animals per group in the treatment (C) n = 8. Differences between treated and untreated animals are highlighted; statistical significance $p < 0.0001$.

membrane drug transporters overexpressed in various cancer cells of mouse lymphoma or human neuroblastoma origin. The ability of the P-gp-mediated MDR inhibition is attributed to the diblock polymer precursor **DB** itself, which is non-toxic, but induces the effective chemosensitization of drug-resistant cancer cells towards cytotoxic drugs. Furthermore, we observed that the addition of the diblock polymer to parent Dox or polymer-Dox conjugates significantly increased the cytotoxicity of various Dox formulations by one order of magnitude. We believe that the combination of the above-mentioned features makes the amphiphilic diblock polymer conjugates excellent candidates for further pharmaceutical development.

Author contributions

T.E., A.B., M.P., O.J. and M.Š. were involved in experimental planning, interpreting data and writing the manuscript. A.B., T.E., L.K. and M.P. planned and completed the synthesis, purification and characterization of the small molecules, polymer precursors and polymer conjugates. A.B., S.F., R.L. and P.Č. planned and conducted characterization of prepared micelles by FFF and LS measurements. L.C., Z.H., O.J., L.S. and M.Š. planned and conducted the biological studies.

Acknowledgements

This work was supported by the Ministry of Health of the Czech Republic (grant 16-28600A), Ministry of Education, Youth and Sports of the Czech Republic within the National Sustainability Program I (Project POLYMAT LO1507), National Sustainability Program II (Project BIOCEV-FAR LQ1604) and by the project "BIOCEV" (CZ.1.05/1.1.00/02.0109).

Appendix A. Supplementary data

Electronic Supplementary Information available: Size of micelles measured by DLS (Fig. S1); stability of micelles in PBS buffer (Fig. S2); calcein efflux assay tested in neuroblastoma resistant cell lines (Fig. S3); EL4 lymphoma tumor growth in C57BL/6 mice treated with DB-

Dox, pHPMA-Dox, or free Dox (Fig. S4); IC_{50} values determined for sensitive NB3, NB4 and P388 cell line (Table S1). Supplementary data associated with this article can be found in the online version, at http://dx.doi.org/10.1016/j.jconrel.2016.11.020.

References

[1] J. Sun, Z.-G. He, G. Cheng, S.-J. Wang, X.-H. Hao, M.-J. Zou, Med. Sci. Monit. 10 (2004) RA5–A14.
[2] A.V. Kabanov, J. Zhu, in: G.S. Kwon (Ed.), Polymeric Drug Delivery Systems, Drugs and the Pharmaceutical sciences, vol. 148, Taylor and Francis Group, CRC press, United States of America 2005, pp. 577–613.
[3] M. Werle, Pharm. Res. 25 (2008) 500–511.
[4] J.L. Markman, A. Rekechenetskiy, E. Holler, J.Y. Ljubimova, Adv. Drug Deliv. Rev. 65 (2013) 1866–1879.
[5] S. Kapse-Mistry, T. Govender, R. Srivastava, M. Yergeri, Front. Pharmacol. (5 Jul, 2014) 1–22.
[6] T. Etrych, J. Strohalm, M. Šírová, B. Tomalová, P. Rossmann, B. Říhová, K. Ulbrich, M. Kovář, Polym. Chem. 6 (2015) 160–170.
[7] F. Danhier, E. Ansorena, J.M. Silva, R. Coco, A. Le Breton, V. Préat, J. Control. Release 161 (2012) 505–522.
[8] M.A. Quadir, R. Haag, J. Control. Release 161 (2012) 484–495.
[9] C. Oerlemans, W. Bult, M. Bos, G. Storm, J.F.W. Nijsen, W.E. Hennink, Pharm. Res. 27 (2010) 2569–2589.
[10] J.S. Lee, J. Feijen, J. Control. Release 158 (2012) 312–318.
[11] J.S. Lee, J. Feijen, J. Control. Release 161 (2012) 473–483.
[12] H. Maeda, Adv. Enzym. Regul. 41 (2001) 189–207.
[13] H. Maeda, T. Sawa, T. Konno, J. Control. Release 74 (2001) 47–61.
[14] S. Hoffmann, L. Vystrčilová, K. Ulbrich, T. Etrych, H. Caysa, T. Mueller, K. Mäder, Biomacromolecules 13 (2012) 652–663.
[15] P. Chytil, T. Etrych, L. Kostka, K. Ulbrich, Macromol. Chem. Phys. 213 (2012) 858–867.
[16] V.Y. Alakhov, E.Y. Moskaleva, E.V. Batrakova, A.V. Kabanov, Bioconjug. Chem. 7 (1996) 209–216.
[17] E.V. Batrakova, S. Li, Y. Li, V.Y. Alakhov, A.V. Kabanov, Pharm. Res. 21 (2004) 2226–2233.
[18] E. Batrakova, S. Lee, S. Li, A. Venne, V. Alakhov, A. Kabanov, Pharm. Res. 16 (1999) 1373–1379.
[19] A. Venne, S. Li, R. Mandeville, A. Kabanov, V. Alakhov, Cancer Res. 56 (1996) 3626–3629.
[20] D.Y. Alakhova, Y. Zhao, S. Li, A.V. Kabanov, PLoS One 8 (2013), e72238.
[21] D.Y. Alakhova, N.Y. Rapoport, E.V. Batrakova, A.A. Timoshin, S. Li, D. Nicholls, V.Y. Alakhov, A.V. Kabanov, J. Control. Release 142 (2010) 89–100.
[22] Y. Shi, C.F. Van Nostrum, W.E. Hennink, ACS Bioemater. Sci. Eng. 1 (2015) 393–404.
[23] Y. Shi, E.T.A. van den Dungen, B. Klumperman, C.F. Van Nostrum, W.E. Hennink, ACS Macro Lett. 2 (2013) 403–408.
[24] M. Barz, M. Tarantola, K. Fischer, M. Schmidt, R. Luxenhofer, A. Janshoff, P. Theato, R. Zentel, Biomacromolecules 9 (2008) 3114–3118.
[25] T. Etrych, M. Jelínková, B. Říhová, K. Ulbrich, J. Control. Release 73 (2001) 89–102.
[26] T. Etrych, T. Mrkvan, P. Chytil, Č. Koňák, B. Říhová, K. Ulbrich, J. Appl. Polym. Sci. 109 (2008) 3050–3061.
[27] P. Chytil, M. Šírová, E. Koziolová, K. Ulbrich, B. Říhová, T. Etrych, Physiol. Res. 64 (2015) S41–S49.
[28] K. Ulbrich, T. Etrych, P. Chytil, M. Pechar, M. Jelínková, B. Říhová, Int. J. Pharm. 277 (2004) 63–72.
[29] P. Chytil, T. Etrych, J. Kříž, V. Šubr, K. Ulbrich, Eur. J. Pharm. Sci. 41 (2010) 473–482.
[30] K. Ulbrich, T. Etrych, P. Chytil, M. Jelínková, B. Říhová, J. Drug Target. 12 (2004) 477–489.
[31] V. Šubr, Č. Koňák, R. Laga, K. Ulbrich, Biomacromolecules 7 (2006) 122–130.
[32] X. Huang, D. Appelhans, P. Formanek, F. Simon, B. Voit, Macromolecules 44 (2011) 8351–8360.
[33] S. Perrier, P. Takolpuckdee, C.A. Mars, Macromolecules 38 (2005) 2033–2036.
[34] V. Šubr, K. Ulbrich, React. Funct. Polym. 66 (2006) 1525–1538.
[35] J. Bednricek, A. Vicha, M. Jarosova, M. Holzerova, J. Cinatl, M. Michaelis, J. Cinatl, T. Eckschlager, Neoplasma 52 (2005) 415–419.
[36] E. Koziolová, O. Janoušková, L. Cuchalová, Z. Hvězdová, J. Hraběta, T. Eckschlager, L. Sivák, K. Ulbrich, T. Etrych, V. Šubr, J. Control. Release 233 (2016) 136–146.
[37] V. Šubr, L. Sivák, E. Koziolová, A. Braunová, M. Pechar, J. Strohalm, M. Kabešová, B. Říhová, K. Ulbrich, M. Kovář, Biomacromolecules 15 (2014) 3030–3043.
[38] T. Minko, L. Rodriguez-Rodriguez, V. Pozharov, Adv. Drug Deliv. Rev. 65 (2013) 1880–1895.
[39] T. Minko, P. Kopečková, V. Pozharov, J. Kopeček, J. Control. Release 54 (1998) 223–233.
[40] B. Tomalova, M. Sirova, P. Rossmann, R. Pola, J. Strohalm, P. Chytil, V. Cerny, J. Tomala, M. Kabesova, B. Rihova, K. Ulbrich, T. Etrych, M. Kovar, J. Control. Release 223 (2016) 1–10.
[41] M. Sirova, T. Mrkvan, T. Etrych, P. Chytil, P. Rossmann, M. Ibrahimova, L. Kovar, K. Ulbrich, B. Rihova, Pharm. Res. 27 (2010) 200–208.

Journal of Controlled Release 269 (2018) 214–224

Contents lists available at ScienceDirect

Journal of Controlled Release

journal homepage: www.elsevier.com/locate/jconrel

Polymer nitric oxide donors potentiate the treatment of experimental solid tumours by increasing drug accumulation in the tumour tissue

M. Studenovsky[a,*], L. Sivak[b], O. Sedlacek[a], R. Konefal[a], V. Horkova[b], T. Etrych[a], M. Kovar[b], B. Rihova[b], M. Sirova[b]

[a] Institute of Macromolecular Chemistry, Academy of Sciences of the Czech Republic, Heyrovsky Sq. 2, 162 06 Prague 6, Czech Republic
[b] Institute of Microbiology, Academy of Sciences of the Czech Republic, Videnska 1083, 142 20 Prague 4, Czech Republic

ARTICLE INFO

Keywords:
Enhanced permeability and retention effect
Nitric oxide donor
Polymer-based cytotoxic drugs
HPMA
Solid tumour treatment
T-cell lymphoma

ABSTRACT

The delivery of nitric oxide (NO) specifically to solid tumours was explored in this study as a strategy to augment the passive accumulation of nanomedicines in tumours induced by the Enhanced Permeability and Retention (EPR) effect. An increase in accumulation was achieved by the binding of the chemical precursor of NO, based on an organic nitrate, to a water-soluble synthetic polymer drug carrier. Four structurally different *N*-(2-hydroxypropyl)methacrylamide (HPMA)-based polymer NO donors were synthesized. Depending on their chemical structure, two of these donors were hydrolytically stable, while two rapidly released the parent nitrate under acidic conditions, mimicking the intracellular environment. The polymer NO donors were shown to overcome the drawbacks related to low-molecular-weight NO releasing compounds, namely systemic toxicity, lack of site specificity, and fast blood clearance. The NO donors showed intracellular NO release upon incubation with tumour cells. *In vivo*, they potentiated the EPR effect, resulting in an increased accumulation of polymer-bound cytotoxic drug doxorubicin (Dox) in EL4 T-cell lymphoma inoculated in mice. This led to a better therapeutic outcome in the treatment of lymphoma with the high-molecular-weight polymer conjugates carrying Dox but not in the treatment with the free Dox. The localized augmentation of the EPR effect *via* the tumour-specific NO delivery system can be viewed as a promising strategy to potentiate polymer-based tumour therapy without increasing systemic toxicity.

1. Introduction

The modern world is confronted with an increasing incidence of cancer. The mainstay of cancer therapy is surgery, radiation, chemotherapy, in the last few years also immuno-oncotherapy. Whilst surgery and radiation are suitable for achieving local control over the tumour, chemotherapy exerts a systemic effect. In current clinical oncology, combinations of drugs with different mechanisms of action are used, with the aim of increasing the treatment benefit without amplifying the non-specific toxicity. Systemic toxicity that severely impairs normal tissues and cells, including the immune system, is indeed a major drawback. Due to the side effects, the drugs must be used at suboptimal doses. This can result in the development of (multi)drug resistance, metastatic disease, and, eventually, failure of the therapy. Viewed in light of recent knowledge, a general approach to developing effective cancer therapy would require a potent anti-cancer effect devoid of side toxicity. Potent anti-cancer effects without any significant systemic toxicity have already been thoroughly documented in high-molecular-weight (HMW) delivery systems – for a review see [1,2].

The concept of HMW drug delivery systems, including water-soluble polymers such as *N*-(2-(hydroxypropyl)methacrylamide (HPMA) copolymers, has become generally accepted. Preferably, low-molecular-weight (LMW) drugs are covalently bound to a polymer *via* spacers, which enables the controlled release of the active drug in target tissues or cells. Polymer drug carriers are designed to alter the drug biodistribution and optimize its pharmacokinetics. Binding of the LMW drug to the HMW carrier results in its prolonged blood clearance, enhanced accumulation in solid tumours, controlled drug release, reduction of systemic toxicity and immunogenicity, and possibility of inducing anti-cancer resistance upon treatment [3,4]. Moreover, the binding to the polymer can solubilize water-insoluble drugs.

The HMW anti-cancer drug delivery systems rely on a passive accumulation in the tissue of solid tumours due to the Enhanced Permeability and Retention (EPR) effect, which is caused by the morphological and physiological differences between healthy and malignant tissue [5]. Numerous studies show higher permeability of blood

* Corresponding author.
E-mail address: studenovsky@imc.cas.cz (M. Studenovsky).

https://doi.org/10.1016/j.jconrel.2017.11.017
Received 9 June 2017; Received in revised form 9 November 2017; Accepted 10 November 2017
Available online 16 November 2017
0168-3659/ © 2017 Elsevier B.V. All rights reserved.

vessels in tumours compared to normal blood vessels [6]. The endothelial lining of the capillaries in the tumour is fenestrated and leaky, thereby permeable to macromolecules. Tumour lymphatic drainage is mostly defective or even missing; therefore, macromolecules are retained within tumours. The discovery of the EPR phenomenon [7] led to the rational development of tumour-selective delivery of polymer conjugates, micellar and liposomal drugs and genes. In HPMA copolymers, the EPR effect was observed in conjugates with a molecular weight (M_w) exceeding 20,000 g·mol^{-1} and grew with the increasing M_w of the polymer [8].

The EPR effect occurs because of defective vascular architecture and is tightly controlled by various factors, including bradykinin, nitric oxide (NO), peroxynitrite, prostaglandins, and vascular endothelial growth factor, present in the tumour. Augmenting the EPR effect without systemic side-effects is therapeutically applicable [9]. Some possibilities have already been tested; for instance, raising the systemic blood pressure by infusing angiotensin II during the administration of an HMW cytotoxic drug led to an enhancement of the tumour drug delivery and better therapeutic outcomes [10,11]. The benefits of the utilization of angiotensin-converting enzyme inhibitor for the regulation of blood flow in the tumour focus have also been documented [12]. NO-releasing agents, such as nitro-glycerin (glyceryl trinitrate, GTN), were among the most important substances that facilitated the EPR effect *via* vasodilation, opening the endothelial cell junction gaps, and increasing the blood flow in hypovascular tumours [13,14]. Topical GTN application was shown to induce the enhanced delivery of macromolecular anti-tumour drugs to tumours [15].

This approach is based on the vaso-dilative action of NO, a molecule with a short half-life of a few seconds in the blood. GTN is the most common NO precursor, used for over a century to treat angina pectoris, myocardial infarction and heart failure. GTN exhibits strong vasodilatation potency [16] and has therefore been used as a standard for augmenting the EPR effect. However, many other organic nitrates have been tested as NO donors with variable vasodilatation potency [17]. Although the synergistic actions of such agents with polymer chemotherapeutics have been extensively demonstrated [18,19], the co-administration of the LMW NO donors suffers from several principal problems. Namely, the LMW agents generally exhibit no tumour specificity; thus, only a small fraction of the administered dose is effective. Thus, the total required dose of the LMW agent is high, and furthermore limited, by its non-specific toxicity. Rapid blood clearance combined with a short-term action is another relevant drawback related to the LMW NO donors. Recently, a new group of nanoparticle-based NO donors have been developed [20–22] where other effects than enhancement of EPR effect in terms of therapy with HMW anticancer agents have been reported. For a comprehensive review of NO release see [23–27].

The aim of the study wad to validate the concept that polymer-bound NO donors could accumulate in the tumour tissue by the EPR-mediated manner, and augment tumour localization and effect of co-administered EPR-driven therapies, capitalizing on the already described phenomenon of vasodilation within the tumour through NO [9,13,15]. Furthermore, polymer NO donors were synthesized to overcome the limitations associated with the LMW NO donors. The polymer conjugates should decrease radically the systemic toxicity of the NO donor and change favorably the pharmacokinetics of the NO donor, resulting in an accumulation of the conjugate in the tumours and thus predominant NO generation localized in the tumour mass. The LMW NO donors were coupled to the HPMA copolymer carrier either by a stable bond or a pH-sensitive biodegradable bond, enabling the LMW NO donor's release, prior to its biotransformation to NO. In this paper, we verify our hypothesis that NO could be generated from the polymer NO donors upon cell internalization. The *in vivo* administration of the donors should lead to increased accumulation of HMW polymer conjugate containing cytotoxic drug (administered concomitantly) in a model tumour, and result in improved treatment efficiency of the conjugate. Supposedly, the polymer NO donors should not substantially enhance the treatment effect of the particular free drug. We present data supporting the usage of HPMA copolymer, as a carrier of chemical precursor of NO donor, which could be delivered preferentially to the solid tumour and operate in a spatiotemporal manner, as an EPR effect enhancer, potentiating the effect of treatment with HMW conjugate containing doxorubicin (Dox), designed for passive accumulation in the tumour tissue.

2. Materials and methods

2.1. Chemicals

Acetic acid, 1-aminopropan-2-ol, 2,2′-azobis(2-methylpropionitrile), 4-(chloromethyl)benzyl alcohol, 3-chloropropiophenone, dicyclohexylcarbodiimide, 4-(dimethylamino)pyridine, hydrazine hydrate, iron(III) acetylacetonate, isopropyl magnesium chloride, levulinic acid, methacryloyl chloride, methyl 6-aminohexanoate hydrochloride, silica gel, silver nitrate, sodium hydrogen carbonate, sodium iodide, sodium thiosulfate and succinic anhydride were purchased from Sigma-Aldrich, Czech Republic, Prague. Acetonitrile, methanol and other common solvents and chemicals were purchased from Merck, Czech Republic, Prague. All chemicals and solvents were analytical grade.

2.2. Analytical methods

Analyses were performed on an HPLC chromatograph (Shimadzu, Japan) using a reverse-phase column (Chromolith Performance RP-18e 100 × 4.6 mm) with UV detection. A mixture of water and acetonitrile was used as the eluent at a gradient 0–100 vol% and a flow rate of 2 ml/min. Elemental composition was determined using a Perkin Elmer Elemental Analyzer 2400 CHN (Perkin Elmer, USA). Melting point temperatures (m.p.) were determined on a Kofler block (VEB Analytik Dresden, Germany). NMR spectra were measured on a Bruker Avance MSL 300 MHz NMR spectrometer (Bruker Daltonik, Germany). Molecular weights M_w and M_n of the polymers were determined by gel permeation chromatography (GPC) using an HPLC Shimadzu system equipped with a GPC column (TSKgel G3000SWxl 300 × 7.8 mm; 5 μm), UV/VIS, refractive index (RI) Optilab®-rEX and multiangle light scattering (MALS) DAWN EOS (Wyatt Technology Co., USA) detectors using a methanol and sodium acetate buffer (0.3 M; pH 6.5) mixture (80:20 vol%; flow rate 0.5 ml/min). The hydrodynamic radius (R_h) and zeta potential (ζ) of the polymer conjugates in water (2 mg/ml) was measured using a Nano-ZS instrument (ZEN3600, Malvern, UK). The intensity of scattered light was detected at angle θ = 173° using a laser with a wavelength of 632.8 nm. Data were evaluated using the DTS (Nano) program. The values were the mean of at least five independent measurements. ATR FTIR spectra were recorded using a Thermo Nicolet NEXUS 870 FTIR spectrometer (Thermo Scientific, Madison, WI, USA) in an H_2O-purged environment with MCT (mercury cadmium telluride) detector in the wavelength range from 400 to 4000 cm^{-1}. MKII Golden Gate™ Heated Diamond ATR Top-Plate single reflection system (Specac Ltd., Orpington, Great Britain) was applied for the measurements of spectra of the samples. Typical parameters used: 256 of sample scans, resolution 4 cm^{-1}, Happ-Genzel apodization, KBr beamsplitter.

2.3. Syntheses

2.3.1. 3-Nitrooxypropiophenone (nitrate I)

A solution of sodium iodide (0.88 g, 5.84 mmol) and 3-chloropropiophenone (0.8 g, 4.75 mmol) in 20 ml of acetone was refluxed under argon in the presence of a small amount of sodium hydrogen carbonate (to prevent acid-catalysed aldol condensation) for 20 h. The reaction mixture was cooled down, stirred with a small amount of fine-grained sodium thiosulphate for 1 h to remove traces of iodine, filtered off and the solvent was evaporated. The obtained 3-iodopropiophenone

(0.78 g) was converted to the corresponding nitrate immediately without further purification. The crude product was diluted with 15 ml of acetonitrile, and a solution of silver nitrate (1.23 g, 7.2 mmol) in 10 ml of acetonitrile was added. The reaction mixture was kept overnight in the dark at room temperature, filtered off, washed with dichloromethane and the solution was then extracted five times with 80 ml of water. The combined organic layers were dried with anhydrous sodium sulphate, filtered off and the solvent was evaporated. Yield: 0.55 g, (59%), elemental analysis: calcd. C 55.39, H 4.65, N 7.18%, found C 55.18, H 4.80, N 6.99%.

^{1}H NMR 300 MHz ($CDCl_3$, 297 K): 3.39 t (2H, $COCH_2CH_2$), 4.91 t (2H, $COCH_2CH_2ONO_2$), 7.46–7.96 m (5H, Ar).

^{1}H NMR and ^{13}C NMR spectra are also shown in Fig. S1 and ATR FTIR spectrum is shown in Fig. S4 in Supplementary information.

2.3.2. 5-Methyl-4-oxohexanoic acid

The synthesis of this precursor was carried out according to the procedures found in the literature [28]. Yield: 3.2 g (53%); elemental analysis: calcd. C 58.32, H 8.39%, found C 58.12, H 8.22%.

2.3.3. 4-(chloromethyl)benzyl-5-methyl-4-oxohexanoate

4-(chloromethyl)benzylalcohol (238 mg, 1.52 mmol), 5-methyl-4-oxohexanoic acid (220 mg, 1.52 mmol), dicyclohexylcarbodiimide (600 mg, 2.91 mmol) and 4-(dimethylamino)pyridine (30 mg, 0.25 mmol) were dissolved in 20 ml of tetrahydrofurane at 0 °C, kept cooled for 2 h and then for the next 2 h at room temperature. The pure product was isolated using column chromatography on silica gel at $R_f \sim 0.7$ in the mixture of hexane/ethyl acetate 3:1. Yield: 114 mg (24.9%).

^{1}H NMR 300 MHz (CD_3OD, 297 K): 1.09 d (6H, CH_3), 2.55–2.78 m (5H, $CHCOCH_2CH_2$), 4.55 s (2H, CH_2Cl), 5.08 s (2H, OCH_2Ar), 7.32 m (4H, Ar).

2.3.4. 4-(chloromethyl)benzyl-4-oxopentanoate

4-(chloromethyl)benzylalcohol (238 mg, 1.52 mmol), 4-oxopentanoic acid (177 mg, 1.52 mmol), dicyclohexylcarbodiimide (600 mg, 2.91 mmol) and 4-(dimethylamino)pyridine (30 mg, 0.25 mmol) were dissolved in 20 ml of tetrahydrofurane at 0 °C, kept cooled for 2 h and then for the next 2 h at room temperature. The pure product was isolated using column chromatography on silica gel at $R_f \sim 0.65$ in the mixture of hexane/ethyl acetate 3:1. Yield: 120 mg (31%).

^{1}H NMR 300 MHz (CD_3OD, 297 K): 2.2 s (3H, CH_3), 2.61–2.78 m (4H, $COCH_2CH_2$), 4.55 s (2H, CH_2Cl), 5.08 s (2H, OCH_2Ar), 7.32 m (4H, Ar).

2.3.5. 4-(nitrooxymethyl)benzyl-5-methyl-4-oxohexanoate (nitrate II)

4-(chloromethyl)benzyl-5-methyl-4-oxohexanoate (114 mg, 0.403 mmol) was dissolved in 5 ml of acetonitrile, and a solution of silver nitrate (0.3 g, 1.77 mmol) in 5 ml of acetonitrile was added. The reaction mixture was kept overnight at room temperature in the dark, filtered off, washed with dichloromethane and the solution was then extracted five times with 50 ml of water. The combined organic layers were dried with anhydrous sodium sulphate, filtered off and the solvent was evaporated. Yield: 0.1 g, (80%), elemental analysis: calcd. C 58.25, H 6.19, N 4.53%, found C 54.99, H 6.44, N 4.31%.

^{1}H NMR 300 MHz ($CDCl_3$, 297 K): 1.1 d (6H, CH_3), 2.57–2.8 m (5H, $CHCOCH_2CH_2$), 5.11 s (2H, OCH_2Ar), 5.41 s (2H, CH_2ONO_2), 7.352 m (4H, Ar).

^{1}H NMR and ^{13}C NMR spectra are also shown in Fig. S1 and ATR FTIR spectrum is shown in Fig. S4 in Supplementary information.

2.3.6. 2-Nitrooxyacetophenone (nitrate III)

The synthesis of this nitrate was carried out according to the procedures found in the literature [29]; briefly, 2-bromoacetophenone (1 g, 5.02 mmol) was dissolved in 15 ml of acetonitrile, and a solution of silver nitrate (1.55 g, 9.13 mmol) in 10 ml of acetonitrile was added. The reaction mixture was kept overnight at room temperature in the dark, filtered off, washed with dichloromethane and the solution was then extracted five times with 100 ml of water. The combined organic layers were dried with anhydrous sodium sulphate, filtered off and the solvent was evaporated. Yield: 0.8 g, (88%), elemental analysis: calcd. C 53.04, H 3.9, N 7.73%, found C 53.40, H 3.77, N 7.69%.

^{1}H NMR 300 MHz ($CDCl_3$, 297 K): 5.61 s (2H, CH_2), 7.55–7.94 m (5H, Ar).

^{1}H NMR and ^{13}C NMR spectra are also shown in Fig. S1 and ATR FTIR spectrum is shown in Fig. S4 in Supplementary information.

2.3.7. 4-(nitrooxymethyl)benzyl-4-oxopentanoate (nitrate IV)

4-(chloromethyl)benzyl-4-oxopentanoate (120 mg, 0.47 mmol) was dissolved in 5 ml of acetonitrile, and a solution of silver nitrate (0.3 g, 1.77 mmol) in 5 ml of acetonitrile was added. The reaction mixture was kept overnight at room temperature in the dark, filtered off, washed with dichloromethane and the solution was then extracted five times with 50 ml of water. The combined organic layers were dried with anhydrous sodium sulphate, filtered off and the solvent was evaporated. Yield: 110 mg, (83%), elemental analysis: calcd. C 55.51, H 5.38, N 4.98%, found C 55.18, H 5.68, N 4.99%.

^{1}H NMR 300 MHz ($CDCl_3$, 297 K): 2.2 s (3H, CH_3), 2.61–2.78 m (4H, $COCH_2CH_2$), 5.08 s (2H, OCH_2Ar), 5.4 s (2H, CH_2ONO_2), 7.36 m (4H, Ar).

^{1}H NMR and ^{13}C NMR spectra are also shown in Fig. S1 and ATR FTIR spectrum is shown in Fig. S4 in Supplementary information.

2.3.8. HPMA

Synthesis of this monomer was carried out according to the procedures found in the literature [30]. Yield: 32 g (75%); elemental analysis: calcd. C 58.72, H 9.15, N 9.78%, found C 58.90, H 9.10, N 9.88%; m.p. 69–71 °C (lit: 70 °C).

2.3.9. 6-Methacrylamidohexanohydrazide (MA-HH)

Synthesis of this reactive co-monomer was carried out using a two-step procedure found in the literature [31]. Yield: 5.6 g (80%); elemental analysis: calcd. C 56.32, H 8.98, N 19.70%, found C 56.49, H 8.63, N 19.83%; m.p. 77–79 °C.

2.3.10. Copolymer of HPMA with MA-HH (poly(HPMA-co-MA-HH))

HPMA (3.2 g, 22.4 mmol), MA-HH (0.36 g, 1.67 mmol) and 2,2′-azobis(2-methylpropionitrile) (150 mg, 0.91 mmol) were dissolved in 20 ml of methanol and dry argon was bubbled through the solution for 20 min. The solution was then heated in a sealed glass ampoule at 60 °C for 17 h. The copolymer was precipitated into ethyl acetate, filtered off and purified by re-precipitation from methanol into ethyl acetate. The suspension was filtered off and the resulting copolymer was dried under vacuum. Yield: 2.7 g (76%); molecular weight (GPC): M_w = 30 kDa, Đ = 2.2; hydrazide content (TNBSA assay [32]): 0.65 mmol/g; molar ratio of HPMA:MA-HH monomer units (calculated from the hydrazide content) ~ 9:1, elemental analysis: calcd. C 58.48, H 9.13, N 10.77%, found C 57.98, H 9.5, N 10.56%.

^{1}H NMR 300 MHz (DMSO-d_6, 297 K): 0.8–1.02 m (CH_3), 1.4–2 m ($(CH_2{-}C)_n$, $(CH_2)_4CO$), 2.9 m ($CH_2{-}N$), 3.66 m (CH), 4.18 m (NH_2), 4.7 m (OH), 7.17 m ($NH{-}CH_2$), 8.96 m (NH−N).

^{1}H NMR and ^{13}C NMR spectra and GPC chromatogram are also shown in Figs. S1 and S2. ATR FTIR spectrum is shown in Fig. S4 in Supplementary information.

2.3.11. Polymer nitrates (general procedure)

Poly(HPMA-*co*-MA-HH) (0.7 g, 0.46 mmol hydrazides) and the nitrate **I–IV** (0.5 mmol) were dissolved in 7 ml of methanol and 1 ml of acetic acid and the reaction mixture was kept for two days at room temperature. The corresponding conjugate **I–IV** was precipitated into ethyl acetate, centrifuged and purified by re-precipitation from

Table 1
Characteristics of polymer nitrates.

Conjugate	Yield (g)	M_w (kDa)/Đ	Average nitrate content (mmol/g)/(units/polymer)	R_h (nm)	ζ (mV)
I	0.65	41/2.6	0.64/26	7.2	1.11
II	0.6	55/2.1	0.33/18	7	0.11
III	0.68	41/1.78	0.37/15	6.6	0.76
IV	0.63	53/2.3	0.35/19	7.1	0.14

methanol into ethyl acetate. The suspension was centrifuged and the resulting polymer nitrate was dried under vacuum. Yields, molecular weights (GPC) and nitrate contents (calculated from ^{1}H NMR, see discussion), Rh and ζ potential for conjugates **I–IV** are summarized in Table 1. Elemental analysis and ^{1}H NMR (300 MHz, DMSO-d_6, 297 K) spectra are listed below. ^{1}H NMR and ^{13}C NMR spectra and GPC chromatograms are also shown in Figs. S1 and S2 and the traces from dynamic light scattering (DLS) measurements are shown in Fig. S3 in Supplementary information. ATR FTIR spectra are listed in Fig. S4.

Conjugate **I**: elemental analysis: calcd. C 58.77, H 8.55, N 10.45%, found C 58.12, H 8.71, N 10.18%.

^{1}H NMR: 0.8–1.01 m (CH_3), 1.38–2.01 m ($(CH_2-C)_n$, $(CH_2)_4CO$), 2.9 m (CH_2-N), 3.14 m ($CH_2CH_2ONO_2$), 3.67 m (CH), 4.02 m ($CH_2CH_2ONO_2$) 3.7–4.6 m (OH), 7.17 m ($NH-CH_2$), 8.68 m (NH−N), 7.39–8.12 m (Ar).

Conjugate **II**: elemental analysis: calcd. C 58.8, H 8.82, N 10.2%, found C 58.32, H 9.01, N 10.05%.

^{1}H NMR: 0.8–1.11 m (CH_3), 1.36–1.9 m ($(CH_2-C)_n$, $(CH_2)_4CO$), 2.49–2.73 m (5H, $CH(C=N)CH_2CH_2$), 2.9 m (CH_2-N), 3.67 m (CH), 5.12 m ($COO-CH_2$) 5.57 m (CH_2ONO_2) 4.71 m (OH), 7.18 m ($NH-CH_2$), 7.35–7.49 m (Ar), 10.2 m (NH−N).

Conjugate **III**: elemental analysis: calcd. C 58.51, H 8.77, N 10.64%, found C 58.2, H 8.98, N 10.51%.

^{1}H NMR: 0.8–1 m (CH_3), 1.42–2 m ($(CH_2-C)_n$, $(CH_2)_4CO$), 2.89 m (CH_2-N), 3.66 m (CH), 4.71 m (OH), 5.1 m (CH_2ONO_2), 7.18 m ($NH-CH_2$), 7.54–8.04 m (Ar), 8.06 m (NH−N).

Conjugate **IV**: elemental analysis: calcd. C 58.56, H 8.75, N 10.27%, found C 58.45, H 8.9, N 10.16%.

^{1}H NMR: 0.8–1.15 m (CH_3), 1.35–1.95 m ($(CH_2-C)_n$, $(CH_2)_4CO$), 2.5–2.7 m (7H, $CH_3(C=N)CH_2CH_2$), 2.9 m (CH_2-N), 3.65 m (CH), 5.11 m ($COO-CH_2$) 5.56 m (CH_2ONO_2) 4.71 m (OH), 7.2 m ($NH-CH_2$), 7.35–7.45 m (Ar), 10.15 m (NH−N).

2.3.12. Star-Dox conjugate

Synthesis of this dendrimer-based (*star*-like) polymer conjugate of Dox (star-Dox) was described here [33]. The conjugate was derived from a second generation of poly(amido amine) (PAMAM) dendrimer (Dendritic Nanotechnologies, Inc., USA) grafted with semitelechelic HPMA copolymers with doxorubicin attached by hydrazone bond in side chains (referred as D_2-P(Dox^H), Table 2 in the cited paper). The final conjugate contains a given amount of amino groups originating from Dox molecules but also certain amount of unreacted amines from the PAMAM core. Consequently, the overall nature of the Star-Dox conjugate is slightly cationic that is in accordance with a positive value of the ζ potential. A sample of the amount sufficient for all experiments (M_w: 250 kDa, Đ: 1.5, Dox: 10.7 wt%, R_h: 12.7 nm, ζ: 16.8 mV) was kindly provided by the authors.

2.4. Tumour cell lines

Murine EL4 T cell lymphoma (ATCC TIB-39), EL4.IL-2 (ATCC TIB-181), 4T1 breast carcinoma (ATCC CRL-2539), and human endothelial cell line EA.hy926 (ATCC CRL-2922) were purchased from ATCC and maintained as recommended by the provider. The murine monocytic leukaemia cell line P388 (parental cell line) and its Dox-resistant subline P388/MDR (cell line overexpressing P-gp) were obtained from Prof. I. Lefkovits (Basel Institute for Immunology, Basel, Switzerland).

2.5. In vitro treatment of tumour cells with polymer NO donors

To determine *in vitro* effects of the polymer NO donors on the tumour cells, the conditions for cell cultivation were adopted for the use of D-MEM, to ensure that no extracellular biotransformation of the organic nitrates to NO occurred, due to glutathione contained in the culture medium. The RPMI 1640 medium contains high levels of nitrate/nitrite that interfere with NO detection in the supernatants of NO donor-treated cells. The D-MEM medium (Sigma-Aldrich) was supplemented with 4 mM L-glutamine, 4.5 g/l glucose, antibiotics (pen/strept, Sigma-Aldrich; 100 U/ml penicillin, 100 μg/ml streptomycin), 10 mM HEPES, and 10% foetal calf serum (FCS).

The cells were cultivated in 96-well flat-bottomed (FB) culture plates (Thermo Scientific) with various concentrations of NO donors or GTN as a positive control for 3 days. Cell counts at the beginning of cultivation were as follows: 5000/well for EL4.IL-2 and EA.hy926, and 2500/well for the 4T1 cell line. Cell proliferation was estimated by the standard ^{3}H-thymidine incorporation assay, or by determination of overall metabolic activity using MTT as a surrogate parameter. EL4.IL-2 subline of EL4 lymphoma was explored in ^{3}H-thymidine incorporation assays, instead of EL4, as the EL4 cells do not incorporate thymidine at a sufficient intensity.

2.6. Cell-based nitric oxide assay

For intracellular NO determination, the water soluble, cell permeable non-fluorescent probe 5-amino-2-(6-hydroxy-3-oxo-3H-xanthen-9-yl) benzoic acid methyl ester (FA-OMe) was used (Nitric Oxide Fluorometric Cell-based assay Kit, Cayman Chemicals) [34]. Cleavage of the probe by intracellular esterases prevents re-transfer across the cell membrane and the active form reacts with NO, generating intensely fluorescent product dA-FA-OMe *via* reductive deamination of the aromatic primary amine [35]. The EL4 cells (5×10^4/well) were seeded onto 96-well FB plates in phenol-free D-MEM supplemented with 10% FCS. The cells were incubated with NO donors (in duplicate) and 10 μM FA-OMe for 8 h at 37 °C under humidified 5% CO_2 atmosphere in darkness. The reaction was terminated by centrifugation (200 G, 5 min, 4 °C), the cell pellets washed twice with 100 μl assay buffer and transferred to black FB plate (Thermo Scientific). The dA-FA-OMe fluorescence was measured at excitation 485 nm, emission 535 (Tecan Infinite). The images were captured using FV-1000 confocal microscope (Olympus) and analysed by FV-ASW image software (Olympus). The fluorescence intensity was determined using ImageJ software. For endogenously generated NO detection, NO generated *via* inducible nitric oxide synthase was measured in RAW 264.7 murine macrophages, stimulated 1 μg/ml of lipopolysaccharide (LPS from *Salmonella sp.*, Sigma-Aldrich).

2.7. In vivo tumour treatment

Inbred C57BL/6 (*H-2b*) female mice were obtained from the Institute of Physiology CAS, v.v.i., Prague, Czech Republic. EL4 T-cell lymphoma (ATCC TIB-39) was used as the *in vivo* model of the solid tumour. The mice (two to three months old, ~23 g) were subcutaneously (s.c.) transplanted at day zero with 1×10^5 EL4 cells, and treated with the polymer conjugates injected intravenously (i.v.)

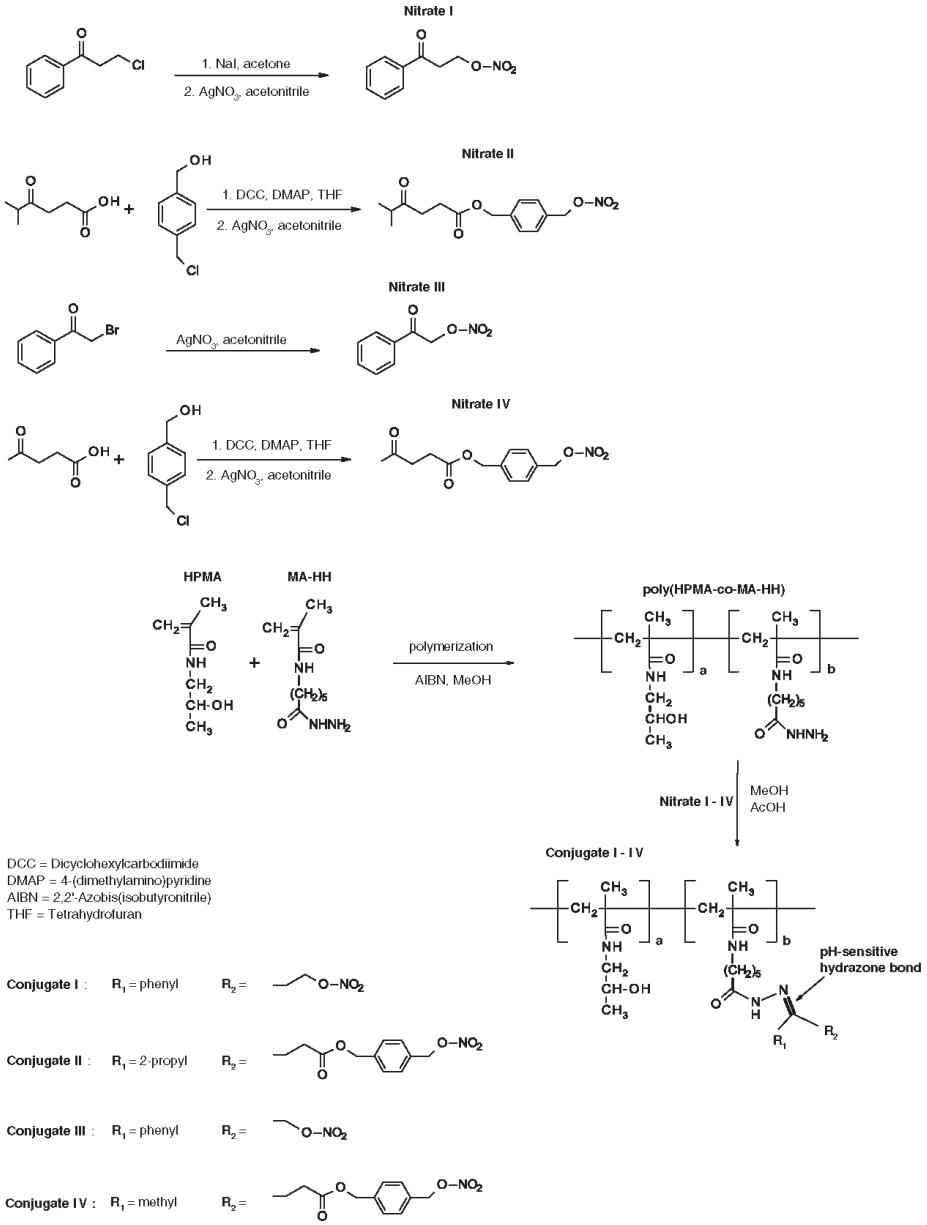

Fig. 1. Synthesis of polymer NO donors I–IV.

starting at day 9, when diameter of the tumour focuses was 6–8 mm. The mice were injected with a single dose of the star-Dox conjugate eq. of 7.5 mg Dox/kg, and with four doses of the polymer NO donors **I** and **II**, each dose eq. to 20 μmol nitrate/kg; for the administration scheme, see the Fig. 5. Tumour growth, body weight as a parameter of overall toxicity, and survival time were monitored. The tumour volume was calculated, as $V = a \cdot b^2/2$, where a = longer diameter, and b = smaller diameter. In all animal work, institutional guidelines for care and use of laboratory animals were strictly followed under a protocol approved by the Institutional Animal Care and Use Committee of the Academy of

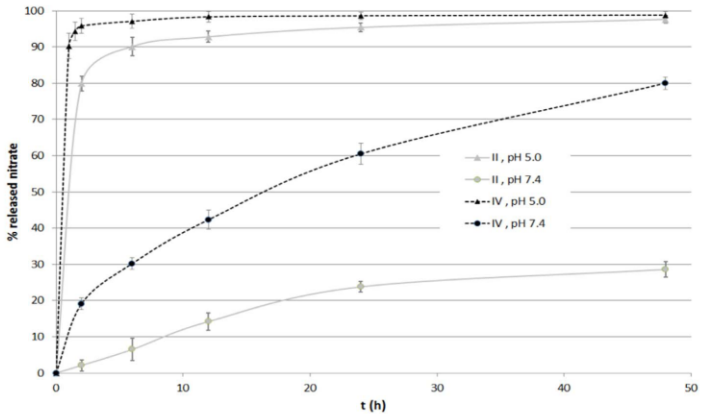

Fig. 2. Kinetics of hydrolysis of conjugates **II** and **IV**. The conjugates were incubated in phosphate buffer pH 5 and pH 7.4, respectively at 37 °C and the released nitrate was quantified by HPLC.

Sciences of the Czech Republic, and conducted in compliance with local and European guidelines.

2.8. Dox accumulation in the tumour

The EL4 tumour-bearing mice were administered i.v. with polymer-Dox conjugate (star-Dox), single dose of 10 mg Dox eq./kg. The exact dosage of the polymer nitrate (conjugate **I**) is shown in the Fig. 6. At specified time intervals, the mice were sacrificed, and samples of tumour, skeletal muscle, and liver were harvested. The weighted tissue was homogenized in 1 ml PBS using glass homogenizer. The homogenates free of coarse tissue remnants were frozen at − 20 °C until the sample processing.

The samples were tested for the total content of Dox (*i.e.*, the sum of free and polymer-bound Dox). Determination of the total Dox content was performed after quantitative acid hydrolysis in 1 M HCl. After incubation for 1 h at 50 °C, the aglycon of Dox (doxorubicinone) was extracted with chloroform, the organic phase was evaporated to dryness, and the remaining solid was completely dissolved in methanol and analysed using a gradient-based HPLC Shimadzu system equipped with a fluorescence detector (Shimadzu RF-10Axl) (λ_{exc} = 488 nm, λ_{em} = 560 nm). A calibration curve was obtained by the injection of exact amounts of free Dox.HCl into the blood and tumour tissues obtained from untreated animals, and the samples were analysed, as described above, after homogenization, hydrolysis, and extraction. All experiments were carried out in quadruplicate.

2.9. Statistical analysis

Analysis of significance was conducted with Student's *t*-test, comparison of the survival times by log-rank (Mantel-Cox) test, and statistical analysis was performed with GraphPad Prism software. Significance was set as $p < 0.05$.

3. Results and discussion

3.1. Chemistry

In this work, we used HPMA copolymer as a carrier for various nitroesters, acting as active compounds, releasing nitric oxide *in vitro* and *in vivo*. Molecular weight of the carrier was 30 kDa thus, exhibiting a solid tumour selectivity *via* the EPR effect. The LMW nitroesters were linked to the linear polymer chain by the hydrazone bond that is generally stable under neutral or alkaline conditions but can be, depending on the structure, susceptible to a rapid hydrolysis at slightly acidic pH, typical for tumour microenvironment. This latter aspect makes it possible to design and prepare hydrolysable or non-hydrolysable hydrazone bond-based conjugates, and then compare the two different systems – one of them releasing the LMW nitrate prior to entering the tumour cell (conjugate **II** and **IV**), and the other acting as an NO donor in its parent polymer form (conjugates **I** and **III**). The reactive polymer carrier was prepared by free radical copolymerization of HPMA with hydrazide group-containing co-monomer MA-HH in methanol using 2,2′-azobis(2-methylpropionitrile) as an initiator. The content of hydrazide groups, determined by TNBS method, was 0.65 mmol/g, which is equivalent to approximately 10 mol% of hydrazide group-containing monomer units in the polymer. Nitrates **I–IV** were linked to the polymer precursor by an acid-catalysed condensation, where their carbonyl groups were coupled with polymer hydrazides, thus forming hydrazone bond. A general synthetic scheme for the polymer NO donors is illustrated in Fig. 1 and Fig. S5 in Supplementary information. The content of the nitrates in the corresponding conjugates was calculated from the ratio of integrals of ^{1}H NMR signals (300 MHz, DMSO-d_6, 297 K) selected from the nitrate molecule (conjugate **I**: 7.39–8.12 m (5H, Ar); conjugate **II**: 5.57 s (2H, CH_2ONO_2); conjugate **III**: 7.54–8.04 m (5H, Ar))); conjugate **IV**: 5.56 s (2H, CH_2ONO_2) and the HPMA co-monomer (3.67 s (1H, CHOH)). Polymer conjugates **I** and **III** are derived from aromatic ketones (nitrates **I** and **III**); thus, they have a phenyl substituent on the hydrazone group resulting in an electron delocalization causing their hydrolytic resistance and they were completely stable at pH 7.4 and 5. However, conjugate **II** and **IV** have no aromatic substituent in the vicinity of the hydrazone bond and exhibited hydrolytic profile shown in Fig. 2 [36] – rapid hydrolysis at pH 5 (mimicking endosomes and lysosomes of tumour cell) but prolonged stability at pH 7.4 (mimicking blood). At pH 5, there was no significant difference between hydrolysis rate of conjugate **II** and **IV** – > 90% of the LMW nitrate was released during first three hours. On the other hand, the conjugate **IV** showed much lower stability at pH 7.4 compared with conjugate **II** (64% *vs.* 22% released in 24 h). Based on this fact, we considered conjugate **IV** unsuitable for further experiments and excluded it from this study. The nitroesters **I–IV** were prepared from the corresponding halides by the reaction with silver nitrate in acetonitrile, where a formation of completely insoluble silver halide, as a by-product, was the main reactive driving force. Because of the low reactivity of 3-chloropropiophenone, a starting compound for synthesis of nitrate **I**, it must be converted to a more reactive 3-iodopropiophenone with sodium iodide in acetone (Finkelstein reaction), prior to the reaction with silver nitrate.

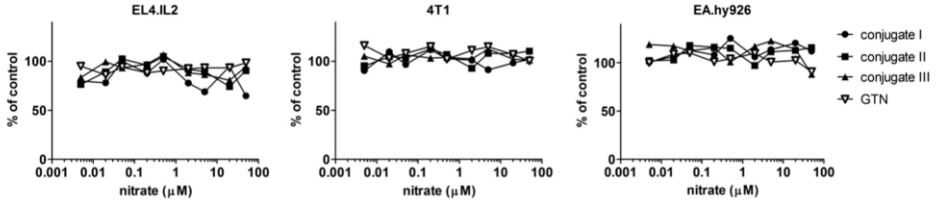

Fig. 3. Cytostatic activity of polymer NO donors and GTN in permanent cell lines. The cells were cultivated with various concentrations of polymer NO donors, and their proliferation was determined after 72 h using ^{3}H-thymidine incorporation. The results are expressed as percent of control (untreated) cell proliferation.

3.2. In vitro toxicity of polymer NO donors

Neither of the polymer NO donors nor GTN showed direct cytostatic or cytotoxic effect, as proved for a wide range of NO donor concentrations tested. No significantly decreased proliferation was observed in selected permanent cell lines, including murine EL4.IL-2 T-cell lymphoma and 4T1 mammary carcinoma, or a prototype human endothelial cell line EA.hy926 (Fig. 3). No cytotoxic effect, as determined by overall metabolic activity using MTT, was also observable (Supplementary information, Fig. S6). The same effect was observed for normal murine splenocytes cultivated in D-MEM culture medium and evaluated using MTT (Supplementary information, Fig. S7) within one to three days. The effect on splenocytes, under the condition of intense proliferation induced by a mitogen (Con A), could not be evaluated, as the presence of a high level of glutathione (as in the RPMI 1640 medium) is needed for adjustment of this condition. We assume that glutathione can trigger biotransformation of organic nitrates to NO; therefore, its extracellular content is undesirable. However, considering the negligible cytostatic/cytotoxic activity observed in the permanent cell lines, no such activity in proliferating normal cells is supposed.

3.3. Intracellular NO release

Upon incubation with EL4 T-cell lymphoma cells, the polymer NO donors showed intracellular NO release, detectable using a cell-captured fluorescent probe. Compared with non-treated controls, the NO release was most prominent in conjugates I and II, whilst conjugate III showed only limited NO release. Various time-periods were tested, of which, 8 h proved the best relationship between the conjugate-related and background fluorescence (Fig. 4). The detected cellular NO content was strictly dose-dependent. Interestingly, lower concentrations of the NO donors induced the highest specific fluorescence, both in polymer donors and LMW nitrates (Supplementary information, Fig. S8) irrespective of the differences in the nature of the donor organic nitrates. To further substantiate these findings we evaluated the intracellular NO release from conjugates I, II, III and GTN using confocal microscopy in parallel with measurements of fluorescence intensity (Supplementary information, Fig. S9).

Together, the results showed a similar intracellular NO profile in the organic nitrates I, II and GTN. However, the biotransformation of GTN and other organic nitrates, mechanisms of activation and action *in vivo* in vasodilation are still not fully elucidated, despite years of their clinical use [37]. The bioactivation pathway appears to differ between low and high concentrations of GTN [16,37,38]. Speculatively, a similar process could exist in the intracellular detection of NO using FA-OMe probe. Obviously, the incubation of cells with the polymer NO donors or GTN did not decrease the overall metabolic activity of the cells, as determined by MTT assay within the concentration range and incubation periods tested (data not shown); thus, the low NO intracellular content at high concentration of NO donors was not caused by their toxicity. Moreover, the FA-OMe probe was sufficient for detecting the increased fluorescence within a wide range of NO concentrations as was proven using the monocyte/macrophage cell line stimulated with lipopolysaccharide (Supplementary information, Fig. S10). This finding documents that any potential quenching of the specific dA-FA-OMe fluorescence, by increased NO production at higher concentrations of polymer NO donors or GTN, did not happen.

Based on the intracellular NO delivery, the conjugates I and II were selected for further *in vivo* experiments. Their intracellular NO release profile showed that NO could be released directly from the polymer conjugate, and the liberation of the organic nitrate from the polymer carrier is not a prerequisite for the intracellular NO generation. According to our previous data on the accumulation of HPMA-based polymer prodrugs in the EL4 lymphoma tumours, we assume similar accumulation also in the case of polymer NO donor. Thus, the crucial range of the polymer NO donors falls within the interval of 0.1–0.05 μM nitrate. It is of note that in this range of the NO donor concentrations a significant intracellular NO generation was demonstrated.

3.4. In vivo combination treatment with polymer NO donors

To prove that polymer NO donors could affect the treatment of solid tumours, we tested their effects in a model of murine EL4 T-cell lymphoma (for the administration scheme, see Fig. 5A). Compared with the untreated control, the conjugates I and II, when applied as a sole treatment, showed virtually no effect on the lymphoma growth. However, survival times were slightly shortened, but the differences *vs.* untreated control were not significant (Fig. 5 B, C). This outcome could be indicative of a short-term improvement in tumour blood supply, induced by the release of NO within the tumour focus. Indeed, a transient increase in the tumour size was observed between days 17 and 21 post tumour transplantation in the cohorts treated with the conjugate I or II. An increase in blood flow and blood vessel permeability in experimental tumours by local administration of GTN as an NO donor has been demonstrated [15].

Notably, compared with the sole star-Dox treatment, when the conjugates I and II were co-administered with star-Dox conjugate, the treatment outcome was better. The star-Dox conjugate was applied deliberately at a suboptimal dose, which, as a sole treatment, compared with untreated animals, brought significant survival benefit ($p < 0.0001$), as it induced complete cure in two out of eight mice in the group. Although the differences between star-Dox and combination of star-Dox with conjugate I or II were not significant, the result demonstrated an increase in the number of cured animals (five cured mice with conjugate I, four with conjugate II *vs* two complete remissions with star-Dox only). This trend was apparent both in the average tumour growth (Fig. 5D) and survival time (Fig. 5E). Thus, the final effect of the combination therapy, probably reduced by the very small contradictory effect of the polymer NO donor itself, was a clear improvement in the treatment effect. Similar to the intracellular *in vitro* NO release (Fig. 4), the liberation of the organic nitrate from the polymer carrier probably is not a prerequisite for the *in vivo* function, as the conjugate I with the non- hydrolysable binding of the NO donor was active as well as the conjugate II with the organic nitrate bound *via* a labile bond.

Not surprisingly, compared with Dox-only treatment, similar

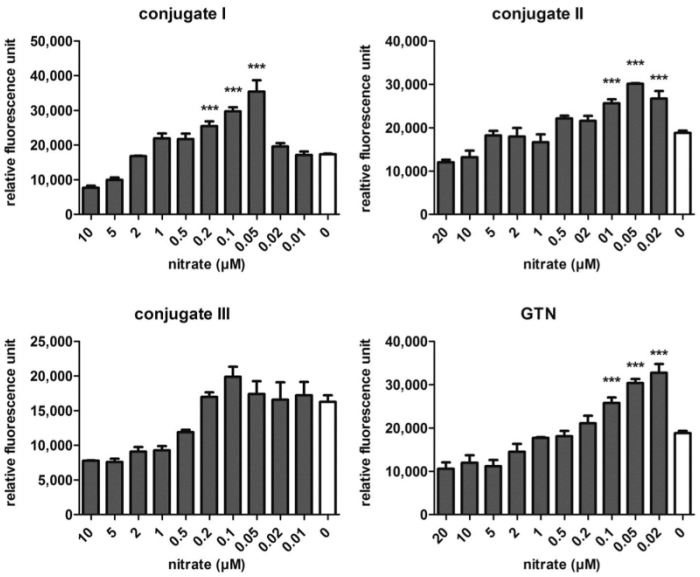

Fig. 4. Intracellular NO detected in EL4 T-cell lymphoma cells using FA-OMe probe. The cells were incubated with titrated concentrations of polymer NO donors (conjugates **I**, **II**, and **III**), or GTN, as a positive control, and FA-OMe probe. After 8 h, the cells were washed and dA-FA-OMe fluorescence measured at excitation 485 nm, emission 535 nm. Cells incubated in medium only were used as control. Fluorescence intensity was determined using microplate reader and expressed as relative fluorescence units (RFUs). All data are the mean ± SD of two independent experiments. Significant differences *vs.* the negative control incubated with FA-OME only are shown ($p \leq 0.05$, $p \leq 0.01$, $p \leq 0.001$).

combination treatment with free Dox and conjugate I neither reduced the tumour growth nor extended the survival time (Fig. 5F, G). Despite that the dose of Dox was set close to the maximum tolerated dose (9 mg/kg i.v., administered as a single dose) [39,40], no decrease in the body weight or occurrence of other signs of systemic toxicity, such as hunched posture, were observed due to the combination with the polymer NO donor (Supplementary information, Fig. S11). The free drug is not subject to the EPR effect and its biological half-life in peripheral blood is short; thus, any increase in the blood supply or improved vasodilation induced by the NO release in the tumour probably could not induce significant improvement in the anti-tumour activity of the free drug.

3.5. Effects of polymer NO donor on drug accumulation in vivo

Indeed, the treatment of EL4 T-cell lymphoma based on polymer therapeutics, whose effect depends on passive accumulation in the tumour driven by the EPR effect, could be improved by NO, generated locally from the chemical precursor. Next, we investigated whether the polymer NO donor could induce the increase in the drug accumulation in the tumour tissue. Total Dox content was determined as the sum of the content of the drug bound to the polymer and the drug liberated from the carrier in tumours, liver, and skeletal muscle of the EL4 tumour-bearing mice treated with conjugate **I**, either two (Fig. 6A), or four doses, in combination with star-Dox conjugate (Fig. 6B). As expected, the Dox content in the liver detected at twelve hours post the treatment was rather high (Fig. 6C), but the drug accumulation decreased at later intervals. The Dox accumulation in the tumour upon administration of conjugate I was significantly higher than that induced by the sole Dox-containing conjugate at 12 h and 24 h (two doses of conjugate **I**), and at 72 h (four doses of conjugate **I**) (Fig. 6E). At 24 h, the difference in the Dox content in the combination treatment was apparent, but less pronounced. Supposedly, the NO generation from the chemical precursor was rather fast; thus, the time interval between 12 and 24 could be rather long for the two doses of conjugate I to maintain the vasodilation and increased permeability of the vasculature in the tumour. As a results the Dox content began to fall back to the level induced by the sole star-Dox conjugate. The Dox content in the samples of skeletal muscle, a tissue also well supplied with blood, was virtually negligible at all time intervals (Fig. 6D). There were no significant differences in the Dox content in the liver or skeletal muscle at the later time points, *i.e.*, 24 and 72 h, between the sole *star*-Dox treatment and the combination with polymer NO donor (Fig. 6C and D). The preferential accumulation of Dox due to the passive accumulation of the HMW star-Dox conjugate driven by the EPR effect was further documented by the ratio between the Dox content detected in the tumour and healthy tissue, such as skeletal muscle (Fig. 6F). The data showed increased accumulation of Dox in the tumour over the muscle tissue, due to the combination treatment with polymer NO donor at all time intervals tested. As expected, the ratio increased over time, and compared with the sole star-Dox, the values rose more steeply in the combination treatment, pointing to a potentiating effect of the polymer NO donor.

The increased efficacy of nano-sized drug delivery systems for cytotoxic drugs is believed to be linked to the enhanced accumulation of the drug in the tumour tissue. Recently, we showed that a decrease in the Dox accumulation in the tumour reduced the number of mice with regressed EL4 tumours following treatment with the HMW polymer Dox conjugate [41]. Thus, *vice versa*, we consider the finding of the increased Dox content in the tumours could be responsible for the observed increase in the therapeutic efficacy of the combination of *star*-Dox with polymer NO donor.

Indeed, NO could play several important roles in cancer, thus the possibility of other mechanisms by which NO generated from the polymer NO donors could affect the tumour growth cannot be ruled out. Some of the already described ones, such as direct killing of cancer cells [42,43], chemosensitization effect [44,45], or increased cytotoxic effect of Dox by inhibiting drug efflux mediated by P-gp or other multidrug resistance-associated proteins [46], can be excluded as the main mechanisms in the EL4 lymphoma model. The direct cytotoxicity of the polymer donors *in vitro* is limited (Fig. 3). Moreover, conjugate I and II do not increase the anti-cancer effect of free Dox *in vitro* [47] and *in vivo* (Fig. 5), which contests the chemosensitivity as the main mechanism. The overexpression of P-gp or other membrane transporters causing

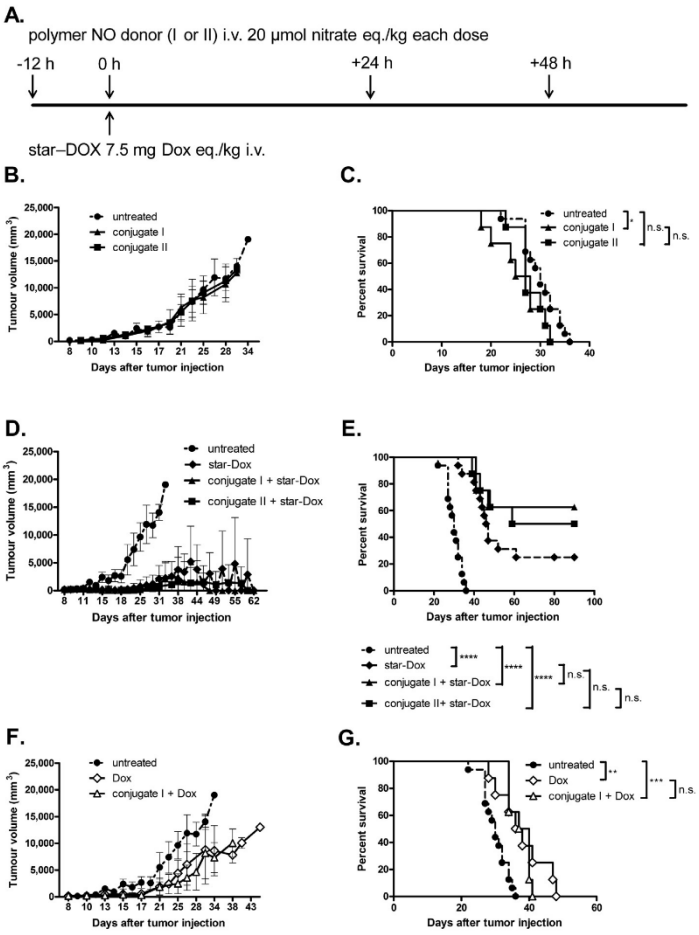

Fig. 5. Combination treatment of EL4 T-cell lymphoma in C57BL/6 mice using polymer-bound Dox or free Dox and polymer NO donors I and II. The mice were injected with 1×10^5 EL4 cells s.c. at day 0 and treated at day 9 with a single i.v. dose of star-Dox, 7.5 mg Dox eq./kg or free Dox, 9 mg Dox eq./kg., and four doses of conjugate I or II, each eq. of 20 μmol nitrate/kg. Eight mice per group were used. Treatment scheme (A), tumour growth and survival of mice treated with polymer NO donors only (B, C), tumour growth and survival of mice with combination of star-Dox and conjugate I or II (D, E), and tumour growth and survival of mice treated with combination of free Dox and conjugate I (F, G). Statistical significance $p \leq 0.05$, $p < 0.01$, $p < 0.001$, and $p < 0.0001$.

multidrug resistance does not come into consideration as the crucial factor; the EL4 lymphoma model was deliberately explored because the EL4 cells do not express detectable levels of these transporters (Supplementary information, Fig. S12), and proved as sensitive to the *in vivo* treatment with Dox and Dox-containing polymer prodrugs. Moreover, the same combination treatment as in Fig. 5D, E (star-Dox conjugate with conjugate I) administered in a model of BCL1 B cell leukaemia, in which the EPR effect does not play a role, did not induced any improvement in the therapy as compared with the sole star-Dox treatment (submitted). On the contrary, the increased accumulation of high-molecular-weight polymer cytotoxic drugs is characteristic of the EPR-driven mechanism. Altogether, the observed data are supportive of the enhanced EPR effect as the leading mechanism of action of the polymer NO donors.

4. Conclusions

In summary, four HPMA copolymer conjugates were designed and synthesized as HMW donors of NO suitable for the highly selective release of NO in solid tumours, thus potentiating tumour uptake of polymer cancerostatics due to the EPR effect by increasing the tumour vascular permeability. The NO-releasing moieties were derived from nitroesters, known for their high NO releasing potency, linked to the polymer carrier *via* a spacer, containing a well-established hydrazone bond that has a tunable hydrolytic stability and, thus, enables variation in their release rate both *in vitro* and *in vivo*. Two of the four polymer NO donors (conjugate I and II) showed effective NO release intracellularly upon incubation with tumour cells *in vitro*, regardless of the pH-stability of the spacer between the nitroester and the polymer carrier. As a sole treatment, these two conjugates do not exhibit toxicity towards tumour cells *in vitro* and do not potentiate the toxicity of Dox towards several tested tumour cell lines. The administration of conjugate I and II to EL4 T-cell lymphoma-bearing mice showed a moderate but not statistically significant trend towards accelerating the tumour growth, most likely caused by increasing the blood supply to the tumour focus. However, when administered in combination with the HMW star HPMA conjugate carrying Dox, but not with the free Dox, the *co*-treatment with polymer NO donors increased the number of completely cured mice from two to five (conjugate II) or even six (conjugate I) mice. Higher Dox accumulation in the combination

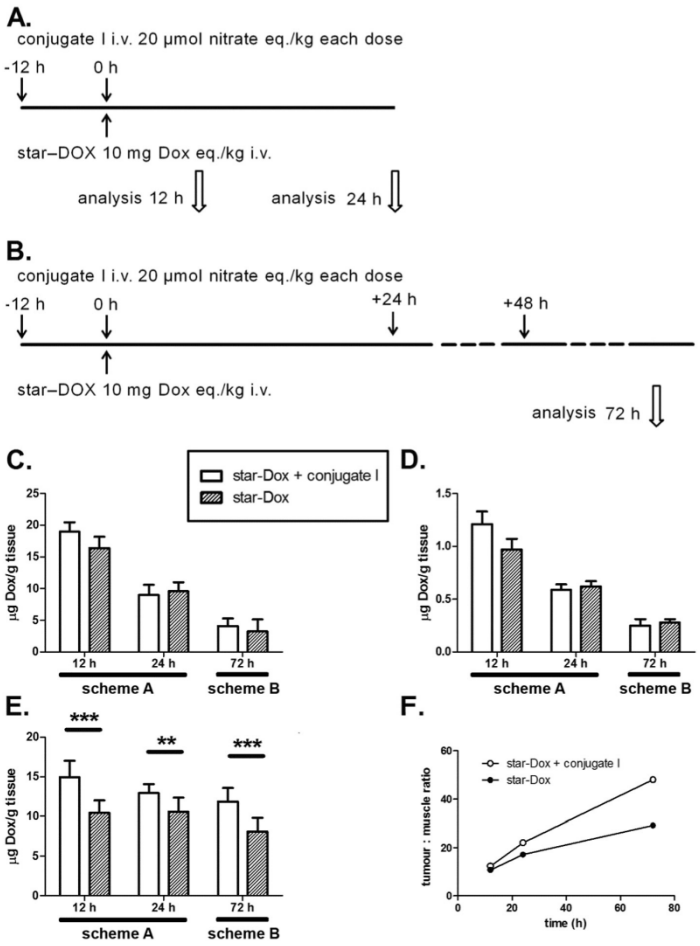

Fig. 6. Dox accumulation in tissues of EL4 T-cell lymphoma-bearing mice at various times after the administration of the star-Dox conjugate. One dose of 10 mg Dox eq./kg was administered i.v. on day 8 post tumour transplantation in combination with two or four doses of the star conjugate I. Treatment scheme (A – two doses of conjugate I) and (B- four doses of conjugate I), Dox accumulation in liver (C), Dox accumulation in skeletal muscle (D), Dox accumulation in tumour (E), Tumour: muscle ratio calculated from the Dox content in the respective tissue at each time interval (F). In each graph, using of the treatment scheme (A) or (B) is depicted. Four mice per group were used for each time interval and condition. Statistical significance: $p < 0.01$ or $p < 0.001$.

therapy substantiated the improved treatment outcome, showing that this enhanced EPR effect could serve as one of several potential strategies to further increasing the passive-accumulation-driven therapeutic effect of polymer conjugates with cytotoxic drugs in solid tumours.

Acknowledgements

Financial support for this work from the Czech Science Foundation (14-12742S), from the Ministry of Health of the Czech Republic (grant 16-28600A), from the Ministry of Education, Youth and Sports of the Czech Republic within the National Sustainability Program II (Project BIOCEV-FAR LQ1604) and the project "BIOCEV" (CZ.1.05/1.1.00/02.0109) is gratefully acknowledged. We thank prof. Karel Ulbrich for critical reading of the manuscript. The authors thank Albert Koválik, Pavlina Jungrova and Helena Misurcova for their excellent technical assistance.

Appendix A. Supplementary data

Supplementary data to this article can be found online at https://doi.org/10.1016/j.jconrel.2017.11.017.

References

[1] R. Duncan, Development of HPMA copolymer–anticancer conjugates: clinical experience and lessons learnt, Adv. Drug Deliv. Rev. 61 (13) (2009) 1131–1148.
[2] J. Kopeček, Polymer–drug conjugates: origins, progress to date and future directions, Adv. Drug Deliv. Rev. 65 (1) (2013) 49–59.
[3] B. Rihova, M. Kovar, Immunogenicity and immunomodulatory properties of HPMA-based polymers, Adv. Drug Deliv. Rev. 62 (2) (2010) 184–191.
[4] M. Sirova, M. Kabesova, L. Kovar, T. Etrych, J. Strohalm, K. Ulbrich, et al., HPMA copolymer-bound doxorubicin induces immunogenic tumor cell death, Curr. Med. Chem. 20 (38) (2013) 4815–4826.
[5] H. Maeda, Tumor-selective delivery of macromolecular drugs via the EPR effect: background and future prospects, Bioconjug. Chem. 21 (5) (2010) 797–802.
[6] S. Taurin, H. Nehoff, K. Greish, Anticancer nanomedicine and tumor vascular permeability; where is the missing link? J. Control. Release 164 (3) (2012) 265–275.
[7] Y. Matsumura, H. Maeda, A new concept for macromolecular therapeutics in cancer chemotherapy: mechanism of tumoritropic accumulation of proteins and the antitumor agent smancs, Cancer Res. 46 (12 Pt. 1) (1986) 6387–6392.
[8] L.W. Seymour, Y. Miyamoto, H. Maeda, M. Brereton, J. Strohalm, K. Ulbrich, et al.,

Influence of molecular weight on passive tumour accumulation of a soluble macromolecular drug carrier, Eur. J. Cancer (5) (1995) 766–770.
[9] H. Maeda, Vascular permeability in cancer and infection as related to macromolecular drug delivery, with emphasis on the EPR effect for tumor-selective drug targeting, Proc. Jpn. Acad. Ser. B Phys. Biol. Sci. 88 (3) (2012) 53–71.
[10] K. Hori, M. Suzuki, S. Tanda, S. Saito, M. Shinozaki, Q.H. Zhang, Fluctuations in tumor blood flow under normotension and the effect of angiotensin II-induced hypertension, Jpn. J. Cancer Res. 82 (11) (1991) 1309–1316.
[11] A. Nagamitsu, K. Greish, H. Maeda, Elevating blood pressure as a strategy to increase tumor-targeted delivery of macromolecular drug SMANCS: cases of advanced solid tumors, Jpn. J. Clin. Oncol. 39 (11) (2009) 756–766.
[12] K. Hori, S. Saito, H. Takahashi, H. Sato, H. Maeda, Y. Sato, Tumor-selective blood flow decrease induced by an angiotensin converting enzyme inhibitor, temocapril hydrochloride, Jpn. J. Cancer Res. 91 (2) (2000) 261–269 (Epub 2000/04/13).
[13] H. Maeda, H. Nakamura, J. Fang, The EPR effect for macromolecular drug delivery to solid tumors: improvement of tumor uptake, lowering of systemic toxicity, and distinct tumor imaging in vivo, Adv. Drug Deliv. Rev. 65 (1) (2013) 71–79 (Epub 2012/10/24).
[14] J. Wu, T. Akaike, H. Maeda, Modulation of enhanced vascular permeability in tumors by a bradykinin antagonist, a cyclooxygenase inhibitor, and a nitric oxide scavenger, Cancer Res. 58 (1) (1998) 159–165 (Epub 1998/01/13).
[15] T. Seki, J. Fang, H. Maeda, Enhanced delivery of macromolecular antitumor drugs to tumors by nitroglycerin application, Cancer Sci. 100 (12) (2009) 2426–2430.
[16] Z. Chen, J.S. Stamler, Bioactivation of nitroglycerin by the mitochondrial aldehyde dehydrogenase, Trends Cardiovasc. Med. 16 (8) (2006) 259–265.
[17] A. Koenig, C. Roegler, K. Lange, A. Daiber, E. Glusa, J. Lehmann, NO donors. Part 16: investigations on structure-activity relationships of organic mononitrates reveal 2-nitrooxyethylammoniumnitrate as a high potent vasodilator, Bioorg. Med. Chem. Lett. 17 (21) (2007) 5881–5885.
[18] L. Santucci, A. Mencarelli, B. Renga, G. Pasut, F. Veronese, A. Zacheo, et al., Nitric oxide modulates proapoptotic and antiapoptotic properties of chemotherapy agents: the case of NO-pegylated epirubicin, FASEB J. 20 (6) (2006) 765–767.
[19] L. Santucci, A. Mencarelli, B. Renga, D. Ceccobelli, G. Pasut, F.M. Veronese, et al., Cardiac safety and antitumoral activity of a new nitric oxide derivative of pegylated epirubicin in mice, Anti-Cancer Drugs 18 (9) (2007) 1081–1091.
[20] S. Kudo, Y. Nagasaki, Facile and quantitative synthesis of a poly(ethylene glycol)-b-poly(L-arginine) block copolymer and its use for the preparation of polyion complex micelles with Polyanions for biomedical applications, Macromol. Rapid Commun. (2015) (Epub 2015/07/29).
[21] S. Kudo, Y. Nagasaki, A novel nitric oxide-based anticancer therapeutics by macrophage-targeted poly(L-arginine)-based nanoparticles, J. Control. Release 217 (2015) 256–262.
[22] H. Nurhasni, J. Cao, M. Choi, I. Kim, B.L. Lee, Y. Jung, et al., Nitric oxide-releasing poly(lactic-co-glycolic acid)-polyethylenimine nanoparticles for prolonged nitric oxide release, antibacterial efficacy, and in vivo wound healing activity, Int. J. Nanomedicine 10 (2015) 3065–3080 (Epub 2015/05/12).
[23] A.W. Carpenter, M.H. Schoenfisch, Nitric oxide release: part II. Therapeutic applications, Chem. Soc. Rev. 41 (10) (2012) 3742–3752 (Epub 2012/03/01).
[24] H. Liang, P. Nacharaju, A. Friedman, J.M. Friedman, Nitric oxide generating/releasing materials, Future Sci. 1 (1) (2015) FSO54.
[25] J.F. Quinn, M.R. Whittaker, T.P. Davis, Delivering nitric oxide with nanoparticles, J. Control. Release 205 (2015) 190–205 (Epub 2015/02/11).
[26] D.A. Riccio, M.H. Schoenfisch, Nitric oxide release: part I. Macromolecular scaffolds, Chem. Soc. Rev. 41 (10) (2012) 3731–3741 (Epub 2012/03/01).
[27] A.B. Seabra, G.Z. Justo, P.S. Haddad, State of the art, challenges and perspectives in the design of nitric oxide-releasing polymeric nanomaterials for biomedical applications, Biotechnol. Adv. 33 (6 Pt. 3) (2015) 1370–1379 (Epub 2015/02/01).
[28] M. Barberis, J. Pérez-Prieto, Enantioselective synthesis of sabina ketone, Tetrahedron Lett. 44 (35) (2003) 6683–6685.
[29] W.D. Emmons, J.P. Freeman, The synthesis of diketones from nitratoketones1, J. Am. Chem. Soc. 77 (16) (1955) 4415–4416.
[30] K. Ulbrich, V. Šubr, J. Strohalm, D. Plocová, M. Jelínková, B. Říhová, Polymeric drugs based on conjugates of synthetic and natural macromolecules. I. Synthesis and physico-chemical characterisation, J. Control. Release 64 (1–3) (2000) 63–79.
[31] M. Hruby, J. Kucka, O. Lebeda, H. Mackova, M. Babic, C. Konak, et al., New bioerodable thermoresponsive polymers for possible radiotherapeutic applications, J. Control. Release 119 (1) (2007) 25–33.
[32] T. Etrych, M. Jelínková, B. Říhová, K. Ulbrich, New HPMA copolymers containing doxorubicin bound via pH-sensitive linkage: synthesis and preliminary in vitro and in vivo biological properties, J. Control. Release 73 (1) (2001) 89–102.
[33] T. Etrych, J. Strohalm, P. Chytil, P. Černoch, L. Starovoytova, M. Pechar, et al., Biodegradable star HPMA polymer conjugates of doxorubicin for passive tumor targeting, Eur. J. Pharm. Sci. 42 (5) (2011) 527–539.
[34] L.J. Chappell, M.K. Whalen, S. Gurai, A. Ponomarev, F.A. Cucinotta, J.M. Pluth, Analysis of flow cytometry DNA damage response protein activation kinetics after exposure to x rays and high-energy iron nuclei, Radiat. Res. 174 (6) (2010) 691–702.
[35] M.D. Pluth, L.E. McQuade, S.J. Lippard, Cell-trappable fluorescent probes for nitric oxide visualization in living cells, Org. Lett. 12 (10) (2010) 2318–2321.
[36] O. Sedláček, M. Studenovský, D. Větvička, K. Ulbrich, M. Hrubý, Fine tuning of the pH-dependent drug release rate from polyHPMA-ellipticinium conjugates, Bioorg. Med. Chem. 21 (18) (2013) 5669–5672.
[37] T. Munzel, S. Steven, A. Daiber, Organic nitrates: update on mechanisms underlying vasodilation, tolerance and endothelial dysfunction, Vasc. Pharmacol. 63 (3) (2014) 105–113 (Epub 2014/12/03).
[38] T. Munzel, A. Daiber, A. Mulsch, Explaining the phenomenon of nitrate tolerance, Circ. Res. 97 (7) (2005) 618–628 (Epub 2005/10/01).
[39] G.T. Colbern, A.J. Hiller, R.S. Musterer, E. Pegg, I.C. Henderson, P.K. Working, Significant increase in antitumor potency of doxorubicin Hcl by its encapsulation in Pegylated liposomes, J. Liposome Res. 9 (4) (1999) 523–538.
[40] B. Tomalova, M. Sirova, P. Rossmann, R. Pola, J. Strohalm, P. Chytil, et al., The structure-dependent toxicity, pharmacokinetics and anti-tumour activity of HPMA copolymer conjugates in the treatment of solid tumours and leukaemia, J. Control. Release 223 (2016) 1–10.
[41] M. Šírová, J. Strohalm, P. Chytil, O. Lidický, J. Tomala, B. Říhová, et al., The structure of polymer carriers controls the efficacy of the experimental combination treatment of tumors with HPMA copolymer conjugates carrying doxorubicin and docetaxel, J. Control. Release 246 (2017) 1–11.
[42] Q. Song, S. Tan, X. Zhuang, Y. Guo, Y. Zhao, T. Wu, et al., Nitric oxide releasing D-α-Tocopheryl polyethylene glycol succinate for enhancing antitumor activity of doxorubicin, Mol. Pharm. 11 (11) (2014) 4118–4129.
[43] E.V. Stevens, A.W. Carpenter, J.H. Shin, J. Liu, C.J. Der, M.H. Schoenfisch, Nitric oxide-releasing silica nanoparticle inhibition of ovarian cancer cell growth, Mol. Pharm. 7 (3) (2010) 775–785.
[44] L.J. Frederiksen, R. Sullivan, L.R. Maxwell, S.K. Macdonald-Goodfellow, M.A. Adams, B.M. Bennett, et al., Chemosensitization of cancer in vitro and in vivo by nitric oxide signaling, Clin. Cancer Res. 13 (7) (2007) 2199–2206.
[45] M.M. Reynolds, S.D. Witzeling, V.B. Damodaran, T.N. Medeiros, R.D. Knodle, M.A. Edwards, et al., Applications for nitric oxide in halting proliferation of tumor cells, Biochem. Biophys. Res. Commun. 431 (4) (2013) 647–651.
[46] C. Riganti, E. Miraglia, D. Viarisio, C. Costamagna, G. Pescarmona, D. Ghigo, et al., Nitric oxide reverts the resistance to doxorubicin in human colon cancer cells by inhibiting the drug efflux, Cancer Res. 65 (2) (2005) 516–525.
[47] M. Sirova, V. Horkova, T. Etrych, P. Chytil, B. Rihova, M. Studenovsky, Polymer donors of nitric oxide improve the treatment of experimental solid tumours with nanosized polymer therapeutics, J. Drug Target. 7 (1–13) (2017).

4 Conclusions

1. We designed and evaluated the biological activity of HPMA copolymer conjugates bearing a P-gp inhibitor and cytostatic drug in sensitive and resistant murine and human cancer cell lines *in vitro* and *in vivo*.
    a. We proved that R121 and RIT, when bound to a polymeric carrier via a pH-sensitive hydrazone bond, were very effective in the inhibition of P-gp activity *in vitro* in both murine and human MDR cancer cell lines in a dose dependent manner. The HPMA copolymer conjugate bearing R121 inhibited P-gp activity even at 12 μM, whereas RIT was effective at higher concentrations. Both conjugates had no effect on sensitive cell lines at these concentrations. The conjugate bearing R121 was also effective *in vivo* as a P-gp inhibitor in P388/MDR tumors.
    b. HPMA copolymer conjugates bearing both an anticancer drug (Dox or THP) and P-gp inhibitor (R121 or RIT) were far more potent than the conjugate bearing Dox alone or a mixture of conjugates bearing either the cytostatic drug or P-gp inhibitor in terms of cytostatic and cytotoxic activity, cell cycle arrest, the accumulation of cytostatic drug in cells and the induction of apoptosis in murine and human cancer cell lines expressing different levels of P-gp *in vitro*.
    c. We showed that the conjugate bearing both Dox and R121 remarkably inhibited the growth of resistant P388/MDR tumors and led to the significantly prolonged survival of treated mice. More importantly, this antitumor activity was more profound in the CT26 tumor model, in which it completely cured six out of eight experimental mice.

2. We evaluated the biological potential of micelle-forming HPMA copolymer-PPO diblock bearing Dox in sensitive and MDR murine and human cancer cell lines *in vitro* and *in vivo*.
    a. We proved that the presence of PPO in the structure of HPMA copolymer-PPO diblock ensures the inhibition of P-gp in murine and human cancer cell lines expressing different levels of P-gp.
    b. HPMA copolymer-PPO diblock without Dox was capable of sensitizing cancer cell lines expressing P-gp to the cytostatic and cytotoxic activity of Dox in a dose dependent manner. HPMA copolymer-PPO diblock bearing Dox showed higher cytostatic activity than the HPMA copolymer conjugate bearing Dox. We observed a significantly higher accumulation of HPMA copolymer-PPO diblock bearing Dox

in comparison to HPMA copolymer-drug conjugates that do not form a micellar structure in both sensitive and MDR neuroblastoma cell lines *in vitro*.

c. HPMA copolymer-PPO diblock bearing Dox showed higher antitumor efficacy in mouse EL4 lymphoma *in vivo*, even at a sub-optimal dose in comparison to the HPMA copolymer conjugate bearing Dox, which does not form a micellar structure.

3. We evaluated the potential of polymeric NO donors to improve the therapeutic activity of HPMA copolymer conjugates bearing Dox in murine tumor cell lines *in vitro* and *in vivo*.
    a. The polymeric NO donors showed intracellular NO release upon incubation with mouse EL4 lymphoma cells after eight hours of incubation.
    b. Polymeric NO donors were capable of chemosensitizing mouse EL4, 4T1 and human EA.hy926 cells to the cytostatic activity of Dox *in vitro*. Polymeric NO donors showed no cytostatic or cytotoxic activity per se within the concentration range used.
    c. No decrease of body weight or the occurrence of other signs of systemic toxicity were observed after the administration of a therapeutic dose of polymeric NO donors.
    d. Two tested polymeric NO donors significantly improved the treatment of EL4 lymphoma bearing mice with HPMA copolymer conjugate bearing Dox by increasing the EPR effect, resulting in a higher accumulation of polymer-bound Dox within the tumors.

5 References

[1] A. Pluen *et al.*, "Role of tumor-host interactions in interstitial diffusion of macromolecules: cranial vs. subcutaneous tumors," *Proceedings of the National Academy of Sciences of the United States of America,* vol. 98, no. 8, pp. 4628-33, Apr 10 2001.

[2] R. K. Jain, "Delivery of molecular and cellular medicine to solid tumors," *Advanced drug delivery reviews,* vol. 64, no. Suppl, pp. 353-365, Dec 1 2012.

[3] R. K. Jain, "Normalizing tumor vasculature with anti-angiogenic therapy: a new paradigm for combination therapy," *Nature medicine,* vol. 7, no. 9, pp. 987-9, Sep 2001.

[4] S. K. Green, A. Frankel, and R. S. Kerbel, "Adhesion-dependent multicellular drug resistance," *Anticancer Drug Des,* vol. 14, no. 2, pp. 153-68, Apr 1999.

[5] R. E. Durand and P. L. Olive, "Resistance of tumor cells to chemo- and radiotherapy modulated by the three-dimensional architecture of solid tumors and spheroids," *Methods Cell Biol,* vol. 64, pp. 211-33, 2001.

[6] H. Thomas and H. M. Coley, "Overcoming multidrug resistance in cancer: an update on the clinical strategy of inhibiting p-glycoprotein," *Cancer control : journal of the Moffitt Cancer Center,* vol. 10, no. 2, pp. 159-65, Mar-Apr 2003.

[7] S. V. Ambudkar, S. Dey, C. A. Hrycyna, M. Ramachandra, I. Pastan, and M. M. Gottesman, "Biochemical, cellular, and pharmacological aspects of the multidrug transporter," *Annual review of pharmacology and toxicology,* vol. 39, pp. 361-98, 1999.

[8] T. Fojo and S. Bates, "Strategies for reversing drug resistance," *Oncogene,* vol. 22, no. 47, pp. 7512-23, Oct 20 2003.

[9] D. B. Longley and P. G. Johnston, "Molecular mechanisms of drug resistance," *The Journal of pathology,* vol. 205, no. 2, pp. 275-92, Jan 2005.

[10] M. M. Gottesman, T. Fojo, and S. E. Bates, "Multidrug resistance in cancer: role of ATP-dependent transporters," *Nature reviews. Cancer,* vol. 2, no. 1, pp. 48-58, Jan 2002.

[11] M. M. Gottesman, "How cancer cells evade chemotherapy: sixteenth Richard and Hinda Rosenthal Foundation Award Lecture," *Cancer research,* vol. 53, no. 4, pp. 747-54, Feb 15 1993.

[12] D. Kessel, V. Botterill, and I. Wodinsky, "Uptake and retention of daunomycin by mouse leukemic cells as factors in drug response," *Cancer research,* vol. 28, no. 5, pp. 938-41, May 1968.

[13] M. N. Goldstein, I. J. Slotnick, and L. J. Journey, "In vitro studies with HeLa cell line sensitive and resistant to actinomycin D," *Annals of the New York Academy of Sciences,* vol. 89, pp. 474-83, Oct 5 1960.

[14] J. L. Biedler and H. Riehm, "Cellular resistance to actinomycin D in Chinese hamster cells in vitro: cross-resistance, radioautographic, and cytogenetic studies," *Cancer research,* vol. 30, no. 4, pp. 1174-84, Apr 1970.

[15] K. Dano, "Active outward transport of daunomycin in resistant Ehrlich ascites tumor cells," *Biochimica et biophysica acta,* vol. 323, no. 3, pp. 466-83, Oct 25 1973.

[16] R. L. Juliano and V. Ling, "A surface glycoprotein modulating drug permeability in Chinese hamster ovary cell mutants," *Biochimica et biophysica acta,* vol. 455, no. 1, pp. 152-62, Nov 11 1976.

[17] H. Zahreddine and K. L. Borden, "Mechanisms and insights into drug resistance in cancer," *Front Pharmacol,* vol. 4, p. 28, 2013.

[18] S. Chai, K. K. To, and G. Lin, "Circumvention of multi-drug resistance of cancer cells by Chinese herbal medicines," *Chin Med,* vol. 5, p. 26, Jul 25 2010.

[19] V. Goler-Baron and Y. G. Assaraf, "Structure and function of ABCG2-rich extracellular vesicles mediating multidrug resistance," *PloS one,* vol. 6, no. 1, p. e16007, Jan 24 2011.

[20] V. Goler-Baron, I. Sladkevich, and Y. G. Assaraf, "Inhibition of the PI3K-Akt signaling pathway disrupts ABCG2-rich extracellular vesicles and overcomes multidrug resistance in breast cancer cells," *Biochemical pharmacology,* vol. 83, no. 10, pp. 1340-8, May 15 2012.

[21] N. Gonen and Y. G. Assaraf, "Antifolates in cancer therapy: structure, activity and mechanisms of drug resistance," *Drug resistance updates : reviews and commentaries in antimicrobial and anticancer chemotherapy,* vol. 15, no. 4, pp. 183-210, Aug 2012.

[22] I. Ifergan, G. L. Scheffer, and Y. G. Assaraf, "Novel extracellular vesicles mediate an ABCG2-dependent anticancer drug sequestration and resistance," *Cancer research,* vol. 65, no. 23, pp. 10952-8, Dec 1 2005.

[23] S. Raz, D. Sheban, N. Gonen, M. Stark, B. Berman, and Y. G. Assaraf, "Severe hypoxia induces complete antifolate resistance in carcinoma cells due to cell cycle arrest," *Cell Death Dis,* vol. 5, p. e1067, Feb 20 2014.

[24] B. Zhitomirsky and Y. G. Assaraf, "Lysosomal sequestration of hydrophobic weak base chemotherapeutics triggers lysosomal biogenesis and lysosome-dependent cancer multidrug resistance," *Oncotarget,* vol. 6, no. 2, pp. 1143-56, Jan 20 2015.

[25] X. Zhou, D. Li, X. Wang, B. Zhang, H. Zhu, and J. Zhao, "Galectin-1 is overexpressed in CD133+ human lung adenocarcinoma cells and promotes their growth and invasiveness," *Oncotarget,* vol. 6, no. 5, pp. 3111-22, Feb 20 2015.

[26] R. Krishna and L. D. Mayer, "Multidrug resistance (MDR) in cancer. Mechanisms, reversal using modulators of MDR and the role of MDR modulators in influencing the pharmacokinetics of anticancer drugs," *European journal of pharmaceutical sciences : official journal of the European Federation for Pharmaceutical Sciences,* vol. 11, no. 4, pp. 265-83, Oct 2000.

[27] T. Fiaschi and P. Chiarugi, "Oxidative stress, tumor microenvironment, and metabolic reprogramming: a diabolic liaison," *Int J Cell Biol,* vol. 2012, p. 762825, 2012.

[28] B. Vincenzi, M. Imperatori, M. Silletta, E. Marrucci, D. Santini, and G. Tonini, "Emerging kinase inhibitors of the treatment of gastric cancer," *Expert Opin Emerg Drugs,* vol. 20, no. 3, pp. 479-93, Sep 2015.

[29] M. B. Meads, R. A. Gatenby, and W. S. Dalton, "Environment-mediated drug resistance: a major contributor to minimal residual disease," *Nature reviews. Cancer,* vol. 9, no. 9, pp. 665-74, Sep 2009.

[30] S. I. Grivennikov, F. R. Greten, and M. Karin, "Immunity, inflammation, and cancer," *Cell,* vol. 140, no. 6, pp. 883-99, Mar 19 2010.

[31] D. W. McMillin, J. M. Negri, and C. S. Mitsiades, "The role of tumour-stromal interactions in modifying drug response: challenges and opportunities," *Nature reviews. Drug discovery,* vol. 12, no. 3, pp. 217-28, Mar 2013.

[32] M. M. Gottesman, "Mechanisms of cancer drug resistance," *Annual review of medicine,* vol. 53, pp. 615-27, 2002.

[33] A. Di Paolo and G. Bocci, "Drug distribution in tumors: mechanisms, role in drug resistance, and methods for modification," *Curr Oncol Rep,* vol. 9, no. 2, pp. 109-14, Mar 2007.

[34] A. Schmidt and O. F. Weber, "In memoriam of Rudolf virchow: a historical retrospective including aspects of inflammation, infection and neoplasia," *Contrib Microbiol,* vol. 13, pp. 1-15, 2006.

[35] S. Paget, "The distribution of secondary growths in cancer of the breast. 1889," *Cancer metastasis reviews,* vol. 8, no. 2, pp. 98-101, Aug 1989.

[36] R. E. Durand and R. M. Sutherland, "Effects of intercellular contact on repair of radiation damage," *Experimental cell research,* vol. 71, no. 1, pp. 75-80, Mar 1972.

[37] R. M. Sutherland, H. A. Eddy, B. Bareham, K. Reich, and D. Vanantwerp, "Resistance to adriamycin in multicellular spheroids," *Int J Radiat Oncol Biol Phys,* vol. 5, no. 8, pp. 1225-30, Aug 1979.

[38] B. A. Teicher *et al.*, "Tumor resistance to alkylating agents conferred by mechanisms operative only in vivo," *Science,* vol. 247, no. 4949 Pt 1, pp. 1457-61, Mar 23 1990.

[39] C. H. Graham, H. Kobayashi, K. S. Stankiewicz, S. Man, S. J. Kapitain, and R. S. Kerbel, "Rapid acquisition of multicellular drug resistance after a single exposure of mammary tumor cells to antitumor alkylating agents," *Journal of the National Cancer Institute,* vol. 86, no. 13, pp. 975-82, Jul 6 1994.

[40] T. P. Szatrowski and C. F. Nathan, "Production of large amounts of hydrogen peroxide by human tumor cells," *Cancer research,* vol. 51, no. 3, pp. 794-8, Feb 1 1991.

[41] A. Klein-Goldberg, S. Maman, and I. P. Witz, "The role played by the microenvironment in site-specific metastasis," *Cancer letters,* vol. 352, no. 1, pp. 54-8, Sep 28 2014.

[42] S. V. Kozin, W. S. Kamoun, Y. Huang, M. R. Dawson, R. K. Jain, and D. G. Duda, "Recruitment of myeloid but not endothelial precursor cells facilitates tumor regrowth after local irradiation," *Cancer research,* vol. 70, no. 14, pp. 5679-85, Jul 15 2010.

[43] J. M. Brown, "Vasculogenesis: a crucial player in the resistance of solid tumours to radiotherapy," *Br J Radiol,* vol. 87, no. 1035, p. 20130686, Mar 2014.

[44] G. Kibria, H. Hatakeyama, and H. Harashima, "Cancer multidrug resistance: mechanisms involved and strategies for circumvention using a drug delivery system," *Archives of pharmacal research,* vol. 37, no. 1, pp. 4-15, Jan 2014.

[45] J. Choi, Y. J. Cha, and J. S. Koo, "Adipocyte biology in breast cancer: From silent bystander to active facilitator," *Prog Lipid Res,* vol. 69, pp. 11-20, Jan 2018.

[46] A. Ribas, "Adaptive Immune Resistance: How Cancer Protects from Immune Attack," *Cancer discovery,* vol. 5, no. 9, pp. 915-9, Sep 2015.

[47] P. C. Tumeh *et al.*, "PD-1 blockade induces responses by inhibiting adaptive immune resistance," *Nature,* vol. 515, no. 7528, pp. 568-71, Nov 27 2014.

[48] H. Roca *et al.*, "Transcription factors OVOL1 and OVOL2 induce the mesenchymal to epithelial transition in human cancer," *PloS one,* vol. 8, no. 10, p. e76773, 2013.

[49] J. A. Engelman *et al.*, "MET amplification leads to gefitinib resistance in lung cancer by activating ERBB3 signaling," *Science,* vol. 316, no. 5827, pp. 1039-43, May 18 2007.

[50] R. Nazarian *et al.*, "Melanomas acquire resistance to B-RAF(V600E) inhibition by RTK or N-RAS upregulation," *Nature,* vol. 468, no. 7326, pp. 973-7, Dec 16 2010.

[51] M. H. Barcellos-Hoff and S. A. Ravani, "Irradiated mammary gland stroma promotes the expression of tumorigenic potential by unirradiated epithelial cells," *Cancer research,* vol. 60, no. 5, pp. 1254-60, Mar 1 2000.

[52] R. Straussman *et al.*, "Tumour micro-environment elicits innate resistance to RAF inhibitors through HGF secretion," *Nature,* vol. 487, no. 7408, pp. 500-4, Jul 26 2012.

[53] T. R. Wilson *et al.*, "Widespread potential for growth-factor-driven resistance to anticancer kinase inhibitors," *Nature,* vol. 487, no. 7408, pp. 505-9, Jul 26 2012.

[54] Y. Sun *et al.*, "Treatment-induced damage to the tumor microenvironment promotes prostate cancer therapy resistance through WNT16B," *Nature medicine,* vol. 18, no. 9, pp. 1359-68, Sep 2012.

[55] P. P. Provenzano, C. Cuevas, A. E. Chang, V. K. Goel, D. D. Von Hoff, and S. R. Hingorani, "Enzymatic targeting of the stroma ablates physical barriers to treatment of pancreatic ductal adenocarcinoma," *Cancer cell,* vol. 21, no. 3, pp. 418-29, Mar 20 2012.

[56] A. A. Van der Veldt *et al.*, "Rapid decrease in delivery of chemotherapy to tumors after anti-VEGF therapy: implications for scheduling of anti-angiogenic drugs," *Cancer cell,* vol. 21, no. 1, pp. 82-91, Jan 17 2012.

[57] L. A. Gilbert and M. T. Hemann, "DNA damage-mediated induction of a chemoresistant niche," *Cell,* vol. 143, no. 3, pp. 355-66, Oct 29 2010.

[58] C. Flotho *et al.*, "A set of genes that regulate cell proliferation predicts treatment outcome in childhood acute lymphoblastic leukemia," *Blood,* vol. 110, no. 4, pp. 1271-7, Aug 15 2007.

[59] N. A. Bhowmick *et al.*, "TGF-beta signaling in fibroblasts modulates the oncogenic potential of adjacent epithelia," *Science,* vol. 303, no. 5659, pp. 848-51, Feb 6 2004.

[60] A. Ostman and M. Augsten, "Cancer-associated fibroblasts and tumor growth--bystanders turning into key players," *Curr Opin Genet Dev,* vol. 19, no. 1, pp. 67-73, Feb 2009.

[61] J. J. Tomasek, G. Gabbiani, B. Hinz, C. Chaponnier, and R. A. Brown, "Myofibroblasts and mechano-regulation of connective tissue remodelling," *Nat Rev Mol Cell Biol,* vol. 3, no. 5, pp. 349-63, May 2002.

[62] H. Y. Chang *et al.*, "Diversity, topographic differentiation, and positional memory in human fibroblasts," *Proceedings of the National Academy of Sciences of the United States of America,* vol. 99, no. 20, pp. 12877-82, Oct 1 2002.

[63] M. Simian, Y. Hirai, M. Navre, Z. Werb, A. Lochter, and M. J. Bissell, "The interplay of matrix metalloproteinases, morphogens and growth factors is necessary for branching of mammary epithelial cells," *Development,* vol. 128, no. 16, pp. 3117-31, Aug 2001.

[64] H. Laklai *et al.*, "Genotype tunes pancreatic ductal adenocarcinoma tissue tension to induce matricellular fibrosis and tumor progression," *Nature medicine,* vol. 22, no. 5, pp. 497-505, May 2016.

[65] A. Orimo *et al.*, "Stromal fibroblasts present in invasive human breast carcinomas promote tumor growth and angiogenesis through elevated SDF-1/CXCL12 secretion," *Cell,* vol. 121, no. 3, pp. 335-48, May 6 2005.

[66] K. Shiga, M. Hara, T. Nagasaki, T. Sato, H. Takahashi, and H. Takeyama, "Cancer-Associated Fibroblasts: Their Characteristics and Their Roles in Tumor Growth," *Cancers,* vol. 7, no. 4, pp. 2443-58, Dec 11 2015.

[67] Y. Jung *et al.*, "Recruitment of mesenchymal stem cells into prostate tumours promotes metastasis," *Nat Commun,* vol. 4, p. 1795, 2013.

[68] E. M. Zeisberg, S. Potenta, L. Xie, M. Zeisberg, and R. Kalluri, "Discovery of endothelial to mesenchymal transition as a source for carcinoma-associated fibroblasts," *Cancer research,* vol. 67, no. 21, pp. 10123-8, Nov 1 2007.

[69] C. Jotzu *et al.*, "Adipose tissue derived stem cells differentiate into carcinoma-associated fibroblast-like cells under the influence of tumor derived factors," *Cell Oncol (Dordr),* vol. 34, no. 1, pp. 55-67, Feb 2011.

[70] S. Dulauroy, S. E. Di Carlo, F. Langa, G. Eberl, and L. Peduto, "Lineage tracing and genetic ablation of ADAM12(+) perivascular cells identify a major source of profibrotic cells during acute tissue injury," *Nature medicine,* vol. 18, no. 8, pp. 1262-70, Aug 2012.

[71] S. Vicent *et al.*, "Cross-species functional analysis of cancer-associated fibroblasts identifies a critical role for CLCF1 and IL-6 in non-small cell lung cancer in vivo," *Cancer research,* vol. 72, no. 22, pp. 5744-56, Nov 15 2012.

[72] A. F. Olumi, G. D. Grossfeld, S. W. Hayward, P. R. Carroll, T. D. Tlsty, and G. R. Cunha, "Carcinoma-associated fibroblasts direct tumor progression of initiated human prostatic epithelium," *Cancer research,* vol. 59, no. 19, pp. 5002-11, Oct 1 1999.

[73] Y. Shintani *et al.*, "IL-6 Secreted from Cancer-Associated Fibroblasts Mediates Chemoresistance in NSCLC by Increasing Epithelial-Mesenchymal Transition Signaling," *J Thorac Oncol,* vol. 11, no. 9, pp. 1482-92, Sep 2016.

[74] T. Sethi *et al.*, "Extracellular matrix proteins protect small cell lung cancer cells against apoptosis: a mechanism for small cell lung cancer growth and drug resistance in vivo," *Nature medicine,* vol. 5, no. 6, pp. 662-8, Jun 1999.

[75] E. H. Cheteh *et al.*, "Human cancer-associated fibroblasts enhance glutathione levels and antagonize drug-induced prostate cancer cell death," *Cell Death Dis,* vol. 8, no. 6, p. e2848, Jun 1 2017.

[76] S. Su *et al.*, "CD10(+)GPR77(+) Cancer-Associated Fibroblasts Promote Cancer Formation and Chemoresistance by Sustaining Cancer Stemness," *Cell,* vol. 172, no. 4, pp. 841-856 e16, Feb 8 2018.

[77] R. Kalluri, "The biology and function of fibroblasts in cancer," *Nature reviews. Cancer,* vol. 16, no. 9, pp. 582-98, Aug 23 2016.

[78] A. Naba, K. R. Clauser, S. Hoersch, H. Liu, S. A. Carr, and R. O. Hynes, "The matrisome: in silico definition and in vivo characterization by proteomics of normal and tumor extracellular matrices," *Mol Cell Proteomics,* vol. 11, no. 4, p. M111 014647, Apr 2012.

[79] D. M. Gilkes *et al.*, "Collagen prolyl hydroxylases are essential for breast cancer metastasis," *Cancer research,* vol. 73, no. 11, pp. 3285-96, Jun 1 2013.

[80] S. Ramaswamy, K. N. Ross, E. S. Lander, and T. R. Golub, "A molecular signature of metastasis in primary solid tumors," *Nature genetics,* vol. 33, no. 1, pp. 49-54, Jan 2003.

[81] M. Allinen *et al.*, "Molecular characterization of the tumor microenvironment in breast cancer," *Cancer cell,* vol. 6, no. 1, pp. 17-32, Jul 2004.

[82] G. Finak *et al.*, "Stromal gene expression predicts clinical outcome in breast cancer," *Nature medicine,* vol. 14, no. 5, pp. 518-27, May 2008.

[83] S. M. Frisch and H. Francis, "Disruption of epithelial cell-matrix interactions induces apoptosis," *J Cell Biol,* vol. 124, no. 4, pp. 619-26, Feb 1994.

[84] N. Boudreau, C. J. Sympson, Z. Werb, and M. J. Bissell, "Suppression of ICE and apoptosis in mammary epithelial cells by extracellular matrix," *Science,* vol. 267, no. 5199, pp. 891-3, Feb 10 1995.

[85] R. Fridman, G. Giaccone, T. Kanemoto, G. R. Martin, A. F. Gazdar, and J. L. Mulshine, "Reconstituted basement membrane (matrigel) and laminin can enhance the tumorigenicity and the drug resistance of small cell lung cancer cell lines," *Proceedings of the National Academy of Sciences of the United States of America,* vol. 87, no. 17, pp. 6698-702, Sep 1990.

[86] C. C. Park *et al.*, "Beta1 integrin inhibitory antibody induces apoptosis of breast cancer cells, inhibits growth, and distinguishes malignant from normal phenotype in three dimensional cultures and in vivo," *Cancer research,* vol. 66, no. 3, pp. 1526-35, Feb 1 2006.

[87] C. C. Park, H. J. Zhang, E. S. Yao, C. J. Park, and M. J. Bissell, "Beta1 integrin inhibition dramatically enhances radiotherapy efficacy in human breast cancer xenografts," *Cancer research,* vol. 68, no. 11, pp. 4398-405, Jun 1 2008.

[88] J. S. Damiano, A. E. Cress, L. A. Hazlehurst, A. A. Shtil, and W. S. Dalton, "Cell adhesion mediated drug resistance (CAM-DR): role of integrins and resistance to apoptosis in human myeloma cell lines," *Blood,* vol. 93, no. 5, pp. 1658-67, Mar 1 1999.

[89] S. Maubant *et al.*, "Altered adhesion properties and alphav integrin expression in a cisplatin-resistant human ovarian carcinoma cell line," *International journal of cancer. Journal international du cancer,* vol. 97, no. 2, pp. 186-94, Jan 10 2002.

[90] C. A. Sherman-Baust *et al.*, "Remodeling of the extracellular matrix through overexpression of collagen VI contributes to cisplatin resistance in ovarian cancer cells," *Cancer cell,* vol. 3, no. 4, pp. 377-86, Apr 2003.

[91] J. H. Uhm, N. P. Dooley, A. P. Kyritsis, J. S. Rao, and C. L. Gladson, "Vitronectin, a glioma-derived extracellular matrix protein, protects tumor cells from apoptotic death," *Clinical cancer research : an official journal of the American Association for Cancer Research,* vol. 5, no. 6, pp. 1587-94, Jun 1999.

[92] S. Kuzmich and K. D. Tew, "Detoxification mechanisms and tumor cell resistance to anticancer drugs," *Medicinal research reviews,* vol. 11, no. 2, pp. 185-217, Mar 1991.

[93] Y. Onishi, Y. Azuma, Y. Sato, Y. Mizuno, T. Tadakuma, and H. Kizaki, "Topoisomerase inhibitors induce apoptosis in thymocytes," *Biochimica et biophysica acta,* vol. 1175, no. 2, pp. 147-54, Jan 17 1993.

[94] H. Sies, "Glutathione and its role in cellular functions," *Free radical biology & medicine,* vol. 27, no. 9-10, pp. 916-21, Nov 1999.

[95] V. I. Lushchak, "Glutathione homeostasis and functions: potential targets for medical interventions," *J Amino Acids,* vol. 2012, p. 736837, 2012.

[96] M. L. O'Brien and K. D. Tew, "Glutathione and related enzymes in multidrug resistance," *European journal of cancer,* vol. 32A, no. 6, pp. 967-78, Jun 1996.

[97] A. K. Godwin, A. Meister, P. J. O'Dwyer, C. S. Huang, T. C. Hamilton, and M. E. Anderson, "High resistance to cisplatin in human ovarian cancer cell lines is associated with marked increase of glutathione synthesis," *Proceedings of the National Academy of Sciences of the United States of America,* vol. 89, no. 7, pp. 3070-4, Apr 1 1992.

[98] R. T. Mulcahy, S. Untawale, and J. J. Gipp, "Transcriptional up-regulation of gamma-glutamylcysteine synthetase gene expression in melphalan-resistant human prostate carcinoma cells," *Molecular pharmacology,* vol. 46, no. 5, pp. 909-14, Nov 1994.

[99] M. Benlloch *et al.*, "Acceleration of glutathione efflux and inhibition of gamma-glutamyltranspeptidase sensitize metastatic B16 melanoma cells to endothelium-induced cytotoxicity," *The Journal of biological chemistry,* vol. 280, no. 8, pp. 6950-9, Feb 25 2005.

[100] M. Shi, E. Gozal, H. A. Choy, and H. J. Forman, "Extracellular glutathione and gamma-glutamyl transpeptidase prevent H2O2-induced injury by 2,3-dimethoxy-1,4-naphthoquinone," *Free radical biology & medicine,* vol. 15, no. 1, pp. 57-67, Jul 1993.

[101] S. N. Hochwald, D. M. Rose, M. F. Brennan, and M. E. Burt, "Elevation of glutathione and related enzyme activities in high-grade and metastatic extremity soft tissue sarcoma," *Ann Surg Oncol,* vol. 4, no. 4, pp. 303-9, Jun 1997.

[102] A. D. Lewis, J. D. Hayes, and C. R. Wolf, "Glutathione and glutathione-dependent enzymes in ovarian adenocarcinoma cell lines derived from a patient before and after the onset of drug resistance: intrinsic differences and cell cycle effects," *Carcinogenesis,* vol. 9, no. 7, pp. 1283-7, Jul 1988.

[103] M. T. Kuo *et al.*, "Frequent coexpression of MRP/GS-X pump and gamma-glutamylcysteine synthetase mRNA in drug-resistant cells, untreated tumor cells, and normal mouse tissues," *Biochemical pharmacology,* vol. 55, no. 5, pp. 605-15, Mar 1 1998.

[104] T. Oguri, Y. Fujiwara, T. Isobe, O. Katoh, H. Watanabe, and M. Yamakido, "Expression of gamma-glutamylcysteine synthetase (gamma-GCS) and multidrug resistance-associated protein (MRP), but not human canalicular multispecific organic anion transporter (cMOAT), genes correlates with exposure of human lung cancers to platinum drugs," *British journal of cancer,* vol. 77, no. 7, pp. 1089-96, Apr 1998.

[105] H. Zhang and H. J. Forman, "Redox regulation of gamma-glutamyl transpeptidase," *Am J Respir Cell Mol Biol,* vol. 41, no. 5, pp. 509-15, Nov 2009.

[106] M. P. Gamcsik, M. S. Kasibhatla, S. D. Teeter, and O. M. Colvin, "Glutathione levels in human tumors," *Biomarkers,* vol. 17, no. 8, pp. 671-91, Dec 2012.

[107] V. Adler *et al.*, "Regulation of JNK signaling by GSTp," *The EMBO journal,* vol. 18, no. 5, pp. 1321-34, Mar 1 1999.

[108] B. Marengo *et al.*, "p38MAPK inhibition: a new combined approach to reduce neuroblastoma resistance under etoposide treatment," *Cell Death Dis,* vol. 4, p. e589, Apr 11 2013.

[109] D. M. Townsend and K. D. Tew, "The role of glutathione-S-transferase in anti-cancer drug resistance," *Oncogene,* vol. 22, no. 47, pp. 7369-75, Oct 20 2003.

[110] P. Bouwman and J. Jonkers, "The effects of deregulated DNA damage signalling on cancer chemotherapy response and resistance," *Nature reviews. Cancer,* vol. 12, no. 9, pp. 587-98, Sep 2012.

[111] R. Ceccaldi, B. Rondinelli, and A. D. D'Andrea, "Repair Pathway Choices and Consequences at the Double-Strand Break," *Trends Cell Biol,* vol. 26, no. 1, pp. 52-64, Jan 2016.

[112] Y. Chen *et al.*, "Oncogenic mutations of ALK kinase in neuroblastoma," *Nature,* vol. 455, no. 7215, pp. 971-4, Oct 16 2008.

[113] R. V. Lord *et al.*, "Low ERCC1 expression correlates with prolonged survival after cisplatin plus gemcitabine chemotherapy in non-small cell lung cancer," *Clinical cancer research : an official journal of the American Association for Cancer Research,* vol. 8, no. 7, pp. 2286-91, Jul 2002.

[114] H. C. Kwon *et al.*, "Prognostic value of expression of ERCC1, thymidylate synthase, and glutathione S-transferase P1 for 5-fluorouracil/oxaliplatin chemotherapy in advanced gastric cancer," *Ann Oncol,* vol. 18, no. 3, pp. 504-9, Mar 2007.

[115] S. Usanova *et al.*, "Cisplatin sensitivity of testis tumour cells is due to deficiency in interstrand-crosslink repair and low ERCC1-XPF expression," *Mol Cancer,* vol. 9, p. 248, Sep 16 2010.

[116] S. Y. Park, W. Lam, and Y. C. Cheng, "X-ray repair cross-complementing gene I protein plays an important role in camptothecin resistance," *Cancer research,* vol. 62, no. 2, pp. 459-65, Jan 15 2002.

[117] C. A. Delaney *et al.*, "Potentiation of temozolomide and topotecan growth inhibition and cytotoxicity by novel poly(adenosine diphosphoribose) polymerase inhibitors in a panel of human tumor cell lines," *Clinical cancer research : an official journal of the American Association for Cancer Research,* vol. 6, no. 7, pp. 2860-7, Jul 2000.

[118] C. Meisenberg *et al.*, "Clinical and cellular roles for TDP1 and TOP1 in modulating colorectal cancer response to irinotecan," *Molecular cancer therapeutics,* vol. 14, no. 2, pp. 575-85, Feb 2015.

[119] S. L. Edwards *et al.*, "Resistance to therapy caused by intragenic deletion in BRCA2," *Nature,* vol. 451, no. 7182, pp. 1111-5, Feb 28 2008.

[120] W. Sakai *et al.*, "Secondary mutations as a mechanism of cisplatin resistance in BRCA2-mutated cancers," *Nature,* vol. 451, no. 7182, pp. 1116-20, Feb 28 2008.

[121] A. Sawant, A. Kothandapani, A. Zhitkovich, R. W. Sobol, and S. M. Patrick, "Role of mismatch repair proteins in the processing of cisplatin interstrand cross-links," *DNA Repair (Amst),* vol. 35, pp. 126-36, Nov 2015.

[122] A. G. Letai, "Diagnosing and exploiting cancer's addiction to blocks in apoptosis," *Nature reviews. Cancer,* vol. 8, no. 2, pp. 121-32, Feb 2008.

[123] C. L. Sentman, J. R. Shutter, D. Hockenbery, O. Kanagawa, and S. J. Korsmeyer, "bcl-2 inhibits multiple forms of apoptosis but not negative selection in thymocytes," *Cell,* vol. 67, no. 5, pp. 879-88, Nov 29 1991.

[124] T. Miyashita and J. C. Reed, "bcl-2 gene transfer increases relative resistance of S49.1 and WEHI7.2 lymphoid cells to cell death and DNA fragmentation induced by glucocorticoids and multiple chemotherapeutic drugs," *Cancer research,* vol. 52, no. 19, pp. 5407-11, Oct 1 1992.

[125] S. Kitada *et al.*, "Expression of apoptosis-regulating proteins in chronic lymphocytic leukemia: correlations with In vitro and In vivo chemoresponses," *Blood,* vol. 91, no. 9, pp. 3379-89, May 1 1998.

[126] T. Ni Chonghaile *et al.*, "Pretreatment mitochondrial priming correlates with clinical response to cytotoxic chemotherapy," *Science,* vol. 334, no. 6059, pp. 1129-33, Nov 25 2011.

[127] Y. Yu, Z. Zhong, and Y. Guan, "The downregulation of Bcl-xL/Bcl-2-associated death promoter indicates worse outcomes in patients with small cell lung carcinoma," *Int J Clin Exp Pathol,* vol. 8, no. 10, pp. 13075-82, 2015.

[128] E. Yang, J. Zha, J. Jockel, L. H. Boise, C. B. Thompson, and S. J. Korsmeyer, "Bad, a heterodimeric partner for Bcl-XL and Bcl-2, displaces Bax and promotes cell death," *Cell,* vol. 80, no. 2, pp. 285-91, Jan 27 1995.

[129] J. Deng, N. Carlson, K. Takeyama, P. Dal Cin, M. Shipp, and A. Letai, "BH3 profiling identifies three distinct classes of apoptotic blocks to predict response to ABT-737 and conventional chemotherapeutic agents," *Cancer cell,* vol. 12, no. 2, pp. 171-85, Aug 2007.

[130] E. T. Olejniczak *et al.*, "Integrative genomic analysis of small-cell lung carcinoma reveals correlates of sensitivity to bcl-2 antagonists and uncovers novel chromosomal gains," *Mol Cancer Res,* vol. 5, no. 4, pp. 331-9, Apr 2007.

[131] S. Kondo *et al.*, "Over-expression of bcl-xL gene in human gastric adenomas and carcinomas," *International journal of cancer. Journal international du cancer,* vol. 68, no. 6, pp. 727-30, Dec 11 1996.

[132] C. Castilla, B. Congregado, D. Chinchon, F. J. Torrubia, M. A. Japon, and C. Saez, "Bcl-xL is overexpressed in hormone-resistant prostate cancer and promotes survival of LNCaP cells via interaction with proapoptotic Bak," *Endocrinology,* vol. 147, no. 10, pp. 4960-7, Oct 2006.

[133] T. Oltersdorf *et al.*, "An inhibitor of Bcl-2 family proteins induces regression of solid tumours," *Nature,* vol. 435, no. 7042, pp. 677-81, Jun 2 2005.

[134] M. Konopleva *et al.*, "Mechanisms of apoptosis sensitivity and resistance to the BH3 mimetic ABT-737 in acute myeloid leukemia," *Cancer cell,* vol. 10, no. 5, pp. 375-88, Nov 2006.

[135] G. Yang *et al.*, "The biphasic role of NF-kappaB in progression and chemoresistance of ovarian cancer," *Clinical cancer research : an official journal of the American Association for Cancer Research,* vol. 17, no. 8, pp. 2181-94, Apr 15 2011.

[136] B. Grabner *et al.*, "Disruption of STAT3 signalling promotes KRAS-induced lung tumorigenesis," *Nat Commun,* vol. 6, p. 6285, Mar 3 2015.

[137] E. B. Haura, Z. Zheng, L. Song, A. Cantor, and G. Bepler, "Activated epidermal growth factor receptor-Stat-3 signaling promotes tumor survival in vivo in non-small cell lung cancer," *Clinical cancer research : an official journal of the American Association for Cancer Research,* vol. 11, no. 23, pp. 8288-94, Dec 1 2005.

[138] A. Bhardwaj *et al.*, "Resveratrol inhibits proliferation, induces apoptosis, and overcomes chemoresistance through down-regulation of STAT3 and nuclear factor-kappaB-regulated antiapoptotic and cell survival gene products in human multiple myeloma cells," *Blood,* vol. 109, no. 6, pp. 2293-302, Mar 15 2007.

[139] G. Szakacs, J. K. Paterson, J. A. Ludwig, C. Booth-Genthe, and M. M. Gottesman, "Targeting multidrug resistance in cancer," *Nature reviews. Drug discovery,* vol. 5, no. 3, pp. 219-34, Mar 2006.

[140] L. R. Kelland, "New platinum antitumor complexes," *Crit Rev Oncol Hematol,* vol. 15, no. 3, pp. 191-219, Dec 1993.

[141] H. Burger, W. J. Loos, K. Eechoute, J. Verweij, R. H. Mathijssen, and E. A. Wiemer, "Drug transporters of platinum-based anticancer agents and their clinical significance," *Drug resistance updates : reviews and commentaries in antimicrobial and anticancer chemotherapy,* vol. 14, no. 1, pp. 22-34, Feb 2011.

[142] I. S. Song *et al.*, "Role of human copper transporter Ctr1 in the transport of platinum-based antitumor agents in cisplatin-sensitive and cisplatin-resistant cells," *Molecular cancer therapeutics,* vol. 3, no. 12, pp. 1543-9, Dec 2004.

[143] A. K. Holzer *et al.*, "The copper influx transporter human copper transport protein 1 regulates the uptake of cisplatin in human ovarian carcinoma cells," *Molecular pharmacology,* vol. 66, no. 4, pp. 817-23, Oct 2004.

[144] P. Noordhuis, A. C. Laan, K. van de Born, N. Losekoot, I. Kathmann, and G. J. Peters, "Oxaliplatin activity in selected and unselected human ovarian and colorectal cancer cell lines," *Biochemical pharmacology,* vol. 76, no. 1, pp. 53-61, Jul 1 2008.

[145] R. Safaei, S. Otani, B. J. Larson, M. L. Rasmussen, and S. B. Howell, "Transport of cisplatin by the copper efflux transporter ATP7B," *Molecular pharmacology,* vol. 73, no. 2, pp. 461-8, Feb 2008.

[146] G. Samimi *et al.*, "Increased expression of the copper efflux transporter ATP7A mediates resistance to cisplatin, carboplatin, and oxaliplatin in ovarian cancer cells," *Clinical cancer research : an official journal of the American Association for Cancer Research,* vol. 10, no. 14, pp. 4661-9, Jul 15 2004.

[147] Y. G. Assaraf and R. T. Schimke, "Identification of methotrexate transport deficiency in mammalian cells using fluoresceinated methotrexate and flow cytometry," *Proceedings of the National Academy of Sciences of the United States of America,* vol. 84, no. 20, pp. 7154-8, Oct 1987.

[148] V. M. Belkov *et al.*, "Reduced folate carrier expression in acute lymphoblastic leukemia: a mechanism for ploidy but not lineage differences in methotrexate accumulation," *Blood,* vol. 93, no. 5, pp. 1643-50, Mar 1 1999.

[149] Y. Wettergren, E. Odin, S. Nilsson, R. Willen, G. Carlsson, and B. Gustavsson, "Low expression of reduced folate carrier-1 and folylpolyglutamate synthase correlates with lack of a deleted in colorectal carcinoma mRNA splice variant in normal-appearing mucosa of colorectal carcinoma patients," *Cancer Detect Prev,* vol. 29, no. 4, pp. 348-55, 2005.

[150] W. Guo *et al.*, "Mechanisms of methotrexate resistance in osteosarcoma," *Clinical cancer research : an official journal of the American Association for Cancer Research,* vol. 5, no. 3, pp. 621-7, Mar 1999.

[151] I. B. Kastrup, J. Worm, E. Ralfkiaer, P. Hokland, P. Guldberg, and K. Gronbaek, "Genetic and epigenetic alterations of the reduced folate carrier in untreated diffuse large B-cell lymphoma," *Eur J Haematol,* vol. 80, no. 1, pp. 61-6, Jan 2008.

[152] A. J. Ferreri *et al.*, "Aberrant methylation in the promoter region of the reduced folate carrier gene is a potential mechanism of resistance to methotrexate in primary central nervous system lymphomas," *British journal of haematology,* vol. 126, no. 5, pp. 657-64, Sep 2004.

[153] A. Qiu *et al.*, "Identification of an intestinal folate transporter and the molecular basis for hereditary folate malabsorption," *Cell,* vol. 127, no. 5, pp. 917-28, Dec 1 2006.

[154] N. K. Diop-Bove, J. Wu, R. Zhao, J. Locker, and I. D. Goldman, "Hypermethylation of the human proton-coupled folate transporter (SLC46A1) minimal transcriptional regulatory region in an antifolate-resistant HeLa cell line," *Molecular cancer therapeutics,* vol. 8, no. 8, pp. 2424-31, Aug 2009.

[155] Y. Saikawa, C. B. Knight, T. Saikawa, S. T. Page, B. A. Chabner, and P. C. Elwood, "Decreased expression of the human folate receptor mediates transport-defective methotrexate resistance in KB cells," *The Journal of biological chemistry,* vol. 268, no. 7, pp. 5293-301, Mar 5 1993.

[156] K. N. Chung *et al.*, "Stable transfectants of human MCF-7 breast cancer cells with increased levels of the human folate receptor exhibit an increased sensitivity to antifolates," *The Journal of clinical investigation,* vol. 91, no. 4, pp. 1289-94, Apr 1993.

[157] M. L. Slovak *et al.*, "The LRP gene encoding a major vault protein associated with drug resistance maps proximal to MRP on chromosome 16: evidence that chromosome breakage plays a key role in MRP or LRP gene amplification," *Cancer research,* vol. 55, no. 19, pp. 4214-9, Oct 1 1995.

[158] Y. Zhu, C. Kong, Y. Zeng, Z. Sun, and H. Gao, "Expression of lung resistance-related protein in transitional cell carcinoma of bladder," *Urology,* vol. 63, no. 4, pp. 694-8, Apr 2004.

[159] W. Berger, L. Elbling, and M. Micksche, "Expression of the major vault protein LRP in human non-small-cell lung cancer cells: activation by short-term exposure to antineoplastic drugs," *International journal of cancer. Journal international du cancer,* vol. 88, no. 2, pp. 293-300, Oct 15 2000.

[160] L. A. Torre, R. L. Siegel, and A. Jemal, "Lung Cancer Statistics," *Advances in experimental medicine and biology,* vol. 893, pp. 1-19, 2016.

[161] S. Awasthi *et al.*, "RLIP76 and Cancer," *Clinical cancer research : an official journal of the American Association for Cancer Research,* vol. 14, no. 14, pp. 4372-7, Jul 15 2008.

[162] S. Awasthi *et al.*, "Adenosine triphosphate-dependent transport of doxorubicin, daunomycin, and vinblastine in human tissues by a mechanism distinct from the P-glycoprotein," *The Journal of clinical investigation,* vol. 93, no. 3, pp. 958-65, Mar 1994.

[163] D. Stuckler, J. Singhal, S. S. Singhal, S. Yadav, Y. C. Awasthi, and S. Awasthi, "RLIP76 transports vinorelbine and mediates drug resistance in non-small cell lung cancer," *Cancer research,* vol. 65, no. 3, pp. 991-8, Feb 1 2005.

[164] J. K. Zolnerciks, E. J. Andress, M. Nicolaou, and K. J. Linton, "Structure of ABC transporters," *Essays in biochemistry,* vol. 50, no. 1, pp. 43-61, Sep 7 2011.

[165] M. Dean, A. Rzhetsky, and R. Allikmets, "The human ATP-binding cassette (ABC) transporter superfamily," *Genome research,* vol. 11, no. 7, pp. 1156-66, Jul 2001.

[166] A. Bodo, E. Bakos, F. Szeri, A. Varadi, and B. Sarkadi, "The role of multidrug transporters in drug availability, metabolism and toxicity," *Toxicol Lett,* vol. 140-141, pp. 133-43, Apr 11 2003.

[167] J. Bryan *et al.*, "ABCC8 and ABCC9: ABC transporters that regulate K+ channels," *Pflugers Archiv : European journal of physiology,* vol. 453, no. 5, pp. 703-18, Feb 2007.

[168] J. Aittoniemi, C. Fotinou, T. J. Craig, H. de Wet, P. Proks, and F. M. Ashcroft, "Review. SUR1: a unique ATP-binding cassette protein that functions as an ion channel regulator," *Philos Trans R Soc Lond B Biol Sci,* vol. 364, no. 1514, pp. 257-67, Jan 27 2009.

[169] J. R. Riordan, "CFTR function and prospects for therapy," *Annual review of biochemistry,* vol. 77, pp. 701-26, 2008.

[170] M. Dean and R. Allikmets, "Complete characterization of the human ABC gene family," *Journal of bioenergetics and biomembranes,* vol. 33, no. 6, pp. 475-9, Dec 2001.

[171] B. Sarkadi, L. Homolya, G. Szakacs, and A. Varadi, "Human multidrug resistance ABCB and ABCG transporters: participation in a chemoimmunity defense system," *Physiological reviews,* vol. 86, no. 4, pp. 1179-236, Oct 2006.

[172] A. K. Tiwari, K. Sodani, C. L. Dai, C. R. Ashby, Jr., and Z. S. Chen, "Revisiting the ABCs of multidrug resistance in cancer chemotherapy," *Curr Pharm Biotechnol,* vol. 12, no. 4, pp. 570-94, Apr 2011.

[173] C. P. Wu, C. H. Hsieh, and Y. S. Wu, "The emergence of drug transporter-mediated multidrug resistance to cancer chemotherapy," *Molecular pharmaceutics,* vol. 8, no. 6, pp. 1996-2011, Dec 5 2011.

[174] E. J. Tarling, T. Q. de Aguiar Vallim, and P. A. Edwards, "Role of ABC transporters in lipid transport and human disease," *Trends Endocrinol Metab,* vol. 24, no. 7, pp. 342-50, Jul 2013.

[175] D. C. Rees, E. Johnson, and O. Lewinson, "ABC transporters: the power to change," *Nat Rev Mol Cell Biol,* vol. 10, no. 3, pp. 218-27, Mar 2009.

[176] I. B. Holland and M. A. Blight, "ABC-ATPases, adaptable energy generators fuelling transmembrane movement of a variety of molecules in organisms from bacteria to humans," *Journal of molecular biology,* vol. 293, no. 2, pp. 381-99, Oct 22 1999.

[177] G. B. Erkens *et al.*, "The structural basis of modularity in ECF-type ABC transporters," *Nature structural & molecular biology,* vol. 18, no. 7, pp. 755-60, Jun 26 2011.

[178] A. L. Davidson and J. Chen, "ATP-binding cassette transporters in bacteria," *Annual review of biochemistry,* vol. 73, pp. 241-68, 2004.

[179] K. P. Locher, A. T. Lee, and D. C. Rees, "The E. coli BtuCD structure: a framework for ABC transporter architecture and mechanism," *Science,* vol. 296, no. 5570, pp. 1091-8, May 10 2002.

[180] R. J. Dawson and K. P. Locher, "Structure of a bacterial multidrug ABC transporter," *Nature,* vol. 443, no. 7108, pp. 180-5, Sep 14 2006.

[181] E. Schneider and S. Hunke, "ATP-binding-cassette (ABC) transport systems: functional and structural aspects of the ATP-hydrolyzing subunits/domains," *FEMS Microbiol Rev,* vol. 22, no. 1, pp. 1-20, Apr 1998.

[182] K. Hollenstein, D. C. Frei, and K. P. Locher, "Structure of an ABC transporter in complex with its binding protein," *Nature,* vol. 446, no. 7132, pp. 213-6, Mar 8 2007.

[183] H. W. Pinkett, A. T. Lee, P. Lum, K. P. Locher, and D. C. Rees, "An inward-facing conformation of a putative metal-chelate-type ABC transporter," *Science,* vol. 315, no. 5810, pp. 373-7, Jan 19 2007.

[184] S. V. Ambudkar, I. W. Kim, D. Xia, and Z. E. Sauna, "The A-loop, a novel conserved aromatic acid subdomain upstream of the Walker A motif in ABC transporters, is critical for ATP binding," *FEBS letters,* vol. 580, no. 4, pp. 1049-55, Feb 13 2006.

[185] J. Zaitseva, S. Jenewein, T. Jumpertz, I. B. Holland, and L. Schmitt, "H662 is the linchpin of ATP hydrolysis in the nucleotide-binding domain of the ABC transporter HlyB," *The EMBO journal,* vol. 24, no. 11, pp. 1901-10, Jun 1 2005.

[186] A. L. Davidson, S. S. Laghaeian, and D. E. Mannering, "The maltose transport system of Escherichia coli displays positive cooperativity in ATP hydrolysis," *The Journal of biological chemistry,* vol. 271, no. 9, pp. 4858-63, Mar 1 1996.

[187] A. E. Senior and S. Bhagat, "P-glycoprotein shows strong catalytic cooperativity between the two nucleotide sites," *Biochemistry,* vol. 37, no. 3, pp. 831-6, Jan 20 1998.

[188] L. W. Hung, I. X. Wang, K. Nikaido, P. Q. Liu, G. F. Ames, and S. H. Kim, "Crystal structure of the ATP-binding subunit of an ABC transporter," *Nature,* vol. 396, no. 6712, pp. 703-7, Dec 17 1998.

[189] S. G. Aller *et al.*, "Structure of P-glycoprotein reveals a molecular basis for poly-specific drug binding," *Science,* vol. 323, no. 5922, pp. 1718-22, Mar 27 2009.

[190] J. Li, K. F. Jaimes, and S. G. Aller, "Refined structures of mouse P-glycoprotein," *Protein science : a publication of the Protein Society,* vol. 23, no. 1, pp. 34-46, Jan 2014.

[191] D. A. Gutmann, A. Ward, I. L. Urbatsch, G. Chang, and H. W. van Veen, "Understanding polyspecificity of multidrug ABC transporters: closing in on the gaps in ABCB1," *Trends Biochem Sci,* vol. 35, no. 1, pp. 36-42, Jan 2010.

[192] P. C. Smith *et al.*, "ATP binding to the motor domain from an ABC transporter drives formation of a nucleotide sandwich dimer," *Molecular cell,* vol. 10, no. 1, pp. 139-49, Jul 2002.

[193] K. P. Hopfner *et al.*, "Structural biology of Rad50 ATPase: ATP-driven conformational control in DNA double-strand break repair and the ABC-ATPase superfamily," *Cell,* vol. 101, no. 7, pp. 789-800, Jun 23 2000.

[194] J. Chen, G. Lu, J. Lin, A. L. Davidson, and F. A. Quiocho, "A tweezers-like motion of the ATP-binding cassette dimer in an ABC transport cycle," *Molecular cell,* vol. 12, no. 3, pp. 651-61, Sep 2003.

[195] C. F. Higgins and K. J. Linton, "The ATP switch model for ABC transporters," *Nature structural & molecular biology,* vol. 11, no. 10, pp. 918-26, Oct 2004.

[196] P. M. Jones and A. M. George, "A reciprocating twin-channel model for ABC transporters," *Q Rev Biophys,* vol. 47, no. 3, pp. 189-220, Aug 2014.

[197] P. M. Jones and A. M. George, "Opening of the ADP-bound active site in the ABC transporter ATPase dimer: evidence for a constant contact, alternating sites model for the catalytic cycle," *Proteins,* vol. 75, no. 2, pp. 387-96, May 1 2009.

[198] A. E. Senior, M. K. al-Shawi, and I. L. Urbatsch, "The catalytic cycle of P-glycoprotein," *FEBS letters,* vol. 377, no. 3, pp. 285-9, Dec 27 1995.

[199] M. Hohl, C. Briand, M. G. Grutter, and M. A. Seeger, "Crystal structure of a heterodimeric ABC transporter in its inward-facing conformation," *Nature structural & molecular biology,* vol. 19, no. 4, pp. 395-402, Mar 25 2012.

[200] A. Breier, L. Gibalova, M. Seres, M. Barancik, and Z. Sulova, "New insight into p-glycoprotein as a drug target," *Anti-cancer agents in medicinal chemistry,* vol. 13, no. 1, pp. 159-70, Jan 2013.

[201] F. Zhang *et al.*, "P-glycoprotein associates with Anxa2 and promotes invasion in multidrug resistant breast cancer cells," *Biochemical pharmacology,* vol. 87, no. 2, pp. 292-302, Jan 15 2014.

[202] M. Pallis and N. Russell, "P-glycoprotein plays a drug-efflux-independent role in augmenting cell survival in acute myeloblastic leukemia and is associated with modulation of a sphingomyelin-ceramide apoptotic pathway," *Blood,* vol. 95, no. 9, pp. 2897-904, May 1 2000.

[203] P. Gros, Y. B. Ben Neriah, J. M. Croop, and D. E. Housman, "Isolation and expression of a complementary DNA that confers multidrug resistance," *Nature,* vol. 323, no. 6090, pp. 728-31, Oct 23-29 1986.

[204] J. E. Chin, R. Soffir, K. E. Noonan, K. Choi, and I. B. Roninson, "Structure and expression of the human MDR (P-glycoprotein) gene family," *Molecular and cellular biology,* vol. 9, no. 9, pp. 3808-20, Sep 1989.

[205] A. van Helvoort *et al.*, "MDR1 P-glycoprotein is a lipid translocase of broad specificity, while MDR3 P-glycoprotein specifically translocates phosphatidylcholine," *Cell,* vol. 87, no. 3, pp. 507-17, Nov 1 1996.

[206] H. Green, P. Soderkvist, P. Rosenberg, G. Horvath, and C. Peterson, "ABCB1 G1199A polymorphism and ovarian cancer response to paclitaxel," *Journal of pharmaceutical sciences,* vol. 97, no. 6, pp. 2045-8, Jun 2008.

[207] H. Green, P. Soderkvist, P. Rosenberg, G. Horvath, and C. Peterson, "mdr-1 single nucleotide polymorphisms in ovarian cancer tissue: G2677T/A correlates with response to paclitaxel chemotherapy," *Clinical cancer research : an official journal of the American Association for Cancer Research,* vol. 12, no. 3 Pt 1, pp. 854-9, Feb 1 2006.

[208] M. M. Gottesman, C. A. Hrycyna, P. V. Schoenlein, U. A. Germann, and I. Pastan, "Genetic analysis of the multidrug transporter," *Annu Rev Genet,* vol. 29, pp. 607-49, 1995.

[209] B. Verhalen *et al.*, "Energy transduction and alternating access of the mammalian ABC transporter P-glycoprotein," *Nature,* vol. 543, no. 7647, pp. 738-741, Mar 30 2017.

[210] M. M. Gottesman, S. V. Ambudkar, and D. Xia, "Structure of a multidrug transporter," *Nat Biotechnol,* vol. 27, no. 6, pp. 546-7, Jun 2009.

[211] T. W. Loo, M. C. Bartlett, and D. M. Clarke, "Simultaneous binding of two different drugs in the binding pocket of the human multidrug resistance P-glycoprotein," *The Journal of biological chemistry,* vol. 278, no. 41, pp. 39706-10, Oct 10 2003.

[212] A. B. Shapiro, K. Fox, P. Lam, and V. Ling, "Stimulation of P-glycoprotein-mediated drug transport by prazosin and progesterone. Evidence for a third drug-binding site," *European journal of biochemistry / FEBS,* vol. 259, no. 3, pp. 841-50, Feb 1999.

[213] S. Dewanjee *et al.*, "Natural Products as Alternative Choices for P-Glycoprotein (P-gp) Inhibition," *Molecules,* vol. 22, no. 6, May 25 2017.

[214] T. W. Loo and D. M. Clarke, "Recent progress in understanding the mechanism of P-glycoprotein-mediated drug efflux," *The Journal of membrane biology,* vol. 206, no. 3, pp. 173-85, Aug 2005.

[215] M. Hennessy and J. P. Spiers, "A primer on the mechanics of P-glycoprotein the multidrug transporter," *Pharmacological research : the official journal of the Italian Pharmacological Society,* vol. 55, no. 1, pp. 1-15, Jan 2007.

[216] C. F. Higgins and M. M. Gottesman, "Is the multidrug transporter a flippase?," *Trends Biochem Sci,* vol. 17, no. 1, pp. 18-21, Jan 1992.

[217] S. Hsing, Z. Gatmaitan, and I. M. Arias, "The function of Gp170, the multidrug-resistance gene product, in the brush border of rat intestinal mucosa," *Gastroenterology,* vol. 102, no. 3, pp. 879-85, Mar 1992.

[218] V. J. Wacher, C. Y. Wu, and L. Z. Benet, "Overlapping substrate specificities and tissue distribution of cytochrome P450 3A and P-glycoprotein: implications for drug delivery and activity in cancer chemotherapy," *Molecular carcinogenesis,* vol. 13, no. 3, pp. 129-34, Jul 1995.

[219] N. Okamura *et al.*, "Digoxin-cyclosporin A interaction: modulation of the multidrug transporter P-glycoprotein in the kidney," *The Journal of pharmacology and experimental therapeutics,* vol. 266, no. 3, pp. 1614-9, Sep 1993.

[220] A. H. Schinkel *et al.*, "Disruption of the mouse mdr1a P-glycoprotein gene leads to a deficiency in the blood-brain barrier and to increased sensitivity to drugs," *Cell,* vol. 77, no. 4, pp. 491-502, May 20 1994.

[221] Z. Binkhathlan and A. Lavasanifar, "P-glycoprotein inhibition as a therapeutic approach for overcoming multidrug resistance in cancer: current status and future perspectives," *Current cancer drug targets,* vol. 13, no. 3, pp. 326-46, Mar 2013.

[222] X. Xu *et al.*, "Dominant effector genetics in mammalian cells," *Nature genetics,* vol. 27, no. 1, pp. 23-9, Jan 2001.

[223] T. Schondorf *et al.*, "Amplification of the mdr1-gene is uncommon in recurrent ovarian carcinomas," *Cancer letters,* vol. 146, no. 2, pp. 195-9, Nov 15 1999.

[224] K. M. Tainton *et al.*, "Mutational analysis of P-glycoprotein: suppression of caspase activation in the absence of ATP-dependent drug efflux," *Cell Death Differ,* vol. 11, no. 9, pp. 1028-37, Sep 2004.

[225] K. Goda, Z. Bacso, and G. Szabo, "Multidrug resistance through the spectacle of P-glycoprotein," *Current cancer drug targets,* vol. 9, no. 3, pp. 281-97, May 2009.

[226] A. J. Slot, S. V. Molinski, and S. P. Cole, "Mammalian multidrug-resistance proteins (MRPs)," *Essays in biochemistry,* vol. 50, no. 1, pp. 179-207, Sep 7 2011.

[227] K. Hollenstein, R. J. Dawson, and K. P. Locher, "Structure and mechanism of ABC transporter proteins," *Curr Opin Struct Biol,* vol. 17, no. 4, pp. 412-8, Aug 2007.

[228] R. G. Deeley, C. Westlake, and S. P. Cole, "Transmembrane transport of endo- and xenobiotics by mammalian ATP-binding cassette multidrug resistance proteins," *Physiological reviews,* vol. 86, no. 3, pp. 849-99, Jul 2006.

[229] M. L. Slovak, J. P. Ho, G. Bhardwaj, E. U. Kurz, R. G. Deeley, and S. P. Cole, "Localization of a novel multidrug resistance-associated gene in the HT1080/DR4 and H69AR human tumor cell lines," *Cancer research,* vol. 53, no. 14, pp. 3221-5, Jul 15 1993.

[230] N. Godinot *et al.*, "Cloning and functional characterization of the multidrug resistance-associated protein (MRP1/ABCC1) from the cynomolgus monkey," *Molecular cancer therapeutics,* vol. 2, no. 3, pp. 307-16, Mar 2003.

[231] L. Ma, S. E. Pratt, J. Cao, A. H. Dantzig, R. E. Moore, and C. A. Slapak, "Identification and characterization of the canine multidrug resistance-associated protein," *Molecular cancer therapeutics,* vol. 1, no. 14, pp. 1335-42, Dec 2002.

[232] K. Nunoya, C. E. Grant, D. Zhang, S. P. Cole, and R. G. Deeley, "Molecular cloning and pharmacological characterization of rat multidrug resistance protein 1 (mrp1)," *Drug metabolism and disposition: the biological fate of chemicals,* vol. 31, no. 8, pp. 1016-26, Aug 2003.

[233] E. Bakos *et al.*, "Characterization of the amino-terminal regions in the human multidrug resistance protein (MRP1)," *Journal of cell science,* vol. 113 Pt 24, pp. 4451-61, Dec 2000.

[234] M. F. Rosenberg *et al.*, "Structure of a human multidrug transporter in an inward-facing conformation," *J Struct Biol,* vol. 170, no. 3, pp. 540-7, Jun 2010.

[235] R. Ernst, P. Kueppers, C. M. Klein, T. Schwarzmueller, K. Kuchler, and L. Schmitt, "A mutation of the H-loop selectively affects rhodamine transport by the yeast multidrug ABC transporter Pdr5," *Proceedings of the National Academy of Sciences of the United States of America,* vol. 105, no. 13, pp. 5069-74, Apr 1 2008.

[236] K. Koike, G. Conseil, E. M. Leslie, R. G. Deeley, and S. P. Cole, "Identification of proline residues in the core cytoplasmic and transmembrane regions of multidrug resistance protein 1 (MRP1/ABCC1) important for transport function, substrate specificity, and nucleotide interactions," *The Journal of biological chemistry,* vol. 279, no. 13, pp. 12325-36, Mar 26 2004.

[237] R. G. Deeley and S. P. Cole, "Substrate recognition and transport by multidrug resistance protein 1 (ABCC1)," *FEBS letters,* vol. 580, no. 4, pp. 1103-11, Feb 13 2006.

[238] K. Ito, S. L. Olsen, W. Qiu, R. G. Deeley, and S. P. Cole, "Mutation of a single conserved tryptophan in multidrug resistance protein 1 (MRP1/ABCC1) results in loss of drug resistance and selective loss of organic anion transport," *The Journal of biological chemistry,* vol. 276, no. 19, pp. 15616-24, May 11 2001.

[239] A. Haimeur, R. G. Deeley, and S. P. Cole, "Charged amino acids in the sixth transmembrane helix of multidrug resistance protein 1 (MRP1/ABCC1) are critical determinants of transport activity," *The Journal of biological chemistry,* vol. 277, no. 44, pp. 41326-33, Nov 1 2002.

[240] D. W. Zhang, K. Nunoya, M. Vasa, H. M. Gu, S. P. Cole, and R. G. Deeley, "Mutational analysis of polar amino acid residues within predicted transmembrane helices 10 and 16 of multidrug resistance protein 1 (ABCC1): effect on substrate specificity," *Drug metabolism and disposition: the biological fate of chemicals,* vol. 34, no. 4, pp. 539-46, Apr 2006.

[241] P. Wu, C. J. Oleschuk, Q. Mao, B. O. Keller, R. G. Deeley, and S. P. Cole, "Analysis of human multidrug resistance protein 1 (ABCC1) by matrix-assisted laser desorption ionization/time of flight mass spectrometry: toward identification of leukotriene C4 binding sites," *Molecular pharmacology,* vol. 68, no. 5, pp. 1455-65, Nov 2005.

[242] S. P. Cole *et al.*, "Overexpression of a transporter gene in a multidrug-resistant human lung cancer cell line," *Science,* vol. 258, no. 5088, pp. 1650-4, Dec 4 1992.

[243] E. Bakos, R. Evers, E. Sinko, A. Varadi, P. Borst, and B. Sarkadi, "Interactions of the human multidrug resistance proteins MRP1 and MRP2 with organic anions," *Molecular pharmacology,* vol. 57, no. 4, pp. 760-8, Apr 2000.

[244] E. Bakos *et al.*, "Functional multidrug resistance protein (MRP1) lacking the N-terminal transmembrane domain," *The Journal of biological chemistry,* vol. 273, no. 48, pp. 32167-75, Nov 27 1998.

[245] I. S. Mohammad, W. He, and L. Yin, "Understanding of human ATP binding cassette superfamily and novel multidrug resistance modulators to overcome MDR," *Biomedicine & pharmacotherapy = Biomedecine & pharmacotherapie,* vol. 100, pp. 335-348, Apr 2018.

[246] S. P. Cole *et al.*, "Pharmacological characterization of multidrug resistant MRP-transfected human tumor cells," *Cancer research,* vol. 54, no. 22, pp. 5902-10, Nov 15 1994.

[247] A. Tamaki, C. Ierano, G. Szakacs, R. W. Robey, and S. E. Bates, "The controversial role of ABC transporters in clinical oncology," *Essays in biochemistry,* vol. 50, no. 1, pp. 209-32, Sep 7 2011.

[248] S. Heimerl, A. K. Bosserhoff, T. Langmann, J. Ecker, and G. Schmitz, "Mapping ATP-binding cassette transporter gene expression profiles in melanocytes and melanoma cells," *Melanoma research,* vol. 17, no. 5, pp. 265-73, Oct 2007.

[249] A. Rajagopal and S. M. Simon, "Subcellular localization and activity of multidrug resistance proteins," *Molecular biology of the cell,* vol. 14, no. 8, pp. 3389-99, Aug 2003.

[250] S. P. Cole, "Targeting multidrug resistance protein 1 (MRP1, ABCC1): past, present, and future," *Annual review of pharmacology and toxicology,* vol. 54, pp. 95-117, 2014.

[251] S. Ryu, T. Kawabe, S. Nada, and A. Yamaguchi, "Identification of basic residues involved in drug export function of human multidrug resistance-associated protein 2," *The Journal of biological chemistry,* vol. 275, no. 50, pp. 39617-24, Dec 15 2000.

[252] C. C. Paulusma *et al.*, "A mutation in the human canalicular multispecific organic anion transporter gene causes the Dubin-Johnson syndrome," *Hepatology,* vol. 25, no. 6, pp. 1539-42, Jun 1997.

[253] J. Kranz *et al.*, "The role of the efflux carriers Abcg2 and Abcc2 for the hepatobiliary elimination of benzo[a]pyrene and its metabolites in mice," *Chemico-biological interactions,* vol. 224, pp. 36-41, Dec 5 2014.

[254] J. Kartenbeck, U. Leuschner, R. Mayer, and D. Keppler, "Absence of the canalicular isoform of the MRP gene-encoded conjugate export pump from the hepatocytes in Dubin-Johnson syndrome," *Hepatology,* vol. 23, no. 5, pp. 1061-6, May 1996.

[255] R. Evers *et al.*, "Vinblastine and sulfinpyrazone export by the multidrug resistance protein MRP2 is associated with glutathione export," *British journal of cancer,* vol. 83, no. 3, pp. 375-83, Aug 2000.

[256] T. Kawabe *et al.*, "Enhanced transport of anticancer agents and leukotriene C4 by the human canalicular multispecific organic anion transporter (cMOAT/MRP2)," *FEBS letters,* vol. 456, no. 2, pp. 327-31, Aug 6 1999.

[257] M. T. Huisman, A. A. Chhatta, O. van Tellingen, J. H. Beijnen, and A. H. Schinkel, "MRP2 (ABCC2) transports taxanes and confers paclitaxel resistance and both processes are stimulated by probenecid," *International journal of cancer. Journal international du cancer,* vol. 116, no. 5, pp. 824-9, Sep 20 2005.

[258] L. A. Doyle *et al.*, "A multidrug resistance transporter from human MCF-7 breast cancer cells," *Proceedings of the National Academy of Sciences of the United States of America,* vol. 95, no. 26, pp. 15665-70, Dec 22 1998.

[259] J. D. Allen, R. F. Brinkhuis, J. Wijnholds, and A. H. Schinkel, "The mouse Bcrp1/Mxr/Abcp gene: amplification and overexpression in cell lines selected for resistance to topotecan, mitoxantrone, or doxorubicin," *Cancer research,* vol. 59, no. 17, pp. 4237-41, Sep 1 1999.

[260] N. K. Diop and C. A. Hrycyna, "N-Linked glycosylation of the human ABC transporter ABCG2 on asparagine 596 is not essential for expression, transport activity, or trafficking to the plasma membrane," *Biochemistry,* vol. 44, no. 14, pp. 5420-9, Apr 12 2005.

[261] Y. Imai *et al.*, "C421A polymorphism in the human breast cancer resistance protein gene is associated with low expression of Q141K protein and low-level drug resistance," *Molecular cancer therapeutics,* vol. 1, no. 8, pp. 611-6, Jun 2002.

[262] R. R. Vethanayagam *et al.*, "Functional analysis of the human variants of breast cancer resistance protein: I206L, N590Y, and D620N," *Drug metabolism and disposition: the biological fate of chemicals,* vol. 33, no. 6, pp. 697-705, Jun 2005.

[263] J. Xu, H. Peng, and J. T. Zhang, "Human multidrug transporter ABCG2, a target for sensitizing drug resistance in cancer chemotherapy," *Current medicinal chemistry,* vol. 14, no. 6, pp. 689-701, 2007.

[264] M. Maliepaard *et al.*, "Subcellular localization and distribution of the breast cancer resistance protein transporter in normal human tissues," *Cancer research,* vol. 61, no. 8, pp. 3458-64, Apr 15 2001.

[265] H. C. Cooray, C. G. Blackmore, L. Maskell, and M. A. Barrand, "Localisation of breast cancer resistance protein in microvessel endothelium of human brain," *Neuroreport,* vol. 13, no. 16, pp. 2059-63, Nov 15 2002.

[266] S. Zhou, Y. Zong, P. A. Ney, G. Nair, C. F. Stewart, and B. P. Sorrentino, "Increased expression of the Abcg2 transporter during erythroid maturation plays a role in decreasing cellular protoporphyrin IX levels," *Blood,* vol. 105, no. 6, pp. 2571-6, Mar 15 2005.

[267] C. Hirschmann-Jax *et al.*, "A distinct "side population" of cells with high drug efflux capacity in human tumor cells," *Proceedings of the National Academy of Sciences of the United States of America,* vol. 101, no. 39, pp. 14228-33, Sep 28 2004.

[268] L. D. Cripe *et al.*, "Zosuquidar, a novel modulator of P-glycoprotein, does not improve the outcome of older patients with newly diagnosed acute myeloid leukemia: a randomized, placebo-controlled trial of the Eastern Cooperative Oncology Group 3999," *Blood,* vol. 116, no. 20, pp. 4077-85, Nov 18 2010.

[269] R. J. Kelly *et al.*, "A pharmacodynamic study of docetaxel in combination with the P-glycoprotein antagonist tariquidar (XR9576) in patients with lung, ovarian, and cervical

cancer," *Clinical cancer research : an official journal of the American Association for Cancer Research,* vol. 17, no. 3, pp. 569-80, Feb 1 2011.

[270] T. Sumizawa *et al.*, "Reversal of multidrug resistance-associated protein-mediated drug resistance by the pyridine analog PAK-104P," *Molecular pharmacology,* vol. 51, no. 3, pp. 399-405, Mar 1997.

[271] M. Qadir *et al.*, "Cyclosporin A is a broad-spectrum multidrug resistance modulator," *Clinical cancer research : an official journal of the American Association for Cancer Research,* vol. 11, no. 6, pp. 2320-6, Mar 15 2005.

[272] S. K. Rabindran *et al.*, "Reversal of a novel multidrug resistance mechanism in human colon carcinoma cells by fumitremorgin C," *Cancer research,* vol. 58, no. 24, pp. 5850-8, Dec 15 1998.

[273] J. D. Allen *et al.*, "Potent and specific inhibition of the breast cancer resistance protein multidrug transporter in vitro and in mouse intestine by a novel analogue of fumitremorgin C," *Molecular cancer therapeutics,* vol. 1, no. 6, pp. 417-25, Apr 2002.

[274] A. Gupta, Y. Zhang, J. D. Unadkat, and Q. Mao, "HIV protease inhibitors are inhibitors but not substrates of the human breast cancer resistance protein (BCRP/ABCG2)," *The Journal of pharmacology and experimental therapeutics,* vol. 310, no. 1, pp. 334-41, Jul 2004.

[275] K. K. To, "MicroRNA: a prognostic biomarker and a possible druggable target for circumventing multidrug resistance in cancer chemotherapy," *J Biomed Sci,* vol. 20, p. 99, Dec 20 2013.

[276] D. D. Feng *et al.*, "Down-regulated miR-331-5p and miR-27a are associated with chemotherapy resistance and relapse in leukaemia," *Journal of cellular and molecular medicine,* vol. 15, no. 10, pp. 2164-75, Oct 2011.

[277] G. Zhang, Z. Wang, F. Qian, C. Zhao, and C. Sun, "Silencing of the ABCC4 gene by RNA interference reverses multidrug resistance in human gastric cancer," *Oncology reports,* vol. 33, no. 3, pp. 1147-54, Mar 2015.

[278] H. Wu, W. N. Hait, and J. M. Yang, "Small interfering RNA-induced suppression of MDR1 (P-glycoprotein) restores sensitivity to multidrug-resistant cancer cells," *Cancer research,* vol. 63, no. 7, pp. 1515-9, Apr 1 2003.

[279] M. Shionoya, T. Jimbo, M. Kitagawa, T. Soga, and A. Tohgo, "DJ-927, a novel oral taxane, overcomes P-glycoprotein-mediated multidrug resistance in vitro and in vivo," *Cancer science,* vol. 94, no. 5, pp. 459-66, May 2003.

[280] T. J. Altstadt *et al.*, "Synthesis and antitumor activity of novel C-7 paclitaxel ethers: discovery of BMS-184476," *Journal of medicinal chemistry,* vol. 44, no. 26, pp. 4577-83, Dec 20 2001.

[281] G. Cassinelli *et al.*, "Cellular bases of the antitumor activity of the novel taxane IDN 5109 (BAY59-8862) on hormone-refractory prostate cancer," *Clinical cancer research : an official journal of the American Association for Cancer Research,* vol. 8, no. 8, pp. 2647-54, Aug 2002.

[282] H. C. Chiu, P. Kopeckova, S. S. Deshmane, and J. Kopecek, "Lysosomal degradability of poly(alpha-amino acids)," *Journal of biomedical materials research,* vol. 34, no. 3, pp. 381-92, Mar 5 1997.

[283] J. B. Lloyd, "Lysosome membrane permeability: implications for drug delivery," *Advanced drug delivery reviews,* vol. 41, no. 2, pp. 189-200, Mar 30 2000.

[284] J. Kopecek and P. Kopeckova, "HPMA copolymers: origins, early developments, present, and future," *Advanced drug delivery reviews,* vol. 62, no. 2, pp. 122-49, Feb 17 2010.

[285] O. Sterba *et al.*, "New types of synthetic infusion solutions. Basic biological properties of poly N-(2-hydroxypropyl) methacrylamide," *Rev Czech Med,* vol. 22, no. 3, pp. 152-6, 1976.

[286] L. Sprincl, J. Exner, O. Sterba, and J. Kopecek, "New types of synthetic infusion solutions. III. Elimination and retention of poly-[N-(2-hydroxypropyl)methacrylamide] in a test organism," *Journal of biomedical materials research,* vol. 10, no. 6, pp. 953-63, Nov 1976.

[287] L. W. Seymour, R. Duncan, J. Strohalm, and J. Kopecek, "Effect of molecular weight (Mw) of N-(2-hydroxypropyl)methacrylamide copolymers on body distribution and rate of excretion after subcutaneous, intraperitoneal, and intravenous administration to rats," *Journal of biomedical materials research,* vol. 21, no. 11, pp. 1341-58, Nov 1987.

[288] K. Ulbrich and V. Subr, "Structural and chemical aspects of HPMA copolymers as drug carriers," *Advanced drug delivery reviews,* vol. 62, no. 2, pp. 150-66, Feb 17 2010.

[289] K. Ulbrich, K. Hola, V. Subr, A. Bakandritsos, J. Tucek, and R. Zboril, "Targeted Drug Delivery with Polymers and Magnetic Nanoparticles: Covalent and Noncovalent Approaches, Release Control, and Clinical Studies," *Chemical reviews,* vol. 116, no. 9, pp. 5338-431, May 11 2016.

[290] P. Kopečková, R. Rathi, S. Takada, B. Říhová, M. M. Berenson, and J. Kopeček, "Bioadhesive N-(2-hydroxypropyl) methacrylamide copolymers for colon-specific drug delivery," *Journal of Controlled Release,* vol. 28, no. 1, pp. 211-222, 1994/01/01/ 1994.

[291] K. Ulbrich, V. Subr, J. Strohalm, D. Plocova, M. Jelinkova, and B. Rihova, "Polymeric drugs based on conjugates of synthetic and natural macromolecules. I. Synthesis and physico-chemical characterisation," *Journal of controlled release : official journal of the Controlled Release Society,* vol. 64, no. 1-3, pp. 63-79, Feb 14 2000.

[292] J. Strohalm and J. Kopeček, "Poly[N-(2-hydroxypropyl)methacrylamide]. IV. Heterogeneous polymerization," *Die Angewandte Makromolekulare Chemie,* vol. 70, no. 1, pp. 109-118, 1978/07/28 1978.

[293] M. Barz, F. Canal, K. Koynov, R. Zentel, and M. J. Vicent, "Synthesis and in vitro evaluation of defined HPMA folate conjugates: influence of aggregation on folate receptor (FR) mediated cellular uptake," *Biomacromolecules,* vol. 11, no. 9, pp. 2274-82, Sep 13 2010.

[294] N. Mohr, M. Barz, R. Forst, and R. Zentel, "A Deeper Insight into the Postpolymerization Modification of Polypenta Fluorophenyl Methacrylates to Poly(N-(2-Hydroxypropyl) Methacrylamide)," *Macromolecular rapid communications,* vol. 35, no. 17, pp. 1522-1527, 2014/09/01 2014.

[295] P. Rejmanova, J. Kopecek, R. Duncan, and J. B. Lloyd, "Stability in rat plasma and serum of lysosomally degradable oligopeptide sequences in N-(2-hydroxypropyl) methacrylamide copolymers," *Biomaterials,* vol. 6, no. 1, pp. 45-8, Jan 1985.

[296] T. Etrych, M. Jelinkova, B. Rihova, and K. Ulbrich, "New HPMA copolymers containing doxorubicin bound via pH-sensitive linkage: synthesis and preliminary in vitro and in vivo biological properties," *Journal of controlled release : official journal of the Controlled Release Society,* vol. 73, no. 1, pp. 89-102, May 18 2001.

[297] W. C. Shen and H. J. Ryser, "cis-Aconityl spacer between daunomycin and macromolecular carriers: a model of pH-sensitive linkage releasing drug from a lysosomotropic conjugate," *Biochemical and biophysical research communications,* vol. 102, no. 3, pp. 1048-54, Oct 15 1981.

[298] D. B. Rozema, K. Ekena, D. L. Lewis, A. G. Loomis, and J. A. Wolff, "Endosomolysis by masking of a membrane-active agent (EMMA) for cytoplasmic release of macromolecules," *Bioconjugate chemistry,* vol. 14, no. 1, pp. 51-7, Jan-Feb 2003.

[299] V. Subr, J. Strohalm, K. Ulbrich, R. Duncan, and I. C. Hume, "Polymers containing enzymatically degradable bonds, XII. Effect of spacer structure on the rate of release of daunomycin and adriamycin from poly [N-(2-hydroxypropyl)-methacrylamide] copolymer drag carriers in vitro and antitumour activity measured in vivo," *Journal of Controlled Release,* vol. 18, no. 2, pp. 123-132, 1992/02/01/ 1992.

[300] K. Ulbrich, M. Pechar, J. Strohalm, V. Subr, and B. Rihova, "Synthesis of biodegradable polymers for controlled drug release," *Annals of the New York Academy of Sciences,* vol. 831, pp. 47-56, Dec 31 1997.

[301] T. W. Chu, J. Yang, and J. Kopecek, "Anti-CD20 multivalent HPMA copolymer-Fab' conjugates for the direct induction of apoptosis," *Biomaterials,* vol. 33, no. 29, pp. 7174-81, Oct 2012.

[302] A. David, P. Kopeckova, T. Minko, A. Rubinstein, and J. Kopecek, "Design of a multivalent galactoside ligand for selective targeting of HPMA copolymer-doxorubicin conjugates to human colon cancer cells," *European journal of cancer,* vol. 40, no. 1, pp. 148-57, Jan 2004.

[303] A. Tang, P. Kopeikova, and J. Kopeckeva, "Binding and cytotoxicity of HPMA copolymer conjugates to lymphocytes mediated by receptor-binding epitopes," *Pharmaceutical research,* vol. 20, no. 3, pp. 360-7, Mar 2003.

[304] H. Maeda, J. Wu, T. Sawa, Y. Matsumura, and K. Hori, "Tumor vascular permeability and the EPR effect in macromolecular therapeutics: a review," *Journal of controlled release : official journal of the Controlled Release Society,* vol. 65, no. 1-2, pp. 271-84, Mar 1 2000.

[305] Y. Matsumura and H. Maeda, "A new concept for macromolecular therapeutics in cancer chemotherapy: mechanism of tumoritropic accumulation of proteins and the antitumor agent smancs," *Cancer research,* vol. 46, no. 12 Pt 1, pp. 6387-92, Dec 1986.

[306] H. Maeda, G. Y. Bharate, and J. Daruwalla, "Polymeric drugs for efficient tumor-targeted drug delivery based on EPR-effect," *European journal of pharmaceutics and biopharmaceutics : official journal of Arbeitsgemeinschaft fur Pharmazeutische Verfahrenstechnik e.V,* vol. 71, no. 3, pp. 409-19, Mar 2009.

[307] A. K. Iyer, G. Khaled, J. Fang, and H. Maeda, "Exploiting the enhanced permeability and retention effect for tumor targeting," *Drug Discov Today,* vol. 11, no. 17-18, pp. 812-8, Sep 2006.

[308] V. Šubr, J. Strohalm, T. Hirano, Y. Ito, and K. Ulbrich, "Poly[N-(2-hydroxypropyl)methacrylamide] conjugates of methotrexate: Synthesis and in vitro drug release," *Journal of Controlled Release,* vol. 49, no. 2, pp. 123-132, 1997/12/15/ 1997.

[309] T. Etrych, M. Sirova, L. Starovoytova, B. Rihova, and K. Ulbrich, "HPMA copolymer conjugates of paclitaxel and docetaxel with pH-controlled drug release," *Molecular pharmaceutics,* vol. 7, no. 4, pp. 1015-26, Aug 2 2010.

[310] D. Putnam and J. Kopecek, "Enantioselective release of 5-fluorouracil from N-(2-hydroxypropyl)methacrylamide-based copolymers via lysosomal enzymes," *Bioconjugate chemistry,* vol. 6, no. 4, pp. 483-92, Jul-Aug 1995.

[311] P. A. Vasey *et al.*, "Phase I clinical and pharmacokinetic study of PK1 [N-(2-hydroxypropyl)methacrylamide copolymer doxorubicin]: first member of a new class of chemotherapeutic agents-drug-polymer conjugates. Cancer Research Campaign Phase I/II Committee," *Clinical cancer research : an official journal of the American Association for Cancer Research,* vol. 5, no. 1, pp. 83-94, Jan 1999.

[312] A. H. Thomson *et al.*, "Population pharmacokinetics in phase I drug development: a phase I study of PK1 in patients with solid tumours," *British journal of cancer,* vol. 81, no. 1, pp. 99-107, Sep 1999.

[313] L. W. Seymour *et al.*, "Phase II studies of polymer-doxorubicin (PK1, FCE28068) in the treatment of breast, lung and colorectal cancer," *International journal of oncology,* vol. 34, no. 6, pp. 1629-36, Jun 2009.

[314] B. Rihova *et al.*, "Cytostatic and immunomobilizing activities of polymer-bound drugs: experimental and first clinical data," *Journal of controlled release : official journal of the Controlled Release Society,* vol. 91, no. 1-2, pp. 1-16, Aug 28 2003.

[315] T. Mrkvan *et al.*, "Chemotherapy based on HPMA copolymer conjugates with pH-controlled release of doxorubicin triggers anti-tumor immunity," *Journal of controlled release : official journal of the Controlled Release Society,* vol. 110, no. 1, pp. 119-29, Dec 10 2005.

[316] B. Rihova and M. Kovar, "Immunogenicity and immunomodulatory properties of HPMA-based polymers," *Advanced drug delivery reviews,* vol. 62, no. 2, pp. 184-91, Feb 17 2010.

[317] T. Etrych, P. Chytil, T. Mrkvan, M. Sirova, B. Rihova, and K. Ulbrich, "Conjugates of doxorubicin with graft HPMA copolymers for passive tumor targeting," *Journal of controlled release : official journal of the Controlled Release Society,* vol. 132, no. 3, pp. 184-92, Dec 18 2008.

[318] T. Etrych, J. Strohalm, P. Chytil, B. Rihova, and K. Ulbrich, "Novel star HPMA-based polymer conjugates for passive targeting to solid tumors," *Journal of drug targeting,* vol. 19, no. 10, pp. 874-89, Dec 2011.

[319] Y. Noguchi *et al.*, "Early phase tumor accumulation of macromolecules: a great difference in clearance rate between tumor and normal tissues," *Jpn J Cancer Res,* vol. 89, no. 3, pp. 307-14, Mar 1998.

[320] K. Ulbrich, T. Etrych, P. Chytil, M. Jelinkova, and B. Rihova, "HPMA copolymers with pH-controlled release of doxorubicin: in vitro cytotoxicity and in vivo antitumor

activity," *Journal of controlled release : official journal of the Controlled Release Society,* vol. 87, no. 1-3, pp. 33-47, Feb 21 2003.

[321] R. Zhang *et al.*, "Synthesis and evaluation of a backbone biodegradable multiblock HPMA copolymer nanocarrier for the systemic delivery of paclitaxel," *Journal of controlled release : official journal of the Controlled Release Society,* vol. 166, no. 1, pp. 66-74, Feb 28 2013.

[322] K. B. O'Hare, R. Duncan, J. Strohalm, K. Ulbrich, and P. Kopeckova, "Polymeric drug-carriers containing doxorubicin and melanocyte-stimulating hormone: in vitro and in vivo evaluation against murine melanoma," *Journal of drug targeting,* vol. 1, no. 3, pp. 217-29, 1993.

[323] M. Kovar, J. Strohalm, T. Etrych, K. Ulbrich, and B. Rihova, "Star structure of antibody-targeted HPMA copolymer-bound doxorubicin: a novel type of polymeric conjugate for targeted drug delivery with potent antitumor effect," *Bioconjugate chemistry,* vol. 13, no. 2, pp. 206-15, Mar-Apr 2002.

[324] L. W. Seymour *et al.*, "Hepatic drug targeting: phase I evaluation of polymer-bound doxorubicin," *Journal of clinical oncology : official journal of the American Society of Clinical Oncology,* vol. 20, no. 6, pp. 1668-76, Mar 15 2002.